NANO BIO-COMPOSITE FOR ENVIORNMENTAL REMEDIATION

Report

Submitted to the University Grants Commission (UGC), New Delhi

as a part of the Emeritus Fellowshipawarded to

Dr. R. RAVEENDRAN

[Award No.- F.6-6/2017-18/ Emeritus -2017-18OBC-9431/(SA-II) Dated 07-04-2017]

DEPARTMENT OF PHYSICS

SREE NARAYANA COLLEGE, KOLLAM

KERALA-601001

Recognised Research Centre, University of Kerala

September- 2020

Dr R Raveendran
G.G.-1, Shiv Ganga
Kavanad PO
Ramankulangara
Kollam-691003
e-mail: rrsnc1960@gmail.com
Mob: 9496847108

Emeritus Fellow
Department of Physics
S N College, Kollam
Kerala-691001
India
Phone : 0474-2741793

CERTIFICATE

This is to certify that the work embodied in the report entitled **"NANO BIO-COMPOSITE FOR ENVIORNMENTAL REMEDIATION"** has been carried out by me as part of the Emeritus Fellowship awarded to me **[*Award No. - F.6-6/2017-18/ Emeritus-2017-18OBC-9431/(SA-II) Dated 07-04-2017*]** by the University Grants Commission (UGC), New Delhi.

Kollam

September-2020

Dr. R. Raveendran

Emeritus – Fellow

ACKNOWLEDGEMENT

It is with deep sense of gratitude that, I wish to express my feelings to the **University Grants Commission (UGC), New Delhi** for the award of this Prestigious Fellowship to me and the financial assistance extended to me to complete this project work .

I wish to thank the Management of S.N. Colleges and the Principal of S.N. College, Kollam, Kerala for providing me with necessary laboratory facilities.

I express my gratitude to the staffs of Sophisticated Test and Instrumentation Centre, CUSAT, Kochi, Central Instrumentation Facility, Pondicherry, S.I.C.C-University of Kerala for extending their help for thecharacterisation of the samples.

I am fortunate to have students like Dr. G. Sajeev Kumar, HOD, Physics Department, Dr.Dedhila Devadethan, Dr.Indulal, Mr. Baiju etc. who had helped me in various capacities during the course of this work.

I also wish to thank **Dr. B. Beena,** Associate Professor in Chemistry, K.S.M.D.B. College, Sasthamcotta and her Research Group for their support to complete the experimental work.

Dr. R. Raveendran

PREFACE

The study of nanomaterials has seen an outburst of scientific and industrial attention over the last few years. Semiconductor nanomaterials of transition metal oxides deserve special attention in view of their tremendous applications in various fields. Nowadays great attention has also been paid to semiconductor / polymer matrix based nanocompositesbecause of their unique quantum confinement nature, which changes the overall properties of materials.They are generally prepared by physical, chemical and biological methods. Compared to physical and chemical methods, biological method is a preferred alternative since it is safe, economical, biocompatible and abides by the principles of green chemistry. In the light of its importance, the present study focuses on the synthesis of transition metal oxides such as Zinc Oxide, Copper Oxide and their composites with bio polymer via. nano cellulose by using herbal extract of Fresh Tinospora Cordifolia plant. The bio nano cellulose was synthesised by using locally available sugarcane bagasse.

The synthesized materials were well characterized by different experimental techniques like XRD, FT-IR, UV-Vis, PL, SEM, TEM and BET surface area. The application potential of the synthesised materials for environmental remediation was investigated through adsorption of heavy metal ions and photodegradation of organic dyes. Further, all the synthesized materials were tested for their antimicrobial properties. The matter presented in the report is summarized under eight chapters.

Chapter I of the report would serve as a general introduction to the necessity of safe environmental protection and various methods adopted in the society and its advantages and limitations of these methods. The chapter also reports a thorough introduction of nanomaterials, their properties, classifications, synthesis methods and applications in different fields. The importance of transition metal oxides and polymer based metal oxides are discussed in detail.The chapter also reveals the broad aim and scope of thepresent work and a brief review of literature on related topics.

Chapter II describes in detail the various characterization techniques used to measure the properties of the synthesized nanomaterials.

Chapter III describes the green synthesis of Nano CuO and nano ZnO and their characterisation by various techniques. The chapter also describes the synthesis and characterisation of Nano Cellulose by using Sugar cane bagasse and the composites of the prepared nano CuO and nano ZnO with nano Cellulose.

Chapter IV gives a detailed analysis of the results of various characterisation techniques adopted in the course of this work.

Chapter V deals with the application studies of the prepared samples on the adsorption of heavy metal ions such as Cd(ll) and Pb(ll) from aqueous solutions and its comparison.

Chapter VI describes the application of the prepared samples in the photo catalytic degradation of organic dyes namely Congo red and Malachite green and its mechanisms were well described and compared with different materials.

Chapter VII deals with the antimicrobial activities of the synthesized nanomaterials towards both bacterial and fungal strains in detail.

In **Chapter VIII** the overall summary of the results and findings of the present study along with future prospectus are given.

List of published papers and conferences/seminars attended are also portrayed in the Annexure-I & Annexure II respectively.

CONTENTS

		Page No.
Preface		**iv**
List of Tables		**xi**
List of Figures		**xii**
CHAPTER - I		
INTRODUCTION		
1.1	WATER POLLUTION	2
1.2	IMPORTANCE OF WASTE WATER TREATMENT	4
1.3.	NANOSCIENCE AND NANOTECHNOLOGY	9
1.4.	PROPERTIES OF NANOMATERIALS	10
1.5.	CLASSIFICATIONS OF NANOMATERIALS	12
1.6.	METHODS FOR THE SYNTHESIS OF NANOMATERIALS	16
1.7.	APPLICATIONS OF NANOTECHNOLOGY	17
1.8.	APPLICATION STUDIES IN THE PRESENT WORK	20
1.9.	LITERATURE REVIEW	21
1.10.	PRESENT STUDY	26
1.11.	OBJECTIVES OF THE PRESENT STUDY	26
CHAPTER - II		
CHARACTERIZATION TECHNIQUES		
2.1.	INTRODUCTION	28
2.2.	ELEMENTAL ANALYSIS	28
2.3.	STRUCTURAL ANALYSIS	29
2.4.	MICROSCOPIC STUDIES	31
2.5.	OPTICAL ANALYSIS	32

CHAPTER - III

SYNTHESIS OF NANO CuO AND NANO ZnO AND ITS CELLULOSE BASED COMPOSITES

3.1.	INTRODUCTION	36
3.2.	METHODS OF SYNTHESIS	36
3.2.a	PREPARATION OF THE PLANT STEM EXTRACT	36
3.2.b	PREPARATION OF ZnO NANOPARTICLES	37
3.2.c	PREPARATION OF CuO NANOPARTICLES.	37
3.2.d	ISOLATION OF NANOCELLULOSE FROM SUGARCANE BAGASSE (SCB)	38
3.2.e	DELIGNIFICATION OF CELLULOSE FROM SUGARCANE BAGASSE	38
3.2.f	EXTRACTION OF CELLULOSE	38
3.2.g	PREPARATION OF NANOCELLULOSE	39
3.2.h	SYNTHESIS OF COMPOSITES OF NANOCELLULOSE WITH ZnO AND CuO	39
3.2.i	PREPARATION OF ZINC OXIDE/ COPPER OXIDE INCORPORATED NANOCELLULOSE (ZnO/NC AND CuO/NC)	39

CHAPTER - IV

CHARACTERIZATION OF NANO CuO AND NANO ZnO AND ITS CELLULOSE BASED COMPOSITES

4.1.	METHODS FOR CHARACTERISATION	41
4.2.	RESULTS AND DISCUSSION	41
4.2. a	XRD	41
4.2. b	FTIR	45
4.2.c	SEM ANALYSIS	48
4.2. d	ENERGY DISPERSIVE X-RAY SPECTROSCOPY ANALYSIS (EDS)	52

4.2. e	TEM ANALYSIS	52
4.2. f	UV-VISIBLE SPECTROSCOPIC STUDIES	59
4.2. g	PHOTOLUMINESCENCE (PL) SPECTRAL ANALYSIS	66
4.2.h	BET SURFACE AREA ANALYSIS	69

CHAPTER - V

APPLICATION STUDIES

5.1.	ADSORPTION STUDIES.	71
5.1.1.	EVALUATION OF ADSORPTION EFFICIENCY	71
5.1.2	MECHANISM OF ADSORPTION	72
5.1.3	EXPERIMENTAL SET UP -BATCH TYPE CONTACT METHOD	73
5.1.4	KINETICS STUDIES.	75
5.1.5	ISOTHERM STUDIES	75
5.2	ADSORPTION STUDIES OF NANO ZnO	77
5.3	ADSORPTION STUDIES OF NANO CuO	84
5.4	ADSORPTION STUDIES OF NANO CELLULOSE (NC),NC/CuO& NC/ ZnO	87
5.4.1	EFFECT OF pH ON ADSORPTION	87

CHAPTER - VI

PHOTODEGRADATION OF DYES

6.1.	INTRODUCTION	90
6.1.1.	CONGO RED (CR)	91
6.1.2	MALACHITE GREEN (MG)	92
6.2	PHOTOCATALYTIC DEGRADATION OF CONGO RED (CR) AND MALACHITE GREEN (MG)	93
6.2.1	EFFECT OF THE OPERATING PARAMETERS	94
6.2.1.1	EFFECT OF TIME ON DEGRADATION	94
6.2.1.2	EFFECT OF pH ON PHOTODEGRADATION	98

6.2.1.3	EFFECT OF INITIAL CONCENTRATION OF DYES ON DEGRADATION	100
6.2.1.4	EFFECT OF CATALYST DOSAGE ON DEGRADATION	103
6.3	KINETICS OF PHOTODEGRADATION	105
6.4	MECHANISM OF PHOTO DEGRADATION	109
6.5	COMPARISON OF PHOTOCATALYTIC ACTIVITIES OF DIFFERENT PHOTO CATALYSTS	111
6.6	REGENERATION AND REUSABILITY OF PHOTO CATALYST	113

CHAPTER-VII

ANTI-MICROBIAL STUDIES

7.1.	INTRODUCTION	114
7.1.1.	ANTIMICROBIAL ACTIVITY – AGAR - WELL DIFFUSION METHOD	115
7.2	EVALUATION OF ANTIMICROBIAL ACTIVITY OF NANO ZnO	115
7.3	EVALUATION OFANTIMICROBIAL PROPERTIES OF NANO CuO	116
7.4	EVALUATION OF ANTIMICROBIAL STUDIES OF NC, ZnO/NC & CuO/NC	117

CHAPTER-VIII

SUMMARY AND FUTURE SCOPE

8.1.	SUMMARY	119
8.2	FUTURE SCOPE	121
	REFERENCES	122 - 133

ANNEXURE – I : - List of Publications and copies of published works during the award period [2017-2019].

ANNEXURE – II : - List of Seminars & Conferences and invited talks attended during the award period[2017-2019].

LIST OF TABLES

Table No.	Title	Page No.
1.1	MAJOR FORMS OF ENVIRONMENTAL POLLUTION	1
4.1	COMPOSITION OF ZnO FROM EDS SPECTRUM	52
4.2	COMPOSITION OF CuO FROM EDS SPECTRUM	53
4.3	BAND GAP VALUES OF DIFFERENT MATERIALS	65
4.4	BET SURFACE AREA OF DIFFERENT MATERIALS	70
5.1	KINETIC PARAMETERS FOR THE ADSORPTION OF Pb(II) AND Cd(II)	81
5.2	LANGMUIR, FREUNDLICH AND SIPS ISOTHERM CONSTANTS FOR THE ADSORPTION OF Pb(II) AND Cd(II) ONTO ZnO	82
5.3	KINETIC PARAMETERS FOR THE ADSORPTION OF Pb (II) AND Cd (II) ONTO CuO	86
5.4	LANGMUIR, FREUNDLICH AND SIPS ISOTHERM CONSTANTS FOR THE ADSORPTION OF Pb(II) AND Cd(II) ONTO CuO	87
5.5	COMPARISON OF ADSORPTION EFFICIENCIES OF METAL OXIDES, NC AND ITS COMPOSITES.	89
5.6	KINETIC PARAMETERS FOR THE ADSORPTION OF Pb (II) AND Cd (II) ON NC, NC/CuO AND NC/ZnO	89
6.1	FIRST-ORDER KINETIC CONSTANTS AND RELATIVE COEFFICIENTS FOR THE PHOTOCATALYTIC DEGRADATION OF CR AND MG OVER THE PHOTOCATALYSTS	109
6.2	PHOTODEGRADATION EFFICIENCY OF VARIOUS PHOTOCATALYSTS	111

Table No.	Title	Page No.
6.3	COMPARISON OF PHOTOCATALYTIC DEGRADATION ABILITY OF ZnO/NC WITH PREVIOUS LITERATURE	112
7.1	COMPARISON OF ANTIMICROBIAL ACTIVITIES OF DIFFERENT ZnO SAMPLES	116
7.2	ZONE OF INHIBITION (MM) OF CuO (300) AND CuO (500) TOWARDS *E. coli* AND *S. aureus*	116
7.3	COMPARISON OF ZONE OF INHIBITION OF NC AND COMPOSITES	117

LIST OF FIGURES

Figure No.	Title	Page No.
1.1	MECHANISM OF ANTIBACTERIAL ACTIVITY	21
2.1 (a) & (b)	EXCITATION OF ELECTRONS BETWEEN MOLECULAR ORBITALS	33
3.1	TINOSPORA CORDIFOLIA PLANT	37
3.2	SUGARCANE BAGASSE	38
3.3	STRUCTURE OF CELLULOSE	39
3.4	PROPOSED STRUCTURE OF ZnO/NC COMPOSITE	40
4.1	XRD PATTERN OF ZnO	42
4.2	XRD PATTERN OF NC	42
4.3	XRD PATTERN OFZnO/NC	43
4.4	XRD PATTERN OF CuO	44
4.5	XRD PATTERN OF CuO/NC	44
4.6	FTIR SPECTRUM OF ZnO	45
4.7	FTIR SPECTRUM OF NC	46
4.8	FTIR SPECTRUM OF ZnO/NC	47
4.9	FTIR SPECTRUM OF CuO	47
4.10	FTIR SPECTRUM OFCuO/NC	48
4.11	SEM IMAGE OF ZnO	49
4.12	SEM IMAGE OF NC	49
4.13	SEM IMAGE OF ZnO/NC	50
4.14	SEM IMAGE OFCuO	51
4.15	SEM IMAGE OF CuO/NC	51

Figure No.	Title	Page No.
4.16	EDS SPECTRUM OF ZnO	52
4.17	EDS SPECTRUM OF CuO	53
4.18	EDS SPECTRUM OF NC	54
4.19	EDS SPECTRUM OF ZnO/NC	54
4.20	EDS SPECTRUM OF CuO/NC	55
4.21	(a)TEM (b) SAED PATTERN(c) HISTOGRAM DEPICTING THE SIZE DISTRIBUTION OF ZnO	56
4.22	(a)TEM (b) SAED PATTERN OF NC	57
4.23	(a)TEM (b) SAED OF ZnO/NC	57
4.24	(a)TEM (b) SAED PATTERN (c) HISTOGRAM DEPICTING THE SIZE DISTRIBUTION OF CuO	58
4.25	(a)TEM OF CuO/NC (b) SAED OF CuO/NC	59
4.26	UV-Vis. SPECTRUM OF ZnO	60
4.27	UV-Vis. SPECTRUM OF NC	60
4.28	UV-Vis. SPECTRUM OF ZnO/NC	61
4.29	UV-Vis. SPECTRUM OF CuO	62
4.30	UV-Vis. SPECTRUM OF CuO/NC	62
4.31	Tauc’s PLOT OF ZnO	63
4.32	Tauc’s PLOT OF NC	63
4.33	Tauc’s PLOT OF ZnO/NC	64
4.34	Tauc’s PLOT OF CuO	65
4.35	Tauc’s PLOT OF CuO/NC	65
4.36	PL EMISSION SPECTRUM OF ZnO	66
4.37	PL EMISSION SPECTRUM OF NC	67

Figure No.	Title	Page No.
4.38	PL EMISSION SPECTRUM OF ZnO/NC	68
4.39	PL EMISSION SPECTRUM OF CuO	68
4.40	PL EMISSION SPECTRUM OF CuO/NC	69
5.1	WATER POLLUTION DUE TO HEAVY METAL IONS AND ORGANIC DYES	71
5.2	REMOVAL EFFICIENCY *vs* pH FOR Pb(ll) AND Cd(ll)	78
5.3	REMOVAL EFFICIENCY *vs* ADSORBENT DOSAGE FOR Pb(ll) and Cd(ll)	79
5.4	ADSORPTION EFFICIENCY vs INITIAL METAL ION CONCENTRATIONS FOR Pb(ll) AND Cd(ll)	80
5.5	KINETIC PLOTS FOR Pb(ll) AND Cd(ll)	81
5.6	EXPERIMENTAL AND MODEL FITS OF LANGMUIR, FREUNDLICH AND SIPS ISOTHERMS OF Pb(II) AND Cd(II) ADSORPTION ONTO NANO ZnO	82
5.7	ADSORPTION –DESORPTION CYCLES FOR Pb (ll) & Cd (ll)	83
5.8	REMOVAL EFFICIENCY *vs*p HFOR Pb(ll) &Cd(ll)	84
5.9	REMOVAL EFFICIENCY *vs* ADSORBENT DOSAGE FOR Pb(ll) &Cd(ll)	85
5.10	KINETIC PLOTS FOR Pb(ll) & Cd(ll)	85
5.11	EXPERIMENTAL AND MODEL FITS OF LANGMUIR, FREUNDLICH AND SIPS ISOTHERMS OF Pb(ll) & Cd(ll)	86
5.12	EFFECT OF PH ON THE ADSORPTION OF Pb (II) AND Cd (II) ON NC, NC/CuO,AND NC/ZnO.	88
5.13	EFFECT OF ADSORBENT DOSE ON ADSORPTION	88

Figure No.	Title	Page No.
6.1	STRUCTURE OF CONGO RED	91
6.2	ABSORBANCE SPECTRUM OF CR	92
6.3	STRUCTURE OF MALACHITE GREEN	92
6.4	ABSORBANCE SPECTRUM OF MG	93
6.5	PHOTODEGRADATION OF CR USING VISIBLE LIGHT ONLY, ZnO/NC ONLY & ZnO/NC WITH VISIBLE LIGHT	93
6.5.1	TIME DEPENDANT ABSORPTION SPECTRA OF CONGO RED DYE UNDER VISIBLE LIGHT IRRADIATION WITH (a) ZnO (b)NC (c) ZnO/NC (d) CuO (e) CuO/NC	95
6.5.2	TIME DEPENDANT ABSORPTION SPECTRA OF MALACHITE GREEN DYE UNDER VISIBLE LIGHT IRRADIATION WITH (a) ZnO (b)NC (c) ZnO/NC (d) CuO (e) CuO/NC	96
6.5.3	DEGRADATION EFFICIENCY vs pH FOR CONGO RED	98
6.5.4	DEGRADATION EFFICIENCY vs pH FOR MALACHITE GREEN	99
6.5.5	DEGRADATION EFFICIENCY VS CONCENTRATION FOR CONGO RED	101
6.5.6	DEGRADATION EFFICIENCY VS CONCENTRATION FOR MG	102
6.5.7	DEGRADATION EFFICIENCY VS CATALYST DOSAGE FOR CR	103
6.5.8	DEGRADATION EFFICIENCY VS CATALYST DOSAGE FOR MG	104

Figure No.	Title	Page No.
6.6	PHOTODEGRADATION OF CR WITH (A) BLANK, ZnO, NC, ZnO/NC, CuO, CuO/NC (B) KINETIC LINEAR SIMULATION PLOT (C) REACTION RATE OF PHOTODEGRADATION OF CR WITH BLANK, ZnO, NC, ZnO/NC, CuO, CuO/NC.	107
6.7	PHOTODEGRADATION OF MG WITH (A) BLANK, ZnO, NC, ZnO/NC, CuO, CuO/NC (B) KINETIC LINEAR SIMULATION PLOT (C) REACTION RATE OF PHOTODEGRADATION OF CR WITH BLANK, ZnO, NC, ZnO/NC, CuO, CuO/NC	108
6.8	MECHANISM OF PHOTO DEGRADATION BY METAL-OXIDE NANOCOMPOSITES	110
6.9	PHOTODEGRADATION CYCLE OF CR ON TO ZnO/NC	113
7.1	MECHANISM OF ANTIMICROBIAL ACTIVITY OF ZnO NANOPARTICLES	114

CHAPTER - I

INTRODUCTION

Ecosystem is a set of connections between living organisms and nonliving components such as water, soil, air and with environment. In the environment there are different interactions between animals, plants, soil, water, and other living and non-living things. Present society takes a large number of steps like hurried industrialization, unintended urbanization, deforestation, over exploitation of natural resources to face the problems created by the population increase. The after effect of these processes involves the releasing of a large number of extraneous materials and energy into environment in an uninterrupted manner, which increases the amount of the objectionable materials in the environment that adversely affects the environment which domino effect in environmental pollution. From the reports of National Academy of Science, USA, pollution is the undesirable change in physical, chemical and biological characteristics of natural resources such as water, air andsoil which unfavorably affect human, animal and plant life. A pollutant is a living or nonliving thing or any physical agent, the excess concentration of which hurtful to theenvironment. Pollutants are classified into non-biodegradable pollutants and bio degradable pollutants. Non-biodegradable pollutants do not break down under the action of microbes which react with other compounds producing harmful substances such as toxins which include wastes like glass, plastics et. and poisons like pesticides, heavy metals etc. Degradable pollutants breakdown by microbial action or by natural processes. Major forms of environmental pollutions and the reasons of pollutions are shown in **Table 1.1**

Table 1.1. Major forms of environmental pollution

Air pollution	Releases of gases such as carbon monoxide, carbon dioxide, chlorofluorocarbons and nitrogen dioxide from industries or vehicles in to air.
Water pollution	The waste waters discharged from textile, nuclear industries and from farms.
Soil pollution	Release of heavy metals, acids, hydrocarbons etc. into soil or underground.

Noise pollution	Noises from factories, aircrafts or roadways.
Thermal pollution	Change in the temperature of the water bodies due to anthropogenic activities

Of the above mentioned pollutions, water pollution is the most threatening problem of the environment.

1.1. WATER POLLUTION

The most fundamental requirement of life is water and one third of our universe is enclosed by water. Of these 97% of the water is in the ocean, salty, and the remaining 3% is fresh water contained in ground and surface waters such as rivers, canals and lakes. Fresh water is available for many activities like drinking, cooking, cleaning, agriculture etc**.** Water has extensive impact on all aspect of human life together with health, food, energy and economy**.** Water is the most indispensable material vital for the subsistence of life and at present water is mostly polluted. About 6.5 billion populations are in the world and should amplified to be 9 million by 2050 The augmented population correlated troubles our flora and fauna by causing environmental pollutions, which in turn affects health of human lives as well as aquatic lives. From the reports of world health organization, nearly 12 million peoples are killed by waterborne diseases in every year. 5000-6000 children die due to diarrhea; a waterborne disease. Water pollution mainly affects surface waters such as rivers, lakes and canals and ground waters. Based on the source from which pollution occurs, pollution sources are categorized into two. Point-source pollution and nonpoint-source pollution. Point sources are the sources of pollution that point directly and the pollution comes from a single location such as discharge pipes from industries, leaking septic tanks, accidental spills, leaking gasoline storage tanks etc. Nonpoint source pollution comes not from a single source but from many scattered sources such as excess metal ion concentrations, organic pollutants like pesticides, dyes, antibiotics, fertilizers etc. The main organic pollutants which are harmful present in waste water are organic molecules such as polychlorinated biphenyls (PCBs), chlorinated and brominated phenols, chlorinated hydrocarbons, atrazines, surfactants, dyes and antibiotics. Mainly water pollution can be divided into two-physical water pollution and chemical water pollution. Physical water pollution is that which caused by physical actions such as

thermal pollution, taste and odour pollution, colour pollution and domestic effluent pollution. Chemical water pollution is caused by the action of a variety of chemical substances poured into different sources of water. The main chemicals include pesticides, dyes, antibiotics and fertilizers. Wide use of dyes and antibiotics in industries, veterinary and poultry farms lead to its accretion in the surrounding environment. Brisk growth of industries and farms lead to the accumulation of dyes and antibiotics in the surrounding environment, they reached the aquatic environment through the direct hammering of waste water from industries, hospitals and farms which are injurious to human health and aquatic lives. Many problems related to aquatic environment that leads to water pollution is associated with the use of chemicals such as fertilizers, disinfectants, algaecides and pesticides therapeutants such as antibiotics and other antibacterial, feed additives etc.

1.1.1. WATER POLLUTION BY INDUSTRIES

The most widespread type of water pollution is water pollution by the industries. More than half of the water pollution is caused by the industries; the products and by products of industries are toxic and dumped into water bodies. The two main industries which cause water pollution are textile industry and nuclear industry. Various industries such as leather, paper, plastic and printing deals with dyes. Of the 7x105 tons of dyestuffs produced per year, about 10-15% is received by water bodies through the waste water from textile industries. The presence of dyes in aquatic environment cause detrimental effects on aquatic life and human health, causing mutation, cancer, birth defects, central nervous system disorder and heart diseases. Dyes with complex aromatic structures are recalcitrant with attendant inhibitory nature. The pollution by dyes caused on aquatic environment leads to the reduction of dissolved oxygen required for aquatic life as these are resistant to light and moderate oxidative agents. Thus, it is noteworthy to take care of these harmful dyes previous to discharging into water bodies. Most of the dyes and antibiotics contain complex aromatic structures, have complex photo degradation mechanism makes them difficult to degrade under vigorous conditions. Normally dyes are of two types, anionic dyes and cationic dyes. Cationic dyes are basic dyes which dissociate into positive ions in aqueous solutions. Anionic dyes are acidic dyes which dissociate into negative ions in aqueous solutions.

All nuclear plants are associated with thermal pollution, the nuclear industries requires a huge amount of water for cooling purpose. As a result almost all the plants sited in the vicinity of the water bodies faces shortage of water and also the waste water from nuclear industries contains radioactive wastes and they are poured into rivers, lakes and oceans, which are hazard to plants, aquatic life and man-kind equally. Nuclear wastes are highly carcinogenic, causing different types of cancer. Nuclear wastes enter the water bodies through medical and industrial wastes and from naturally arising radioactive materials. The radioactive elements from nuclear industry remain perilous for years depending on their half-life periods. Majority of nuclear plants are older; leaks are common and can pollute drinking water and food supplies which in turn terrorize human society. The spent nuclear fuels contain transuranic elements and isotopes of iodine-131, caesium-137 etc. which are radioactive and carcinogenic.

1.1.2. WATER POLLUTION BY FARMS

Antibiotics are widely used in veterinary and poultry farms to treat for infections and to promote the growth and meat productions. Tetra cyclones and fluoroquinolones are the common antibiotics used as growth promoters in chickens and for the treatment of cholera, respiratory and urinary tract infections in humans. These antibiotics reach the aquatic environment through the wastewater from hospitals, poultry and veterinary farms and from nursing homes. The amount of antibiotics in excess concentration than that allowed will adversely affect the environment and in turn unbalancing of ecosystem**.** Countries like EU and the US introduced poultry farming standards and legislation to regulate the use of antibiotics, as these antibiotics are hurtful. It is necessary to eradicate the antibiotics by the usage of suitable photocatalyst to convert toxic substances into nontoxic gases.

1.2. IMPORTANCE OF WASTE WATER TREATMENT

Waste water containing dyes and antibiotics can harmfully affect aquatic environment by diminishing sunlight penetration, have an effect on human health causing mutation and cancer. It is crucial to be aware of noxious waste providence and effects for pollution management strategies supplementary to the normal methods for handling of effluent waste streams. Waste water management has turn out to be a decisive intimidation due to increased population and industrial pollution, is the

necessitate of this new decades due to the scarceness of drinking water**.** During the last decades due to fast population growth, environmental pollutions such as high chemical contamination in air, water and soil are tremendously increased. Water pollution cause insufficiency of fresh water for drinking and become a solemn intimidation in the present situation. Hence the purification of water from pollutants is very obligatory in present circumstances. Pollution by dyes and antibiotics are extremely pernicious as these are toxic and non-biodegradable pollutants. It is necessary to convert these dyes and antibiotics into most stabilized nontoxic forms otherwise they become menace to the environment. The pollutants in waste water and pollutants in ground water must be removed prior to their discharge in the environment. Most of the dyes and antibiotics are photo stable and refractory towards chemical oxidation which inhibits the degradation by normal physical and chemical methods. Even a trace amount of these pollutants in water affects water transparency, gas solubility and consequently reducing the photosynthetic activity of aquatic biota.

1.2.1. METHODS FOR WASTEWATER TREATMENT

There are various methods for the treatment of wastewater. The conventional methods can be categorized into three: physical, biological and chemical. The main physical methods are distillation, ion exchange, reverse osmosis, coagulation, flocculation, membrane filtration processes like microfiltration, ultra-filtration, nano filtration etc. and these methods are less attractive due to expensive costs and have limited lifetime are some of the physical methods. Water purification can also be done biologically using microorganisms such as bacteria. These microorganisms react in wastewater, decompose the organic matter within the water and thereby reducing the amount of organic suspended matter**.** Also, biological methods such as activated sludge and biological trickling filters requires large land area, shows less flexibility in design and operation are unable to remove the pollutants as these compounds are soluble in effluent. Chemical methods include waste incineration, anaerobic digestion, chlorination, ozonation**,** chemical addition, clarification, deionization, softening etc. and these methods are expensive, use an outsized amount of chemicals and produce slush which are venomous and itself requires treatment. Chemical oxidation is the main physiochemical method for the conversion of organic pollutants into carbon dioxide, water, and other fully oxidized species like nitrates and sulfates. Chemical oxidation

processes come under two categories: conventional and advanced. Wet chemical oxidizing agents including ozone, persulfate, and Fenton reagents (Fe_3+/H_2O_2) are the major conventional methods. Conventional methods have advantages as well as limitations as this embrace toxicity and their high reactivity leads to incomplete combustion liberating toxic intermediates. The advanced oxidation involves sonolysis, radiolysis, or photolysis. It is essential to produce drinking water of high quality; there must be an established method of cost of use to supply fresh water in sufficient amount. The method must be stable, cost effective and economic than any other conventional methods.

1.2.1a. ADSORPTION

Heavy metal ions are introduced into water reservoirs by industries, manufacturing chemicals and battery, metallurgical operations, leather tanning and mining. The increase in the level of toxic heavy metal ions causes a hazardous effect on human beings and the environment. The increasing concentration of Pb(II) and Cd(II) in water became an eco-toxicological hazard of prime importance due to non-biodegradability, toxicity and accumulation in living organisms and diligence in nature even at low concentrations. Current Pb (II) ionconcentration in natural water (2 to 10 $ngmL^{-1}$) is higher as the upper limit suggested by the World Health Organization (which is less than10 $ngmL^{-1}$). Since this unrestrained augment of Pb (ll) ions causes severe environmental issues, there is a very urgent need to protect the environment from these hazardous metal ions. The exposure to Cd^{2+} has been associated with renal damage, osteoporosis, prostate and renal cancer [Jarup2003]. Both Cd^{2+} and Pb^{2+} have been associated with adverse renal and negative bone effects. The permissible limit of Cd^{2+} in the drinking water set by the World Health Organization guidelines is 5 μg/L. Adsorption is considered as a spotless and green technique for the removal of heavy metal ions and has been used in industries for a variety of separations and purification processes.

Though traditional sorbents can remove heavy metal ions from wastewater, their low sorption capacities and efficiencies limit the application. To solve these defects of traditional sorbents, advanced techniques in material design are required. Hence nanomaterials are used as the novel ones to remove heavy metal ions in

wastewater [1&2]. Nanomaterials due to their size, exhibit an array of novel properties that can be used to develop new technologies and improve existing ones. Characteristics such as large surface area, the potential for self-assembly, high specificity, high reactivity and catalytic potential make nanomaterials excellent candidates for water treatment applications [3&4]. Nanoadsorbents because of their high specific surface area and the absence of internal diffusion resistance are quite efficient for the fast adsorption of heavy metal ions and organic molecules from aqueous solutions [5]. To be used as sorbents for removing heavy metal ions in wastewater, nanomaterials should satisfy the following criteria: The nanosorbents themselves must be nontoxic, the sorbents must present relatively high sorption capacities and selectivity to the low concentration of pollutants, the adsorbed pollutant could be removed from the surface of the nanoadsorbents very easily and the sorbents could be recycled infinitely. A variety of nanomaterials such as carbon nanotubes, carbon-based material composites, graphene, nanometal or metal oxide and polymeric sorbents have been studied in the removal of heavy metal ions from aqueous solutions and thesenanomaterials showed high adsorption capacity compared to conventional materials [6,7&8].

1.2.1b. ADVANCED OXIDATION PROCESS (AOP) AND PHOTOCATALYSIS

Advanced oxidation process is the main technology used for the effective treatment of waste water which involves the production of very reactive species like hydroxyl radicals which can oxidize highly toxic organic pollutants into nontoxic inorganic salts. Hydroxyl radicals reacts with almost organic compounds with rate constants usually in the order of 106-109 moll-1s-1 and these are second most strong oxidant after fluorine having an oxidation potential of 2.8V**.** AOP include the generation of hydroxyl radicals and other reactive oxygen species such as superoxide anion radical, hydrogen peroxide and singlet oxygen used for the effective degradation of pollutants from waste water. Generally AOPs can be categorized into two groups: homogeneous and heterogeneous processes. In homogeneous processes, hydrogen peroxide, ozone and or UV lights are utilized but in heterogeneous processes photoreactive semiconductors are utilized. Heterogeneous reactions have a large number of advantages than homogeneous including the reuse of photocatalysts, capability of mineralization of a wide range of organic compounds and utilization of

solar light to excite the catalysts. Heterogeneous photo catalysis is a type of AOP, a promising technology for waste water treatment and is considered as an alternative technology to classical best technologies for both environmental detoxification and for energy production. This technology employs on the surface of the photo catalyst under the irradiation of photons, which involves the degradation of pesticides, dyes, organic - inorganic pollutants and other deleterious pollutants. The promoting of photoreaction in presence of a catalyst is termed as heterogeneous photo catalysis, a low cost and sustainable technology for the treatment of organic and inorganic pollutants present in water. For water purification, heterogeneous photo catalysis is considered as an emerging technology as it can degrade complex toxic organic pollutants into simpler degradable non-toxic fragments. Photocatalysis is a combination of two words photo means light and catalysis means decompose and the substance help to decompose is a catalyst. Photo catalysis an emerging destructive technology is cheap and ecofriendly compared to other AOPs like reverse osmosis, nano filtration, ultra-filtration and can mineralize the toxic pollutants almost completely into nontoxic products and photodegradation means photocatalytic oxidation or photomineralization to CO_2, H_2O, NO_3-, PO_4- and halide ions. The environmental applications of heterogeneous photocatalysis mainly focused on the remediation of polluted water streams as the reactions in aqueous phase are more complex compared to that in gas phase. In aqueous phase reactions, many reaction parameters such as pH, concentration of the photocatalyst and partial pressure of dissolved oxygen are taken into account and are carefully controlled. In photocatalysis, organic pollutants are degraded by using reusable photocatalysts, energetic light source such as sunlight or an artificial light and an oxidizing agent such as oxygen or air. For a photo catalyst, as the particle size decreases, surface area increases and the number of active sites increases which leads to high reactivity. As the number of active sites increases, the absorbance of pollutants on the surface of the catalyst increases. Photo catalytic degradation of dyes and antibiotics does not take place in the absence of O_2, and the systems are highly spontaneous with G0 = 0 and lead to the mineralization of organic pollutants. Chemical modification of the photo catalyst enhances the quantum yield of the electron transfer processes by discharging photoelectrons and providing an oxidation reduction pathway with low over potential. Rapid growth of global population, limited supply of drinking water,

increased environmental problems and the direct relationship between the water quality and human health needs to identify and applying effective water treatment methods for the proper balancing of our environment. Prevalent applications of photo catalysis are significantly constrained due to low separation probability of the photo induced electron hole pairs of the photo catalyst [9]. Therefore, it is necessity of the present situation to develop photo catalysts that promote the charge carrier separations and thereby extending the applications for environment remediation. A catalyst is one which alters the rate of a chemical reaction due to its efficiency in shifting the rate of a chemical reaction by tumbling the activation energy. Photocatalyst is a catalyst which utilizes light energy to trigger rate of a chemical reaction without being involved itself. Numerous metal and metaloxide nanomaterials are considered to be efficient photocatalysts.

1.2.1c.ANTIMICROBIAL ACTIVITY

With their unique physical, chemical, electrical, magnetic, optical and biological properties, metal oxide-nanoparticles are of immense interest to scientists as antimicrobial agents. Information on the molecular mechanisms of antimicrobial activity of metal oxide nanoparticles is still in its infancy and elucidation of the molecular mechanisms is the subject of rigorous research. The possible mechanisms of antimicrobial activity revealed from recent studies is shown in Figure 1.1. Although the mechanisms are not exhaustive, research has revealed that retardation/killing of bacterial growth is brought about by a combination of one or more mechanisms and it varies with the nature of the metal oxide. The principal mode of antimicrobial activity is the generation of reactive oxygen species (ROS). Besides ROS production, damage to cell membranes by electrostatic interaction, disturbance in metal / metal ion homeostasis, protein and enzyme dysfunction, genotoxicity and photokilling are other modes of action [10].

1.3. NANOSCIENCE AND NANOTECHNOLOGY

The word ‘Nano’ is gaining popularity in almost all the fields of Science and Technology. Nanoscience refers to the science & discipline, whereas Nanotechnology refers to the applied part of it including the Engineering to control, manipulate and structure the matter at an unambiguously small scale, which is nanoscale. This scale is

also referred to as atomic or molecular scale, which indicates one billionth of a meter (10^{-9} m).

The leaves of lotus have a self-cleaning mechanism, as water droplets roll over its surface, they wash away particles of dust and dirt leaving the leaves always cleans. This is due to the hydrophobic nature of the surface that no water can find refuge over the surface. Today's nanotechnology is a reflection of this natural phenomenon, and similar use of nano coating is being widely used in the manufacture of paints, bodies of aero-planes, wind shield glasses etc. The water striders are able to walk over the water surface without getting wet due to the nano-grooves present in the micro hairs of their legs [11]. Besides, the brightly coloured plumage of birds like peacock, pigeon and the sparkling wings of butterflies are all but a natural reflection of Nanotechnology.

The nano objects are not new; the new thing is the facilities available nowadays to characterize them on that small scale, which allows us to design and modify such kind of materials instead of getting them accidentally. So the study of nano particles, especially metal nano particles is only made possible by the use of the latest technological discoveries in instrumental analysis. About 20 years after Feynman's prediction, a new era of nanoscience and nanotechnology was developed with the invention of the Scanning Tunneling Microscope (STM) and High Resolution Transmission Electron Microscope (HRTEM) which led to the discovery of fullerenes in 1985 and carbon nanotubes in 1991[12].The invention of STM and AFM (Atomic Force Microscope) provided new important tools for viewing, characterizing and manipulating nanostructures at atomic level [13]

Nanotechnology can be achieved by focusing on the intrinsic properties of nanostructured materials and on the possibility of using, manipulating them into assemblies in order to perform specific functions [14]

1.4. PROPERTIES OF NANOMATERIALS

The physical and chemical properties of nanomaterials can differ significantly from their bulk counter parts because of their small size. In principle, it is difficult to define an exact dimension for the grain size below which the materials can be classified as 'nano'. Nanomaterials may be defined as "*those materials which have at least one of*

their dimensions in the nanomatric range where there is significant variations in the property of interest compared to microcrystalline materials".

The physical properties are comparatively same for micrometer scaled and bulk objects while the objects in the nanoscale may exhibit physical properties entirely different from that of the bulk ones. In the nanoscale some opaque substances become transparent; some inert materials attain catalytic properties; some solids change into liquids even at room temperature; some insulators become conductors and so on. Unexpected visual properties are shown by these nanoparticles because they are small enough to confine their electrons and produce quantum effects [15]. Discovery of particles smaller than subatomic particles acts as a catalyst for the development of the modern field of nanoscience and technology. Nanoparticle research is currently an area of intense scientific research including biological, optical, electrical and electronic fields.

Nanosized materials have large surface to volume ratio compared with their micro sized or bulk counterparts. Consider a particle of 1x1x1 nm^3. This contains nearly 4^3 =64 atoms of which 85% are at the surface. All the properties and applications of nanomaterials are dominated by surface atoms and thus they possess unique properties in the nano form.

1.4.1. OPTICAL PROPERTIES

Nanomaterials have attracted interest for their novel optical properties, which are comparatively different from their bulk counterparts. Due to these enhanced optical properties in nano meter scale, they have wide range of applications in solar cell, photocatalysis, optical detectors, laser and biomedicines. Various parameters such as size and shape, doping and interaction with the surrounding environment have dramatic influence on optical properties of nanomaterials [16].

1.4.2. MECHANICAL PROPERTIES

Mechanical properties such as hardness and elastic modulus, fracture toughness, scratch resistance, fatigue strength and hardness of crystalline nanomaterials follow the Hall-Petch relationship, which increase with decreasing particle size, down to a particle size, d_c~10nm.

1.4.3. MAGNETIC PROPERTIES

Nanomaterials have greater value of magnetization and magnetic anisotropy in comparison with their bulk counter parts while there is a difference in the Curie and Neel temperature. The size effects and charge transfer characteristics of the nanomaterial have significant influence in magnetic properties. Magnetic nanoparticles have been extensively studied in the areas of biomedical applications such as hyperthermia, magnetic resonance contrast enhancement and drug delivery. Super-paramagnetic behavior of nanomaterials has significant influence in various applications.

1.4.4 CATALYTIC PROPERTIES

When the particle size of a nanomaterial is reduced then the surface area and number of surface atoms are increased. This increase in surface area always causes an increase in the catalytic activity of nanomaterials.

1.5. CLASSIFICATIONS OF NANOMATERIALS

According to the dimensionality Sigel classified nanomaterials as Zero Dimensional (0D), One Dimensional (1D), Two Dimensional (2D) and Three Dimensional (3D).

Based on composition, morphology and distribution of nanocrystalline component Gleiter classified the materials as follows,

1.5.1 CARBON NANOTUBES

Carbon nanotubes (CNTs) are faultless cylinders derived from a honey comb lattice representing a single atomic layer or multiple atomic layers of crystalline graphite, called graphene sheets. The nanometer-scale size and hollow cylindrical shape of carbon nanotubes suggests that they may have many potential applications as molecular sieves, nano-test-tubes, and hydraulic actuators.

1.5.2 FULLERENES AND GRAPHENE

Fullerenes are carbon allotropes. Of the large family of fullerenes, the Buckminister fullerene (C_{60}), show anomalous properties of bulk modulus and specific heat as compared with their bulk counter parts. Due to the low water solubility of

fullerenes, a lot of research is devoted to functionalization and a myriad of derivatives of C_{60} has been synthesized which all have their peculiar characteristics and properties.

Graphene, a new type of two dimensional carbon material, has attracted tremendous interest since its discovery in 2004. It has shown great potential for applications in various technological fields due to its exceptional physical properties, including high intrinsic mobility, unique surface area, excellent thermal conductivity and optical transmittance.

1.5.3. NANOPARTICLES

They are small clusters of atoms about 1 to 100 nm long. Noble metal nanoparticles such as gold, silver and their alloys are of great interest for the creation of new functional materials. Among various properties, the optical properties of silver and gold nano particles have received much attention due to their marked size and shape dependence in particular to their Surface Plasmon Resonance (SPR). Light induced collective oscillation of free electrons on the metal surface resulting in specific bands in the UV-Visible spectrum is termed as SPR. Molecules adsorbed on the surface of these metal nano particles undergo surface enhanced Raman scattering effect due to the coupling of the Plasmon band of the irradiated metal with electronic states of the molecules. The creation and examination of numerous metal nano particles in various shapes, size and assemblies has demonstrated the importance of each of these parameters to tailor the resulting plasmonic characteristics of the materials and as a result noble metal nano particle stimulate great interest in photonics, biotechnology and space applications [17].

1.5.4 NANOMETAL OXIDES

Metal oxide nanostructures have received steadily growing interest as a result of their peculiar and fascinating properties superior to their bulk and particle counterpart. To achieve different morphologies such as rods, wires, thin films, or fibers at the nanoscale, novel fabrication techniques need to be adopted. The major goal of nanometal oxides is the design of nano-sensors and catalysts that could be easily integrated with modern electronic fabrication techniques. Most of the applications are highly sensitive to changes in the surface chemistry of the materials, their chemical environment and most sensors are based on appropriately structured doped oxides. In

the current interdisciplinary age of nanotechnology, metal oxide semiconductor nanomaterials have gained substantial interest due to their promising applications in a diversity of technological areas, such as electronics, optoelectronics, bio/chemical sensors, coating systems, and catalysis.

Owing to the large fraction of surface atoms of these oxides as compared to the bulk implies that oxide nanomaterials can exhibit enhanced sensitivity and catalytic activity. Nanostructured transition metal oxides (MOs), a particular class of nanomaterials, are the indisputable prerequisite for the development of various novel functional and smart materials. These transition MO nanocrystals have been attracting much attention not only for fundamental scientific research, but also for various practical applications because of their unique physical and chemical properties. These physical and chemical properties are strongly dependent on the sizes, shapes, compositions, and structures of the nanocrystals. Interesting phenomena such as remarkable increase in surface-to-volume ratio, significant change in surface energy, and quantum confinement effects occur when transition MOs are reduced to nanoscale dimension [18]. These phenomena result in a variety of new physical and chemical properties that are not feasible for materials with bulk dimensionality. Consequently, various nanostructured transition MOs have been synthesized by diverse chemical, physicochemical, and physical strategies. Compared with their micro or bulk counterparts, nanostructured transition MOs exhibit unique structural characteristics and size confinement effects as well as novel properties. These properties contribute to the potential of transition MOs as candidates for both theoretical studies and practical applications in micro/nanodevices [19].

1.5.5. NANOCOMPOSITES

With the increasing demand for nanotechnology, natural materials are inadequate for challenging properties of materials with newer and newer technological applications. The meaning of composite is “consisting of two or more distinct parts”. The nanocomposite is a multiphase solid material where one of the phases has one, two or three dimensions of less than 100 nanometers (nm) or structures having nano-scale repeat distances between the different phases that make up the material. The mechanical, electrical, thermal, optical, electrochemical, catalytic properties of the

nanocomposite will differ entirely from that of the component materials. Examples of nanocomposites in nature are the structure of the abalone shell and bone. In mechanical strength, nanocomposites differ from conventional composite materials due to the exceptionally high surface to volume ratio of the reinforcing phase and/or its high aspect ratio. In nanocomposites, covalent bonds, ionic bonds, van der Waals forces or hydrogen bonding could exist between the matrix and filler components [20]. Better dispersion of the fillers in a given matrix material can be achieved by using fillers in the form of nanopartic1es [21]. Nanocomposites offer unique properties that arise from their small size, large surface area, the interactions of phases and are attractive for their potential to improve the performance of drugs, biomaterials, catalysts and other high-value-added materials. Nanocomposites can be simply classified into the ceramic matrix, metal matrix, and polymer matrix composites.

1.5.5.a CERAMIC MATRIX COMPOSITES

Ceramic matrix composites (CMCs) consist of ceramic fibers embedded in a ceramic matrix. The matrix and fibers consist of any ceramic material, including carbon and carbon fibers. The ceramic occupying most of the volume is often from the group of oxides, nitrides, borides, silicates, whereas the second component is often a metal. Ideally, both components are finely dispersed in each other to develop particular optical, electrical and magnetic properties as well as corrosion-resistance and other protective properties.

1.5.5. b METAL MATRIX COMPOSITES

Metal matrix nanocomposites can be defined as there inforced metal matrix composites. This type of composites can be classified as continuous and non-continuous reinforced materials. One of the important nanocomposites is carbon nanotubes - metal matrix composites. The advantages of these materials are high tensile strength and electrical conductivity.

1.5.5.c POLYMER-MATRIX NANOCOMPOSITES

Polymer nanocomposites are materials in which inorganic particles in the nano range in at least one dimension are dispersed in an organic polymer matrix to improve the properties of the polymer. The major advantage of polymer nanocomposites is their

huge interfacial surface area, which may result in a peculiar three-dimensional network structure. Nanofillers are also expected to be able to strongly influence the wear performance of polymers and composites. A range of polymeric nanocomposites is used for biomedical applications such as tissue engineering, drug delivery and cellular therapies [22&23]. Due to unique interactions between polymer and nanoparticles, a range of property combinations can be engineered to mimic native tissue structure and properties. A range of natural and synthetic polymers are used to design polymeric nanocomposites for biomedical applications including starch, cellulose, alginate, chitosan, collagen, gelatin, and fibrin, poly(vinyl alcohol) (PVA), poly(ethylene glycol) (PEG), poly(caprolactone) (PCL), poly(lactic-co-glycolic acid) (PLGA), and poly(glycerol sebacate) (PGS). A range of nanoparticles including ceramic, polymeric, metal oxide and carbon-based nanomaterials are incorporated within the polymeric network to obtain desired property combinations.

Polymer matrix composites can be processed at a lower temperature than other composites. Nowadays, nanostructured metal-polymer and metal oxide polymer composites are the area of increased attention of researchers in different areas of science and technology. The electrical, mechanical, optical and biological properties of the nanocomposites are improved by dispersing a metallic phase in a polymeric matrix, opening up applications in various technical areas.

1.6. METHODS FOR THE SYNTHESIS OF NANOMATERIALS

Nanoparticles can be synthesized by a variety of methods. Some of the important methods are purely physical, chemical, biological or hybrid. Whatever be the method of synthesizing, it is essential to avoid the coalescence of particles into larger particles and achieve chemical stability over a longer period. Therefore the synthesis routes which protect or passivate the particles have become attractive compared to those which do not take care of long term stability.

The important physical methods include methods like vacuum sputtering, ion beam method, consolidation, gas aggregation of monomers, ball milling etc. Each has its own merits and demerits. Chemical methods include different techniques like chemical capping, micro emulsion, aerosol method, precursor compound method, sol-gel method, co-precipitation method etc. [16].

1.6.1. PHYSICAL METHODS

Physical methods involve gas-solid transformation. The various processes used in this method are physical vapor deposition (PVD), chemical vapor deposition (CVD), pulsed laser deposition (PLD), ion implantation (II), atomic layer deposition (ALD), molecular beam epitaxy (MBE) and spray pyrolysis (SP).

1.6.2. CHEMICAL METHODS

This involves the liquid-solid transformation. The important chemical methods used for preparing nanoparticles are hydrothermal, precipitation and micro emulsion routes, sol-gel, microwave, sonochemical, electrochemical and photochemical processes [24&25].

These physical and chemical preparation methods are typically pricey, labor-intensive and also hazardous to the environment [26].

1.6.2 (a) BIOLOGICAL METHODS

The biological method of synthesizing nanoparticles is according to the 12 fundamental principles of green chemistry [27]. This method utilizes naturally occurring molecules for the formation of nanomaterials with different properties. This method involves minimizing the use of toxic chemicals and maximizing the efficiency of chemical processes [28]. The synthesized nanoparticles induce a less toxicological effect on the environment and human health compared with the chemical methods. Hence this approach finds tremendous applications of nanoparticles in various fields. In this method, nanoparticles are synthesized by bio reduction of metal salt. Biogenic synthesis of nano metals or metal oxides using extracts of plant parts or microorganisms are more advantageous [29&30]. Various metabolites present in the extract of plants and microorganisms act as reducing agents in the synthesis of nanomaterials. The advantages of using green synthesis are easy availability of the raw materials, safety and environmental friendliness and the presences of various metabolites that act as reducing and stabilizing agents.

1.7. APPLICATIONS OF NANOTECHNOLOGY

Ability of materials to dramatically change their property at nanoscale has opened up the possibility of marketing new devices, instruments and consumer goods

to function in much better ways than was possible earlier. Thus nanotechnology is often called *"the next industrial revolution"*. Owing to the new and unique properties of nanostructured materials, they have wide range of applications in many fields; some of them are discussed here;

1.7.1. MEDICINE

Nanotechnology brings a breakthrough in the field of medicine. Nanomedicine is used for diagnosing, treating and preventing diseases and also used for preserving and improving human health with the help of molecular tools and molecular knowledge of the human body. Integration of nanotechnology into complex biological systems leads to detection and prevention of diseases at the earliest stages of its development.

The properties and applications of nanomaterials such as contrast agents for cell imaging and therapeutics for treating cancer in the biological and medical research field are well explored. Due to the similarity of most of the biological molecules and nanomaterials, they are commonly used for both *in vivo* and *in vitro* biomedical research and applications.

1.7.1.(a) DIAGNOSIS

Functionalized nanoparticles when conjugated with biomolecules have shown the ability to detect antibodies, proteins and damaged or diseases cells by various methods. There are several reports and ongoing research on the use of nanotechnology for early detection of diseases like Alzeimer's, Parkinson's disease, Cancer etc.

1.7.1.(b) DRUG DELIVERY

Nanotechnology has been a boon for the medical field by delivering drugs to specific cells using nanoparticles. The overall drug consumption and side effects can be lowered significantly by depositing the active agents in the morbid region only and in no higher dose than needed [11].

1.7.1.(c)TISSUE ENGINEERING

Nanotechnology can help reproduce or repair damaged tissues. Tissue engineering makes use of artificially stimulated cell proliferation by using suitable nanomaterial based scaffolds and growth factors. Tissue engineering might replace

today's conventional treatments like organ transplants. Advanced forms of tissue engineering may lead to life extension.

1.7.2. SPECIAL APPLICATIONS OF NANOMATERIALS

1.7.2.(a) SENSORS

Nanoscience and Nanotechnology have created possibilities for the development of nanosensors and nanoprobes for sensing chemical and biological species with high sensitivity and selectivity. These sensors with dimensions in the nanometer scale offer significant improvement over the classical sensing system because of their high surface to volume ratio.

1.7.2.(b) COATINGS

Coatings are extensively used to paint the walls, doors and windows. Coating should provide a protective layer which is bound to the base material to produce a surface of the desired protective or functional properties. The coatings should have self healing capabilities through a process of "self-assembly". Nanotechnology is being applied to paints to obtain the coatings having self-healing capabilities and corrosion protection under insulation.

1.7.2.(c) DISPLAYS

The production of displays with low energy consumption could be accomplished using Carbon nanotubes (CNT). Carbon nanotubes are electrically conductive and due to their smaller diameter of several nanometers, they can be used as field emitters with extremely high efficiency for field emission displays (FED).

1.7.3. ENVIRONMENTAL APPLICATIONS

1.7.3.(a) RENEWABLE ENERGY

Development of nanotechnology has the potential to revolutionize the approaches to energy production. Some of the promising new areas for the use of nanotechnology in this field are, use of nanomaterials to extract hydrogen from water, to harvest energy from the sun and biomass, to store energy in fuel cells, batteries, capacitors etc.

1.7.3.(b) CATALYSIS

Extremely large surface to volume ratio will enhance the catalytic properties of nanomaterials compared to its bulk form. The application potential of nanoparticles in catalysis ranges from fuel cell to catalytic converters and photocatalytic devices [11]

1.7.3.(c) AGRICULTURE

Applications of nanotechnology have the potential to change the entire agricultural sector and food industry from production to conservation, processing, packaging, transportation and even waste treatment. Major challenges related to agriculture like low productivity in cultivable areas, large uncultivable areas, shrinkage of cultivable lands, wastage of inputs like water, fertilizers, pesticides, wastage of products and of course food security for growing numbers can be addressed through various applications of nanotechnology.

1.8 APPLICATION STUDIES IN THE PRESENT WORK

Applications of nanomaterials for environmental remediation are of immense interests since the modern world is facing challenges in meeting the requirements for clean environment. Nanostructured materials are used as powerful tools for the detection and treatment of pollutants from the environment. Recently the main focus on nanomaterials is to solve environmental problems and to clean the environment for the future [5].

The major problems concerning the various environmental protection agencies are the pollutants coming from industrial, radiological and agricultural wastes running all over the world. In this modern era of industrialization, all these types of pollutants are actively present in water as well as air. The scarcity of potable water is a major problem in the modern world. The pollutants which affect water are of physical, chemical, biological and physiological types. A detailed study of chemical and biological contaminant removal techniques is adopted in this report. The important techniques applied for the removal of chemical contaminants are adsorption and photocatalysis.

1.9. LITERATURE REVIEW

This section comprises a literature review on the recent developments in the synthesis, characterization and applications of nanomaterials based on CuO, ZnO and its composites with Nano Cellulose. In recent years the importance of metal-oxide nanoparticles synthesized by green methods is increased due to their enhanced efficiency in different areas. Green synthesis of nanoparticles or composites is preferred because of its cost-effectiveness, environmental compatibility and biomedical applications. The methods and advantages of commonly applicable green and safe routes for the synthesis of nanoparticles are discussed in brief to show the effect of this strategy. Green-synthesized nanoparticles have been utilized for the removal of heavy metals from wastewater [32&32]

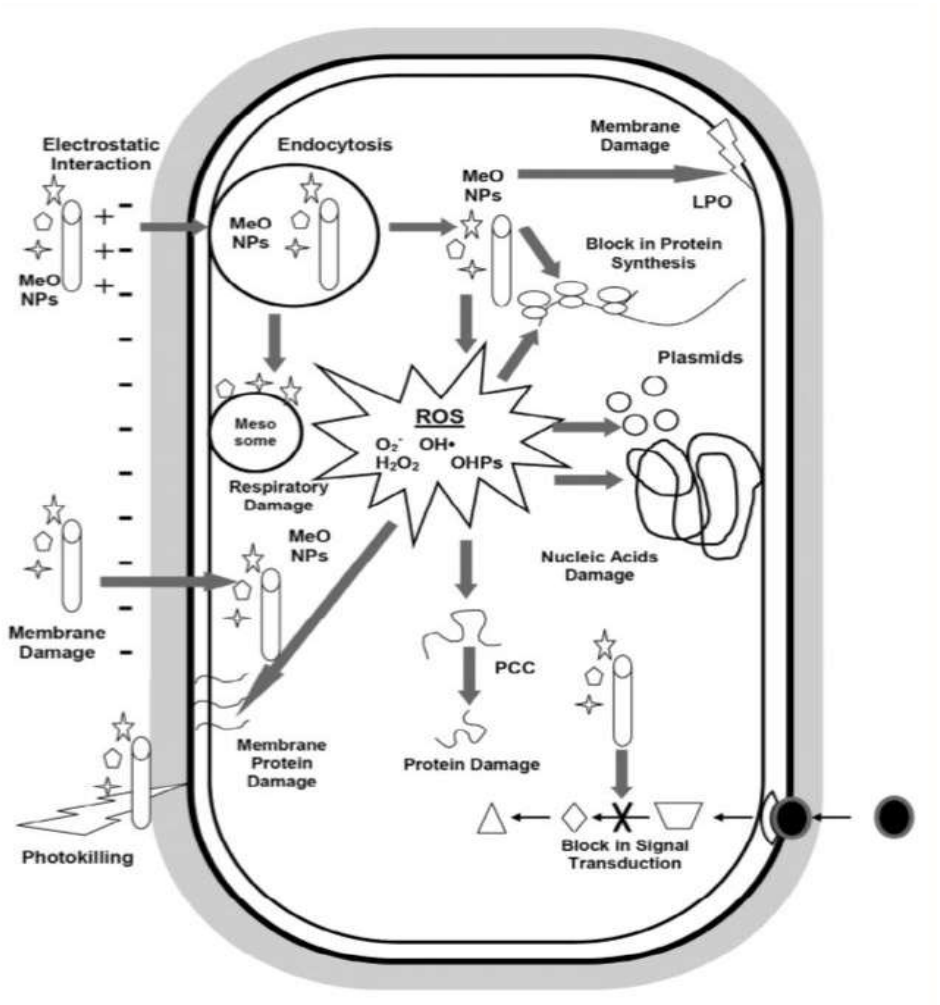

Figure 1.1. Mechanism of antibacterial activity

Acharylu and co-workers synthesized CuO nanoparticles from copper sulfate solution and Phyllanthusamarus leaf extract and reported their activity against multi drug-resistant bacteria. They found that CuO produced by this method has greater antibacterial activity against gram-positive bacteria than gram-negative bacteria [33]. CuO nanoparticles have been prepared from copper acetate and Centella Asiatica leaf extract and used for the degradation of methyl orange dye in UV irradiation [34]. The enhanced antioxidant efficacy of CuO reported from Andean blackberry fruit (89.02%) and leaf (75.92%) was studied by Kumar and workers [35]. Ansilin et al. reported the synthesis and characterization of CuO nanoparticles from aqueous leaf extract of Azadirachtaindica (Neem)[36]. The study of Mekala and Rajan successfully demonstrated the utilization of Hyptissuveolensaqueous leaf extract for synthesizing nano CuO and reported the potential antibacterial activity against S.aureus, C. albicans and E. coli [37]. Niraimathi et al. reported the synthesis of spherical CuO nanoparticles by bio-reduction of copper sulfate solution using aqueous leaf extract of Alternantheraselis[38]. The study on the comparison of the toxicological effect of plant-mediated (Pterospermumacerifolium*)* and engineered CuO has shown that plant-mediated CuO nanoparticles are less toxic than engineered [39]. Eichhoornia mediated CuO nanoparticles synthesized had highest antifungal activity against plant pathogens [40]. The biosynthesized CuO nanoparticles using banana feel extract had 90% degradation efficiency towards Congo Red dye under sunlight irradiation as reported by Aminuzzaman et al. [41]. Prasad and coworkers reported the synthesis of nanospheres of CuO having diameter 13-15 nm using aqueous leaf extract of Saraca indica and copper chloride [42]. Green synthesized nanoparticles of CuO using Ocimum sanctum and Piper nigrum leaf extract showed good antibacterial activity against multidrug resistance bacteria like *B.* subtills, S. aureus, E. coliand *P.* aeruginosa[43]. Narasaiah and coworkers studied the degradation of congo red dye using $NaBH_4$ and biosynthesized CuO nanomaterial [44]. Anticancer activity towards breast cancer cells and antimicrobial activity against various multidrug resistance bacteria were reported by Yugandhar et al. for green synthesized CuO nanoparticles using Syzygiumalternifolium[45]. Antibacterial activity of nano CuO synthesized using Hibiscusrosa-sinensisflower extract showed good activity for S. flexneri and B.

subtils[46]. Studies on adsorption of Congo red in presence of H_2O_2 and bioinspired CuO nanoparticle showed 75% degradation [47].

Many workers have studied the photodegradation of dyes using nano CuO particles under UV light or visible light irradiation. CuO nanomorphs synthesized by chemical precipitation and hydrothermal methods were used for the degradation of Methylene blue under sunlight illumination and showed 72.57% degradation [48]. The photodegradation efficiency of CuO nanoparticle prepared by the wet chemical method for Methylene blue degradation was 45.12% under visible light illumination [49]. Shape dependent properties of nano CuO for the adsorption of Pb(II) ions were reported by Farghali, et. al. [50]. CuO nanoparticle prepared from Murryakoenigiaqueous leaf extract showed 80% degradation of reaction black under UV light irradiation [51]. Nanostructured CuO synthesized by the facile solution-phase method showed 100% degradation of Methylene blue in presence of NaOCl [52]. Katwal et. al. prepared CuO nanoparticles by electrochemical method and they performed the antibacterial and photocatalytic activity in the presence of sunlight. They concluded that nano CuO had high antimicrobial activity and degradation efficiency towards Methylene blue and methyl red than Congo Red [53]. Ijaz et al reported the preparation of CuO nanoparticles from aqueous leaf extract of Abutilon Indicum and photodegradation of acid black 210 dye into water and CO_2. The authors assign a high disintegrative ability due to the higher crystalline nature of the CuO obtained. They also attributed the superior antimicrobial activity of the synthesized CuO [54]. Radhakrishnan and coworkers reported the photodecomposition of malachite green (72%) and Congo red (62%) for CuO nanoparticles prepared using pomegranate fruit extract under UV light irradiation [55]

Elumalaia*et al*., synthesized zinc oxide nanoparticles using leaf aqueous extract of Azadirachta indica (L.) and studied its antimicrobial activities. The results depicted that green synthesized ZnO NPs was more potent than bare ZnO exhibited interesting antimicrobial activity with both Gram positive and Gram negative bacteria and yeast at micromolar concentrations [56]. The influence of green synthesized ZnO nanoparticles calcined at 600 °C for 2 h on protein ase K was investigated by Mansoore *et al*. The enzyme activity of proteinase K showed that ZnO nanoparticles inhibited the activity of

the enzyme and its thermal stability was increased by enhancing the concentration of nanoparticles [57].

Sheela *et al* investigated the utilization of the zinc oxide nanoparticles (ZnO) as an adsorbent for the removal of Zn (II), Cd (II) and Hg (II) ions from aqueous solution. In her studies, the adsorption properties of ZnO towards Zn (II), Cd (II) and Hg (II) ions were systematically investigated, including pH effect, adsorption equilibrium, adsorption kinetics and temperature. The adsorption capacity was found to decrease with the increase of temperature, and thermodynamic calculations suggested that the adsorption of Zn (II), Cd(II) and Hg(II) ions onto ZnO nanoparticles was exothermic [58].

Wang *et al* found that the photo reactivity of ZnO nanoflowers were more than that of ZnO nanorods for the degradation of 4-chlorophenol under UV light irradiation [59]. ZnO hollow spheres for the degradation of reactive brilliant red X-3B increased by a factor 4.66 compared with that of ZnO nanoparticles [60]. Mohajerani *et al* synthesized ZnO nanostructures in the shape of particles, rods, flower-like and microsphere that were tested for the decolorization of CI acid red 27 under direct sunlight irradiation. The photoactivity of the nanorods was slightly superior to that of the nanoparticles. The flower-like and microsphere 3D nanostructures showed much lower photoactivity [61]. The superior performance of the nanoflowers resulted from the larger content of oxygen vacancy on the surface of the 1D nanomaterials. Likewise, 3D flower-like ZnO hierarchical microstructures prepared by a low-temperature aqueous solution route were more active than other nanostructured ZnO powders (nanoparticles, nanosheets, and nanorods [62].

The effects of synthesis conditions during flame-spray pyrolysis (FSP) and annealing post-treatment on the characteristics and photocatalytic activities of ZnO nanoparticles have been investigated by OkornMekasuwandumronga *et al*. The degradation rate over FSP-ZnO-47.0 nm was much higher than those of the commercially available photocatalysts. Their studies suggested a balance between high crystalline quality that enhanced photo phenomena and the surface area available for substrate adsorption in order to obtain high photocatalytic activity of ZnO nanoparticles [63].

Influence of the thermal treatment temperature on the ZnO thin film microstructure and photocatalytic efficiency towards the organic dyes malachite green (MG) and reactive black (RB5) was investigated by Nina et al. The films obtained by both methods had a better photocatalytic activity in the degradation of RB5 compared to MG due to the weaker N=N bond in comparison with the C-C bond between the central carbon atom and N,N-dimethylaminobenzyl in MG [64].

ZnO nanostructures with variable sizes and shapes have been successfully synthesized using microwave (MW) heating in an aqueous solution containing Zn(II) salt, CTAB and NaOH by Subrata Kundu. This process exclusively generated different shapes, e.g., 'bacteria-like', 'larva-like', 'flake-like' and 'flower-like', and they have been utilized as excellent photocatalyst for the degradation of methyl red (MeR) under UV illumination. Among the various shapes examined, the 'flower-like' nanostructure exhibited superior photocatalyst activity due to its special structural features [65].

Mesoporous ZnO particle with high specific surface area was synthesized by a reverse micro emulsion- based evaporation-induced self-assembly (EISA) technique, using zinc nitrate as metal precursor and sucrose as porogen by Wen Zhang et al. The prepared ZnO possessed a wurtzite structure and spherical morphology and exhibited strong antibacterial activity against both Gram-negative bacterium Escherichia coli and Gram-positive bacterium Staphylo coccus [66].

Nanocellulose(NC) has a range of applications in the field of material science and biomedical engineering. It is a renewable and biodegradable material having a large surface area with plenty of hydroxyl groups, porosity and anion sulfate ester groups on the surface. Hence it is a perfect substrate for making composite materials. Li reported that nano crystalline cellulose (NCC) with surface modification by amino group has greater tendency to remove acid red than NCC [67]. Surface modification of NCC with phosphate group resulted in 99% efficient material for removing heavy metal ions like Cu (II) and Fe (III) [68]. Anirudhan et al studied the adsorption of Cd (II) using magnetic NCC polymerized with Itaconic acid [69]. NCC was used to prepare membrane materials as adsorbent for removing Rhodamine B [70]. ZnO-cellulose composites was found to have enhanced thermal stability and antibacterial activity compared to cellulose or ZnO [71]. Zhang et al reported that functional

nanocellulose could be prepared by mixing NC with antibacterial agent. The functional application of NC could be increased by the surface modification through the introduction of functional groups with antibacterial and antioxidative action [72]. Nanocellulose based composites like NC-TiO2, NC/Ag, NC-CuO were used in wastewater treatment [73,74,75,76 & 77], detection of pesticides [78], biomedical applications [79] and multifunctional nanocomposite films [80&81].

1.10. PRESENT STUDY

In view of the importance of nano metal oxides like CuO&ZnO revealed by the vast literature, it was thought of interest to synthesize these metal oxides and composites. Although a large quantum of work has been carried out on these metal oxides, very few reports are available on the green synthesis of their composites. In the present study green method of synthesis for these metal oxides and their composites were adopted. Nanocellulose was selected as the biopolymer for composite synthesis because of its biocompatible nature, easy availability and rigidity for device applications. Before studying the nanocomposites the individual metal oxides are also studied in detail. All the green synthesized materials have been studied for environmental applications like adsorption of heavy metal ions, photodegradation of dyes and antibacterial properties.

1.11. OBJECTIVES OF THE PRESENT STUDY

The objectives of the present study are:

1. To synthesize nano ZnO & nano CuO by follows green synthesis (by using Tinospora Cordifolia plant stem extract) and to synthesis its composites using bio-Polymer such as Nano Cellulose prepared from Sugar Cane Bagasse (NC).
2. To characterize the prepared nanomaterials and its composites by different characterization techniques like XRD, FT-IR, UV-Vis, PL, SEM, TEM and BET surface area. The information on the particle size, phase purity, surface morphology, optical properties and surface area are obtained.
3. To investigate the adsorption potential of these nanomaterials for removal of toxic heavy metal ions like Pb (II) and Cd (II), two prime toxic heavy metal ions present in water bodies.

4. To evaluate the photodegradation efficiency of the prepared nanomaterials for the degradation of organic dyes (Congo red and Malachite green) under sunlight irradiation.
5. To study the antibacterial properties and arrive at a relation between surface area and antimicrobial property of the prepared nanomaterials. The different disease causing pathogens selected for the present study are Escerichia coli, a gram-negative bacterium, causing food poisoning, neonatal meningitis and urinary tract infection and Staphylococcus aureus, a gram-positive bacterium, causing food poisoning.
6. To compare the performance of the materials in the application Studies.

CHAPTER - II
CHARACTERIZATION TECHNIQUES

2.1. INTRODUCTION

Characterization is a major part of nanomaterial research. The advent of nanoscience and nanotechnology demands appropriate techniques to assess the structure and properties of nanomaterials. The characterization techniques also relate to the nature of material under investigation. Some techniques are qualitative, while some other techniques are quantitative. The qualitative techniques provide information such as appearance, presence, morphology etc. and quantitative techniques provide the information about chemical compositions, exact size, concentration etc. The recent technological developments help to obtain two or three dimensional information about the materials. The invisible information of the samples can be brought into the light by using powerful characterization techniques.

Highly sophisticated and advanced characterization techniques are being used for the analysis of nanomaterials. In this section the basic principles and applications of those techniques used in the characterization of materials in the present study are discussed. It includes powder X-Ray Diffraction (XRD), Energy Dispersive X-Ray Spectroscopy (EDS), Scanning Electron Microscopy (SEM), Transmission Electron Microscopy (TEM), Brunauer-Emmett-Teller Gas Adsorption (BET) Surface Area Measurements, Fourier Transform Infrared Spectroscopy (FT-IR), Photoluminescence Spectroscopy (PL), Ultra Violet – Visible Spectroscopy (UV/Vis).

2.2. ELEMENTAL ANALYSIS

For the determination of purity and composition of nanomaterials and elemental analysis, Fourier Transform Infrared Spectroscopy (FT-IR) and Energy Dispersive Spectroscopy (EDS) were used.

2.2.1-FTIR

The advantages of infrared spectroscopy over other spectroscopic techniques include wide applicability, non-destructiveness, measurement under ambient atmosphere and the capability of providing detailed structural information. Infrared spectroscopy by Fourier transform (FTIR) has additional merits such as higher

sensitivity, higher precision, quickness of measurement and extensive data processing capability.

In the present study FTIR spectra of the samples were recorded using Perkin-Elmer FT-IR Spectrophotometer in the wave number range 400 cm^{-1} to 4000 cm^{-1} by KBr disc method.

2.2.2. ENERGY DISPERSIVE X-RAY SPECTROSCOPY (EDS)

Energy dispersive X-ray Spectroscopy (EDS) is an important technique for the elemental analysis of the samples. Interaction of an electron beam with a sample target produces a verity of emissions, including X-rays. An energy-dispersive (EDS) detector is used to separate the characteristic X-rays of different frequencies.

EDS is coincided to be a relatively rapid, inexpensive and basically non-destructive method. It is used to study the purity and composition of the products. It can also be used to survey surface analytical problems, elemental analysis from carbon to uranium and semi-quantitative analysis with detection limits of 0.5 weight % for most of the elements.

In the present study, the elemental analyses of the nanomaterials were carried out using JEOL Model JSM 5600LV scanning electron microscope with EDS.

2.3. STRUCTURAL ANALYSIS

It is very important to determine the structure of nanomaterials as considerable amount of properties are dependent on structure and size. The techniques used for structural determination of nanoparticles are X- Ray Diffraction Studies (XRD), BET surface area measurement and Microscopic studies (Scanning electron microcopy (SEM), Transmission Electron microscopy (TEM).

2.3.1. X-RAY POWDER DIFFRACTION (XRD) ANALYSIS.

It is a powerful analytical method for phase identification of crystalline materials. X-ray is a relatively simpler and easier technique for the determination of crystallite sizes of the powder samples. The average particle size can be determined from the XRD line broadening using the Debye-Scherer equation, $d=0.9\lambda/\beta \cos\theta$,

where βrepresents the full width at half maximum (FWHM), θ is the Braggs angle and λ is the wavelength of X-rays used.

X-ray powder diffraction technique is most widely used for identification of unknown crystalline materials (eg. minerals, inorganic compounds etc.). Determination of unknown solids is critical in almost all branches of science such as geology, environmental science, material science, engineering and biology. Other applications of XRD include characterization of crystalline materials, identification of fine-grained minerals such as clays and mixed layer clays that are difficult to determine optically, determination of unit cell dimensions, measurement of sample purity, textural measurements such as the orientation of grains in a polycrystalline sample.

In the present study, X-ray diffractograms of the samples were taken from XPERT-PRO Powder diffractometer employing in a step size of 0.020^{o} at 35 mA, and 40 KV.

2.3.2. BET SURFACE AREA ANALYSIS

Surface area is an intrinsic property of powdered porous materials that can reveal important informations regarding the usefulness of a material for an application. Surface area plays an important role in the bio-availability, pharmaceutical dispersions, adsorption capacity etc. BET method has been widely used as a standard tool for the determination of surface area [82]. The method was introduced by Brunauer, Emmet and Teller. Gas physisorption method is commonly used for surface area measurements and nitrogen gas is normally used for the purpose [83]. Nitrogen gas is less expensive, easily available, inert and is able to penetrate even the finest pores and all these features make it a good candidate for this method. The nitrogen physisorption measurements are performed at liquid nitrogen temperature (77 K). Here adsorption is characterized by an isotherm which represents the equilibrium amount of gas adsorbed on a solid at a given temperature as a function of time. This theory assumes that materials possess uniform, localized site in which adsorption at one site is independent of others, adsorption is multilayer and the heat of adsorption at each layer is constant and equal to the liquefaction of the adsorbate. This theory is extended from Langmuir model to multilayer adsorption.

This technique provides detailed information about the specific surface area, pore volume and pore size distributions of the sample. The sample generally includes activated carbon, zeolites and also any type of sample like alumina, silica, metal supported catalysts, metal oxide powders, pigments, pharmaceutical powders etc.

In the present study the BET surface area of the synthesized nanomaterials were measured by using SMART SORB 93 Surface area analyzer.

2.4. MICROSCOPIC STUDIES.

Microscopy is the most ancient and widely used method for determination of the morphology and size of small particles and objects. Electron microscopy is the only method for the direct determination of the size of nanoparticles, nanocrystallites and solid nanomaterials and for determining the constitution of the nanoparticles produced from the colloid solutions. All other methods are indirect because the information obtained about the mean particle size is from the data based on the variation of some properties of the nanomaterials. In the present study microscopic analysis were done by Scanning Electron Microscopy (SEM) and Transmission Electron Microscopy (TEM).

2.4.1. SCANNING ELECTRON MICROSCOPY (SEM)

Scanning electron microscopy is one of the most widely used electron microscopic techniques for morphological analysis. Because of its versatility, various modes of imaging, wide range of magnifications, ease of sample preparation and easy interpretation of the images, SEM is widely used. With the recent development in the electron source and the advancement in the technologies of the detectors, higher resolution have been achieved that can be utilized to examine nanomaterials. Scanning Electron Microscopy (SEM) is a type of electron microscope capable of producing high resolution images of the sample and gives information about the surface morphology, composition, shape, size and arrangement of particles.

In the present study, the surface morphology of the nanomaterials was obtained from SEM images using JEOL Model JSM 5600LV scanning electron microscope.

2.4.2. TRANSMISSION ELECTRON MICROSCOPY (TEM).

Transmission electron microscopy is an imaging technique whereby a beam of electrons is focused onto a specimen causing an enlarged version to appear on a

fluorescent screen or a layer of photographic film, or to be detected by a CCD camera. TEM operates on the same principle as the light microscope but uses electrons instead of light. The transmission mode measures the intensity from an electron source after it has been passed through a transparent sample. TEM can be used to characterize nanomaterials to gain information about particle size, shape, crystallinity and inter particle interaction.

TEM is useful for determining the size, shape and arrangement of the particles which make up the specimen. Direct information about the structure is obtained by high resolution transmission electron microscopy (HRTEM). The possibility for high magnifications has made the TEM an important tool in both medical, biological and materials research. It is highly useful for the determination of the lattice planes and the detection of atomic –scale defects localized in areas of few nanometers in diameter with the help of selected area electron diffraction (SAED) technique. A TEM can achieve much greater resolution than SEM, the instrument itself is costlier and much work is required to prepare a sample for a TEM than a SEM.

In the present study the TEM image of the samples were taken with a PHILIPS model CM200 transmission electron microscope in an accelerating voltage of 20-200KV and a resolution of 2.4 A^{o}

2.5. OPTICAL ANALYSIS

The optical properties of the prepared nano materials were determined by the UV-Visible Spectroscopy (UV-Vis.) and Photoluminescence Spectroscopy (PL).

2.5.1. UV-VISIBLE SPECTROSCOPY

Ultraviolet and visible (UV-Vis.) absorption spectroscopy refers to absorption or reflectance spectroscopy in the UV-Visible spectral region. In this region of the electromagnetic spectrum, molecules undergo electronic transitions. The electronic transitions shown in **Figure 2.1(a)** describe that these transitions occur from various occupied level to empty levels, but in reality, excitation only occurs between the two lowest transitions, the outer electron, $\pi \rightarrow \pi *$and the $n \rightarrow \pi *$ levels for the energy range of 200-800 nm associated with UV-Vis radiations. In general, these transitions occur between the highest occupied molecular orbital (HOMO) to the lowest

unoccupied molecular orbital (LUMO) as shown in **Figure 2.1 (b)** When the photon is absorbed, a portion of the energy is absorbed as the electron is promoted to the exited state.

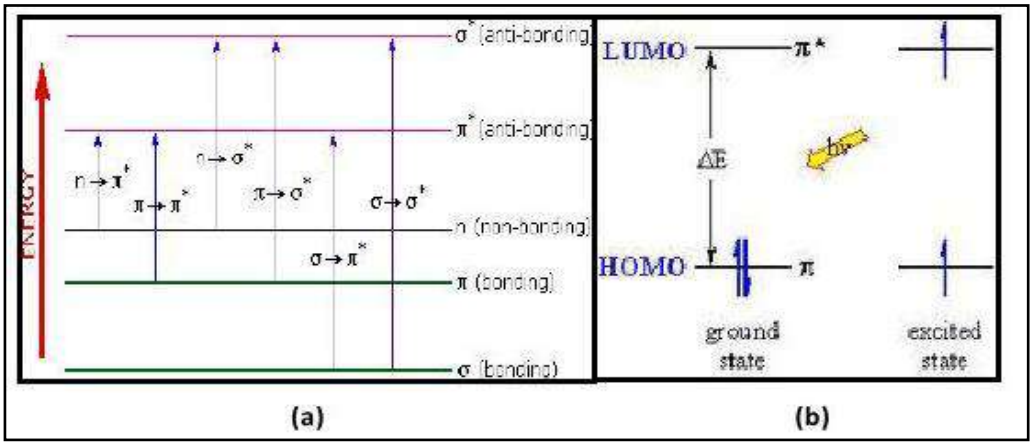

Figure 2.1 (a) & **(b) Excitation of electrons between molecular orbitals**

Calculation of band gap from UV/Visible absorption spectrum

The UV-Visible spectra are used to study the optical properties of the synthesized nanoparticles, from which the band gap and the type of electronic transitions can be determined. When a semiconductor absorbs photons of energy larger than the gap of the semiconductor, an electron is transferred from the valence band to the conduction band and there occurs an abrupt increase in the absorbency of the material to the wave length corresponding to the band gap energy. The relation of the absorption coefficient (α) to the incidental photon energy depends on the type of electronic transitions. When this transition occurs, if the electron momentum is conserved, the transition is direct. If the momentum is not conserved in transition, it must be attended by a photon and it is an indirect electronic transition. To analyze the electronic properties of the synthesized nanoparicles, the emission function F(R'∞) is used, which is represented as,

$$F(R'\infty) = \frac{(1-R'\infty)^2}{2R'\infty} = \frac{\infty}{S} \qquad (2.1)$$

where, α is the absorption coefficient (cm^{-1}) and S is the dispersion factor which is independent of the wavelength for particles larger than 5μm. α is related to the incident photon energy (hυ) by means of the Tauc equation (Devi *et al*, 2007).

$$\alpha h\upsilon = A(h\upsilon - Eg)^n \qquad (2.2)$$

In the above equation, A is a constant that depends on the properties of the material, Eg is the band gap and 'n' is a constant that can take different values depending on the type of electronic transition. For permitted direct transition n=1/2 and for a permitted indirect transition n=2, for forbidden direct transitionn=3/2 and for forbidden indirect transition n =3. The slope of the plot of (αhυ) versus (hυ-E_g) gives the value of "n". Plotting $(\alpha h\upsilon)^{1/n}$ versus hυ and extrapolating the straight line portion of the graph to hυ axis gives the optical band gap of the material. The band gap values of nanostructured materials increase with decrease in particle size due to the quantum confinement effects.

In the present study the UV-Visible spectra of the samples were obtained using JASCO V650, UV/Vis spectrophotometer.

2.5.2. PHOTOLUMINESCENCE SPECTROSCOPY

In photoluminescence (PL), there is a spontaneous emission of light from a material under optical excitation. Emission spectrum can be used to identify details related with surface, interface and impurity levels. PL signal intensity provides information on the quantity of surfaces and interfaces. Photoluminescence spectra can also be applied in the size determination of semiconductor nanocrystals [84]. The PL spectrum gives information about the energy levels available to electrons in a material [85].When light is incident upon a material with suitable frequency, photos are absorbed and electronic excitations are generated. Eventually, these excitations relax and as a result the electrons return to the ground state. If irradiative relaxation occurs, the emitted light is called photoluminescence.

Photoluminescence (PL) technique is very useful to determine the band gap of a semiconductor material, impurity levels, defects present in the compound and material quality. Analysis of photoluminescence also helps to understand the underlying physics of the recombination mechanism in the semiconductor material.

In the present study the photoluminescence spectra of the samples were recorded on Horiba Jobin Yvon Flourolog (III) spectroflourometer equipped with 450 W Xenon lamp and Hamatsu R928-28 photomultiplier.

CHAPTER - III
SYNTHESIS OF NANO CuO AND NANO ZnO AND ITS CELLULOSE BASED COMPOSITES

3.1. INTRODUCTION

In this chapter the experimental approaches used for the synthesis of the materials and their results are described. The chapter also sketches the chemicals and reagents used in the study as well as their origin and purity together with the analytical instruments used. In the present work five photo catalysts namely Zinc oxide (ZnO), Copper oxide (CuO), Nano cellulose (NC), Zinc oxide incorporated nanocellulose (ZnO/NC) and Copper oxide incorporated nano cellulose (CuO/NC) were taken into account.

3.1.1. CHEMICALS AND REAGENTS

All the chemicals such as Zinc acetate dihydrate, Copper acetate, Aureomycine Hydrochloride (AM), Ciprofloxacin Hydrochloride (CF), Enrofloxacin Hydrochloride (EN) were purchased from Sigma Aldrich, London .Sulfuric acid, Hydrogen peroxide and Sodium hydroxide was procured from Merck, Darmstadt, Germany .Other chemicals such as Congo red(CR), Malachite green(MG) and other reagents were of analytical grade and used as such without further purification. Tinospora Cordifolia leaves were collected from Puthoor, a village of Kerala state. Sugarcane bagasse was collected locally.

3.2 METHODS OF SYNTHESIS

In the present work, metal oxides were synthesized by means of biological methods using Tinospora Cordifolia plant stem extract. Nanocellulose was prepared by acid hydrolysis method and the composites by the *exsitu* oxidative polymerization.

3.2.a. PREPARATION OF THE PLANT STEM EXTRACT

Fresh Tinospora Cordifolia plant (Fig.1) stems were collected locally. The stems were washed several times with water to remove the dust particles and then sun dried to remove the residual moisture, cut into small pieces. The extract was cooled to

room temperature and filtered using filter paper. The extract was stored in a refrigerator in order to be used for further experiments.

Fig. 3.1. Tinospora Cordifolia plant

3.2. b. PREPARATION OF ZnO NANOPARTICLES

For the synthesis of ZnO nanoparticles, 50 ml of Tinospora Cordifolia plant stem extract was taken and boiled to 50-70 ^{o}C using a stirrer heater. As the temperature reaches 50^{0}C, 5grams of Zinc Acetate Dihydrate was added to the solution. This mixture is then irradiated with 300 W microwave radiations in a domestic microwave oven for 30 min and then boiled until it is reduced to a deep yellow coloured paste. This paste was then collected in a ceramic crucible and heated in an air heated furnace at 300^{0}C for 2 hours. A light yellow colored powder was obtained.

3.2.c. PREPARATION OF CuO NANOPARTICLES.

For the synthesis of CuO nanoparticles, 0.20 gm of Copper Acetate was dissolved in 50 ml of Tinospora Cordifolia plant stem extract and made up to 250 ml. The resulting solution was then stirred well for 45 min to obtain a homogeneously turbid liquid, which was then irradiated with a 300 W domestic microwave oven for 30 min, allowed to settle at room temperature, filtered, washed with distilled water and dried. The black powder obtained was calcined in a muffle furnace at 400^{0}C for 2 h and collected for further experiments.

3.2.d. ISOLATION OF NANOCELLULOSE FROM SUGARCANE BAGASSE (SCB)

Sugarcane bagasse (Fig.2) was used as the source for the synthesis of Nanocellulose, collected from Sasthamcotta, Kerala. Hot water was used for cleaning sugar cane bagasse and then dried in the sunlight .After that SCB was cut into small pieces, grinded into powder. Sulfuric acid, hydrogen peroxide and sodium hydroxide were used to remove lignin and hemicellulose from SCB.

Fig.3.2. Sugarcane bagasse

3.2. e. DELIGNIFICATION OF CELLULOSE FROM SUGARCANE BAGASSE

About 25 g of the powder of sugarcane bagasse was dewaxed using water and the mixture was boiled for 2h, the process was repeated for three times to remove off waxes. The dewaxed powder was then bleached using 5% sulfuric acid water solution(250ml) with constant stirring at 50^0C for 2h.Again the mixture was washed with water and the process was repeated for five times to remove the lignin and hemicellulose. Finally the residue was filtered and washed with distilled water till neutral pH was reached.

3.2. f. EXTRACTION OF CELLULOSE

The residue obtained was subjected to bleaching using 24% hydrogen peroxide and water solution with stirring in a magnetic stirrer at 60^0Cfor 2h to completely

remove lignin and hemicellulose. Finally the residue was filtered and washed with distilled water to reach neutrality.

3.2.g. PREPARATION OF NANOCELLULOSE

Cellulose (Fig 3) obtained was dried to constant weight at 60^0C.Nanocellulose was prepared using acid hydrolysis. The cellulose was treated 65 ml of 3N H_2SO_4, stirred well using a magnetic stirrer for 4 hrs. The resulting solution was washed with distilled water for three times until the pH of the solution became neutral and then sonicated in an ultrasound sonicator for 1 hr ,filtered, washed and dried to obtain Nanocellulose.

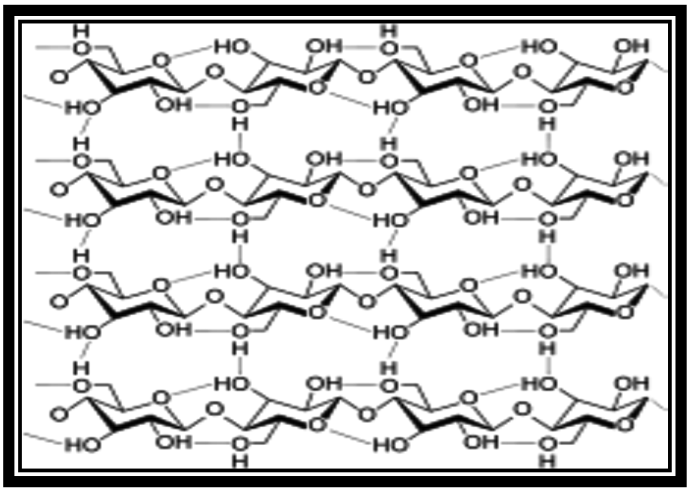

Fig.3. 3. structure of cellulose

3.2.h. SYNTHESIS OF COMPOSITES OF NANOCELLULOSE WITH ZnO AND CuO

In the present work, *ex situ* approach was followed for the synthesis of metal oxide incorporated nanocellulose. In *ex situ* key approach, other samples are impregnated into the extracted nanocellulose matrix.

3.2.i. PREPARATION OF ZINC OXIDE/ COPPER OXIDE INCORPORATED NANOCELLULOSE (ZnO/NC AND CuO/NC)

ZnO/CuO and NC in 1:2 ratio was mixed with 100 ml of water, stirred well using a magnetic stirrer for 5h, sonicated for 2h.The sonicated solution was filtered, washed well and dried at room temperature. The obtained nanocomposites were collected for further experiments.

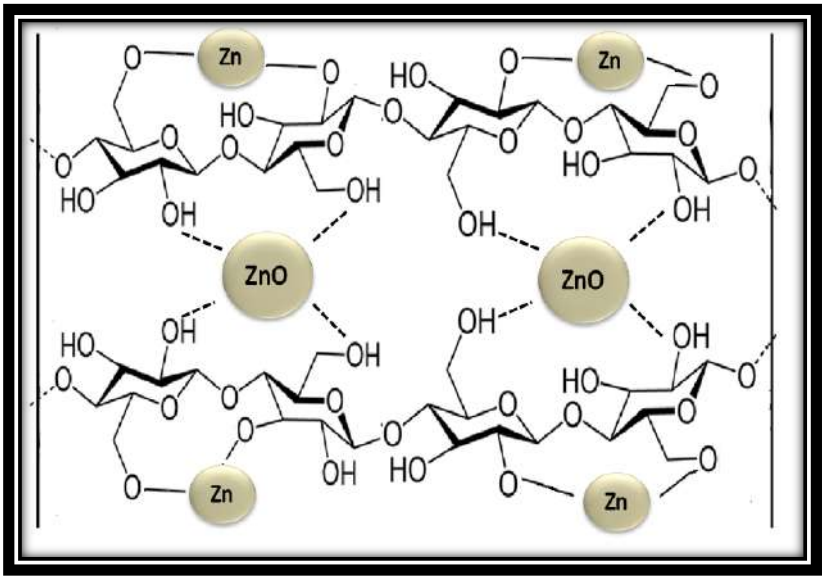

Fig.3.4. Proposed structure of ZnO/NC composite

CHAPTER - IV

CHARACTERIZATIONOF NANO CuO & NANO ZnO AND ITS CELLULOSE BASED COMPOSITES

4.1. METHODS FOR CHARACTERISATION

Nanomaterial characterization is a prime tool in the field of research as it provides a good idea about the size, shape, dimensions and functional groups present. Also characterization helps to find out the properties and applications associated with the samples. The composition and concentration of nanoparticles are not satisfactory for the complete explanation of nanoparticles as they vary in the physical properties such as size, shape, surface properties, crystallinity and dispersion state. Nature of the material plays an important role in the characterization techniques, some are qualitative and others are quantitative. The information regarding the appearance and morphology are given by qualitative techniques while the chemical composition, size, concentration etc. are given by quantitative techniques. Powerful characterization techniques give invisible information of the sample. Analysis of nanomaterials is carried out by using highly sophisticated and advanced characterization techniques explained in Chapter -II. For the characterization of metal oxides and composites, a large number of analytical techniques were used.

4.2. RESULTS AND DISCUSSION

The prepared materials are characterized by various characterization techniques explained in Chapter-2 and this section deals with all the analytical results of the samples.

4.2. a. XRD

The XRD pattern of ZnO [Fig4.1] show 2θ values at 31.96^{o}, 34.61^{o}, 36.44^{o}, 47.72^{o}, 56.75^{o}, 63.02^{o} and 68.09^{o}and corresponds to the (100), (002), (101), (102), (110), (103), and (200) peaks respectively which is consistent with previous works . Hexagonal Wurtzite and cubic zinc blend are the two crystalline forms of ZnO. Of these wurtzite structure is the most common and most stable at ambient conditions. The peaks of ZnOare typical for the hexagonal ZnO wurtzite structure and are reliable with

the JCPDS files (36-1451) and no other crystalline phases were detected which suggest that high purity zinc oxide was obtained.

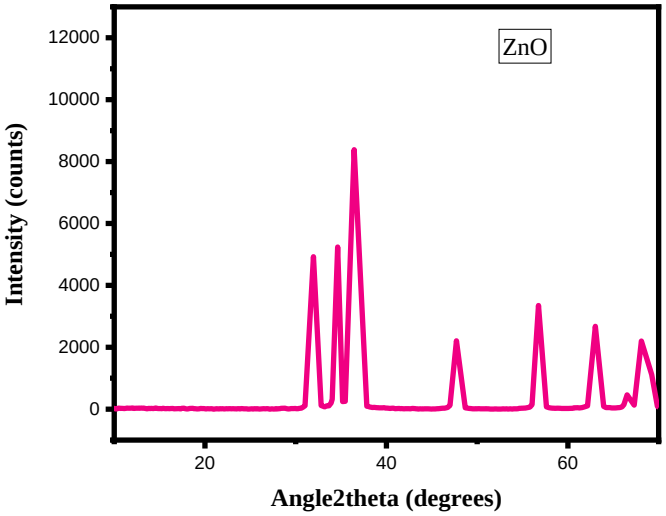

.

Fig.4.1. XRD pattern of ZnO

The XRD analysis of NC [Fig 4.2] revealed significant peaks at $2\theta = 16.10^0$, 23.02^0 and 34.8^0 corresponds to (101), (002) and (004) planes respectively. These peaks correspond to NanoCellulose and were indexed to the database of ID number COD 4114994 .The NC obtained has crystalline nature contrary to the amorphous nature of hemicellulose and lignin, due to hydrogen bonding interaction and Vander Waals forces between adjacent molecules .

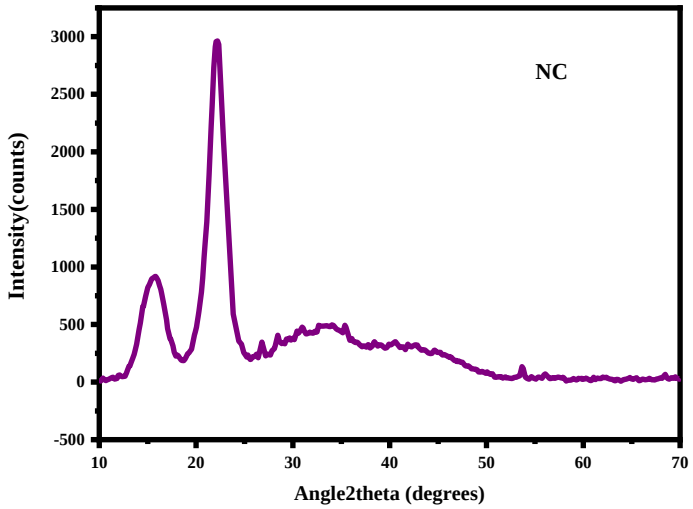

Fig.4.2. XRD pattern of NC

Fig4.3 shows the XRD pattern of ZnO/NC which displays two sets of diffraction peaks corresponding to ZnO and NC, in 2θ range of 10°–70°. The ZnO/NC composite exhibits all the characteristic peaks ofZnO and NC. Neither a new peak nor a peak shift compared with the pure NC indicate that theZnO/NC composite consist of two phase structures that may be polymer and nanoparticles. These observations show that the addition of the ZnO causes an inclusive upturn in crystallinity of ZnO/NC polymer blend,that can be effective on the final properties of biocomposites.

The sharp peak at 2θ of 23.02^{o}indicates polymer doping of NC. This specified the presence of smaller particle size in the nanocomposite containing high NC content.

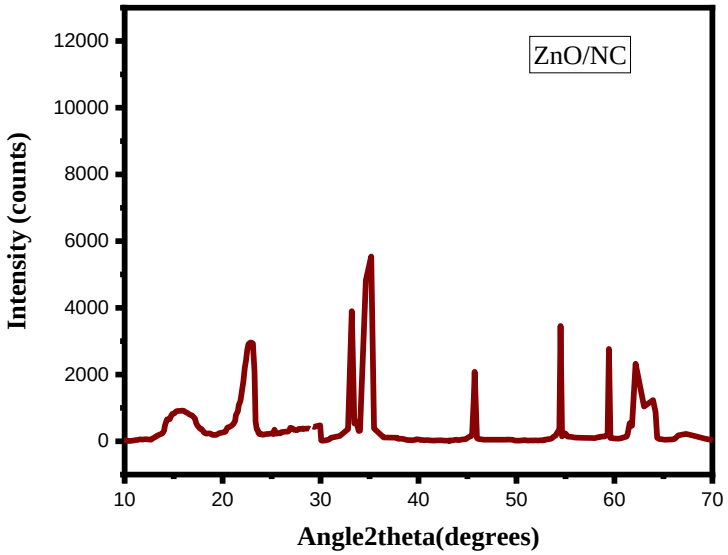

Fig 4.3 XRD pattern of ZnO/NC

The XRD of CuO [Fig.4.4] show 2θ values at 32.6^{0}, 35.8^{0}, 38.9^{0}, 48.9^{0}, 56.4^{0}, 58.5^{0}, 61.7^{0}, 66.4^{0} and 68.2^{o} which can be attributed to the Miller indices of the (110), (-111), (200), (-202), (020), (202), (113),(311) and (220) planes of monoclinic CuO respectively with lattice parameters of a=4.84A^{0}, b=47 A^{0}, c=5.33A^{0}. In the XRD spectra no impurity peaks from secondary phase of Cu_2O or Cu were detected. The intensities and positions of peaks are in good agreement with the standard datas of JCPDS card number 89-2531.The peaks are broad due to the nano-size effect.

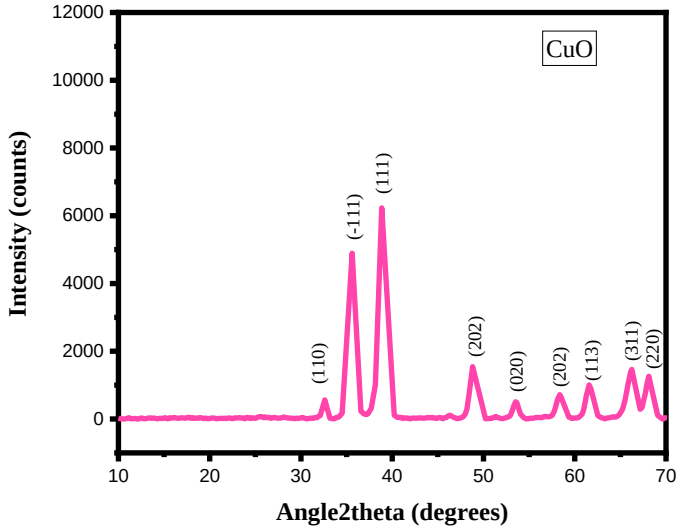

Fig.4.4 XRD pattern of CuO

Fig.4.5 shows the XRD pattern of as-prepared CuO/NC. The appearance of sharp peaks in the XRD of CuO/NC composite indicates some degree of crystallinity. The well-defined peaks corresponding to the crystal planes (110),(-111),(111)and (202) of nano CuO were found to be incorporated into the XRD of NC. From this it is clear that the CuO particles are well distributed in the polymer matrix. Also a change in intensity of all the characteristic peaks of CuO and NC observed in CuO/NC confirms the formation of the composite. The observed broadening of the peaks for the CuO/NC was mainly due to nanoscale size effect.

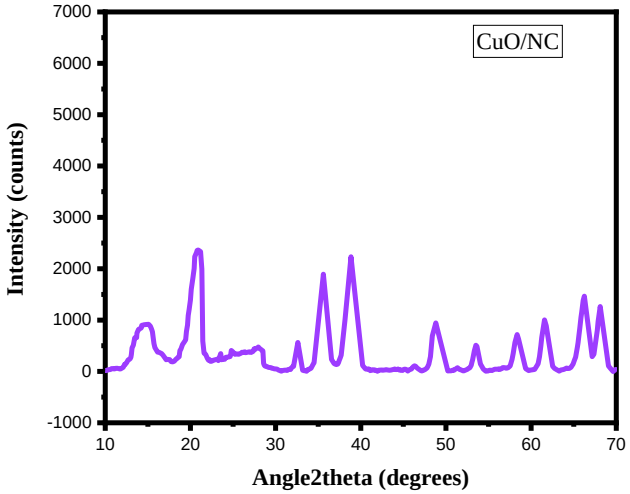

Fig.4.5 XRD pattern of CuO/NC

In order to estimate the average crystallite size, the obtained peaks were analysed and the Debye-Scherrer's equation has been used.

$$D=\frac{k\lambda}{\beta cos\theta} \quad \ldots\ldots\ldots\ldots\ldots\ldots\ldots\ldots\ldots\ldots\ldots\ldots \quad (1)$$

Where D is the crystal size,the value of the coefficient is 0.90,ɵ (radian)is the diffraction angle λ is the X-ray wavelength (1.5405 A^0) and β is the width of XRD peak at half height. The mean sizes of ZnO and CuO was calculated to be 15 nm and 23 nm respectively.

4.2.b. FTIR

To evaluate the chemical composition of ZnO nanoparticles FTIR was used at room temperature in the range of 500-3500 cm^{-1}.Fig.4.6 shows the typical FTIR spectra of ZnO nanoparticles. The bands near the region of 3000-3470 $cm^{-1}$is only because of -OH group. The absorption bands at 900-1000 cm^{-1} in the IR spectrum can be ascribed to the stretching and bending vibrations of C=O species. The band located near 400-500 cm^{-1}indicating the formation of stretching mode of ZnO.

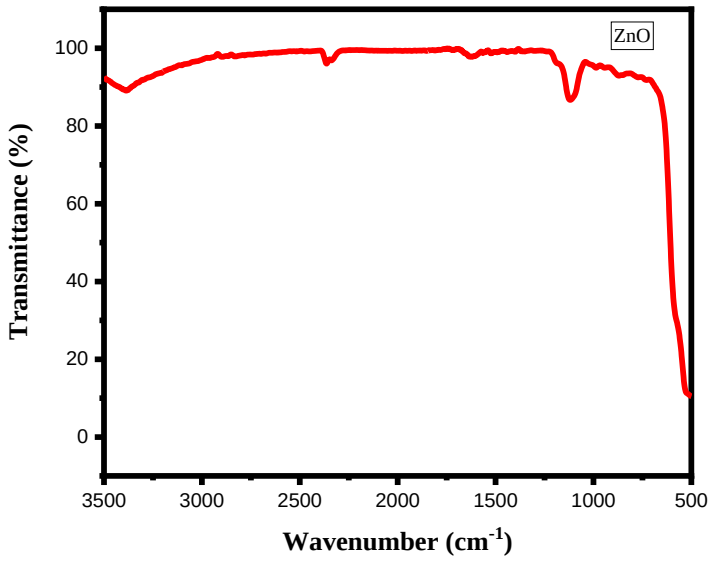

Fig.4.6. FTIR spectrum of ZnO

The spectrum of NC (Fig 4.7) displays peaks at 660 cm^{-1} due to C-OH out of plane bending vibrations of cellulose ,893 cm-1 due to –C-O-C pyranose ring stretching vibration 057cm $^{-1}$-C-O antisymmetric stretching vibration of glucosidic ring in cellulose 1160 due to pyranose ring C-O-C asymmetric stretching of cellulose ,1320

due to -CH2 wagging frequency of cellulose [NC 3]1450 of -C-H asymmetric deformations,2900 of -C-H stretching vibrationand3340 of -O-H stretching vibration of hydroxyl group .In the FTIR spectrum of NC, the distinctive peaks of hemicellulose and lignin were absent due to complete exclusion via acid hydrolysis .

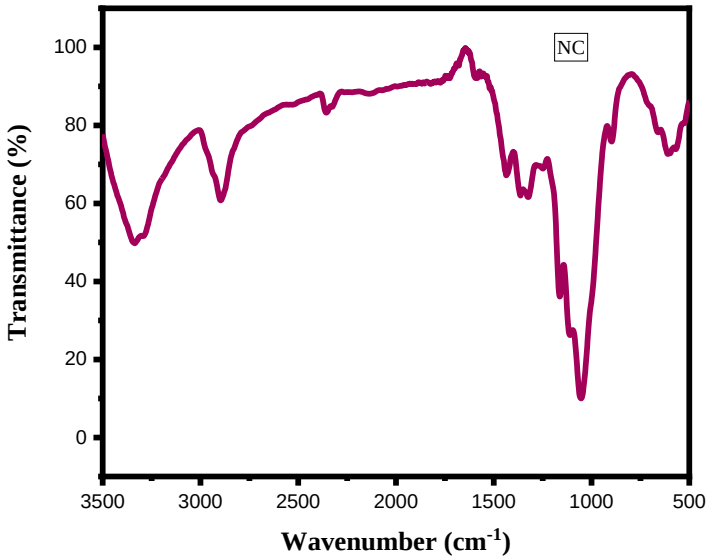

Fig .4.7 FTIR spectrum of NC

FTIR studies were carried out to confirm the identification and bond structure of associated functional groups of as-synthesized ZnO/NC and the infrared absorption spectra was observed in the range of 500-3500 cm^{-1}(Fig 4.8). NC had the characteristic peak at 1057 cm^{-1} and 1167 cm^{-1} while the correlated bands of ZnO/NC centered at around 1127 cm^{-1} and 1517 cm^{-1}respectively. The NC has a peak at 3340 cm^{-1}(OH-group of cellulose) that reduced to 3426 cm^{-1} for ZnO/NC. This broadening may be due to the intermolecular hydrogen bonding between ZnO nanoparticles and NC. In the spectrum of ZnO/NC, characteristic band of ZnO is almost enclosed with NC indicating that the hydroxyl groups of NC are occupied with ZnO. A similar situation in cellulose-based nanoparticles has also been reported for cellulose-Fe_2O_3nanocomposites and cellulose-calcium silicate nanocomposites.

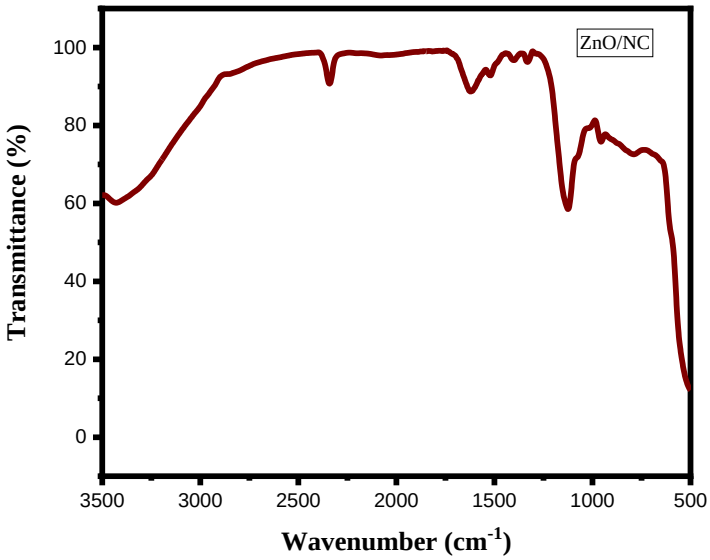

Fig.4.8 FTIR spectrum of ZnO/NC

The quality and composition of the synthesized CuO structures were characterized by the Fourier Transform Infra-red (FTIR) spectroscopy (Fig.4.9).The presence of a weak absorption at 3340 cm^{-1} is caused by the stretching vibration of the adsorbed water and surface hydroxyls as the nanocrystalline materials have high surface to volume ratio and thus absorbs moisture. No infrared active modes from Cu_2O were detected. The absorption bands at 1623 cm^{-1} are bending vibrational modes of combined water molecules. The appearance of a weak and small absorption at 2354 cm^{-1} could be attributed to CO_2 present in air. The absorption bands observed at493cm^{-1},865 cm^{-1} are characteristic of Cu-O vibrational modes.

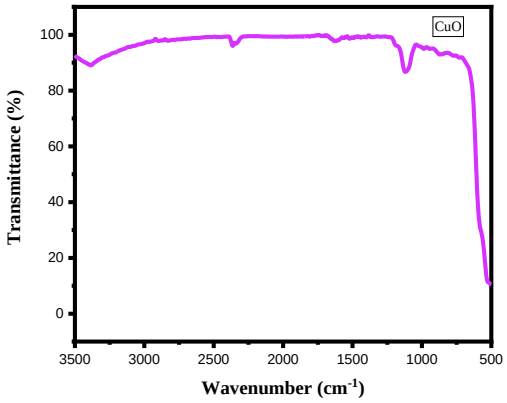

Fig 4.9 FTIR spectrum of CuO

FTIR study is a significant proof to specify the successful compositing. In the FTIR spectrum of CuO/NC (Fig.4.10), the characteristic bands of CuO and NC are retained. Moreover FTIR spectra showed that the characteristic FTIR peaks of NC are shifted to higher wave numbers in CuO/NC, which could indicate that the first CuO layer is closely linked to the surface of NC through covalent bonds. This hetero junction could hypothetically profit photons to be relocated from NC to CuO, which could permit for more photogenerated e^-/h^+ carrier and thus improve the photo catalytic activity of the semiconductor.

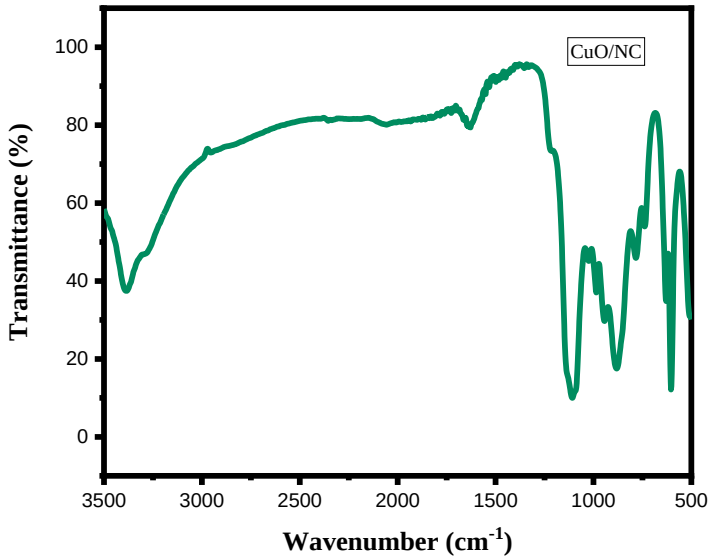

Fig.4.10.FTIR Spectrum of CuO/NC

4.2.c. SEM ANALYSIS

The morphologies and structures of the samples are characterized by using SEM. The SEM image of ZnO nanoparticles are presented in Fig.4.11 showing homogeneous and spherical–like appearance. From the figure we can evidently realize that the samples are demonstrating nanostructured morphology of the ZnO particles.

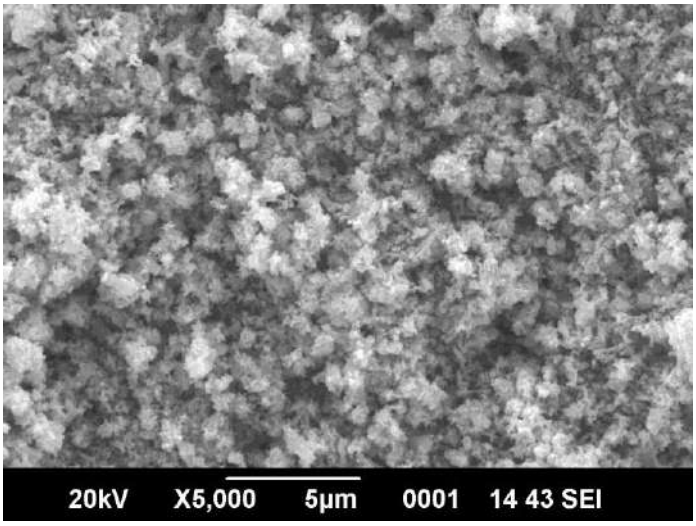

Fig.4.11 SEM image of ZnO

The NC was characterized by SEM to attain information about their morphology, which is also important for the evaluation of their potentialities for specific applications. Fig4.12 shows the SEM micrographs of NC reveals sheet like morphology with diameters in the nanometer range.

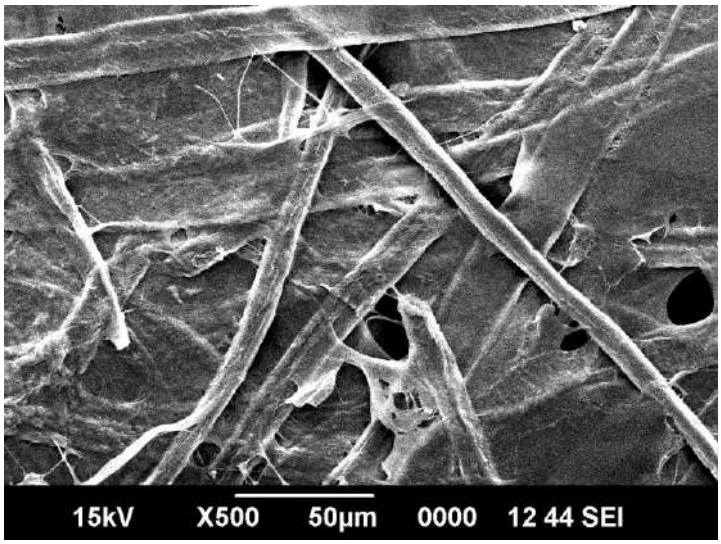

Fig 4.12 SEM image of NC

The surface morphology of the prepared nanocomposite ZnO/NC was investigated by Scanning Electron Microscopy techniques. Fig 4.13 shows the surface morphology of the ZnO/NC. The spherical shaped ZnO particles are well dispersed and embedded on the NC network without aggregation.NC network act as a template letting the high dispersity of ZnO nanostructures in the aqueous dispersion, so that the

individual ZnO could adsorb stably on the NC by trapping with each other. Also it can be observed that the surfaces of the NC are quite smooth, but with the addition of ZnO nanostructures, this smoothness decreases and the particle surface become very loose, this surface gathering can afford a boosted adsorption environment and more active sites for the photocatalytic reaction.

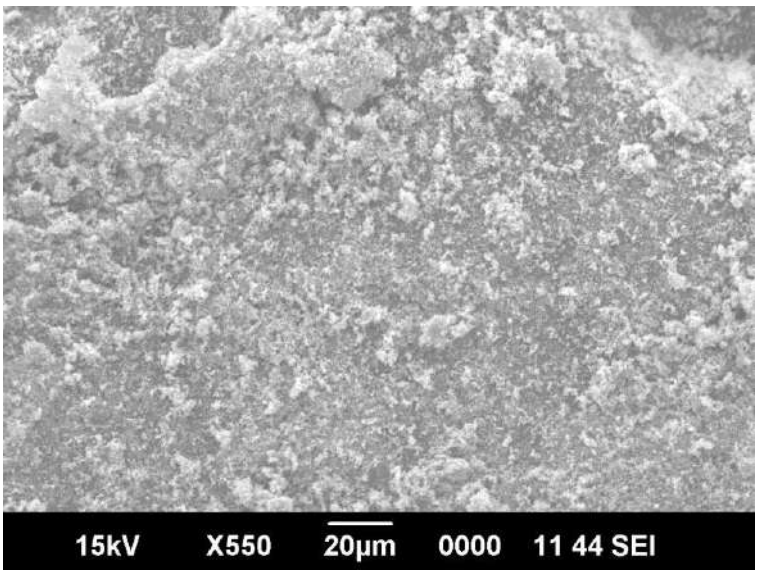

Fig.4.13 SEM image of ZnO/NC

The Scanning Electron Microscope (SEM) image [Fig4.14] of CuO nanoparticles shows flower like morphology with uniform size and shape .The individual nanoparticles align with respect to each other so that they share identical crystal faces and are self assembled through an oriented attachment mechanism. CuO, a polar material and the applied microwave rotation induces rotation of the polarized dipole of CuO causing heat due to molecular inner friction. The orientation effects occur due to the presence of internal electric field resulting reduction of activation energy which is the primary driving force for nucleation.

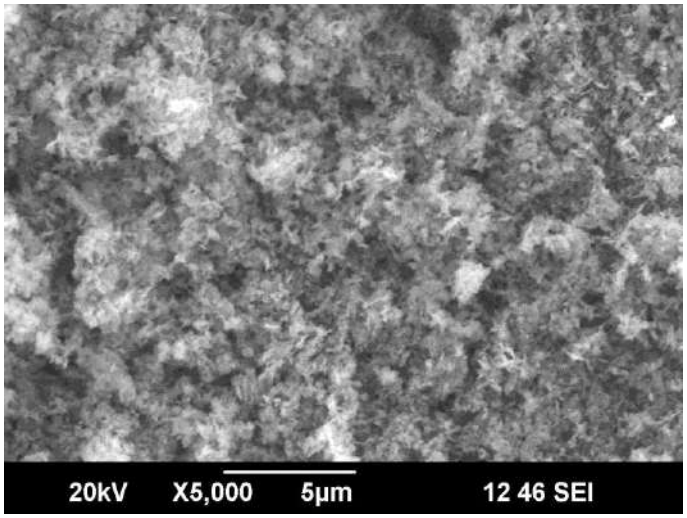

Fig.4.14 SEM image of CuO

SEM has been a principal tool for defining the particleshape, porosity and appropriate size distribution of the composite, Via Scanning Electron Microscopy (SEM),the morphologies and structures of the sample CuO/NC was characterized. In the case of CuO/NC [Fig .4.15], large number of –OH functional groups on NC can bind to the surface of CuO and the nano CuO particles cannot move freely and are dispersed uniformly throughout the nano-network. The CuO/NC composite produced were globular clusters,as shown in Figure. Additionally there was an agglomeration of CuO/NC composites, which was possibly due to the presence of cellulose during the drying process and the formed composite experienced greater resistance to growth, flocculation, leading to smaller size.

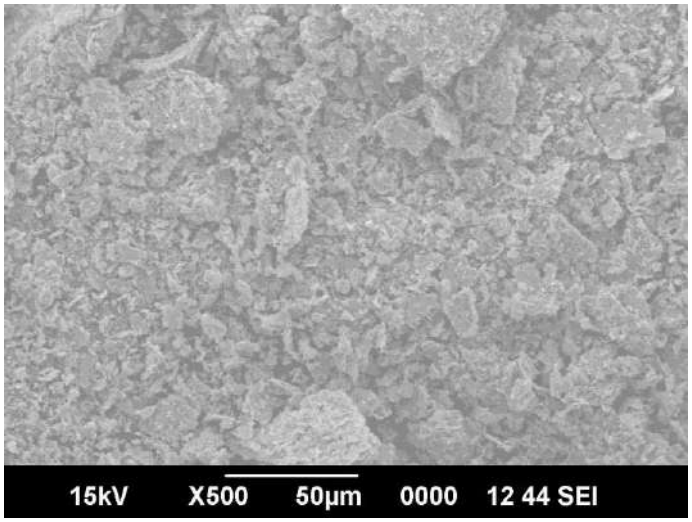

Fig.4.15 SEM image of CuO/NC

4.2.d. ENERGY DISPERSIVE X-RAY SPECTROSCOPY ANALYSIS (EDS)

The EDS spectrum of ZnO is shown in fig4.16. It confirms the presence of only Zinc and Oxygen in the sample. The mass percentage and composition data are shown in Table 1.

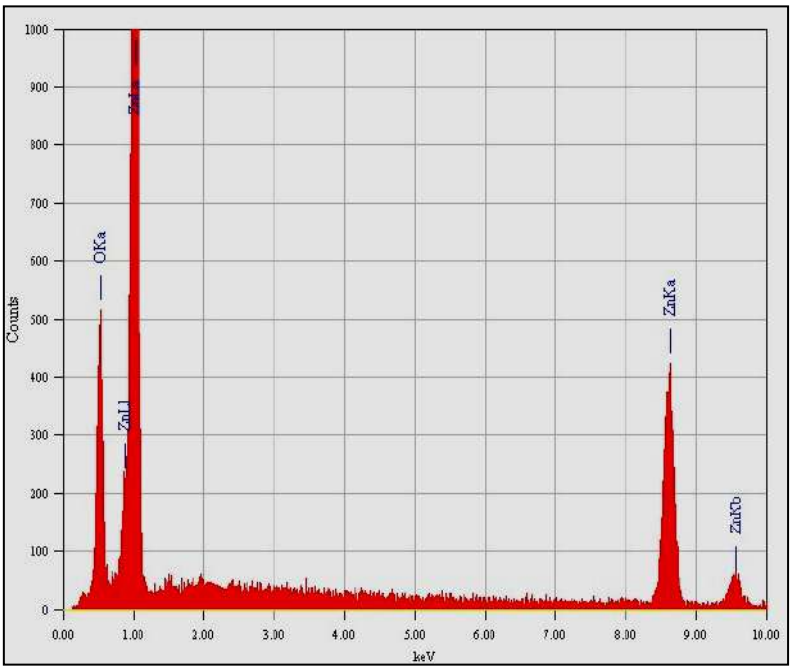

Fig .4.16 EDS Spectrum of ZnO

Table 4. 1 Composition of ZnO from EDS Spectrum

Element	(keV)	Mass %	Atom %	Cation
O K	0.528	11.84	39.25	0.2184
Zn K	8.23	88.16	60 .75	1
Total		100	100	

The EDS spectrum of CuO(Fig 4.17) confirms the presence of Copper and Oxygen in the sample and the mass percentage and composition are shown in Table 2.

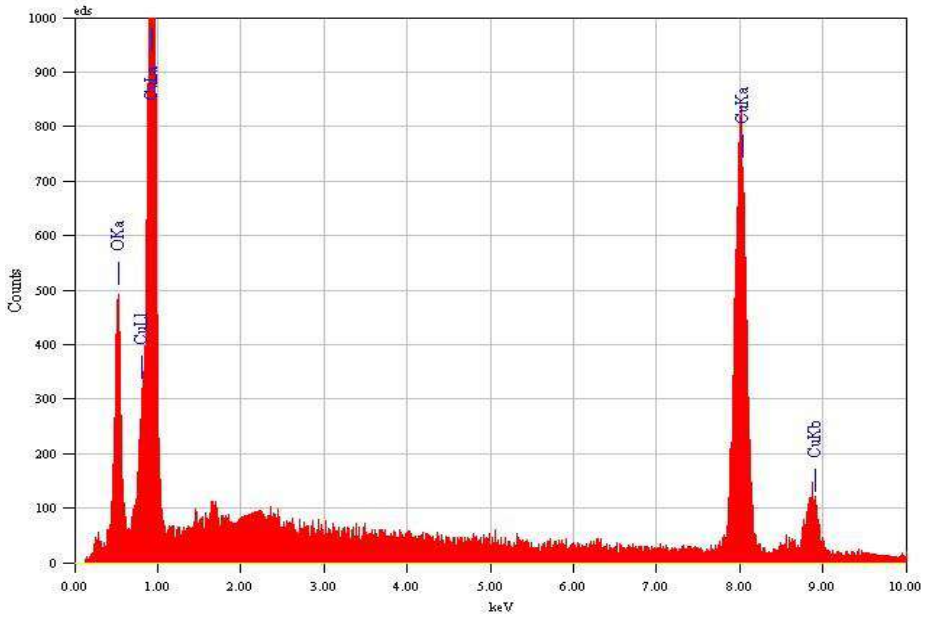

Fig 4.17 EDS Spectrum of CuO

Table 4. 2 Composition of CuO from EDS Spectrum

Element	(keV)	Mass %	Atom %	Cation
O K	0.514	8.54	31.26	0.2712
Cu K	8.013	91.46	68.74	1
Total		100	100	

The chemical compositions of the polymers are different at different point as they have extended chains. Therefore EDS are not used to confirm the chemical composition of polymers. The EDS spectrum of NC is shown in Fig 4.18.

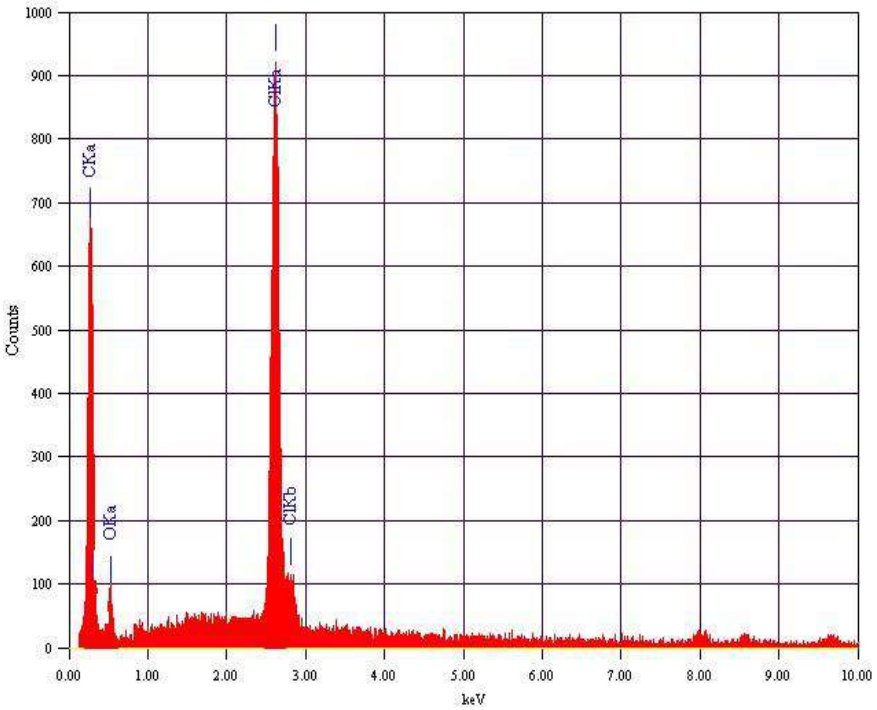

Fig .4.18 EDS Spectrum of NC

The EDS spectrum of ZnO/NC is given in Fig.4.19. In addition to C and O peak, ZnO/NC has a peak of Zn. The intensity of the peaks C and O is reduced, which indicates the modification of ZnO through composite formation. EDS spectrum has provide clear idea about the incorporation of ZnO in NC in the composite ZnO/NC.

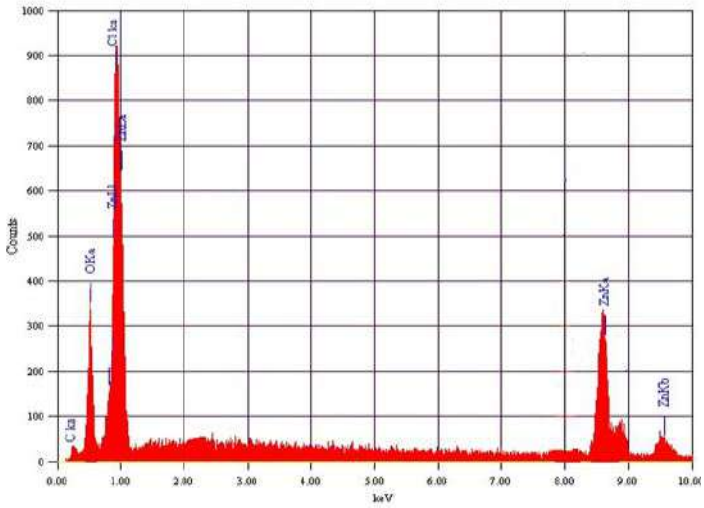

Fig.4.19 EDS Spectrum of ZnO/NC

The EDS spectra of CuO/NC (Fig.4.20) shows the presence of Copper (Cu) in addition to Carbon(C) and Oxygen (O) which again confirms the formation of CuO/NC composite.

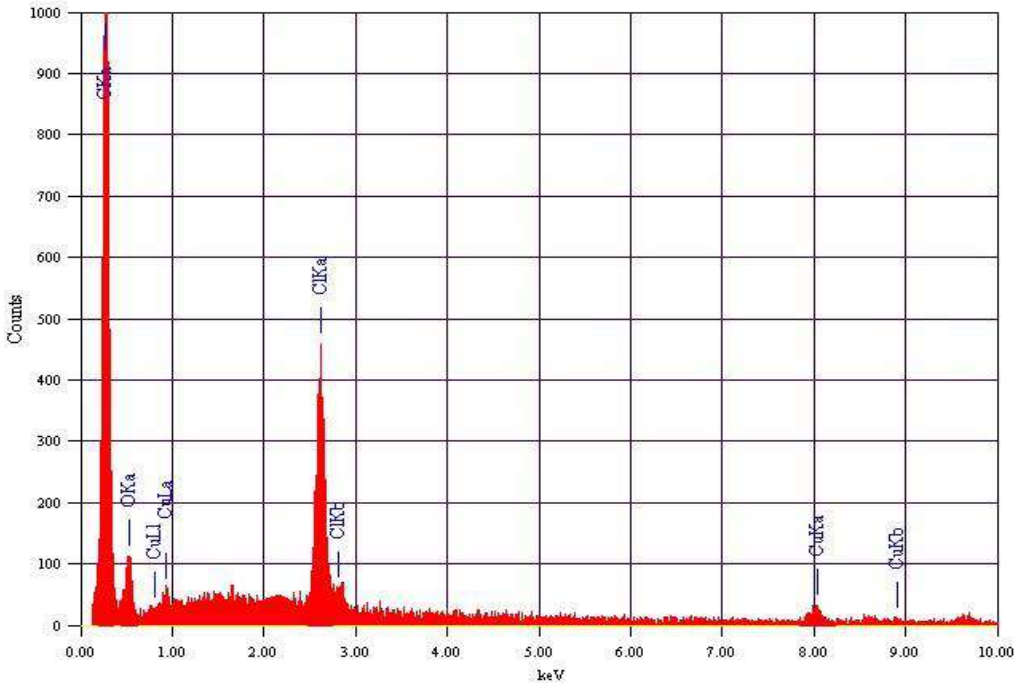

Fig.4.20. EDS Spectrum of CuO/NC

4.2.e. TEM ANALYSIS

The morphology and structure of ZnO sample was investigated by Transmission Electron Microscopy as seen in Fig.4.21 and it reveals that the powder composed of spherical shaped particles with a particle size 20nm which is almost same size with the crystallite size determined from XRD. The powder shows the tendency to break down into smaller pieces with various shapes and sizes. The particle size distribution is shown using the histogram.The SAED pattern of ZnO comprises of broken rings depicting six fold symmetry (hexagonal) corresponding to the crystalline nature of ZnO and the pattern consist of clear lattice fringes which indicates the polycrystalline nature of ZnO.

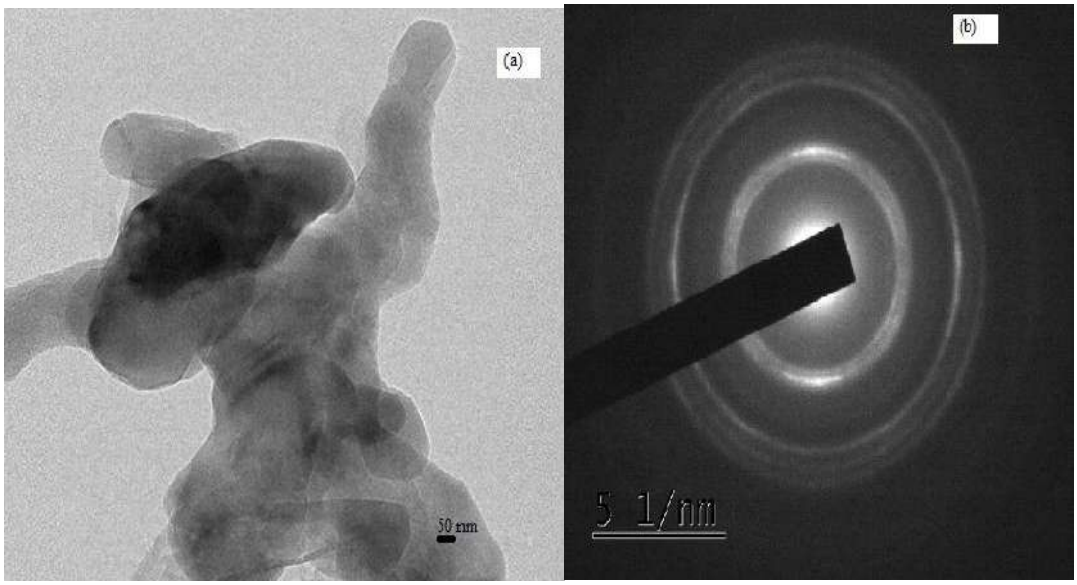

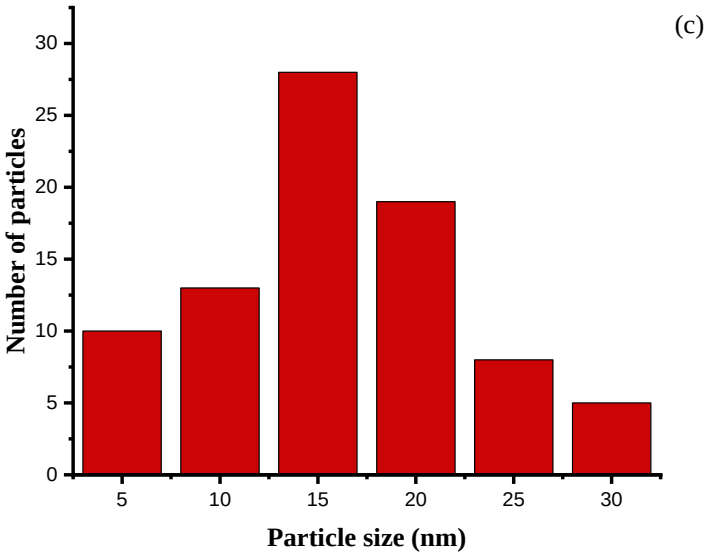

Fig.4.21.(a)TEM (b) SAED pattern(c) Histogram depicting the size distribution of ZnO

Fig.4.22. shows the TEM image of NC which reveals that the as-prepared NC has uniform diameter distribution and adjoins together to form a network structure. During the preparation of NC, the relatively weak interfaces between the cellulose could break mainly by vander Waals forces resulting in decentralizing of the overall NC and the SAED pattern confirms its crystalline nature.

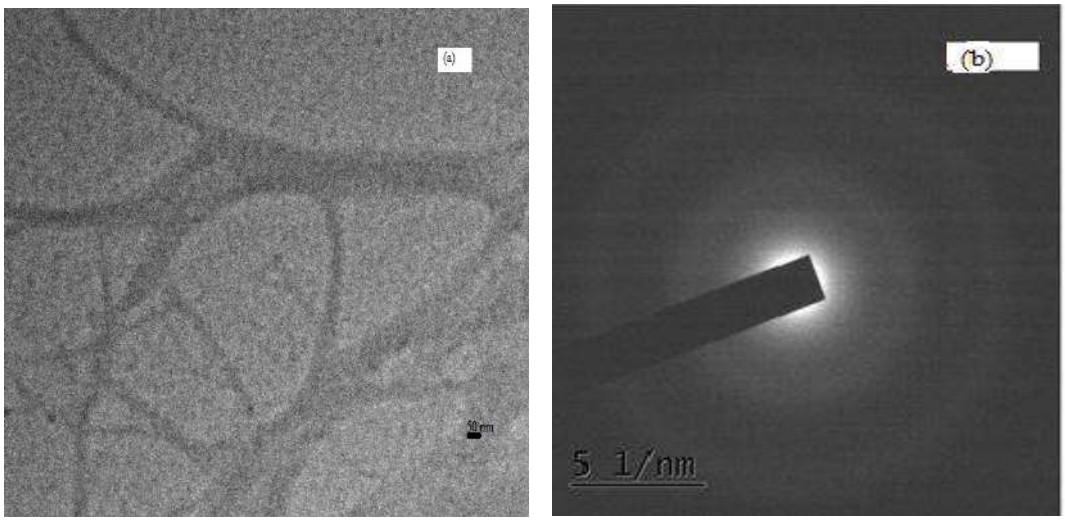

Fig.4.22 a)TEM b) SAED pattern of NC

Fig.4.23. shows the TEM image of ZnO/NC composite. The images portrayed the uneven distribution of ZnO particles in the NC matrix and the ZnO nanoparticles have a tendency to aggregate, to get incorporated into the pores of NC. The ZnO/NC has a spherical shape and dimension with a particle size of 50 nm. The image of the nanocomposite reveals a structure of ZnO inside the polymer matrix. In other words the polymer matrix captures the ZnO. The SAED pattern of the composite consist of some well resolved spots indicates the incorporation of hexagonal six fold symmetry of ZnO into the polymer matrix.

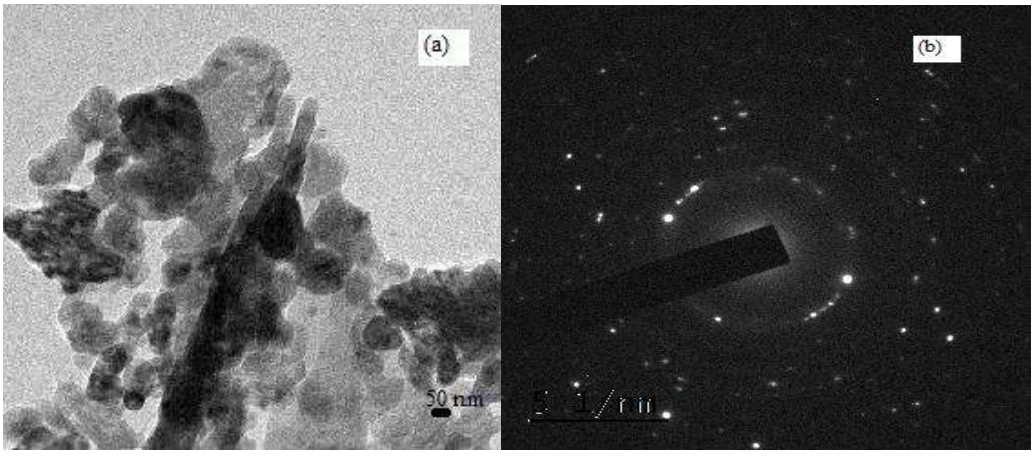

Fig.4.23 (a)TEM (b) SAED of ZnO/NC

The morphology and atomic structure of CuO nanoparticles was further studied using TEM. Fig.4.24.shows the morphology and internal structure of the CuO

nanoparticles. The crystallite size calculated for CuO from XRD results closely matches with the average particle size obtained from TEM. The SAED pattern obtained for CuO nanoparticles consists of bright rings indicating the crystalline nature. Also the diffraction points are slightly stretched indicating that the CuO composed of naocrystals that were assembled via oriented attachment process .The particle size distribution is shown using the histogram.

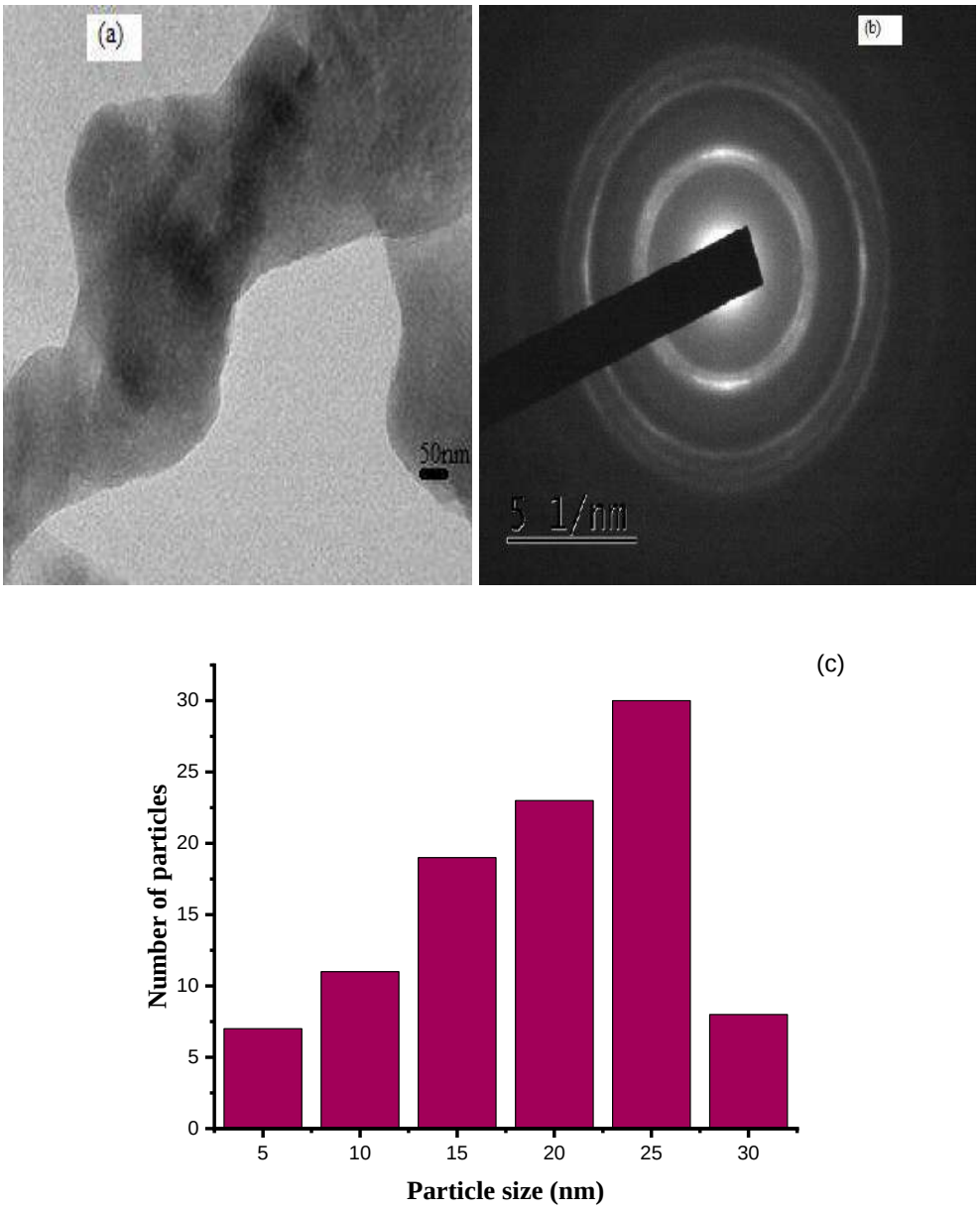

Fig.4.24. (a)TEM (b) SAED pattern (c) Histogram depicting the size distribution of CuO

The surface morphology of the composite CuO/NC was characterized by TEM analysis. Fig.4.25. shows the surface morphology of CuO/NC. In CuO/NC, the NC molecules combines with Cu^{2+} ions or OH^- ions reach a certain amount; they can interpenetrate to form a nano-network. Additionally, there was an agglomeration of CuO/NC composites, which was possibly due to the presence of NC during the drying process and the SAED pattern of CuO/NC comprising of broken rings due to the increasing number of crystals having similar orientations in the composite.

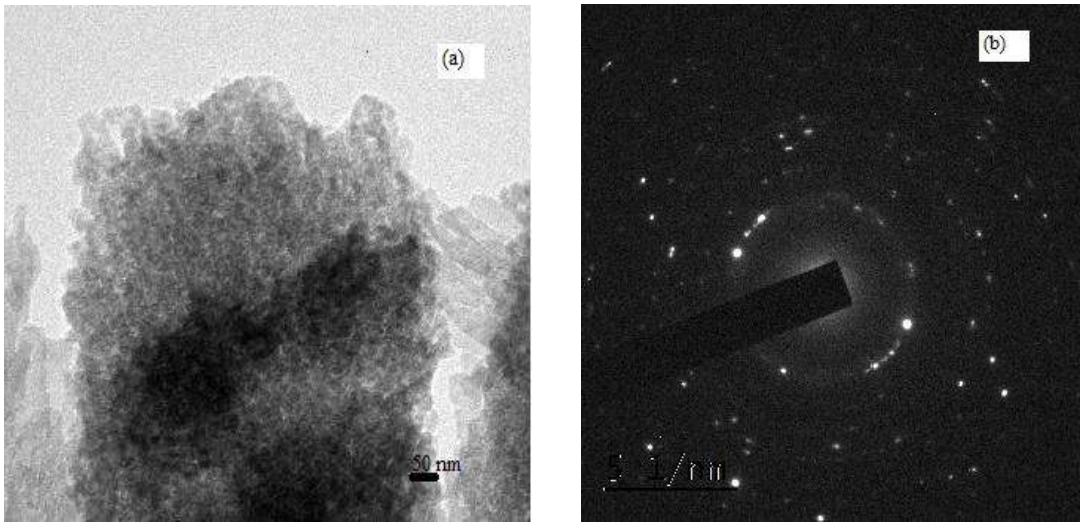

Fig.4.25.(a)TEM of CuO/NC (b) SAED of CuO/NC

4.2.f. UV-VISIBLE SPECTROSCOPIC STUDIES

The optical properties of the prepared samples were investigated by UV-Visible spectroscopy taken in a wavelength range of 200 to 800 nm. The optical band gap of the materials were calculated from the Tauc's plot by the following equation

$(\alpha h\upsilon)=A(h\upsilon-Eg)^n$

Where n is 0.5,1.5,2 and 3 for direct, indirect forbidden, direct forbidden and indirect transitions , α is the absorption coefficient, A is the band edge sharpness constant, h is Plank constant ,υ is the light frequency and Eg the band gap energy. The Eg value can be estimated by extrapolating the straight portion of the $(\alpha h\upsilon)^2$-(hυ) plot to hυ=0 .It is observed that for all the particles, the best straight line is obtained for n=1/2,which is expected for direct allowed transition. The band gap energy values of the photocatalysts are given in Table 3.

The UV visible spectra (Fig.4.26.) for ZnO nanoparticles displayed exciton absorption peak at 363 nm which implies a low ZnO crystallite size. The excitonic absorption peaks have shown significant hypsocromic shift compared to the bulk ZnO due to decrease of particle size and the UV-Visible spectrum of NC (Fig.4.27) shows band at 304nm.

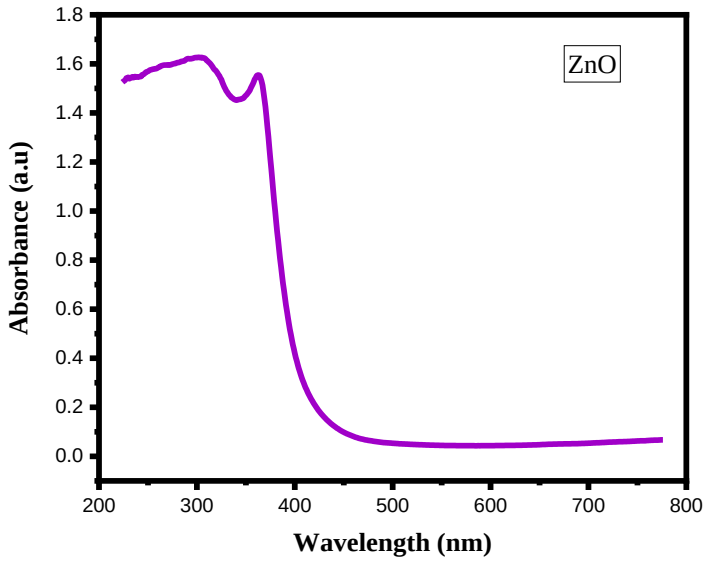

Fig .4.26 UV-Visible spectrum of ZnO

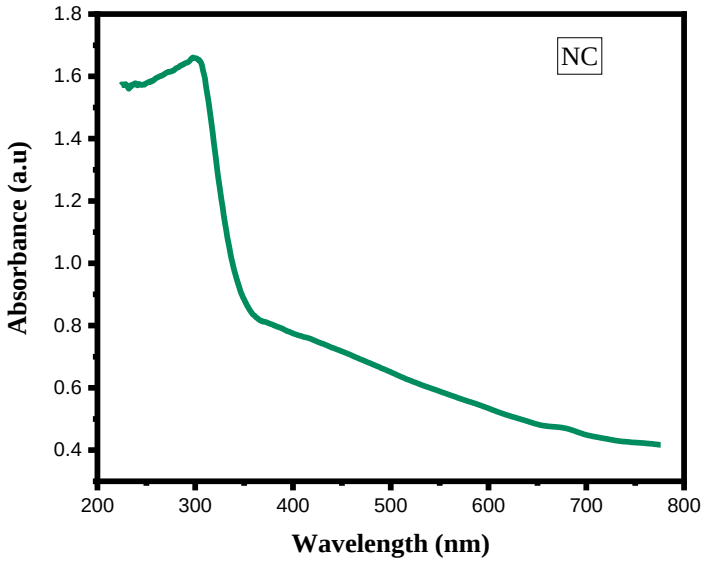

Fig.4.27. UV-Visible spectrum of NC

The UV-Visible spectrum of ZnO/NC (Fig4.28) shows two peaks at 365nm and 302nm which clearly indicates the incorporation of ZnO to NC. Also change in

intensity of the peaks is observed which confirms the formation of the composites. The absorbance spectra reveals that the ZnO/NC composite has increased in visible light region and showed red shift of absorption edge compared to bare ZnO. ZnO/NC composite shows maximum absorption of visible light which can be visibly noticed from the absorption spectra. The increase in the visible light absorbance of composite may be due to the increase of surface electric charge of the oxides in the composite and the alteration of the process of electron-hole pair formation during irradiation. Also, the results clearly indicate the importance of NC introduction on the optical properties of ZnO by suggesting that the introduction of NC on ZnO improves the absorption of visible light.

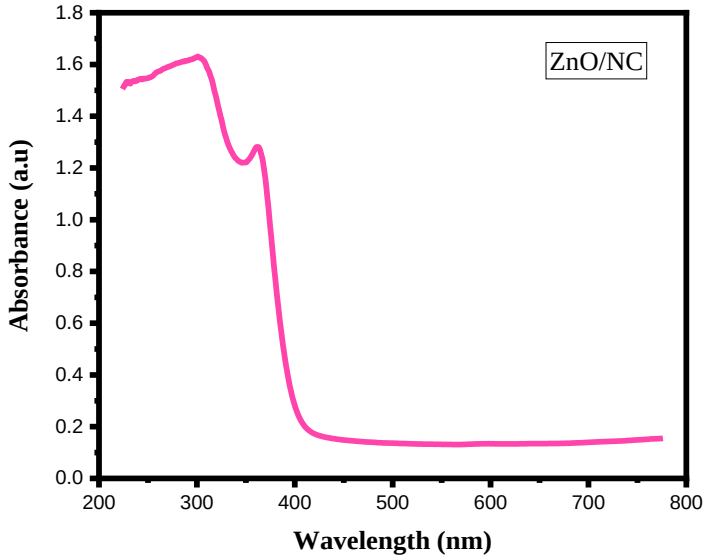

Fig.4.28. UV-Visible spectrum of ZnO/NC

The UV-Visible absorbance spectra of the samples CuO and CuO/NC are shown in Fig.4.29-Fig4.30. All the samples show an absorption maximum in the visible region. The spectrum shows a slight shift in both adsorption bands and the band edges towards higher wavelength with different adsorption intensities. These absorption band shifts provide an awareness of the formation of inter/intra molecular hydrogen bonding existing between Cu ions with the adjacent -OH groups of the NC. As the concentration of CuO increases, more and more inter/intra hydrogen bonding occurs resulting an increase in absorption .The shift in the adsorption edge of the composite is due to the variation in crystalline parameters which in turn changes the band gap energy.

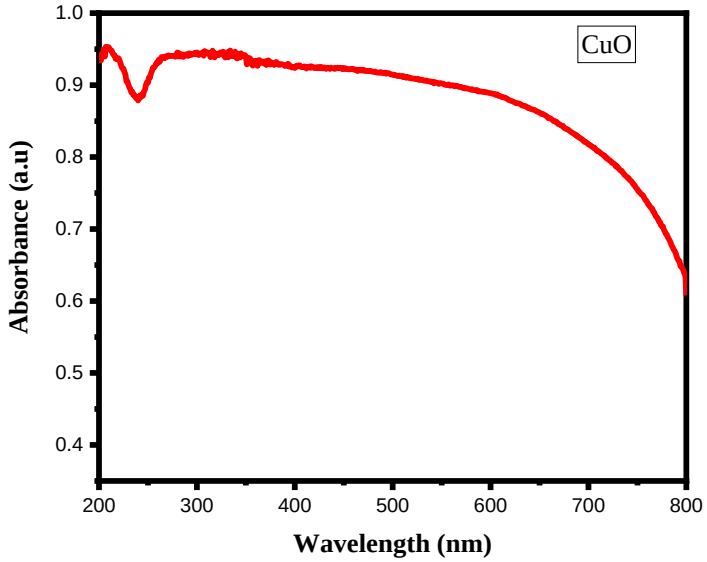

Fig.4.29. UV-Visible spectrum of CuO

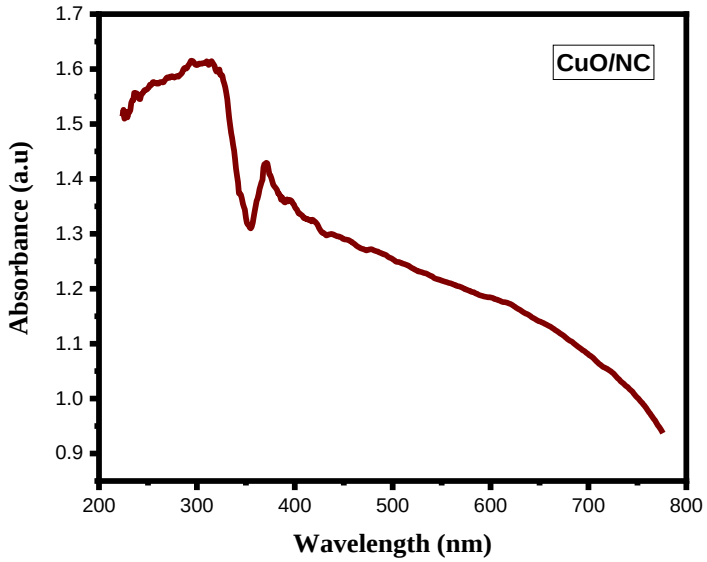

Fig.4.30 UV-Visible spectrum of CuO/NC

The band gap energy of ZnO, NC and ZnO/NC is 3.07, 3.62 and 2.19 respectively. The calculated band gap value of nano ZnO(3.07ev) is smaller than that of bulk ZnO (3.37ev). This difference may originate from the introduction of defects during the decomposition reaction. The band gap energy of semiconductors is due to the residual strain, defects, charged impurities, disorder at the grain boundaries and also

particle size confinement. The particles which are crystalline with smaller size has higher surface area and can cause more band bending effect.

The observed red shift in the adsorption edge of the composite compared to ZnO indicates that the synthesized ZnO/NC can be used as photocatalyst and the composite could absorb more photons from the visible light, the red shift observed in the absorption spectrum could enhances the photodegradation efficiency.

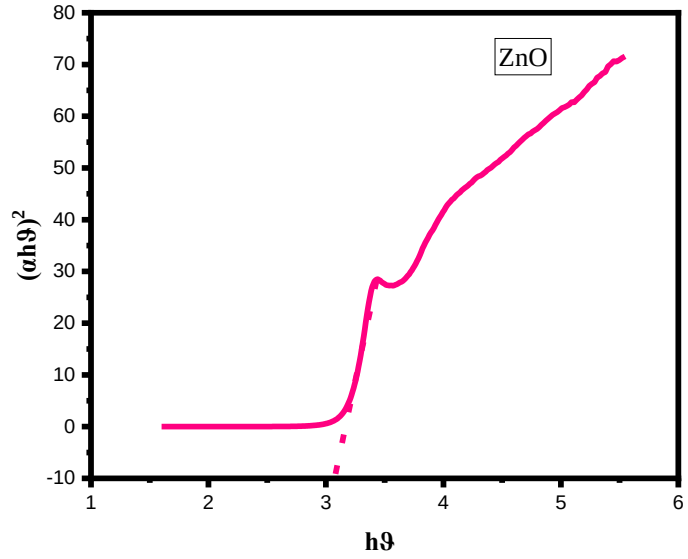

Fig.4.31Tauc's plot of ZnO

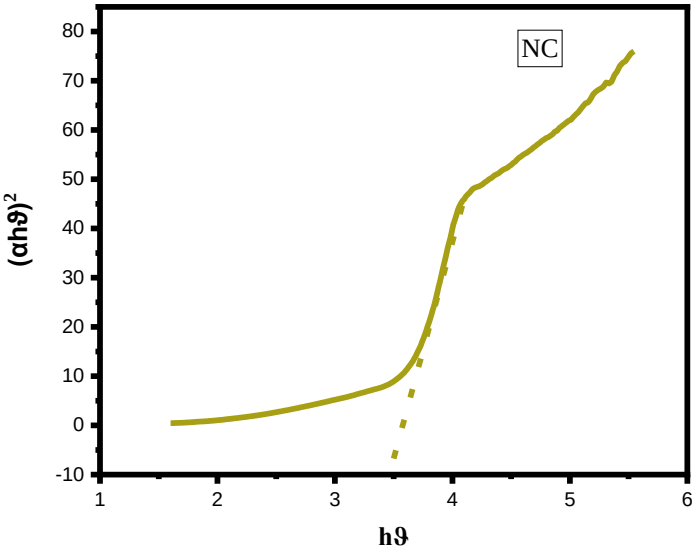

Fig.4.32.Tauc's plot of NC

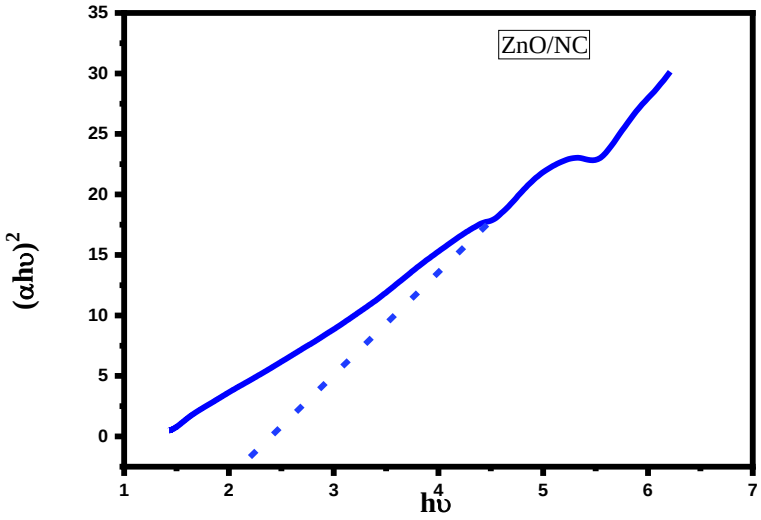

Fig.4.33Tauc's plot of ZnO/NC

The band gap energy of CuO and CuO/NC was found to be 3.2 and 2.9 respectively. CuO/NC have extended optical absorption in the 400-550 nm visible range compared to CuO. This extended optical absorption of metal oxides to the visible light, when incorporated with NC ,may recommend that NC could augment the visible light photocatalytic activity of metal oxides since more photons can now be absorbed by the photocatalyst and used for producing more Reactive Oxygen Species(ROS) during photocatalysis process .The red shift observed in the absorption maximum and in the band gap energy of CuO/NC compared to CuO can be attributed to the increased agglomeration, change in crystallinity and also due to the interaction of CuO with NC .Also, the decrease in band gap energy of the composite is due to the presence of local cross linking that occurred within the polymer present in the composite. As the local cross-linking increases, the degree of ordering in polymer backbone increases which decreases the band gap energy values.

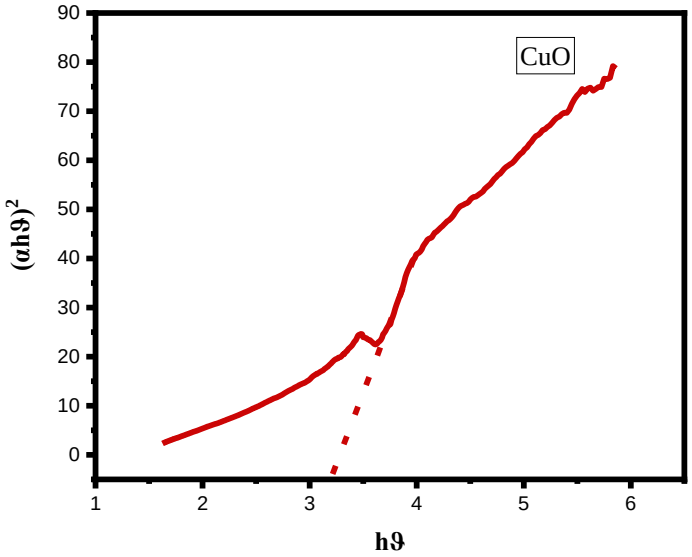

Fig 4.34 Tauc's plot of CuO

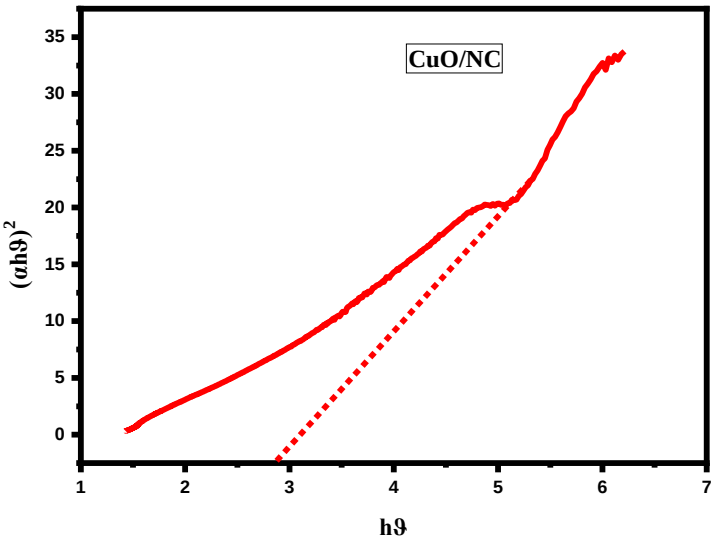

Fig.4.35 Tauc's plot of CuO/NC

Table 4.3 Band gap values of different materials

Photocatalyst	Band Gap (eV)
ZnO	3.07
CuO	3.2
NC	3.62
ZnO/NC	2.2
CuO/NC	2.9

Of the above mentioned photocatalysts, ZnO/NC has the lowest band gap energy due to the quantum confinement effect of the ZnO in the ZnO/NC composite.

4.2. g. PHOTOLUMINESCENCE (PL) SPECTRAL ANALYSIS

Photoluminescence spectroscopy is an effective technique for evaluating the optical properties. The PL spectra were recorded in the spectral range of 350-600 nm at room temperature. The samples have been measured with an excitation of the 320 nm. Fig4.36 presents the PL spectra of the ZnO powder and the results show that the as-synthesized sample have a Wurtzite structure with a weak UV emission at about 395-400 nm,two blue-green emissions, one centered at 450-460 nm and a second at 480 nm, and a green emission at around 520 nm.

At 395-400 nm, a weak emission band is obtained and is consigned to the overlap of the free exciton emission from the wide band gap of ZnO. The emission bands at 450,480 and 520 nm in the blue-green range are defect related emissions. The bands at 450 and 480 nm are caused by the transition from the level of the ionized oxygen vacancies to the valence band. The green band at 520 is assigned to many different kinds of defects such as oxygen vacancies, donor acceptor recombinations, orantisiteoxygen. The absence of the yellow orange and the presence of the blue-green and green band can be a strong symptomatic that only defects associated with oxygen deficiency are presented in ZnO sample .

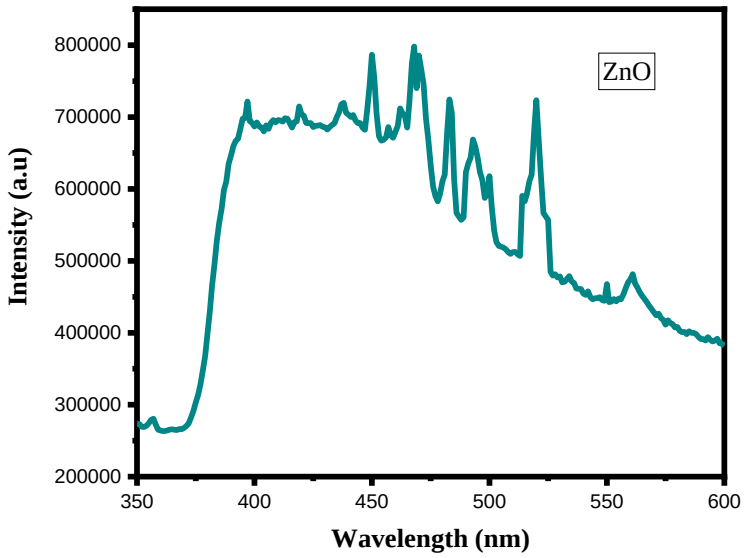

Fig.4.36 PL emission spectrum of ZnO

The emission spectrum for NC excited with a light of wavelength 325 nm is shown in Fig.4.37. The spectrum of NC shows the emission peaks at 416 and 440 nm and a green emission at 510 nm.

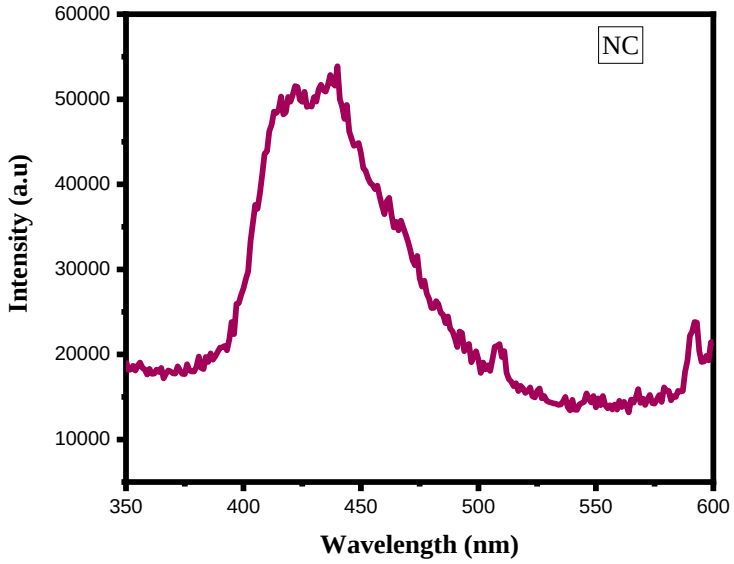

Fig.4.37. PL emission spectrum of NC

The PL spectrum of the nanocomposite ZnO/NC [Fig.4.38.] is observed to be smaller than that for the ZnO. The observed decrease in the overall intensity of the PL spectrum is attributed to the decrease in the oxygen vacancies. The oxygen vacancies present in the case of ZnO are mainly restricted to the surface. The incorporation of the NC into ZnO, leads to decrease in the concentration of oxygen vacancies. Luminescence quenching of the emission of ZnO is observed when it is anchored on the NC surface. As ZnO is a good electron donor, the PL quenching is due to the electron transfer from the conduction band of ZnO to NC and the electron transfer may reduce the recombination of photogenerated electron-hole pairs. Therefore the composite ZnO/NC is expected to show better photocatalytic activity than ZnO.

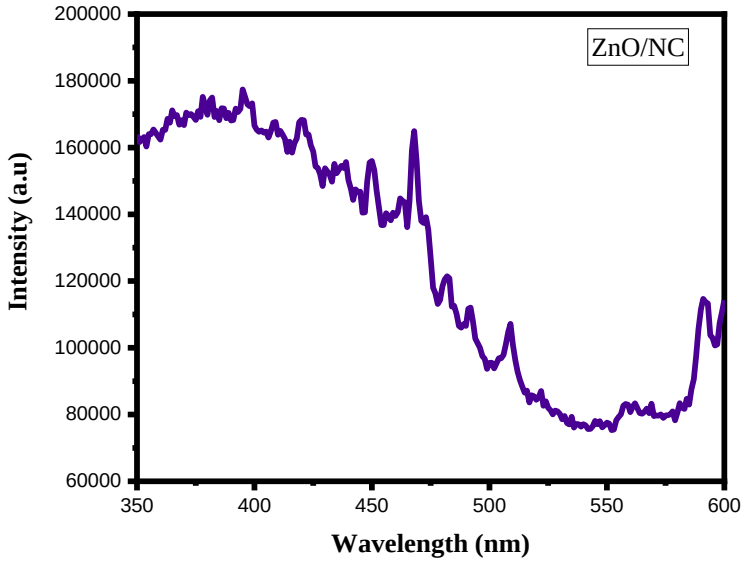

Fig.4.38. PL emission spectrum of ZnO/NC

The room temperature photoluminescence spectra of as prepared CuO nanoparticles are shown in Fig.4.39.Three strong emission peaks are observed at 382,450 and 530 nm. The violet band at 382 nm is due to the band edge emission, the blue band at 450 nm is because of artifact and due to the presence of singly ionized oxygen vacancy, green emission occurs at 530 nm as there are recombination of photogenerated hole with a singly ionized electron in valence band .The emission bands extending from 585 to 600 nm correspond to deep level defects of CuO .

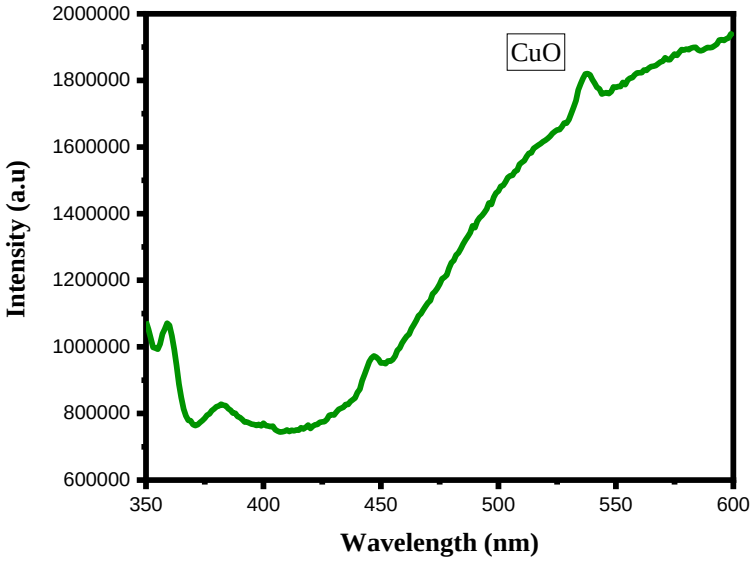

Fig.4.39. PL emission spectrum of CuO

The PL spectrum of CuO/NC [Fig.4.40.] shows broad bands centered at 396,420,480 and 550 nm. A slight red shift occurs in the case of all absorption bands. Red shift and blue shift of the PL peak may be due to quantum chemical effect and specific surface effect. The green band emission at 550 nm corresponds to the singly ionized oxygen vacancy in CuO which results from the recombination of a photogenerated hole with the single ionized charge state of this defect. The CuO/NC composite absorbed heavily in the visible region and the luminescence bands have lower intensity compared to CuO. In the PL spectrum of CuO/NC, missing of peaks and a number of additional peaks are observed which may be due to the interaction between NC and CuO. The additional peaks and shifting of peak positions in the case of CuO/NC can be attributed to the interactions between CuO and NC leading to rearrangement in the electronic-band structure.

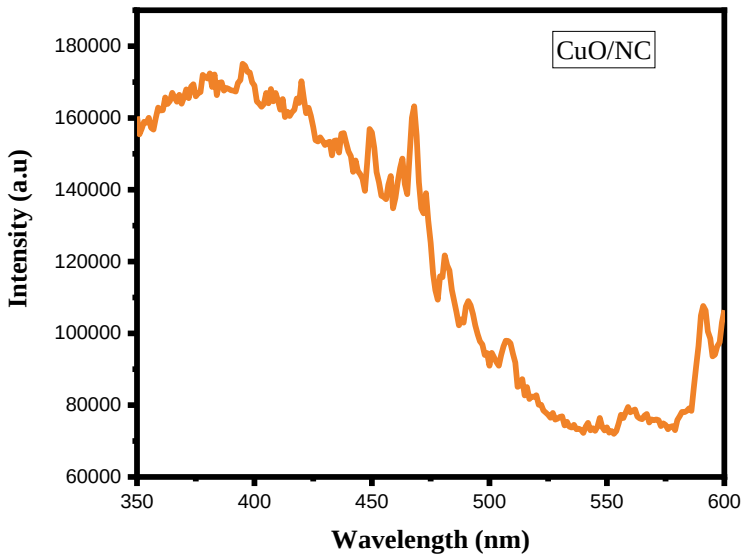

Fig.4.40.PL emission spectrum of CuO/NC

4.2.h. BET SURFACE AREA ANALYSIS

As specific surface area of photocatalysts plays an important role in affecting the photocatalytic reaction, we measured the Brunauer-Emmet-Teller (BET) specific area of the prepared photocatalysts and the results are given in table 4. The table shows that the specific surface area of NC is relatively low (67.84).The composites have higher specific areas (for ZnO/NC for CuO/NC) compared to metal oxides and NC. Metal oxides have small particle size, high density of surface groups and high degree of

agglomeration which results low specific area. In the case of ZnO/NC , the growth of ZnO on the surface of NC makes the ZnO particles homogenously dispersed within the composite, which avoids the ZnO nanoparticles from aggregation and results in much less aggregates and higher surface area .But in the case of CuO/NC, inter and intra hydrogen bonding occurs between Cu^{2+} ions and –OH group of NC resulting a surface area lower than that of ZnO/NC.

Table 4 BET surface area of different materials

Photocatalyst	**Specific surface area (m^2/g)**
ZnO	102.58
CuO	89.69
NC	67.84
ZnO/NC	184.02
CuO/NC	163.52

Based on surface area measurement results, ZnO/NC are supposed to yield the highest photo catalytic activity.

CHAPTER - V

APPLICATION STUDIES

5. APPLICATION STUDIES OF NANO ZnO, NANO CuO & NANO CELLULOSE BASED COMPOSITE OF ZnO&CuO

The application studies mainly included in this report are adsorption, photocatalysis and antimicrobial activity of the prepared nanomaterials. The nanomaterials prepared in the present study were found to be suitable for the above applications.

5.1. ADSORPTION STUDIES

5.1.1. EVALUATION OF ADSORPTION EFFICIENCY

Environmental pollution caused by burning of conventional energy sources is a serious day-to- day problem faced by the developing and developed nations in the world. The common pollutants include toxic organic compounds like chlorinated and non chlorinated aliphatic and aromatic compounds, dyes, heavy metals, insecticides, pesticides and pathogens like bacteria, fungi and virus. Hence strict environmental legislations on the safe disposal of recalcitrant pollutants drive the research community to develop clean and green processes to degrade the pollutants before they are admitted into the atmosphere and water bodies**.**

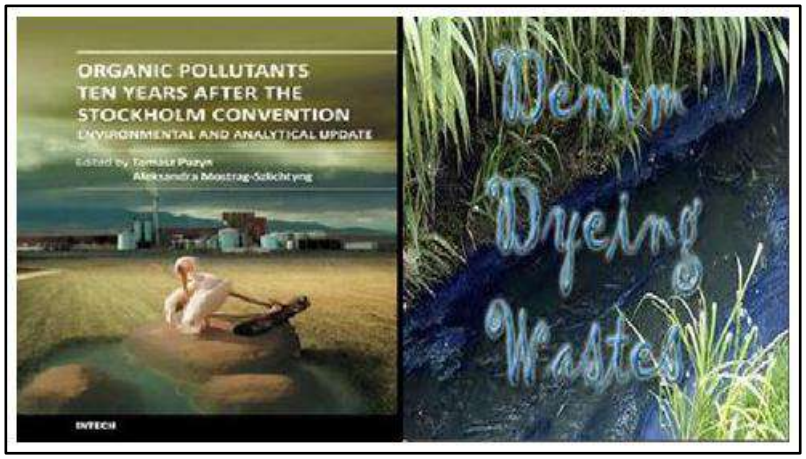

Figure 5.1 Water pollution due to heavy metal ions and organic dyes

Today about 200 million people in India do not have access to safe drinking water due to water pollution. Heavy metals and dyes play an important role in water pollution. Their presence in aquatic ecosystem poses human health risks and causes harmful effects to living organisms. So it is essential to remove metal ions and dyes from industrial waste water before discharging it in to natural water sources. The conventional methods for removing heavy metals are chemical precipitation, electrochemical treatment, ion exchange etc. However, the application of these treatment processes has been found to be restricted, because of expensive investment, operational costs and the potential generation of secondary pollution. Adsorption has been considered as a cheap and green technique for removal of heavy metal ions.

The term adsorption was first used by 'Kayser' in 1881 and it refers strictly to the existence of higher concentration of any particular component at the surface of the liquid or solid phase than in the bulk. Adsorption may be of two types namely physical and chemical. The physical adsorption occurs mainly due to weak forces like ion-dipole, dipole-dipole, polarization or induced dipole, van der Waals forces etc. The physical adsorption is reversible and temporary in character. It usually involves lesser heat exchange, while chemical adsorption is due to the formation of a chemical linkage between the adsorbate and adsorbent. The chemical adsorption is not reversible and carried out at high temperature. It is characterized by a large heat change during adsorption.

5.1.2. MECHANISM OF ADSORPTION

A solid surface in contact with a solution has the tendency to accumulate a layer of solute molecules at the interface due to imbalance of surface forces. This accumulation of molecules is a vectorial sum of the forces of the attraction and repulsion between the solution and the adsorbent. Majority of the solute ions or molecules accumulated at the interface are adsorbed on the large surface area within the pores of the adsorbent and relatively a few are adsorbed on the outside surface of the adsorbent. Adsorption from aqueous solution is influenced largely by the competition between the solute and solvent molecules for adsorption sites. The tendency of a particular solute to get adsorbed is determined by the difference in the adsorption potential between the solute and solvent when the solute- solvent affinity is large. In

general, the lower the affinity of adsorbent for the solvent, the higher will be the adsorption capacity for solutes. Many factors influence the rate of adsorption and extent to which a particular solute can be adsorbed. Some more important factors like nature of adsorbent and adsorbate, concentration, extent of agitation, P^H, temperature, contact time etc. also affect the rate of adsorption.

Lead has been ranked as 2nd in the Environmental Protection Agency's "*Top Hazardous Substance Priority List"*. It is a soft, malleable metal and accounts for most of the cases of pediatric heavy metal poisoning. It has been used in pipes, drains and soldering materials for many years. Every year, industry produces about 2.5 million tons of lead throughout the world. Most of this lead is used in batteries. Reminder is used for cable covering, plumbing, ammunition, and as fuel additives. Target organs are the bones, brain, blood, kidneys and thyroid glands.

Cadmium has been ranked as 7th in the *"Top Hazardous Substance Priority List".* Remarkable characteristics of cadmium involves its great resistance to corrosion, low melting point and excellent electrical conductivity because of which it plays a critical role in several cutting edge technologies such as solar cells. Cadmium is one of the few elements that have no constructive purpose in the human body. The exposure to Cd^{2+} has been associated with renal damage, osteoporosis, prosthetic and liver cancer.

In the present study, the adsorption potential of all the prepared samples was evaluated for the adsorption of Cd^{2+} and Pb^{2+}.

5.1.3. EXPERIMENTAL SET UP -BATCH TYPE CONTACT METHOD

In the present study, the adsorption of heavy metal ions namely Pb(II) and Cd(II) on the nanomaterials have been studied by batch type contact method. Experiments were carried out in a thermostatic water bath shaker at 150 rpm at a particular temperature for predetermined time intervals using 100m1 clean and dried stoppered bottles. The adsorption conditions for the adsorbents were optimized by varying the experimental parameters such as contact time, pH, initial concentration of adsorbate, temperature and adsorbent dose. The metal ion concentrations in liquid phase were measured using atomic absorption spectroscopic studies *(Perkin-Elmer, PinAAcle900 H).*

Metal ion solutions of Pb(II) and Cd(II) of 1000 ppm concentration were prepared and the desired concentrations were taken and used as adsorbates. The amount of metal ions adsorbed in mg/g at equilibrium (q_e) was calculated from the mass balance of initial and final metal concentrations in the aqueous phase. The amount of metal ion adsorbed at time qe was calculated from mass balance equation [86].

$$qe = \frac{(Co - Ce)V}{m} \quad (5.1)$$

where qe is the adsorbed metal ions per unit mass of adsorbent(mg/g), V is the sample volume in L and m is the weight of the adsorbent.

The removal efficiency of various adsorbents was calculated by using the equation,

$$\% \text{ removal } = \frac{(Co - Ce)}{m} X100 \quad (5.2)$$

where, Co and Ce are the initial and the equilibrium concentrations of heavy metal ions.

The quantity of metal ions adsorbed at selected time intervals was determined and used for kinetic analysis.

Recovery of the adsorbent through regeneration of its adsorption properties is an economic necessity in reference to the practical applications of treatment of waste water effluents. To examine this practical side experiments pertaining to adsorbent regeneration and metal readsorption were carried out in six consecutive cycles. Desorption efficiency of the spent adsorbents was checked with HCl solutions having different concentrations ranging from 0.001 to 0.1 M. After each adsorption-desorption cycle, the adsorbents were washed thoroughly with ultrapure water to neutrality and reconditioned for adsorption in the succeeding cycle and the adsorption/desorption procedures were repeated for several times. Once equilibrium was reached, the adsorbents were separated and the metal ions in the concentrated supernatant solution were analyzed using Atomic Absorption Spectroscopy (AAS).

5.1.4. KINETICS STUDIES

The feasibility of adsorption reactions and applicability of the prepared adsorbents were evaluated by kinetics studies. The most commonly used kinetic expressions to explain the solid/liquid adsorption processes are the pseudo first order kinetic and pseudo second-order kinetic models. The adsorption kinetic data were described by the Lagergren pseudo-first-order model, which is the earliest known equation describing the adsorption rate based on the adsorption capacity. In the present study the pseudo-first-order rate equation is written in the exponential form,

$$q_t = q_e(1 - {}_e - k_1{}^t) \qquad (5.3)$$

where q_e and q_t are the amounts of adsorbate adsorbed (mg/g) at equilibrium and at contact time t (min) respectively and k_1 is the pseudo-first-order rate constant (min^{-1}). Parameters of the pseudo-first-order are evaluated from the experimental data using non-linear curve fitting procedure. The Pseudo-second-order kinetic model [87] can be represented in the following form,

$$q_t = \frac{k_2 q_e^2 t}{1 + k_2 q_e t} \qquad (5.4)$$

where k_2 is the rate constant of adsorption (mg/g min), t is the reaction time, qe and qt are the amounts of solute adsorbed per unit mass of the adsorbent at equilibrium and at time *t* respectively. Parameters of the pseudo-second-order are also evaluated from the experimental data using non-linear curve fitting procedure.

5.1.5. ISOTHERM STUDIES

The most conventional and practical method for presenting the adsorption equilibrium data is the adsorption isotherm. Equilibrium relationship between adsorbate and adsorbent are usually determined by the adsorption isotherms, generally the ratio between the amounts of adsorbate adsorbed to the amount of adsorbate remaining in the solution at equilibrium is measured to establish the equilibrium. Isotherms provide a significant amount of information about the adsorbent used and the interaction with the adsorbate in the adsorption process. The theoretical Langmuir adsorption isotherm is

based on three assumptions, namely: adsorption cannot proceed beyond monolayer coverage, all surface sites are equivalent and can accommodate almost one adsorbed atom, and the ability of a molecule to adsorb at a given site is independent of the occupation of neighboring sites. At equilibrium, there is no net charge of surface coverage. The non-linear equation of Langmuir isotherm model is expressed as follows,

$$q_e = \frac{q_m b C_e}{1 + b C_e} \tag{5.5}$$

where q_e and C_e are the equilibrium concentrations when an adsorbate gets adsorbed onto the adsorbent and q_m denotes the maximum adsorption capacity and b is the Langmuir constant. The Freundlich isotherm an empirical equation used to describe adsorption at multilayer and on a heterogeneous surface is represented as,

$$q_e = k_n C_e^{\frac{1}{n}} \tag{5.6}$$

Here, k_n and 1/n are the Freundlich constants. If the 1/n value is less than 1, then it can be assumed that the adsorbent material is heterogeneous in nature. Sips isotherm [88] is a combination of Langmuir and Freundlich isotherm models. At lower adsorbate concentrations, this isotherm follows Freundlich isotherm model (multilayer adsorption) and at higher concentration it predicts Langmuir isotherm (monolayer adsorption). The equation is written as,

$$q_e = \frac{Q_s K_s C_e^{n_s}}{1 + K_s C_e^{n_s}} \tag{5.7}$$

Q_s, K_s and ns are the Sips constants related to adsorption capacity, adsorption equilibrium constant and intensity of adsorption respectively and q_e and C_e are the equilibrium concentrations that are getting evaluated during the adsorption experiments. Parameters of Langmuir, Freundlich and Sips isotherms in the present work were evaluated from the experimental data using non-linear curve fitting procedure.

The kinetic and isotherm model parameters were assessed by nonlinear regression analysis using Origin 9, software. The model parameters were determined by minimizing the distance between the experimental data points and the model predictions. The degrees of fitness of the models with the experimental data were determined using Chi-square test (x^2) given by:

$$x^2 = \sum_{i=1}^{n} \frac{\left(q_{exp-q_{cal}}\right)^2}{q_{cal}} \qquad (5.8)$$

where q_{exp} and q_{cal} correspond to the experimental and model data and m is the number of observations in the experiment. If data from model are similar to the experimental data, x^2 will be a smaller number.

A dimensionless constant, R^2 indicates the adsorption nature to be either unfavourable ($R^2 > 1$), linear ($R^2 = 1$), favourable ($0 < R^2 < 1$) or irreversible ($R^2 = 0$).

5.2. ADSORPTION STUDIES OF NANO ZnO

Present study focuses on the feasibility of synthesized ZnO as high efficient adsorbents for the removal of Lead ions (Pb(ll)) and Cadmium ions (Cd(ll)) from aqueous solutions. The effect of various operational conditions such as pH, adsorbent dosage and contact time was systematically studied.

The effect of pH on the adsorption capacity of metal ions such as Pb(ll) and Cd(ll) was evaluated in a pH range of 2.0 to 9.0 by agitating 100 ppm metal ion solution with 0.1g of ZnO. From Figure 5.2 it is observed that the percentage of adsorption of metal ions increased with increase in the solution pH. The low adsorption in the acidic region can be attributed to the competition between hydrogen and metal ions for the same sites. The increase in pH makes the ZnO surface more negative, thus enhancing electrostatic interactions between metal ions and the adsorbent, resulting in higher retention of metal species.

In the case of lead it exists as Pb^{2+}, $PbOH^{+}$ and $Pb(OH)^{3-}$ depending on pH. At lower pH value, low metal ion uptake was observed. At low pH values, the adsorbent is positively charged due to the presence of H^{+} ions on its surface and hence offers repulsive force to approaching Pb^{2+}ions. However, more Pb^{2+} uptake is observed as the pH increases which are due to the fact that at high pH values, lead still has a net positive charge but exists as $PbOH^{+}$ while most active sites on the adsorbent are deprotonated. This leads to net attractive force that is responsible for high Pb removal from solution. But at elevated pH values i.e, in strong basic region, the uptake of metal ions decreased, may be due to the hydroxide formation. In the present study the removal efficiency is found to increase with pH and attained maximum at pH 6 and then it was found to decrease.

The pH of the solution was found to have a great effect on the adsorption of Cd(II)ions also. The adsorption increased sharply with pH and attained almost a constant value from pH 8 onwards and then showed a slight decrease in adsorption level [Figure 5.2]. The hydrolysis and precipitation of metal ions affect adsorption by changing the concentration and form of soluble metal species those are available for adsorption. Depending upon the pH of the solution, various species of cadmium can be formed during the hydrolysis. The hydrolysis extent of Cd(II) ions is unimportant up to approximately pH 8 and cadmium is in the form of Cd(II) ions at this pH**.**

After each adsorption process, the final pH of the solution was recorded. It was found that after adsorption pH of the solution was lower compared to initial pH. This decrease in pH is an indication for ion exchange mechanism for removal of metal ions and the adsorption of metal ions onto ZnO surface by the release of H+ ions.

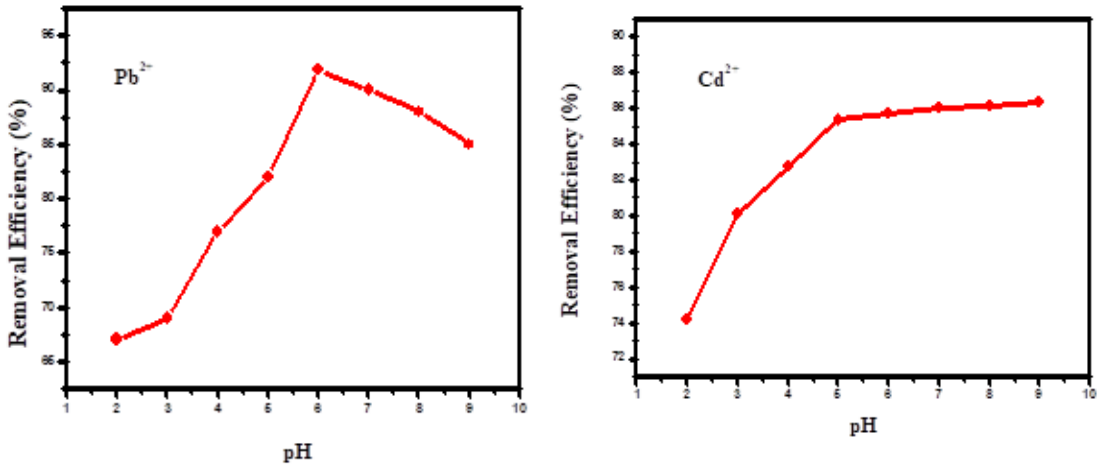

Figure 5.2 Removal efficiency *vs* pH for Pb(ll) and Cd(ll)

The dependence of adsorbent dosage on metal ion adsorption was studied by varying the amount of adsorbents from 0.025 to 0.2mgL^{-1}. From Figure 5.3 it can be observed that the removal efficiency of the adsorbents are enhanced by raising the adsorbent dosage and reached a saturation level at higher dosage. This is expected due to the fact that at higher concentrations of adsorbents greater is the availability of exchangeable sites for the ions. But increase in dosage beyond a certain level results in no further increase in adsorption, may be due the fact that the amount of ions bound to the adsorbent and the amount of free ions in the solution remains constant[89].

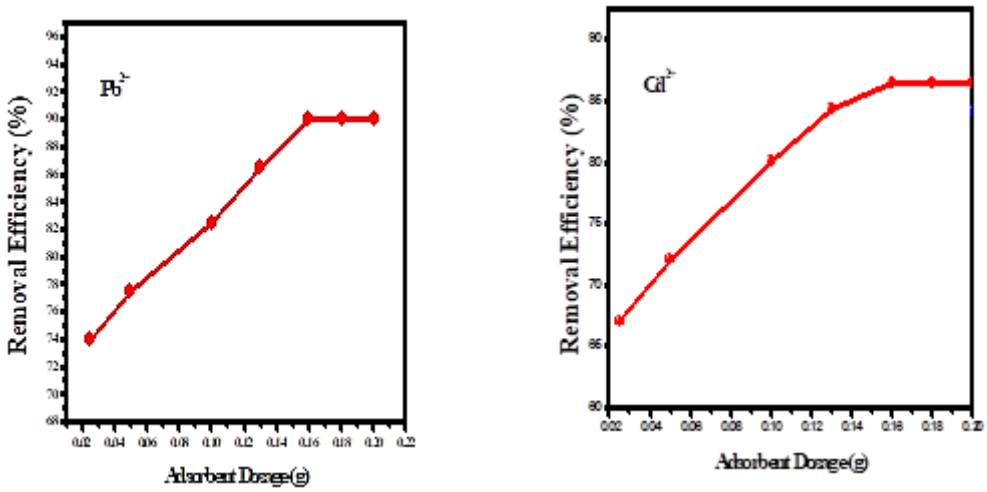

Figure 5.3 .Removal Efficiency *vs* adsorbent dosage for Pb(ll) and Cd(ll)

The dependence of adsorption capacity of nano ZnO on the initial concentrations of Pb(ll) and Cd(ll) ranging between 50 to 200mg/L using 0.1 gm of the adsorbent is represented in Figure5.4 The adsorption capacities increased steadily with increase in metal ion concentrations. The increase in the concentration gradient acts as a driving force for the adsorption process. When the concentration of metal ions increases, the active sites of ZnO are surrounded by more metal ions, and the number of metal ions competing for available binding sites increases leading to an increased uptake of metal ions from the solution. Therefore the value of q_e increased with increase of initial metal ion concentration (C_0). The results also show that adsorption capacity for Pb(ll) is slightly more than Cd(ll) which could be attributed to the higher electro negativity of lead (2.33) than cadmium (1.69), which results in a stronger affinity for the metal oxides (Sheela *et al.*, 2012).

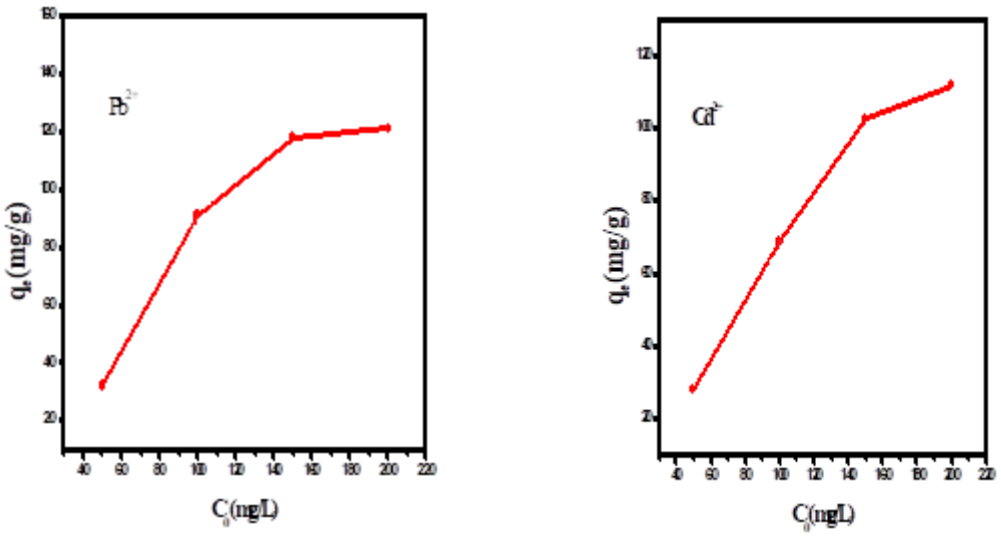

Figure 5.4 .Adsorption efficiency vs initial metal ion concentrations for Pb(ll) and Cd(ll)

The kinetic data were analyzed using the pseudo-first-order and pseudo-second-order kinetic models [Figure 5.5]. The pseudo-first-order and pseudo-second-order kinetic parameters were estimated from the experimental data using non-linear curve fitting procedure and the results are given in Table 5.1 .The pseudo-first-order equation showed a poor correlation with experimental data, whereas the pseudo-second-order equation indicated a good correlation as indicated by a lower value of $\chi^2$and higher value of R^2(nearing unity). In addition, q_e, which is the adsorption capacity, agreed very well with both the experimental and calculated values. The kinetic data indicates that the adsorption process is controlled by pseudo second- order equation. Also, this suggests the assumption behind the pseudo-second-order model that the metal ion uptake process is due to chemisorptions involving valence forces through the sharing or exchange of electrons between adsorbent and adsorbate.

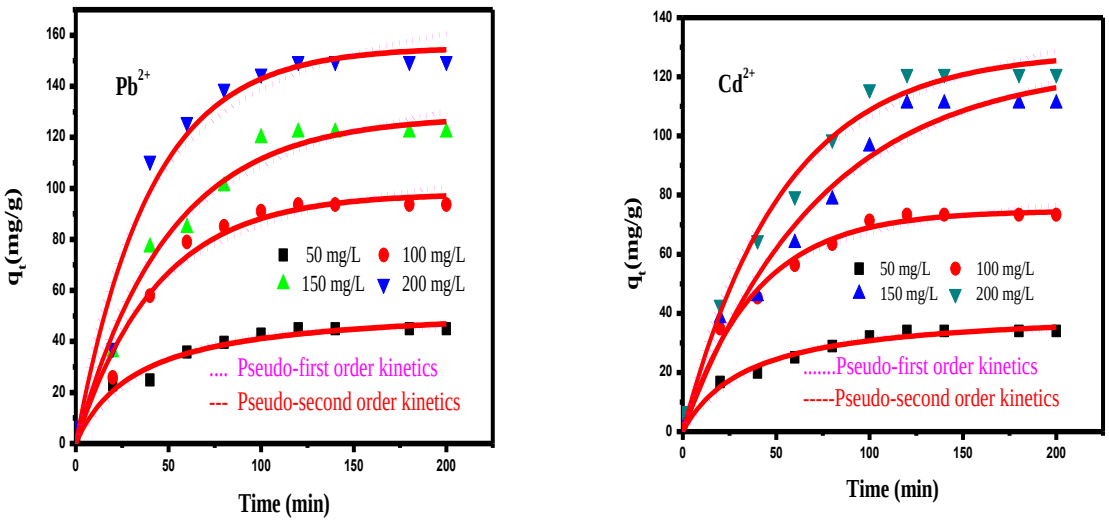

Figure 5.5.Kinetic plots for Pb(ll) and Cd(ll)

Table 5.1 Kinetic parameters for the adsorption of Pb(ll) and Cd(ll)

Metalion	**q_e(mg/g)**	**Pseudo-first-order**				**Pseudo-second-order**			
	Exp	q_e(mg/g)	k_1/min	R^2	χ^2	q_e(mg/g)	k_2 min^{-1}	R^2	χ^2
Pb(ll)	44.98	54.6	0.02	0.96	3.5	45.82	$0.5x10^{-4}$	0.96	0.61
	93.65	122	0.02	0.97	6	97.99	$0.1x10^{-4}$	0.95	0.23
	121.91	162.11	0.02	0.98	8	128.32	$0.1x10^{-4}$	0.96	0.57
	149.87	190.61	0.01	0.95	9	155.32	$0.1x10^{-4}$	0.99	0.17
Cd(ll)	34	41.44	0.02	0.96	3.5	34.59	$0.6x10^{-4}$	0.96	3.21
	73.33	89.66	0.02	0.98	8	74.69	$0.3x10^{-4}$	0.98	3.62
	110.91	163.65	0.01	0.96	4.7	124.22	$0.4x10^{-4}$	0.95	5.71
	121	168.81	0.01	0.98	2.9	128.47	$0.1x10^{-4}$	0.97	4.62

The adsorption of metal ion on ZnO was examined by well –known models to interpret equilibrium isotherm data. The experimental and model fits of Langmuir, Freundlich and Sips isotherms of Pb(ll) and Cd(ll) adsorption onto nano ZnO are shown in Figure 5.6. The isotherm constants were calculated using nonlinear regression analysis and the results are listed in Table 5.2. Here also the values of R^2 and χ^2 showed that the adsorption of metal ions onto ZnO was best fitted with Sips isotherm model over the concentration ranges studied. Sips isotherm model is a combination of

Langmuir and Freundlich adsorption isotherm models. At higher concentration Sips favors Langmuir model while at lower concentration it favors Freundlich model. The R^2 values for all the three isotherms models were beyond 0.99 which indicate the suitability of models in explaining adsorption mechanism. Lower value of χ^2 and higher value of R^2 show a very good mathematical agreement with Sips isotherm model. Sips isotherm gives the idea of multilayer adsorption at lower concentration and monolayer at higher concentration of the metal ion.

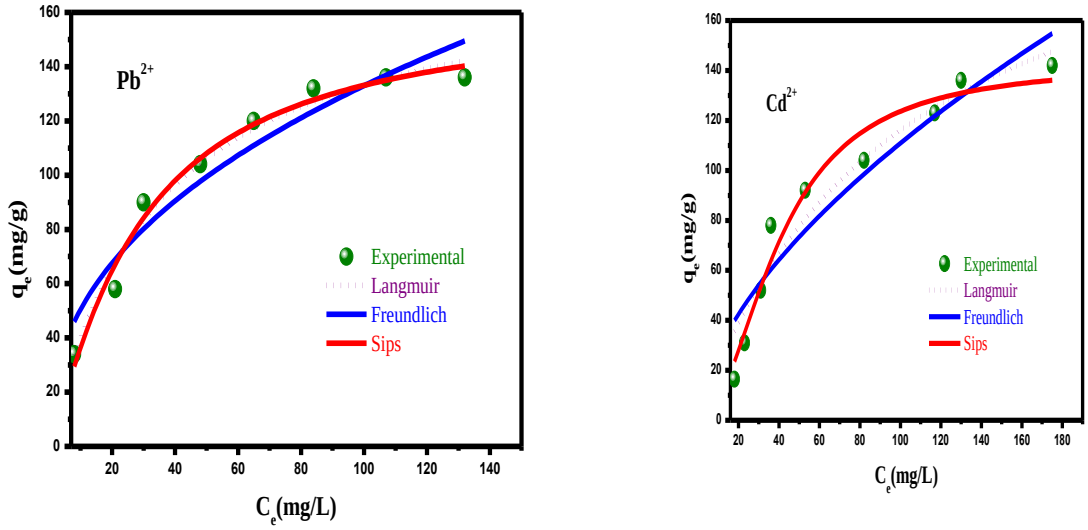

Figure 5.6. Experimental and model fits of Langmuir, Freundlich and Sips isotherms of Pb(ll) and Cd(ll) adsorption onto nano ZnO

Table 5.2. Langmuir, Freundlich and Sips isotherm constants for the adsorption of Pb(ll) and Cd(ll) onto ZnO

Metal ions	Langmuir				Freundlich				Sips				
	q_m mg/g	b L/mg	R^2	χ^2	k_F mg $^{1-1/n}L^{1/n}/g$	1/n	R^2	χ^2	Q_s mg/g	K_s L/mg	$1/n_s$	R^2	χ^2
Pb(ll)	166.67	0.19	0.99	4.5	44.47	0.27	0.98	2.0	169.23	0.10	0.73	0.99	1.1
Cd(ll)	130.62	0.01	0.93	14	7.12	0.59	0.88	2.2	149.21	0.005	2.03	0.95	8.3

In the present work the maximum adsorption capacity obtained using ZnO for Pb(II) adsorption was 169.23 mg g^{-1} and for Cd(II)it was 149.21 mg g^{-1} under optimum conditions. It is found that the metal ion adsorption capacity of ZnO synthesized by green protocols is significantly higher than conventionally synthesized ZnO [89].This result suggests that the ZnO prepared in the present study can be considered as a promising material for the removal of heavy metal ions from industrial waste water.

The desorption capacity of the prepared ZnO was checked with HCl having different concentrations, ranging from 0.001 to 0.1 M. It was observed that the adsorbed Pb(ll) and Cd(ll) could be desorbed from the spent adsorbent using 0.1 M HCl and hence it could be used for the regeneration of nano ZnO. The adsorption–desorption process was carried out for six cycles with 0.1M HCl[Figure 5.7] and it was found that there was only a slight decrease in the adsorption capacity with respect to the regeneration cycles. However desorption capacity decreases to some extent because of the possible penetration of metal ions into inner cavities (pore diffusion or intraparticle diffusion).Therefore, it could be included in the list of very effective adsorbent for Pb(ll) and Cd(ll) in real process such as industrial waste water treatment.

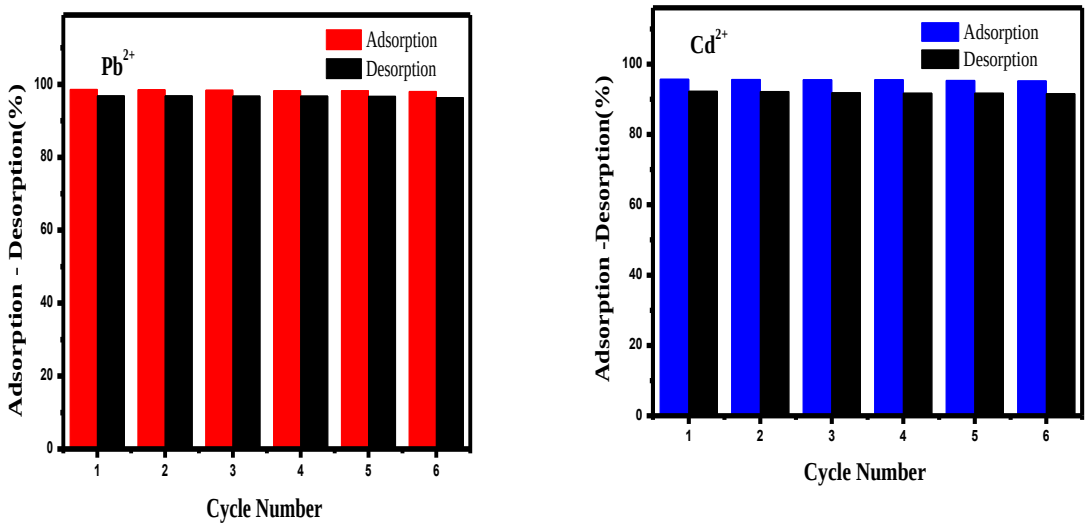

Figure 5.7: Adsorption –desorption cycles for Pb (ll) and Cd (ll)

The practical efficiency and effectiveness of the adsorbents prepared were tested with industrial waste water. The collected waste water sample had Pb(ll) and Cd(ll) concentrations higher than the acceptable concentration for drinking water.

Batch experiments conducted with industrial waste water showed that higher amount of adsorbent was needed compared to original metal ion solution. This discrepancy was due to the competitive adsorption of matrix ions with binding sites/screening effect by other metal ions.

5.3. ADSORPTION STUDIES OF NANO CuO

The Synthesised Nano CuO was analyzed for the adsorption properties towards Pb(ll) and Cd(ll). The effect of pH on the adsorption of Pb(ll) and Cd(ll), nano structured CuO at a pH range of 2 to 12 are shown in Figure 5.8. From the figure it is observed that the percentage of adsorption of metal ions increased with increase in the solution pH of the adsorbent. This study show that the maximum adsorption occurs at a pH of 7 for Pb(ll) and 9 for Cd(ll) onto CuO nanomaterial .

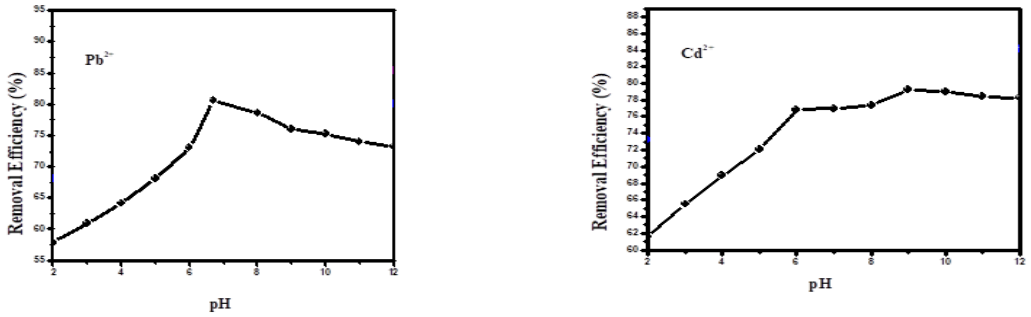

Figure 5.8.Removal efficiency *vs* pH for Pb(ll) and Cd(ll)

From the Figure 5.9 it is clear that as the adsorbent dosage increases the removal efficiency of Pb(ll) and Cd(ll) ions also increases .The results show the amount of adsorption increased with adsorbent concentration from 0.025 g to 0.1 g and from 0.1 g onwards the adsorption percentage had attained an equilibrium level. Since the synthesized CuO have high surface area, hence minimum amount is required for maximum removal of metal ions from solutions.

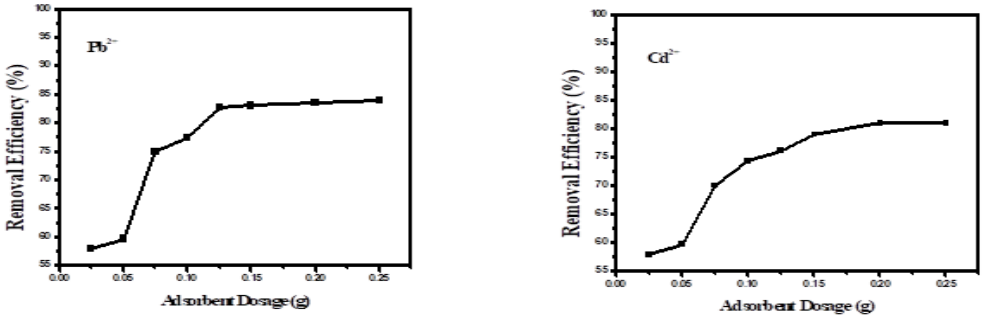

Figure 5.9.Removal Efficiency *vs* adsorbent dosage for Pb(ll) and Cd(ll)

The kinetic data were analyzed using the pseudo-first-order and pseudo-second-order kinetic models[Figure 5.10].With the increase of initial metal ion concentration from 50 to 200 mg/L, the adsorption capacity was found to increase from 32.99 to 138.43 for Pb(ll) and from 28.30 to128.64 mg/g for Cd(ll),indicating that adsorption depends on the initial metal concentration [Table 5.3].The kinetic data indicates that the adsorption process is controlled by pseudo second- order kinetics.

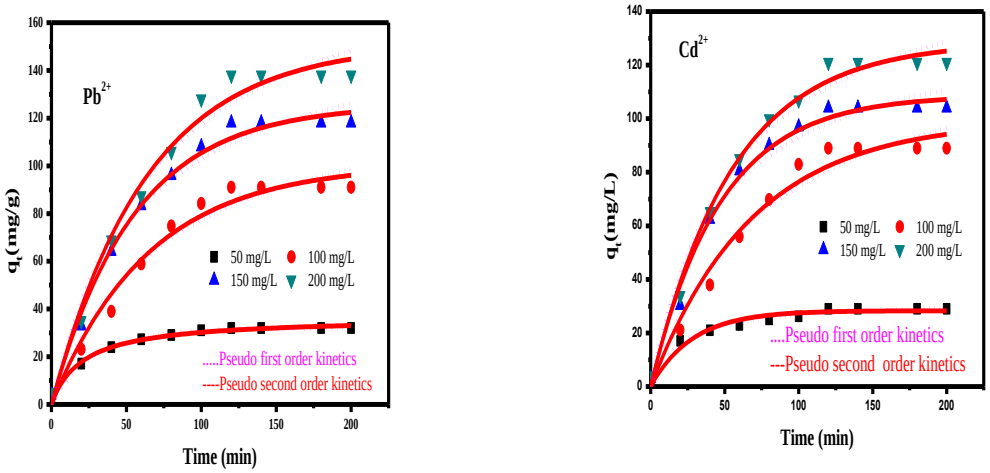

Figure 5.10. Kinetic plots for Pb(ll) and Cd(ll)

Table 5.3. Kinetic parameters for the adsorption of Pb(ll) and Cd(ll) onto CuO

Metal ion	q_e (mg/g)	Pseudo-first-order				Pseudo-second-order			
	Exp	q_e(mg/g)	k_1/min	R^2	χ^2	q_e(mg/g)	k_2 min^{-1}	R^2	χ^2
Pb(ll)	32.05	31.92	0.03	0.97	0.85	32.99	$0.7x10^{-4}$	0.99	0.98
	90.95	80.61	0.01	0.97	0.15	91.09	$0.6x10^{-4}$	0.98	0.96
	118.09	105.66	0.01	0.99	0.24	120.21	$0.4x10^{-4}$	0.99	0.36
	132.21	111.23	0.01	0.98	0.41	138.43	$0.2x10^{-4}$	0.99	0.69
Cd(ll)	29.86	32.29	0.001	0.96	0.25	28.30	$0.9x10^{-4}$	0.98	0.98
	88.93	135.55	0.09	0.97	0.24	99.47	$0.4x10^{-4}$	0.99	0.65
	104.96	136.79	0.02	0.97	0.12	108.76	$0.1x10^{-4}$	0.99	0.33
	121.64	166.42	0.01	0.98	0.15	128.64	$0.1x10^{-4}$	0.99	0.36

The experimental and model fits of q_e and C_e corresponding to various isotherm models for the adsorption of Pb (ll) and Cd (ll) are shown in Figure 5.11.The values of isotherm constants were calculated using non-linear regression analysis and the results are listed in the Table 5.4.

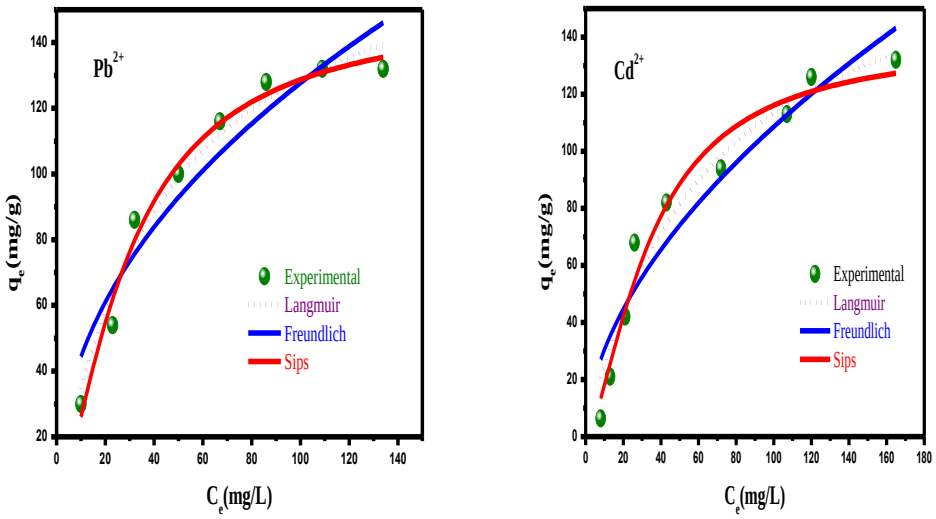

Figure 5.11.Experimental and model fits of Langmuir, Freundlich and Sips isotherms of Pb(ll) and Cd(ll)

Table 5.4. Langmuir, Freundlich and Sips isotherm constants for the adsorption of Pb(ll) and Cd(ll) onto CuO

Metal ions	Langmuir				Freundlich				Sips				
Pb(ll)	q_m mg/g	b L/mg	R^2	χ^2	k_F mg $^{1-1/n}L^{1/n}/g$	1/n	R^2	χ^2	Q_s mg/g	K_s L/mg	$1/n_s$	R^2	χ^2
	150.67	0.02	0.99	4.6	15.43	0.45	0.90	14	172	0.07	1.1	0.99	3.1
Cd(ll)	134.45	0.01	0.95	9.1	8.5	0.55	0.91	18	161	0.004	1.2	0.98	7.3

On verifying the results from Figure 5.11 and Table 5.4, it is clear that the experimental equilibrium data had agreed well with the Sips model. Sips model gave higher Qmax values (172 and 161 mg/g for Pb(ll) and Cd(ll) respectively) than Langmuir model. Lower values of χ^2 and higher values of R^2 show a very good mathematical agreement with Sips isotherm model.

5.4. ADSORPTION STUDIES OF NANO CELLULOSE (NC), NC/CuO & NC/ ZnO

5.4.1. EFFECT OF pH ON ADSORPTION

Adsorption behaviour of Nano Cellulose (NC) and its composites for Pb (II) and Cd(II) were studied through experimental procedure as detailed earlier. The uptakes of metal ions were found to be dependent on pH of the solution and amount of adsorbent.

The effect of pH on adsorption of Pb (II) and Cd (II) was conducted over a range of pH 3 to 9. The metal removal efficiency increases with increase in pH (Figure 5.12). For Pb (II), the maximum removal efficiency was observed at pH 6 for NC and all the composites. For Cd (II), the highest removal efficiency was obtained for pH 6 for NC and pH 7 for NC/CuO and NC/ZnO respectively. This change in the optimum pH of composites is attributed to the surface property of the respective metal oxide.

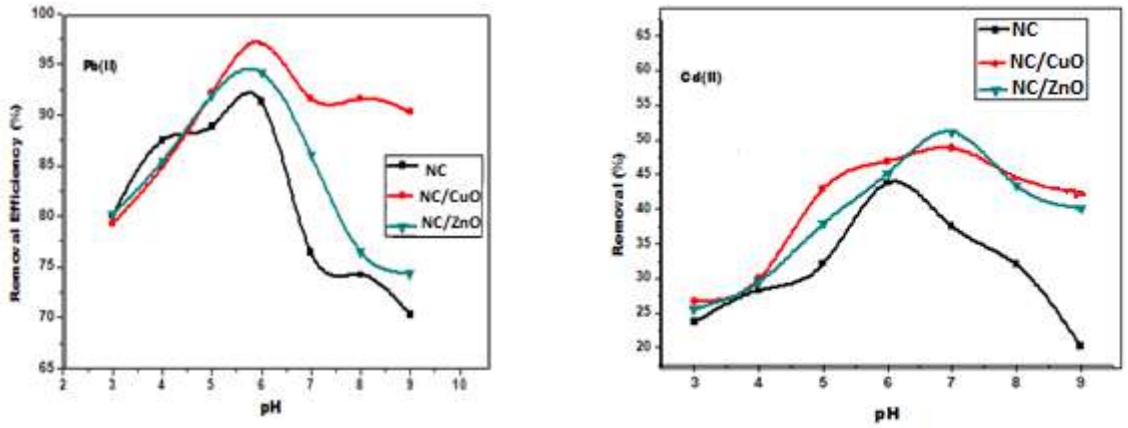

Figure 5.12 Effect of pH on the adsorption of Pb (II) and Cd (II) on NC, NC/CuO, and NC/ZnO

The effect of adsorbent dose on the adsorption efficiency of the prepared materials is shown in Figure 5.13.

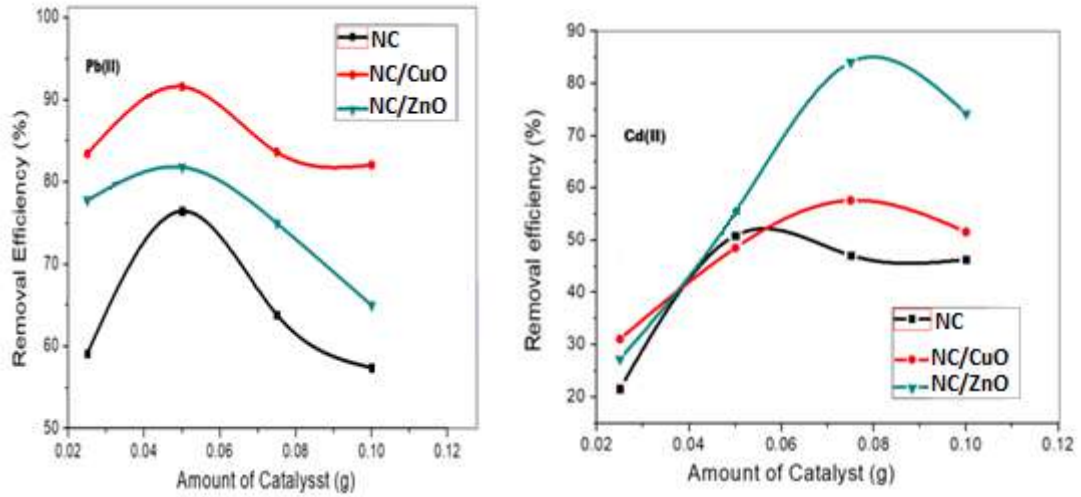

Figure 5.13 Effect of adsorbent dose on adsorption

The removal efficiency increases with adsorbent dose for both NC and composites. The optimum dose of catalyst for Pb (II) adsorption is 0.05g. But in the case of Cd (II), this dose is 0.05g for NC and 0.075g for composites (figure 5.14)

Table 5.5 shows a comparison of adsorption efficiencies of individual metal oxides, NC and composites. It is clear from the table that, almost complete adsorption of Pb (II) is possible using nano ZnO and its cellulose composite NC/ZnO under optimum conditions. It is found that the efficiency of the NC-Zinc Oxide composite (NC/ZnO) is enhanced considerably compared to NC and individual metal oxide. This may be due to the large surface area of the composite. The percentage removal of Cd

(II) by these materials is comparatively less than Pb (II). This may be due to the high electro negativity of lead (2.33) compared to cadmium (1.69), which increases the affinity of Pb for the surface of the metal oxides or composites.

Table 5.5 Comparison of Adsorption Efficiencies of Metal Oxides, NC and its Composites

Material	SA (m^2/g)	Pb (II)		Cd (II)	
		pH	% Removal	pH	% Removal
CuO	26.3	6	95	7	89
ZnO	93.66	7	99	6	95
NC	40.2	6	90	6	50
NC/CuO	52.6	6	95	7	55
NC/ ZnO	150.8	6	99	6	70

Table 5.6 reveals the parameters of Pb (II) and Cd (II) adsorption for first order and second order kinetics. Here also R^2 is more close to unity for pseudo- second order kinetics suggesting chemisorptions through the sharing or exchange of electrons between adsorbent and adsorbate.

Table 5.6 Kinetic parameters for the adsorption of Pb (II) and Cd (II) on NC, NC/CuO and NC/ZnO

Metal ion	Pseudo- first order						Pseudo – second order			
	Sample	Expq_e (mg/g)	q_e (mg/g)	k_1 min^{-1}	R^2	χ^2	q_e (mg/g)	k_2 $M^{-1}min^{-1}$	R^2	χ^2
Pb (II)	NC	23	26	0.04	0.93	32	25	0.004×10^{-4}	0.98	2.3
	NC/CuO	34	36	0.01	0.94	18	33	0.001×10^{-4}	0.99	1.9
	NC/ZnO	18	20	0.04	0.94	13	18	0.004×10^{-4}	0.98	1.6
Cd (II)	NC	11	9.7	0.01	0.93	21	10	0.001×10^{-4}	0.98	1
	NC/CuO	22	23.45	0.05	0.94	31	22	0.004×10^{-4}	0.97	1.9
	NC/ZnO	15	16.46	0.01	0.94	3	14	0.005×10^{-4}	0.98	1.6

CHAPTER - VI

PHOTODEGRADATION OF DYES

6.1. INTRODUCTION

Environmental pollution by hazardous waste materials is becoming the global serious problem which is mainly due to rapid industralisation and population growth. Dyes are the major organic pollutants used in textile industries. The sewages from textile industries standpoint a prime intimidation to water bodies owing to the discharge of dyes. In a single dyeing procedure, large number of dyes from different classes of chemical substances can be used and the resulting sewage containing a complex mixture of coloured, potentially toxic compounds. The colour in the water may be either from natural phenomenon or from artificial phenomenon such as the disposal of dyes effluents. Light is necessary for the proper functioning of aquatic lives and the presence of dyes in water prevents the penetration of light into water resulting an imbalance in aquatic life. Organic dyes are chemically and biologically stable and are difficult to remove by natural degradation. Eradication of these dyes by physical methods such as filtration, adsorption and coagulation are very effective but large amount of coagulated wastes are produced. In the case of chemical treatment, incomplete mineralization occurs resulting the production of toxic and carcinogenic by-products. The simplest, low cost biological methods are beneficial but they are not effective as these dyes are resistant to aerobic biodegradation. Semiconductor photo catalysis is considered to be the most efficient process for the removal of dyes from contaminated water. From the reported works, it was confirmed that ZnO and CuO exhibits better efficiency for the photo degradation of dyes even in aqueous solution. Due to the large band gap energies of ZnO and CuO, they can be excited under an ultra violet irradiation, which only accounts for less than 5% of the whole solar spectrum. This has stimulated the scientific community to develop photo catalysts with a reduced band gap energy (Eg) to enhance the response to the more abundant visible light photons. Various modified ZnO and CuO materials have been fabricated as the visible light driven photocatalysts. Titanium dioxide nanoparticles have been widely premeditated for the photodegradation of organic pollutants. Advance studies have shown that ZnO may have a similar efficiency of photodegradation and is a better

substitution for TiO_2 in many applications. The main disadvantage of nanosized particles are their recyclability and their low adsorption ability for organic pollutant. Doping of these nanoparticles with polymeric substrates is highly recommended for wider practical applications.NC can be well-thought-out as a latent ancillary material to develop the adsorption and removal efficiency of the photocatalysts, in addition to its role in the adsorption of the organic pollutants, which increases the possibility of interaction between the catalyst and the pollutant. To observe the efficiency of the fabricated photo catalysts for the degradation of dyes, an anionic dye Congo Red (CR) and a cationic dye Malachite Green (MG) was selected. To demonstrate the potential applications of ZnO/NC and CuO/NC composites in waste water treatment, their photocatalytic activities in the degradation of CR and MG has been investigated and their activities has been compared with pure ZnO and CuO nanoparticles.

6.1.1. CONGO RED (CR)

Congo red, a benzidine based anionic dye having two azo (N=N) groups as chromophores and is the sodium salt of 3, 3'-([1,1'-biphenyl]-4, 4'-diyl) bis (4-aminonaphthalene-1-sulfonic acid). CR is a secondary diazo dye widely used in textile industries and is soluble in water yielding as a red colloidal solution. It has strong, non-covalent affinity to cellulose fibres.CR has a strong tendency to change colour when touched by sweaty fingers. So CR in cellulose industries has long been abandoned.CR easily metabolizes into harmful human carcinogen benzidine when reaches the environment. The structure of congo red is given in **Figure6.1.**

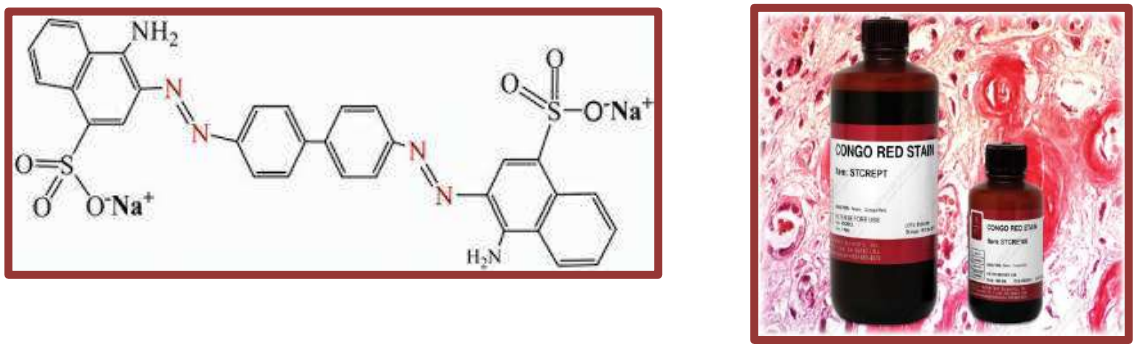

Figure 6.1. Structure of Congo Red

UV-Visible absorbance spectra of congo red is shown in **Figure 6.2**. There are two absorption peaks at 498 nm and 344 nm.

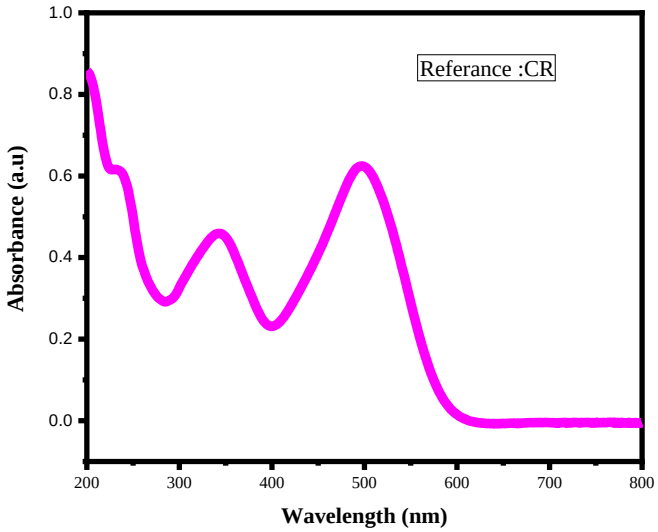

Figure 6.2.Absorbance spectrum of CR

6.1.2. MALACHITE GREEN (MG)

MG a broadly established cationic triphenylmethane dye and formally refers to the chloride, oxalate salt. The chloride and oxalate ions have no significance effect on colour of MG and the colour is mainly due to the strong absorption band at 620 nm.MG is commonly used as fungicide, antiseptic and in textile industries and is destructive to the immune and reproductive systems due to its potential genotoxicity and carcinogenicity and the structure of MG is shown in **Figure 6.3**.

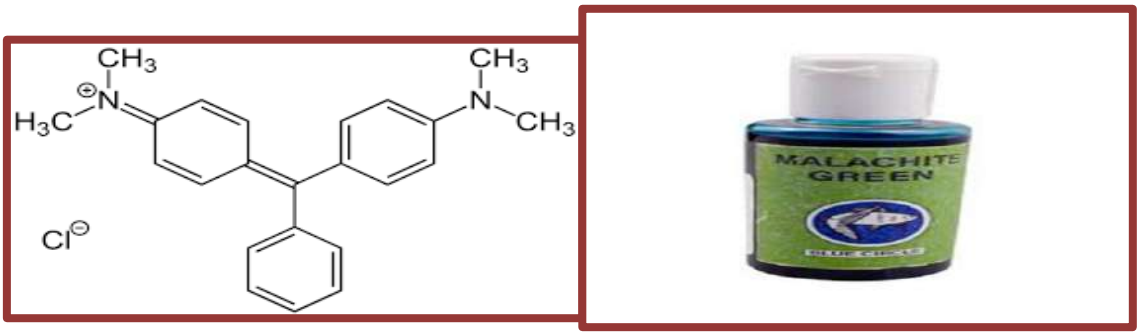

Fig 6.3. Structure of Malachite Green

UV-Visible absorbance spectra of pure malachite green solution shows peaks at 369 and 616 nm. (**Figure 6.4**)

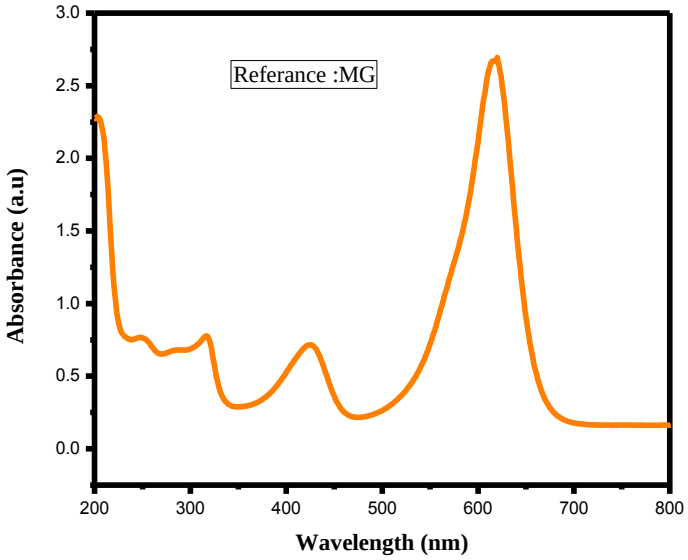

Figure 6.4.Absorbance spectrum of MG

6.2. PHOTOCATALYTIC DEGRADATION OF CONGO RED (CR) AND MALACHITE GREEN (MG)

In order to investigate the effect of the presence of various photocatalysts for the photodegradation of the dyes CR and MG in aqueous solution, a typical experiment was set up using 0.1g of ZnO/NC for the photodegradation of dye CR of 25 ppm concentration at pH 7 using different experimental sets:(i) Visible light irradiation only (ii) photocatalyst only in the dark (iii) visible light in the presence of photocatalysts at a time interval of 30 minutes.

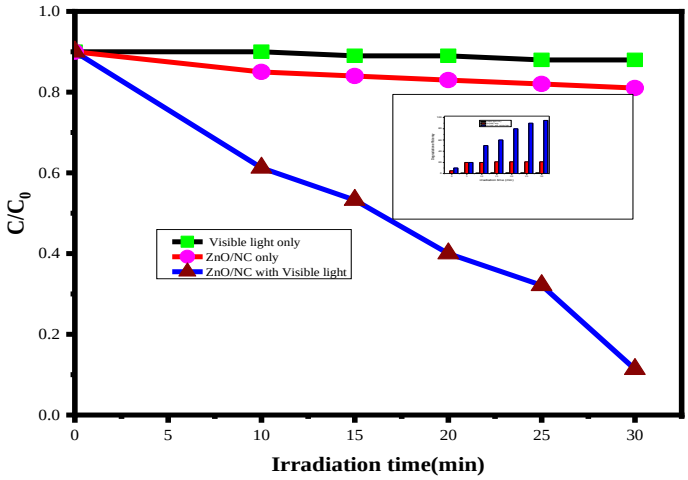

Figure 6.5.Photodegradation of CR using visible light only, ZnO/NC only and ZnO/NC with visible light

Photodegradation of CR using visible light, ZnO/NC and ZnO/NC with visible light are carried out and the results are shown in **Figure 6.5**. From the figure, it is clear that, in the absence of photocatalyst, even though CR is irradiated with visible light over a long period of time, the molecule does not reveal any sign of degradation. Results also showed that the degradation of CR is very slow when only pure ZnO/NC particles are present in the medium. However, the results show that CR undergoes a rapid degradation under visible light in the presence of ZnO/NC.

6.2.1. EFFECT OF THE OPERATING PARAMETERS

To optimise various factors affecting the photocatalytic degradation of dyes, factors like time, amount of catalyst, pH and dye concentration have been systematically studied.

6.2.1.1. EFFECT OF TIME ON DEGRADATION

The time dependent UV-Visible absorption spectra of CR and MGon treatment with 0.1gof different photocatalysts of concentration 25ppm at pH 7under visible light irradiation for different time intervals are shown in **Figure 6.5.1**.The photocatalytic degradation efficiency of ZnO and CuO for the degradation of CR after a time interval of 120 minute was found to be 88% and72% respectively.NC shows a maximumof52%after a time interval of 120 minute. The percentage degradations efficiency of CR with sample ZnO/NC after 120 minutes was found to be higher (99.2%) compared to CuO/NC(95%).

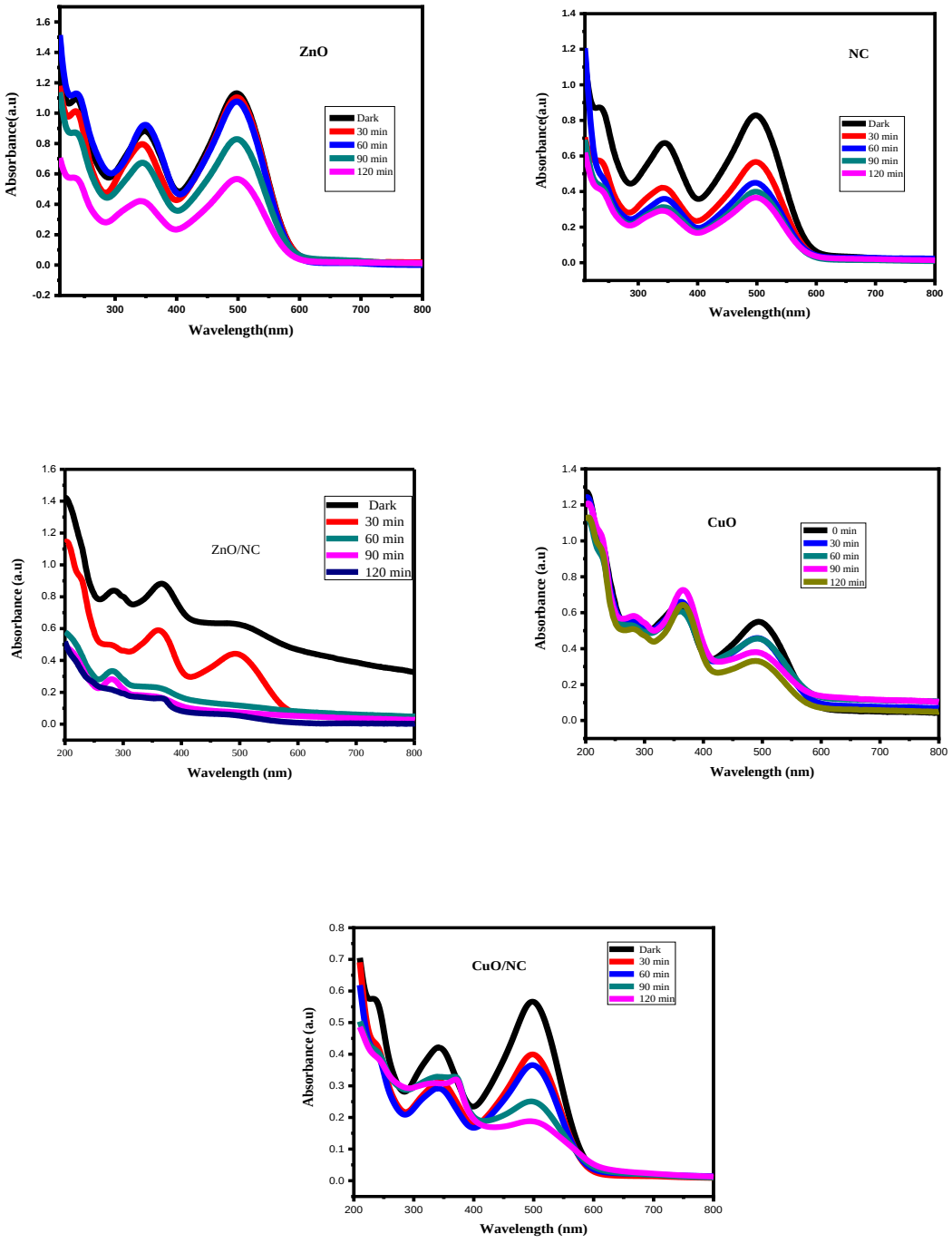

Figure 6.5.1. Time dependent absorption spectra of congo red dye under visible light irradiation with(a)ZnO (b)NC (c) ZnO/NC (d)CuO (e) CuO/NC

In the case of photo degradation of MG (**Figure 6.5.2**), the photodegradation efficiency of NC after 120 minute was found to be 68% whereas for ZnO and CuO it was found to be 89% and 80%. But in the case of ZnO/NC and CuO/NC, at a time

interval of 120 minutes, the photodegradation efficiency was found to be 99.9% and 96% respectively.

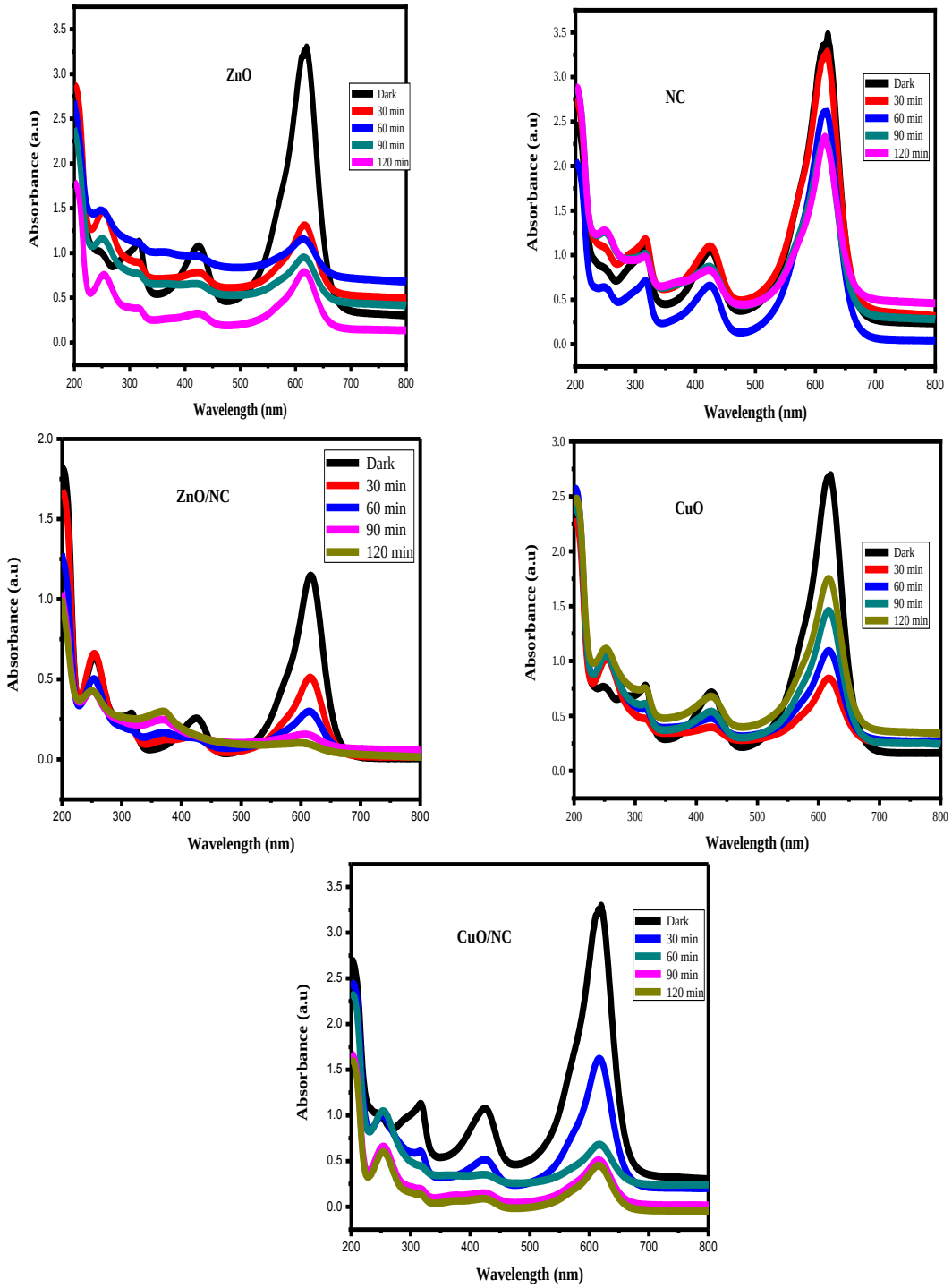

Figure 6.5.2. Time dependent absorption spectra of Malachite Green dye under visible light irradiation with (a)ZnO (b)NC (c) ZnO/NC (d)CuO (e) CuO/NC

ZnO has a large number of oxygen vacancies, and these defect centers will enhance the photodegradation efficiency. Also, the decreased band gap energy and increased surface defects will augment the degradation efficiency of ZnO under visible light. The synthesized CuO have flower like morphology and it is composed of tiny petals with dominant (111) facet show comparatively higher surface area and higher photodegradation efficiency. The surface area of CuO is lower than that of ZnO and show comparatively lower photodegradation efficiency. In all the cases NC shows the least photodegradation and it is due to the fact that unmodified NC usually does not exhibit good adsorption performance. Therefore it needs to be explicitly tailored to provide selective and enhanced interactions for a positive outcome. The essential fundamental characteristics of NC include its hydrophilicity, functionalization ability and ease of tenability.

In the case of composites, the solution containing dye and photocatalysts shows rapid decolorisation which is evident from the decrease in intensities of the prominent peaks. The presence of NC in the composites increases the degradation capacity for dyes due to the hydrophilic ability of the cross linked polymer composites. Also, the chemical modification of NC with the metaloxides is able to improve the adsorption capacity of composites due to formation of new functional group and increased active binding sites that support higher uptake of pollutants. The percentage degradation of dyes was highest for zinc oxide incorporated nanocellulose compared with all other photocatalysts. This is due to the large surface area of ZnO/NC which increases the number of photoactive sites leads to increase in photodegradation efficiency. High surface area can actually promote the dye adsorption on the surface of the photocatalyst and lead to faster decomposition by a direct reaction with the photo-induced holes at the surface of the photocatalyst.

With increase in irradiation time, the formation of strong HO• and $O_2^{-2\bullet}$ radicals increases and thus by breaking different bonds in the dyes, lead to its full degradation in the course of time. The percentage degradation efficiency of malachite green was found to be high as compared to CR. CR is associated with the presence of two azo(-N=N-) groups as chromophores and the decolorization of dyes may be due to the initial electrophiliccleavage of this azo bondsin CR which requires high energy than that of MG.Also, in the case of azo dyes, due to the presence of azo bonds molecular weight increases ,which leads to decreased degradation rate of azo dyes. In azo dyes, the more

reactive azo bonds can be oxidized by positive holes or hydroxyl radicals and can be reduced by electrons in the conduction band which results in the decolorisation of the dyes.

6.2.1.2. EFFECT OF pH ON PHOTODEGRADATION

Photodegradation capability of the photocatalyst depends on solution pH. In order to find out the optimum pH conditions for the degradation of CR, pH was studied over a range of 2.0 to 9.0 by setting the concentration of dyes at 25 ppm and a catalyst dosage as 0.1g with visible light irradiation at 120 minutes. The pH of the solution was altered by using dil. HCl or NaOH. The results obtained for CR degradation was presented in **Figure 6.5.3**, which shows that ZnO, NC and ZnO/NC has maximum photodegradation at pH 7, 4 and 5 respectively. CuO shows maximum degradation at pH 7 and CuO/NC has maximum degradation efficiency at pH 6 for the degradation of CR.

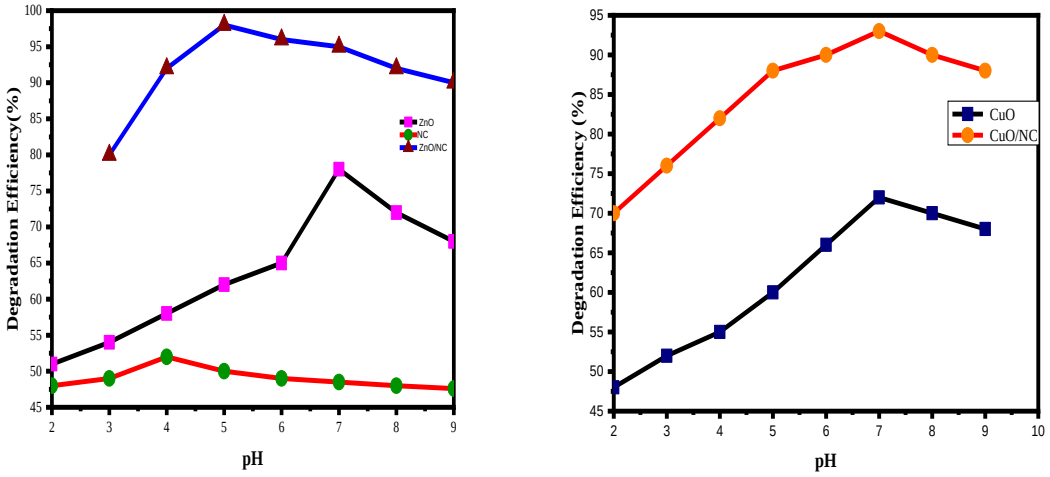

Figure 6.5.3. Degradation efficiency vs pH for Congo Red

In the case of MG (**Figure 6.5.4**.), it was found that the degradation efficiency increased with increasing pH over the entire range for all the photocatalysts.

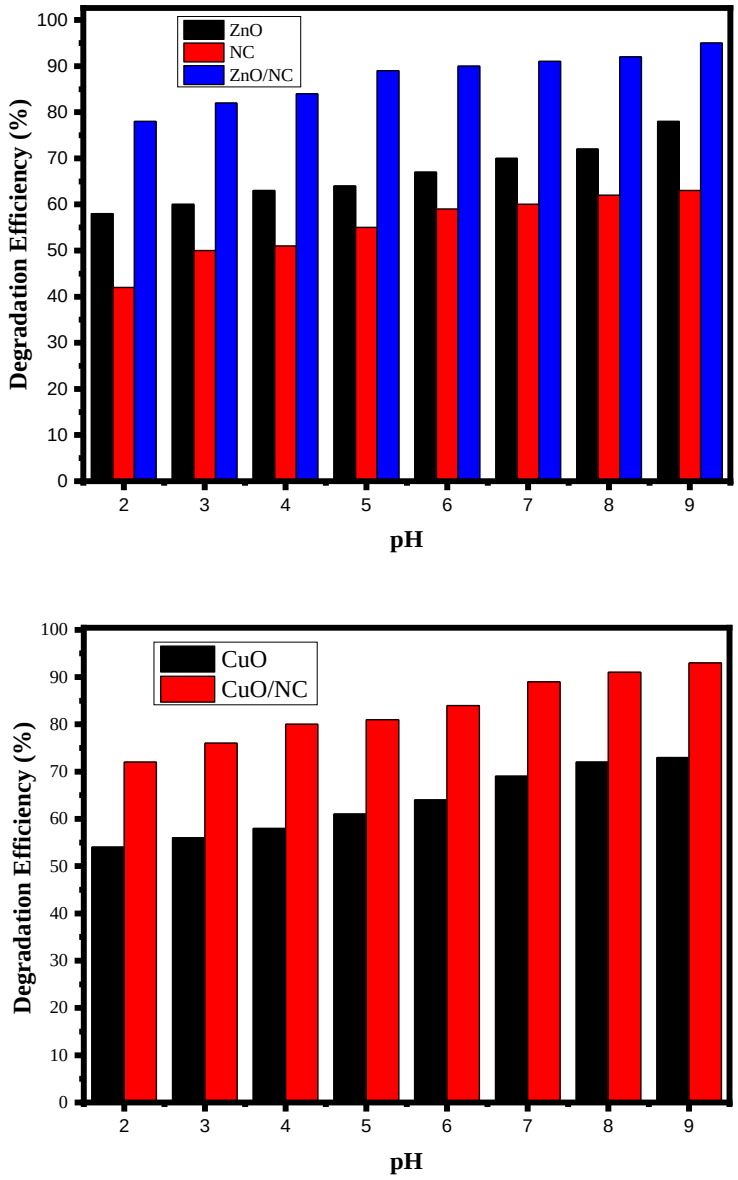

Figure 6.5.4. Degradation efficiency vs pH for Malachite Green

The effect of pH is very important in the photo degradation of dyes since it influences both the surface charge of the photocatalyst and the ionic form of the dye, hence influencing the electrostatic interactions between the dye and the catalyst surface. It was reported that ZnO has a zero point charge (zpc) of approximately 8. Hence the surface of ZnO is positively charged in acidic solutions (pH<8), which is favorable for attracting anions, and ZnO deprotonates in alkaline solutions (pH>8) hence its surface becomes negatively charged, which is favorable for repelling anions .At higher pH, the availability of hydroxyl ions increases which adsorbed on the catalyst surface making it negatively charged. Due to the coulumbic attraction between oppositely charged dye

molecules and catalyst surface, the cationic dye molecules approaches to the surface of the catalyst. The dye molecules undergo photo oxidation by the $OH^{\cdot}$ radicals on the surface. After a limiting value of pH, further increase of pH decreases the rate of degradation because of the fact that with the further increase of OH^{-}concentration, the dye cannot remain as cation, decrease of coulumbic attraction occurs resulting in the decrease of rate.

The photodegradation efficiency of NC was low compared to metal oxides and composites. In the case of NC, the abundant surface –OH groups act as hydrophilic sites. During the drying process, the hydrophilic nature of NC might cause it to aggregate. Therefore the presence of abundant surface –OH groups can produce an opposing effect, which is not ideal for photodegradation. The improvement of the properties of composites is due to the presence of large number of –OH groups on the surface of NC it acts as a multifunctional cross linker and reinforcing agent.

As CR an anionic dye shows higher degradation efficiency at lower pH. At higher pH, the cationic dye MG shows higher degradation efficiency. Moreover, pH influences the sizes of photocatalysts, interaction of the solvent molecules with the catalyst and the type of radicals or intermediates formed during the photocatalytic reaction. All of these factors have a significant influence on the photodegradation of dyes by the catalysts.

6.2.1.3. EFFECT OF INITIAL CONCENTRATION OF DYES ON DEGRADATION

Initial dye concentration has significant effect on the photocatalytic degradation rate and was investigated by varying concentration of dyes from 10 to 50 ppm on treatment with 0.1g photocatalysts of pH 7under visible light irradiation for 120 minutes. The results are shown in **Fig 6.5.5**. Photodegradation efficiency of ZnO for CR increased from 61 to 88% on increasing the concentration from 10 ppm to 25ppm.NC shows maximum degradation efficiency of 64% for the concentration of 10 ppm. But in the case of ZnO/NC, photodegradation efficiency increased from 77 to 95% when the concentration increased from 10 to 30 ppm. CuO shows a maximum degradation of 82% at concentration of 20ppm whereas CuO/NC has a maximum of 91% when the concentration was increased from 10 to 25 ppm.

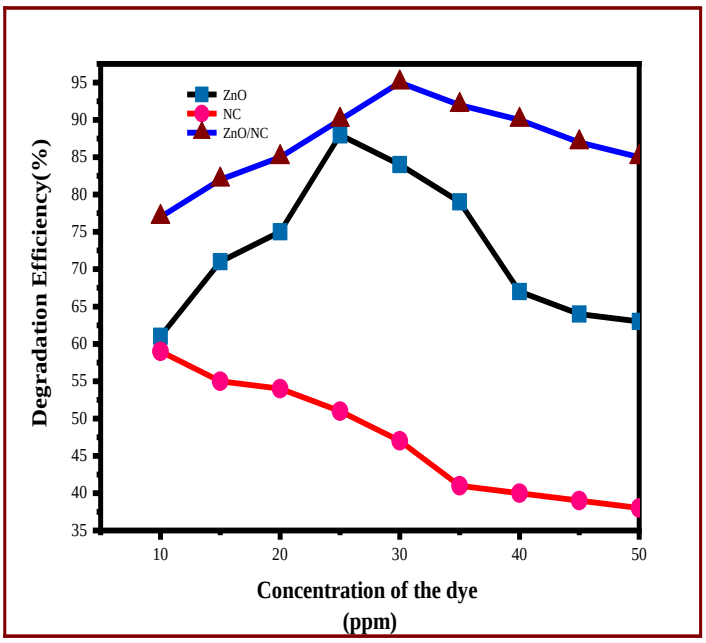

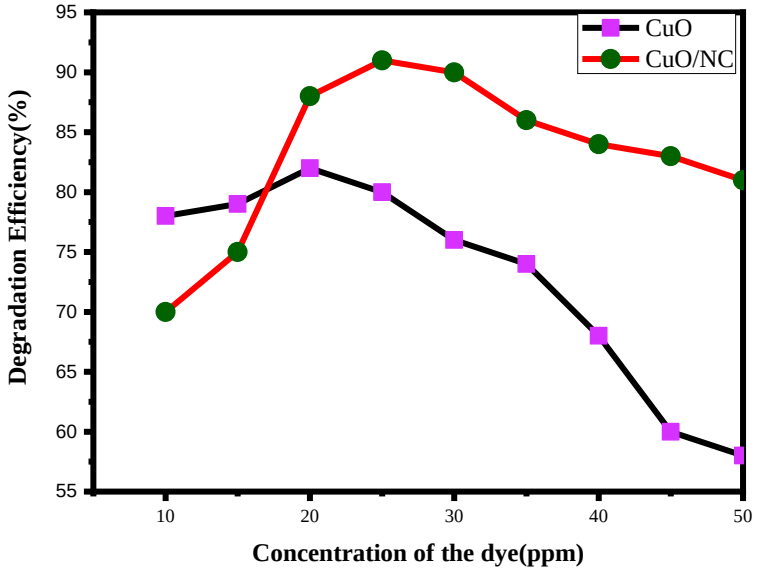

Figure 6.5.5. Degradation efficiency vs concentration for Congo Red

In the case of MG, dye concentration of 10 to 50 was selected for the study. From the **Fig 6.5.6**, it was clear that ZnO and CuO shows a maximum degradation efficiency of 90% and 88% at a concentration of 25ppm. In the case of NC, a maximum of 64% at concentration 10ppm.But the composites ZnO/NC and CuO/NC has maximum degradation efficiencies of 98% and 96% at a concentration of 30ppm.

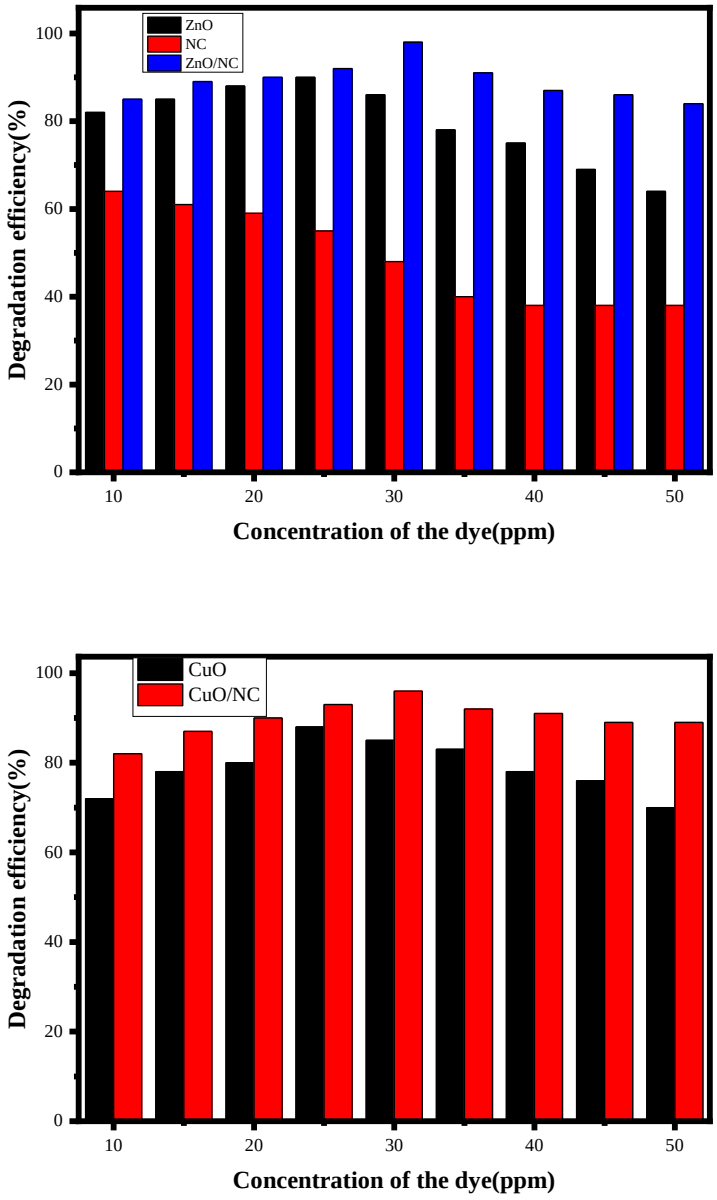

Figure 6.5.6. Degradation efficiency vs concentration for MG

Too low concentration of the dyes was not sufficient for photodegradation studies. At low concentration, adsorption rate become too low resulting low photodegradation. As concentration increases, photodegradation also increases and the reaction rate levels off or become independent when the catalyst concentration reaches a certain limit. Further increase in concentration of dyes beyond this limit, dye molecules act as internal filters which prevents the light to reach the surface of the photo catalyst. This decreases the rate of photocatalytic degradation of the dyes. ZnO

has large number of oxygen vacancies which are responsible for the higher degradation efficiency. The degradation efficiency of CuO may be due to the more number of surface oxygen atoms. The photodegradation efficiency of composites was higher compared to metaloxides and nano cellulose.NC can easily adsorb on metaloxide surface layers and provide additional –OH groups on the surface of metaloxides. As a result, the surface area of the composites is expected to increase, which increases the photodegradation efficiency of the composites. Among all photocatalysts, ZnO/NC shows maximum degradation due to the highest surface area of ZnO/NC.

6.2.1.4. EFFECT OF CATALYST DOSAGE ON DEGRADATION

The effect of catalyst dosage on the degradation of CR (**Figure 6.5.7**.) and MG (**Figure 6.5.8**.) were carried out by varying the catalyst amount from 0.025 to 0.25gm of 25ppm concentration under visible light irradiation for 120 minutes.

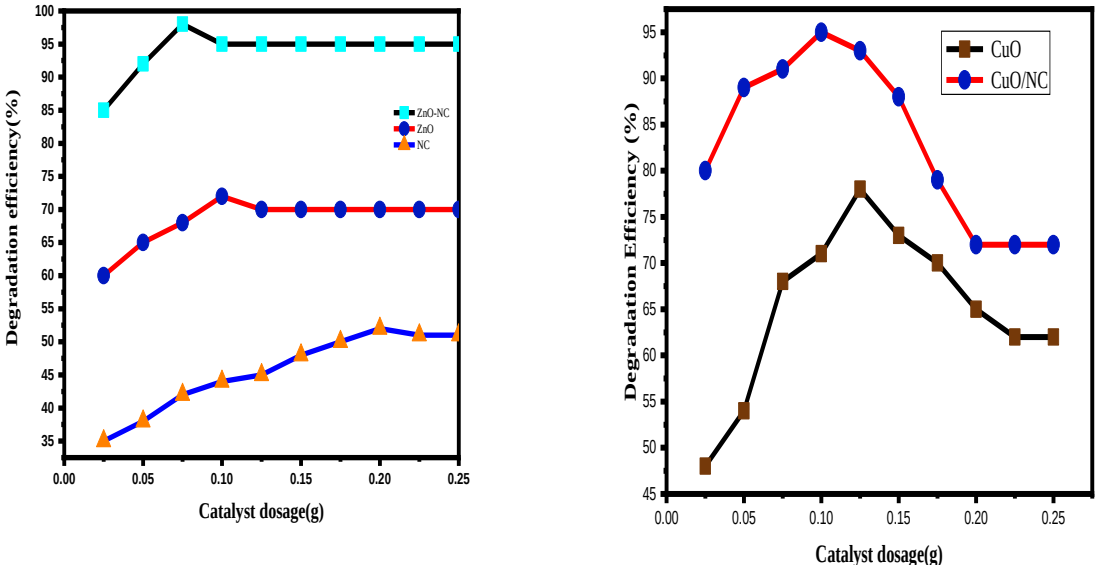

Figure 6.5.7. Degradation efficiency vs catalyst dosage for CR

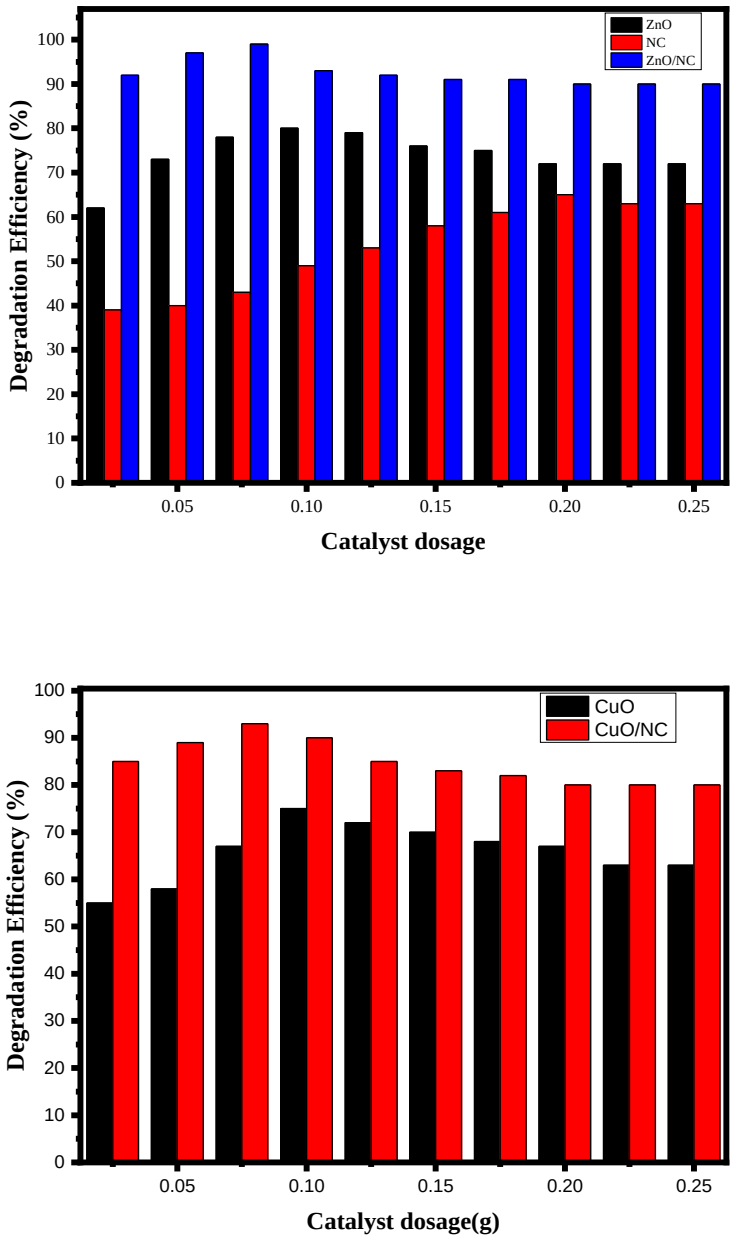

Figure 6.5.8.Degradation efficiency vs catalyst dosage for MG

As the amount of catalyst dosage increases, degradation efficiency also increases, reached a maximum and there after decreases. The increase of catalyst dose increases the number of active sites on the catalyst surface which increases the degradation efficiency. It was found that increasing the catalyst dose above the optimum amount resulted in the aggregation of photo catalyst particles. This leads to decrease in the surface area for contact between the photo catalysts and the dyes result

in the reduction of the active sites and leads to lower photo degradations efficiency .Also as the dosage of catalyst increases, the degradation efficiency decreases because of the decrease in the penetration of UV light due to shielding effect.

The higher degradation efficiency of ZnO is ascribed to the increased amount of oxygen vacancies.NC alone exhibits limited photocatalytic activity under visible light irradiation, semiconductor materials like ZnO and CuO have been added to enhance the photocatalytic activity. The presence of –OH binding sites and network like structure of NC can facilitate the adsorption of metaloxides to its surface. In comparison with metal oxide and nanocellulose, very small amount of nanocomposite were required for maximum degradation for both CR and MG. It was found that; the metaloxides can interact with NC effectively, resulting in the enhancement of nanocomposites properties due to their strong hydrogen bond, divalent character and relatively small ionic radius. The degradation efficiency is more in the case of ZnO/NC due to the increased amount of oxygen vacancies and high surface area. The generation of oxygen vacancies under visible light irradiation is lower in the case of all other photo catalysts.

6.3. KINETICS OF PHOTODEGRADATION

In order to explain the photo degradation efficiency of the nanocomposites for the dyes, experiments of photo degradations of CR and MG was carried out without the catalyst, with ZnO, CuO, NC, ZnO/NC and with CuO/NC and the results are depicted in **Figure 6.6 and Figure 6.7** respectively.From the results it was clear that without the photocatalyst, there occurs slight photo catalytic degradation for CR and MG. By using ZnO/NC, the photodegradation ability of CR and MG was found to be 98.0% and 99.7% within 60 minute. The kinetics for the photodegradation of dyes by means of illuminated ZnO/NC can be described by the kinetic model of Langmuir-Hinshelwood (L-H) eqn.

$$\frac{-dc}{dt} = \frac{kKc}{1+Kc} \qquad (1)$$

where dc/dt is the degradation rate, k is the apparent reaction rate constant, K is the adsorption coefficient of the substance to be degraded and c is the concentration at a time t. When the concentration of dyes (Kc) was very low L-H eqn becomes

$$\frac{-dc}{dt} = kc \qquad (2)$$

When t=0c=c_0,initial dye concentration then

$c=c_0e^{-kt}$ (3)

A linear form of this eqn. is

$\ln c=\ln c_0-kt$ (4)

or

$\ln c/c_0=-kt$ (5)

This eqn. is of the form of straight line eqn,y=mx+c

Thus the plot of lnc as a function of t is a straight line and this eqn fit for a pseudo first-order kinetics. The experimental data was verified by using L-H kinetic model and best correlated with pseudo first order kinetics. Linear regression analysis was done using Origin pro.8 software. From the plots, the rate constants (k) and $R^2$for CR and MG with blank, ZnO, NC , ZnO/NC, CuO and CuO/NC are obtained which are depicted in the **Table 6.1**.

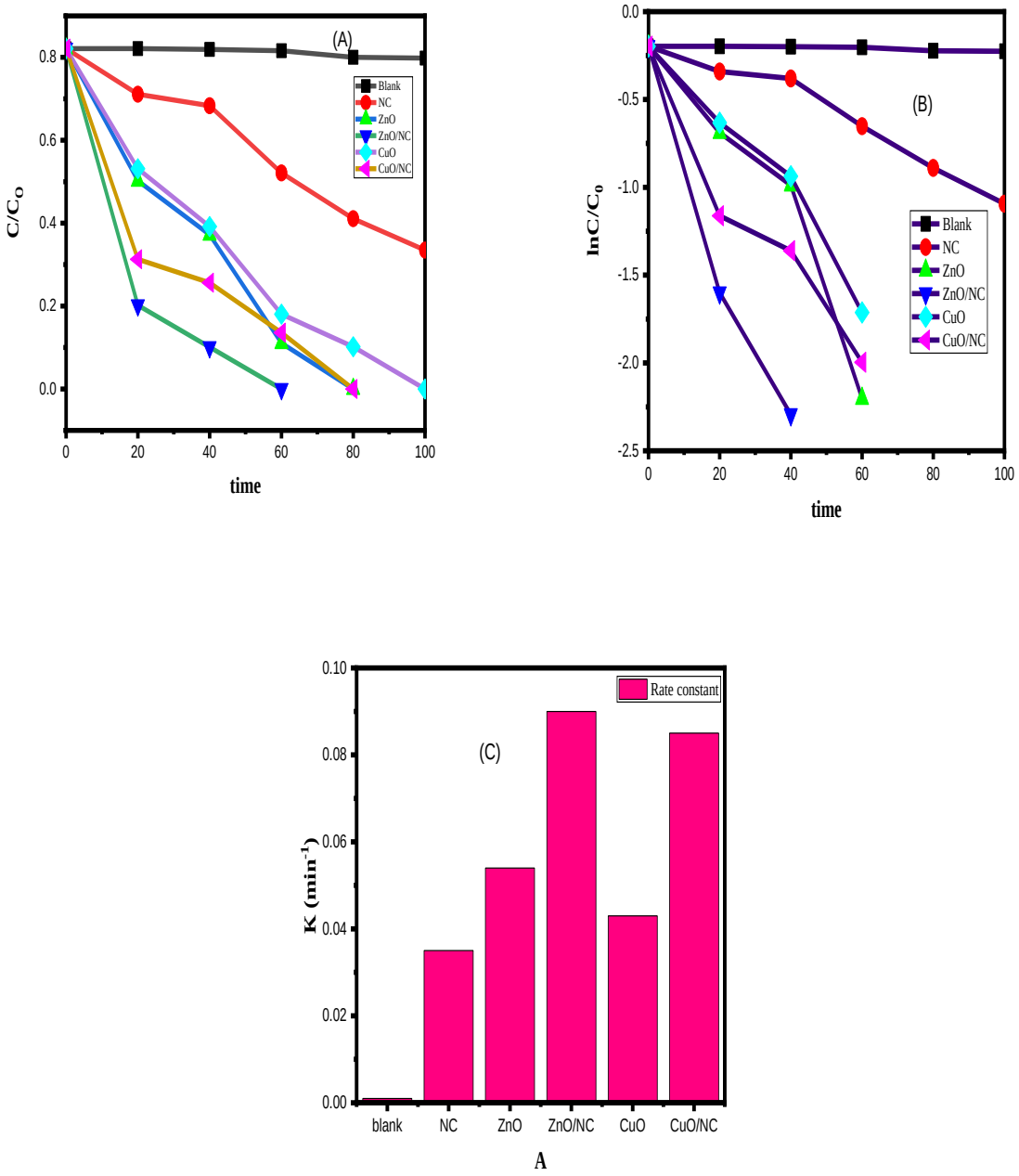

Figure 6.6.Photodegradation of CR with (A) blank, ZnO, NC, ZnO/NC, CuO, CuO/NC (B) Kinetic linear simulation plot (C) Reaction rate of photodegradation of CR with blank, ZnO, NC, ZnO/NC, CuO, CuO/NC.

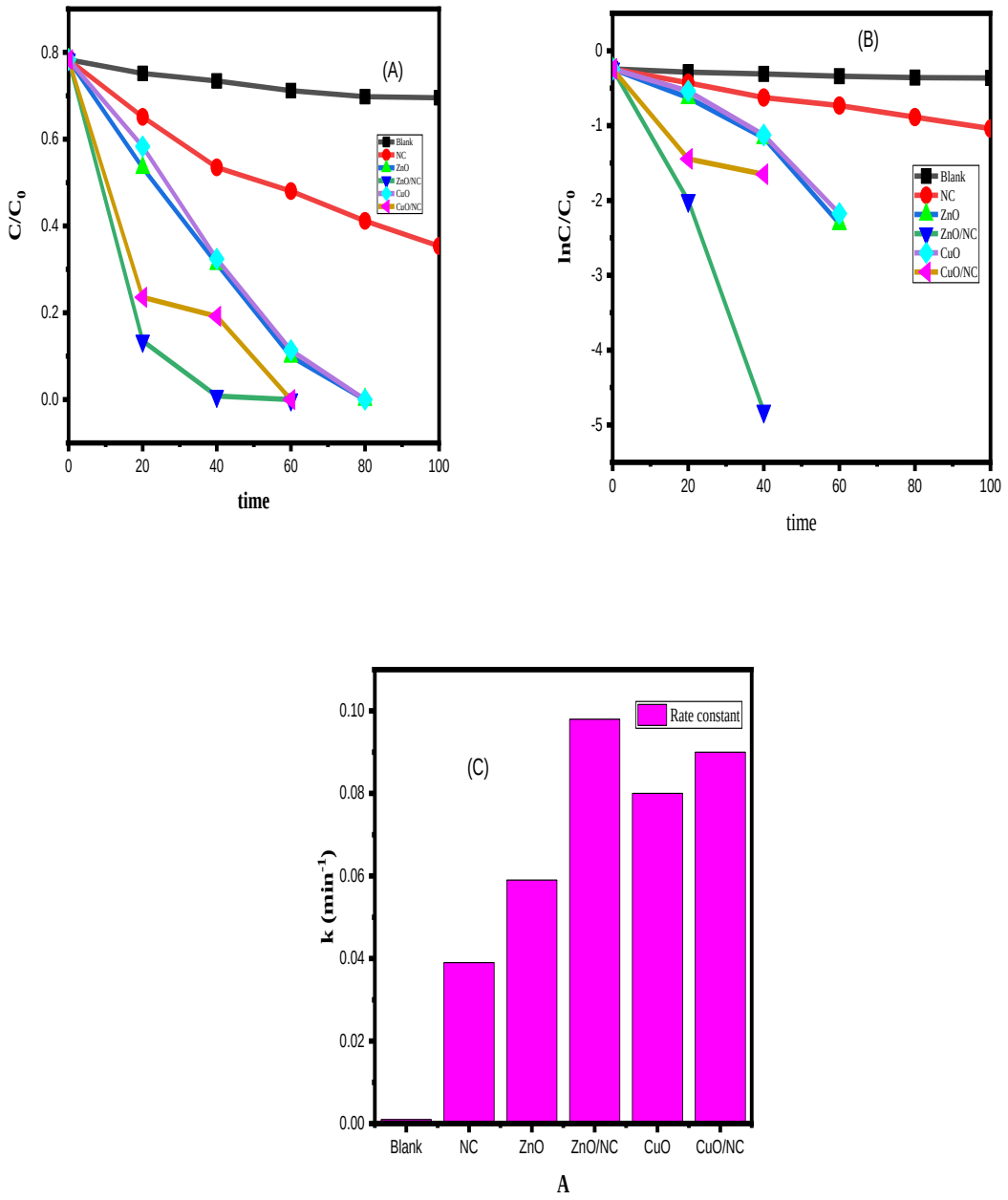

Figure 6.7.Photodegradation of MG with (A) blank, ZnO, NC, ZnO/NC, CuO, CuO/NC (B) Kinetic linear simulation plot (C) Reaction rate of photodegradation of CR with blank, ZnO, NC, ZnO/NC, CuO, CuO/NC.

Table 6.1 First-order kinetic constants and relative coeifficients for the photocatalytic degradation of CR and MG over the photocatalysts.

DYE	PHOTOCATALYSTS	k min^{-1}	R^2
CR	Blank	$0.1X10^{-2}$	0.9411
	ZnO	$3.5X\ 10^{-2}$	0.95418
	NC	$5.4X10^{-2}$	0.94638
	ZnO/NC	$9.0X10^{-2}$	0.99421
	CuO	$4.3X10^{-2}$	0.9658
	CuO/NC	$8.5X10^{-2}$	0.9897
MG	Blank	$0.01X10^{-2}$	0.9381
	ZnO	$5.9X10^{-2}$	0.9625
	NC	$3.9X10^{-2}$	0.9419
	ZnO/NC	$9.8X10^{-2}$	0.9841
	CuO	$4.8X10^{-2}$	0.9426
	CuO/NC	$9.0X10^{-2}$	0.9801

The values of $R^2$from the table indicates that the photodegradation of dyes onto all the photocatalysts was best with pseudo first order kinetics. The R^2values of the composite for the degradation of two dyes were beyond 0.94 which indicates the suitability of pseudo first order kinetics in explaining photodegrdation mechanism. The degradation abilities of the two nanocomposites were significantly higher as compared to their metaloxides and polymer. Also the composite ZnO/NC show higher degradation ability compared to CuO/NC which may be due to the existence of polyfunctional groups present in NC and also due to the high surface area of ZnO/NC.

6.4. MECHANISM OF PHOTO DEGRADATION

When metal oxide nanocellulose (MO-NC) composite was illuminated with visible light, the nanocomposite absorbs photons with energies equal to or higher than band gap energy. The photon with this required energy hits the electrons in the Highest

Occupied Molecular Orbital (HOMO) to the Lowest Unoccupied Molecular Orbital (LUMO) of NC and subsequently into the conduction band of metal oxide resulting holes in the HOMO of NC. The electrons in the VB of metal oxide can migrate to HOMO of NC to recombine with holes generating holes in the VB of metal oxide. The photo generated electrons react with O_2 to generate $O_2^{\cdot -}$ and holes react with OH^- or H_2O to generate $OH^{\cdot}$, which are the Reactive Oxygen Species (ROS) and react with organic dyes. The enhanced photo degradation of dyes can be promoted by the increase in the concentration of hydroxyl groups and molecular oxygen. Increase in the amount of hydroxyl groups increases the trapping sites for photogenerated electrons and holes, leads to increase in the number of hydroxyl radicals. The degradation of dye molecules takes place by the reaction of dyes with ROS which are finally oxidised to CO_2 and H_2O .The detailed mechanism is shown in **Figure 6.8**.

$$MO\text{-}NC \rightarrow MO\text{-}NC^+ + e^- \quad (6)$$

$$e^- + O_2 \rightarrow O_2^{\cdot -} \quad (7)$$

$$MO\text{-}NC^+ \rightarrow MO\text{-}NC + h^+ \quad (8)$$

$$OH^- + h^+ \rightarrow {}^{\cdot}OH \quad (9)$$

$$H_2O + h+ \rightarrow {}^{\cdot}OH + H^+ \quad (10)$$

$$Dye + (O_2^{\cdot -} \text{ or } HO^{\cdot}) \rightarrow \textit{intermediate} \rightarrow \textit{products} \quad (11)$$

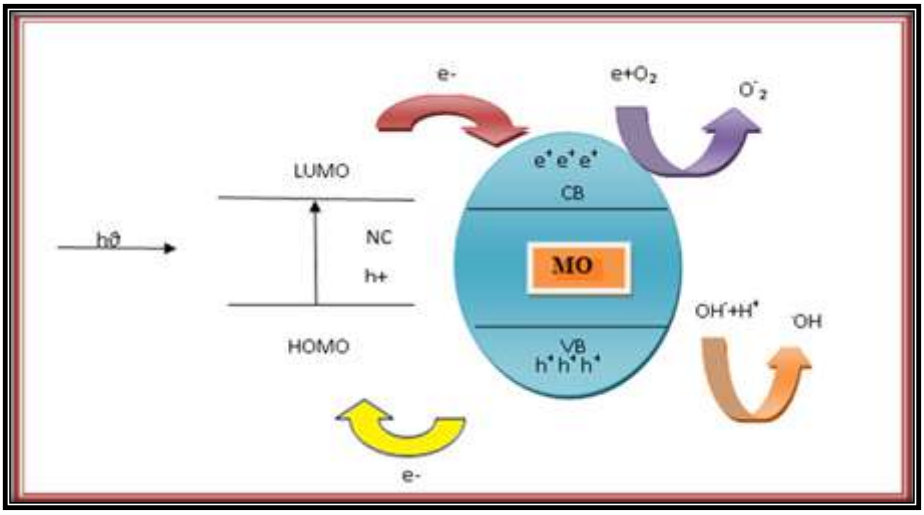

Figure 6.8.Mechanism of photo degradation by metal-oxide nanocomposites

6.5. COMPARISON OF PHOTOCATALYTIC ACTIVITIES OF DIFFERENT PHOTOCATALYSTS

In order to evaluate the photo degradation efficiency of various photo catalysts studied, identical experiments were carried out with ZnO, CuO, NC, ZnO/NC and CuO/NC for the degradation of CR and the results were depicted in **Table 6.2**.From the results it was clear that the highest removal efficiency of CR (99.9%) occurred by ZnO/NC using visible light as energy source. The trend of photo catalytic activity of studied nano photo catalysts for the degradation of CR was ZnO/NC>CuO/NC>ZnO>CuO>NC. Obviously doping of metal oxides with NC increases the degradation efficiency and in the case of ZnO/NC doping increases the surface area, hydroxyl radicals ,oxygen vacancies and hence improve the photo degradation efficiency compared to CuO/NC.

Table 6.2 Photodegradation Efficiency of various photocatalysts

Nano photocatalyst	Removal %
ZnO/NC	99.9
CuO/NC	95.1
ZnO	85.2
CuO	81.9
NC	72.6

The photodegradation ability of the photocatalysts was compared with already reported materials and is shown in **Table 6.3**. Comparisonof the results reveals the superiority of the prepared material which exhibited higher degradation within less time.

Table 6.3 Comparison of photocatalytic degradation ability of ZnO/NC with previous literature

Sl.No.	Photocatalyst used	Dye	Observed result	References
1	Visible light/ZnO	Methyl red	82.65% degradation after 50 min	Shanavas Khan Ph.D Thesis (2018) [103]
2	Visible/ZnO-Cellulose	Methylene Blue	69.5% degradation after 60min	Ali et al,2016[99]
3	UV/TiO2/Mt	Methylene Blue	80% degradation after 60 min	Daneshvar et al,2003 [100]
4	UV/TiO2/Mt	Congo Red	22.1% degradation after 350min	Luttrell et al,2014[101]
5	UV/TiO2/halloysite	Rhodammine B	88% degradation after 360min	Mishra et al,2017
6	UV/GO	Methylene Blue	56.25 % degradation after 140min	Hosseini et al,2017 [102]
7	UV/Amylose-TiO2/halloysite	Methylene blue	91% degradation after 240min	SreekalaPh.D Thesis (2020) [104]
8	UV/ZnO	Malachite Green	100% degradation after 120 min	RejaniPh.DTheisis(2016) [105]
9	Visible/GO-ZnO	Methyl Orange	97% degradation after 120min	RejaniPh.D Thesis(2016) [105]
10	UV/GO/ZnO	Methylene Blue	99% degradation after 140min	Hosseini et al,2017 [102]
11	UV/CNT/ZnO	Methylene Blue	98 % degradation after 140min	Hosseini et al,2017 [102]
12	UV/TiO2/halloysite	Gentian violet dye	60% degradation after 360min	Asha Radhakrishnan Ph.D Thesis(2016) [106]
13	Visible/ZnO/NC	Congo Red	99.2% degradation after 120min	**Present work**
14	Visible/ZnO/NC	Malachite Green	99.9 % degradation after 120min	**Present work**

6.6. REGENERATION AND REUSABILITY OF PHOTO CATALYST

Main advantage of heterogeneous photo catalytic process is the recovery and reuse of the photo catalysts. Experiments to observe the performance of reusing the catalysts were conducted .Five cycles of the photocatalytic experiment for ZnO/NC nanocomposite were carried out under visible light irradiation using 0.2g of the catalyst loaded with CR of 20 ppm solution .It was observed from **Figure 6.9** that the recovered catalyst could be reused and the photo catalytic degradation capacity of the catalyst was reduced from 98.2% on first cycle to 85% on fifth cycle. From the above observation it was found that the efficiency of the recovered catalyst was lower than that of fresh catalyst .For recovered catalyst ,decrease in the number of photo active sites occurs due to chemical reaction and visible light irradiation .

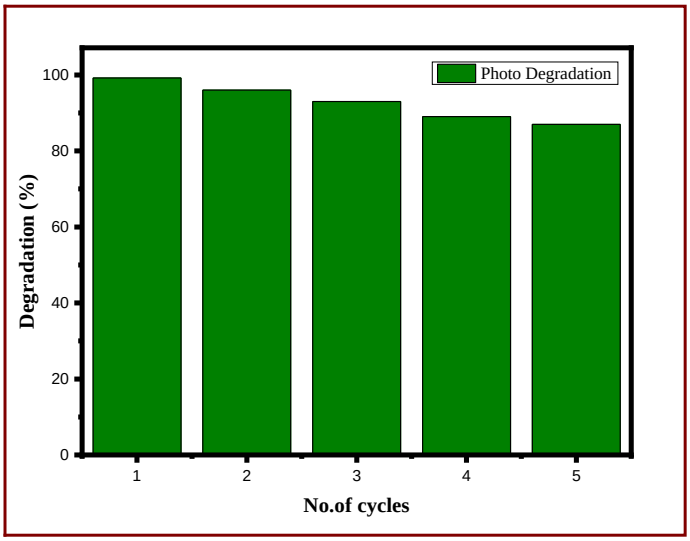

Figure 6.9. Photodegradation cycle of CR on to ZnO/NC

CHAPTER - VII

ANTI-MICROBIAL STUDIES

7.1. INTRODUCTION

This chapter deals with the application of Metal oxides such as ZnO and CuO and its various composites in the anti- microbial field. The contamination of ground water sources by pathogenic bacteria possess a public health concern. Nowadays, nanomaterials are used as antimicrobial agents. As particles are reduced from a micrometer to a nanometer size, the resultant properties can change drastically. For example, electrical conductivity, hardness, active surface area, chemical reactivity and biological activity are all known to be altered. The bactericidal effectiveness of metal nanoparticles has been suggested to be due to both their size and high surface-to-volume ratio. Such characteristics should allow them to interact closely with bacterial membranes, rather than the effect being solely due to the release of metal ions. There are several mechanisms to explain the antimicrobial activity of the nanomaterials including the release of antimicrobial ions, interactions of nanoparticles with microorganisms subsequently damaging the integrity of bacterial cell and the formation of ROS by the effect of light radiation. The release of Zn^{2+} antimicrobial ions has been suggested about the toxicity of ZnO against bacterial strains. Zn^{2+} ions are soluble in the medium containing the microorganisms.

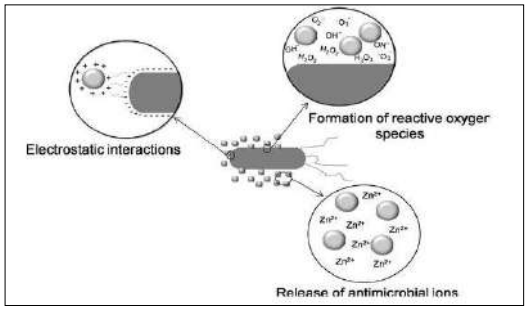

Figure 7.1 Mechanism of antimicrobial activity of ZnO nanoparticles

The nanoparticles can directly interact with the microbial cells and they can oxidize the cell components or they can produce secondary products such as Reactive Oxygen Species (ROS), that cause cell damage [90]. The nanomaterials are reported to

change the structure of bacterial cell membrane by increasing membrane permeability leading to accumulation of nanoparticles on the cell membrane and subsequent internalization [91]. Thus it seems that nanoparticles might have two mode of action to inhibit bacterial survivability. In one mode they induce membrane damage and in other mode they increase cellular ROS. The radical formation occurs on the particle surface. Hence particles with larger surface area demonstrate stronger antibacterial activity. In theory, metal nanoparticles could be combined with polymers or coated onto surfaces, which may then have a variety of potential antimicrobial applications. In recent years, severe fungal infections have significantly contributed to the increasing morbidity and mortality of immune compromised patients who need intensive treatment including broad-spectrum antibiotic therapy.

7.1.1 ANTIMICROBIAL ACTIVITY - AGAR- WELL DIFFUSION METHOD

The antibacterial activities of the prepared samples were evaluated by Agar-Well diffusion method against pathogenic microbial species, *Escherichia coli,* and *Streptococcusaureus*. The culture medium was prepared by dissolving 33.8 g of the commercially available Muller Hinton Agar Medium (MHI Agar Media) in 1000ml of distilled water. The dissolved medium was autoclaved at 15 lbs pressure at 121°C for 15 minutes. The autoclaved medium was mixed well and poured onto 100mm Petri plates (25-30ml/plate) while still molten. Petri plates containing 20ml Muller Hinton Agar Medium were seeded with the bacterial culture of *E. coli a*nd *S. aureus* (growth of culture adjusted according to McFarland Standard, 0.5%). Wells of approximately 10mm was bored using a good cutter and different concentrations of the sample such as 250µg/mL, 500µg/mL and 1000µg/mL were added. The plates were then incubated at 37°C for 24 hrs. The antibacterial activity was assayed by measuring the diameter of the inhibition zone formed around the well in units of milli meter (NCCLS, 1993a). Streptomycin was used as a positive control.

7.2 EVALUATION OF ANTIMICROBIAL ACTIVITY OF NANO ZnO

The synthesized nano structures of ZnO were evaluated for their antimicrobial properties towards bacterial and fungal strains. The antimicrobial studies showed that samples annealed at different temperatures show different antimicrobial activities against microbial strains. It is clear that ZnO annealed at 400^0C has shown greater

antimicrobial activity against *B. subtilis* and *S. aureus.* The decrease in activity of samples annealed at higher temperatures can be attributed to decrease in surface to volume ratio due to increase in particle size. The antimicrobial activity of the nanoparticles is generally known to be a function of the surface area which is in contact with the microorganisms [92]. **Table 7.1** gives the values of zone of inhibition of different samples.

Table 7.1 Comparison of antimicrobial activities of different ZnO samples

Sample	Zone of inhibition(mm)					
	E. coli	***Pseudomonas aeruginosa***	***Bacillus subtilis***	***Streptococcus aureus***	***Penicilliumchrysogenum***	***Aspergillus flavus***
ZO-4	5	6	10	17	8	7
ZO-6	3	5	7	10	7	5
ZO-8	2	3	4	7	6	4

7.3. EVALUATION OFANTIMICROBIAL PROPERTIES OF NANO CuO

The synthesized materials such as nano CuO annealed at 400^0C and 600^0 were investigated for their antimicrobial activity against a Gram-negative bacterium (*E. coli*) and a Gram-positive bacterium (*S.aureus*) using Agar-Well Diffusion method. The presence of an inhibition zone indicated the antibacterial effect of synthesized CuO against both Grams – positive and negative bacterial strains. The zone of inhibition of CuO annealed at (400) and CuO (600) towards *E. coli* and *S. aureus* are CuO(400) exhibited stronger antibacterial property against both gram-positive and gram-negative bacteria as indicated by higher values of the inhibition zone measured in mm (Table 7.2).

Table 7.2 Zone of inhibition (mm) of CuO(400) and CuO(600) towards *E. coli* and *S. Aureus*

Sample	ZOI (mm) of *E. coli*	ZOI (mm) of *S. aureus*
Streptomycin(Control)	20	28
CuO (400)	17	18
CuO (600)	14	15

A tentative mechanism for antibacterial activity is that when bacteria are exposed to nano CuO, copper ions released from nanoparticles neutralize the charge on Lipopolysaccharide (LPS) in bacterial cell wall and increases the permeability of the outer membrane. As a result more CuO NPs enter into the bacterial cell and retard their growth .These materials entering into the bacteria generate ROS (superoxide anion, hydrogen peroxide, organic hydroperoxide, and hydroxyl radicals) and they cause bacterial death. The change in electronic properties and reduction in the size of the particles enhances the production of ROS [10]. Hence CuO (400) has higher antibacterial property than CuO (600).

7.4. EVALUATION OF ANTIMICROBIAL STUDIES OF NC, ZnO/NC & CuO/NC

The antibacterial activities of the cellulose composites were tested with Gram positive (*S.aureus*) and Gram negative (*E. coli*) bacteria by Agar- well diffusion method. NC can act as a template and stabilizer for metal oxide nanoparticles. Thus the nanocomposites can penetrate into the cell wall of bacteria more effectively than NC [93]. Here also that zone of inhibition is higher in gram negative (*E.coli*) than gram positive (*S.aureus*) bacteria (Table 7.3). This is because gram negative bacteria have a single peptidoglycan layer while gram positive bacteria have several peptidoglycan layers [94].

Table 7.3 Comparison of Zone of Inhibition of NC and Composites

Material	**SA(m^2/g)**	**Zone of Inhibition (mm)**	
		E.coli	***S.aureus***
NC	40.2	15	NIL
NC/CuO	52.6	16	11
NC/ZnO	150.8	17	10

Comparison of the antibacterial activity of NC and its composites are summarized in Table 7.3. Nanocellulose itself has no antibacterial activity for bacteria like *S. aureus*. But when active metal oxides are incorporated to its matrix, it shows significant antibacterial activity. In the case of *E. coli*, the activity of the composites is higher than that of NC. This may be due to increased surface area and the activity of the metal oxide component in the composite [95&96].

The mechanism of antibacterial activity of nanocellulose - metal oxide composites may be due to the formation of highly reactive species like superoxide, hydrogen peroxide and hydroxyl on the surface of metal oxide activated by both UV and visible light. Many researchers proposed that the inhibition of bacterial growth is due to the generation H_2O_2 on the surface of metal oxide [97 &98]. The proposed reaction for the generation of H_2O_2 is as follows:

$$MO + h\upsilon \rightarrow e^- + h^+ \quad (1)$$

$$h^+ + H_2O \rightarrow H^+ + {}^{\bullet}OH \quad (2)$$

$$O_2 + e^- \rightarrow O_2^{\bullet-} \quad (3)$$

$$O_2^{\bullet-} + H^+ \rightarrow HO_2^{\bullet} \quad (4)$$

$$HO_2^{\bullet} + e^- \rightarrow HO_2^- \quad (5)$$

$$HO_2^- + H^+ \rightarrow H_2O_2 \quad (6)$$

Even though NC has low antibacterial property by itself, its composites with metal oxides show significant antibacterial property. This could be utilised in the fabrication of antibacterial and bioactive papers, food packing materials, bacteria resistant clothing, etc. Metal oxides because of their powder nature could not be moulded by itself, while cellulose because of its stiffness is easy to be moulded in to devices like clothing, packing materials, filter paper etc. Thus cellulose composites could expand the application potential of both cellulose and metal oxides. Metal oxide incorporated cellulose could be used to prepare antimicrobial papers which could use in bacterial resistant textiles, food packaging, biomedical application and health care.

CHAPTER - VIII

SUMMARY AND FUTURE SCOPE

8.1. SUMMARY

The present work primarily covers the synthesis, characterization and applications of ZnO, CuO and their nanocomposites with a biopolymer nanocellulose. ZnO and CuO are synthesized by using green method from the Tinospora cordifolia plant stem extract. Nanocellulose was prepared by acid hydrolysis method using sugarcane bagasse as the cellulose source. Nanocellulose based composites like Zinc oxide incorporated nanocellulose (ZnO/NC) and Copper oxide incorporated nanocellulose (CuO/NC) were prepared using the ex situ approach. All the prepared samples were subjected to the characterization techniques such as SEM, EDS, TEM, XRD, FTIR, PL, UV-Visible and BET analysis for their qualitative and quantitative analysis.

JCPDS comparison of XRD's of metal oxides confirmed the formation of ZnO and CuO. XRD of Nanocellulose was matched with that in literature. XRD of nanocomposites confirmed their formations. The various morphologies and structures of all the samples are given by the SEM images. From EDAX analysis, the mass percentage, composition and purity of metal oxides and nanocellulose were confirmed. The EDAX of nanocomposites confirmed the presence of metal oxides in nanocellulose. TEM images of all the samples gave the morphology and particle size which is in consistence with that from XRD and SEM.

FTIR confirmed the presence of various functional groups and composition of metal oxides, nanocellulose and nanocellulose based metal oxides formed. UV/Vis absorption spectra and PL analysis of the samples gave exact information about the optical properties. UV/Vis spectra of the metal oxide samples and Nanocellulose showed visible absorption. But the UV/Vis spectra of the nanocomposites resulted in the increase of surface defects which has resulted enhancement of absorption in the visible region. In the case of nanocomposites the range of absorption wasfound to be broader.

From PL analysis, it was clear that all nanocomposites and their counterparts showed very good photoluminescent property such that these materials could be used as light emitters in visible region and near UV region. BET surface area analysis clearly indicated that the nanocomposites possess high surface area compared to its counterparts.

Systematic studies on the adsorption behaviour of all the different nanomaterials prepared were carried out for the removal of heavy metal ions of Pb(II) and Cd(II). The factors affecting adsorption process such as contact time, pH, the concentration of adsorbate and adsorbent dose were studied in detail. The efficiency of adsorption was found to be higher for nanocomposites when compared to their counterparts. The biocomposites could remove Pb(II) ions completely from aqueous solutions under the experimental conditions. Kinetic studies of the experimental data fitted very well with the pseudo-second-order kinetic model showing chemisorptions as the type of adsorption.

A detailed study on the photocatalytic behavior of the metal oxides, nanocellulose and the nanocomposites were carried out for the degradation of dyes such as Congo red and Malachite green. The factors affecting photodegradation such as contact time, pH, concentration of dye and catalyst dosage were studied in detail. The studies reveal that the catalytic activity depends on the size and morphology of the nanometal oxides and nanocellulose based composites. The efficiency of photodegradation was found to be higher for nanocomposites when compared to metal oxides and nanocellulose. Kinetic studies of the experimental data were analyzed using first- order kinetic models and all the systems fitted very well with first-order kinetic model. Thus it could be concluded that the materials prepared in this study are ideal for the photodegradation of organic pollutants using visible light.

The antimicrobial activity of the synthesized nano materials was analyzed for *E.coli* and *S. aureus*. The results indicate that nanometal oxides and their composites are effective against gram-positive and gram-negative bacterial strains. The activity was highest for nanocomposites compared to nanocellulose and individual metal oxides. The antibacterial activity of nanocellulose/metal oxide composites were enhanced which make them suitable for fabricating bacterial resistant clothing,

bioactive paper, food packaging materials, bacterial resistant films and filter for water treatment.

8.2. FUTURE SCOPE

In the present study, metal oxides are synthesized by green method. Future research and development of green synthesis of metal oxides should be directed by extending laboratory based work to an industrial scale by considering present issues such as health and environmental effects. The present work described the photodegradation of organic pollutants including Congo red and Malachite green in synthetic solutions using photocatalytic processes. In future, the same procedure should be used for the removal of these pollutants from real waste water streams. Further this work could be extended to the removal of pesticides and other toxic chemicals. The chemistry and mechanism of the by-products formed in the photodegradation reactions could be studied further using HPLC,GC/MS,LC/MS and Ion chromatography .

From the BET surface area measurements, the surface area of the composites was found to be higher and thus more sites for adsorption. So the prepared samples could be used for the adsorption of heavy metal ions such as Ni(II), Cd(II) and Pb(II). The prepared nanocomposites are likely to be applied extensively both in the field of environmental remediation and in other important areas like pharmaceutical, food and cosmetic industries. The nanomaterials prepared could be used for the evaluation of anticancer, antibacterial, antifungal, antidiabetic and antioxidant properties.

The nanocomposites obtained in the present work are in powder form only. Current research and development focuses the synthesis of thin films due to the wide applications in the field of photovoltaic devices, sensors, etc. Hence the work could be extended for the preparation of thin film of the samples. The nanocomposites in the present study indicate enhancement in the optical properties. So proper tuning can extent their applications to the fields of anti UV applications such as antiUV glass, anti UV sunscreen etc. Proper tuning of the nanomaterials could extend their application to the fields such as deodorizing, air purifying, anti-fogging and purification of various surfaces.

REFERENCES

1. Kobya M., Demirbas E., Senturk E and Ince M, Adsorption of heavy metal ions from aqueous solutions by activated carbon prepared from apricot stone, Bioresour. Technol, 96, 2005, 1518-1521.
2. Sun S., Wang L and Wang A, Adsorption properties of cross linked carboxymethyl-chitosan resin with Pb(II) as template ions, J. Hazard. Mater, 136, 2006, 930-937.
3. Gao C., Zhang W., Li H., Lang L and Xu Z, Controllable fabrication of mesoporous MgO with various morphologies and their absorption performance for toxic pollutants in water, Cryst Growth Des., 8, 2008, 3785-3790.
4. Goswami A., Raul P.K and Purkait M.K, Arsenic adsorption using copper(II) oxide nanoparticles, Chem. Eng. Res. Des.. 90, 2012, 1387-1396.
5. Zhang S., Cheng F., Tao Z., Gao F and Chen J, Removal of nickel ions from wastewater by Mg(OH)2/MgO nanostructures embedded in Al2O3 membranes, J. Alloys Compd, 426,2006, 281-285.
6. Luo T., Cui J., Hu S., Huang Y and Jing C, Arsenic removal and recovery from copper smeltingwastewater using TiO2, Environ Sci Technol, 44, 2010, 9094-9098.
7. Fabrega J., Luoma S.N., Tyler C.R., Galloway T.S and Lead J.R, Silver nanoparticles: Behaviour and effects in the aquatic environment. Environ Int., 37, 2011, 517-531.
8. Feng L., Cao M., Ma X., Zhu Y and Hu C, Superparamagnetic high-surface area Fe3O4 nanoparticles as adsorbents for arsenic removal, J. Hazard Mater., 217-218, 2012, 439-446.
9. Pare B, Jonnalagadda S B, Tomar H, Singh P and Bhagwat V W, ZnO assisted photo catalytic degradation of acridine orange in aqueous solution using visible light irradiation, Desalination, 232,2008, 80-90.

10. Raghunath A. and Perumal E., Metal oxide nanoparticles as antimicrobial agents: a promise for the future, International Journal of Antimicrobial Agents, 49, 2017, 137-152.

11. Murthy Y. L. N., Diwakar B. S., Govindh B., Nagalakshmi K, KasiViswanath I. V.and Rajendra Singh. J., Nano copper ferrite: A reusable catalyst for the synthesis of β, γ-unsaturated ketones, J. Chem. Sci. May, 124,,2012, 639-645.

12. Iijima S, Helical microtubules of graphitic carbon, Nature 354, 1991, 56–58

13. Charles P.P and Frank J.O, Jr., Introduction to Nanotechnology, A John Wiley 81 Sons, Inc., Publication, John Wiley &Amp; Sons, Inc., Hoboken, New Jersey, 2003.

14. Balzani., Alberto Credi and Margherita Venturi, Concepts and Perspectives for the Nanoworld, Molecular Devices and Machines, 2nd Ed, 2008.

15. Pradeep T, Nano: The essentials, Tata McGraw –Hill publishing company limited, New Delhi, 2007.

16. Guozhong Cao and Jeffrey Brinker C, Annual review of nano research, World scientific publishing company, USA, 2, 2011.

17. Guozhong Cao, Nano structures and nano materials, synthesis, properties and applications, Imperial College Press, 2006.

18. Tiwari J.N., Tiwari R.N and Kim K.S, Zero-dimensional, one-dimensional, twodimensional and three-dimensional nanostructured materials for advanced electrochemical energy devices, Prog Mater Sci, 57, 2012, 724–803.

19. Lignier P., Bellabarba R and Tooze R.P.R, Scalable strategies for the synthesis of well-defined copper metal and oxide nanocrystals, Chem Soc Rev, 41, 2012, 1708–20.

20. Horrocks A.R and Price D, Fire retardant materials, Woodhead Publishing, Cambridge, 2001.

21. Wang X., Hall J.E., Warren S., Krom J., Magistrelli J.M., Rackaitis M and Bohm G.G.A,Synthesis, characterization, and application of novel polymeric nanoparticles, Macromolecules, 40, 2007, 499–508.

22. Gaharwar, Akhilesh K.; Peppas, Nicholas A.; Khademhosseini and Ali, Nanocomposite hydrogels for biomedical applications, Biotechnology and Bioengineering. 111, 2014, 441–453.

23. Carrow J. K. and Gaharwar A. K., Bioinspired Polymeric Nanocomposites for Regenerative Medicine, Macromolecular Chemistry and Physics, 216, 2014, 248– 264.

24. Music S, Dragcevic D, Maljkovic M, Popovic S, Influence of chemical synthesis on the crystallization and properties of zinc oxide. Mater Chem Phys., 77, 2003, 521–530.

25. Khashan K. S, Sulaiman G. M. and Abdulameer F. A, Synthesis and antibacterial activity of CuO nanoparticles suspension induced by laser ablation in liquid. J Sci Eng., 41, 2016, 301–310.

26. Wilson N, Nanoparticles: environmental problems or problem solvers?, Bioscience, 68, 2018, 241–246.

27. Anstas P. T. and Warner J. C. Green chemistry: theory and practice. New York: Oxford University Press, Inc; 1998.

28. Ahmed F., Arbab A. A., Jatoi A., Khatri M., Memon N., Khatri Z. and Kim I. S., Ultrasonic-assisted deacetylation of cellulose acetate nanofibers: A rapid method to produce cellulose nanofibers. Ultrason. Sonochem., 36, 2017, 319-325.

29. Anthony K. J. P., Murugan M, Jeyaraj M and Gurunathan S. Multiple strategic approaches for green synthesis and application of silver and gold nanoparticles. In: Rai M, Posten M, editors. Green biosynthesis of nanoparticles: mechanisms and applications. CAB International, 2013, 13–30.

30. Moghaddam A. B, Moniri M, Azizi S, Rahim R. A, Ariff A. B, Saad W. Z, Namvar F, Navaderi M, Mohamad R. Biosynthesis of ZnO Nanoparticles by a new Pichia kudriavzevii yeast strain and evaluation of their antimicrobial and antioxidant activities, Molecules, 22, 2017, 872–89.

31. Ahmad M. A., El-Katori E. E. and Gharni, Z. H., Photocatalytic degradation of methylene blue dye using Fe2O3/TiO2 nanoparticles prepared by sol−gel method. J. Alloys Compd., 553, 2013, 19−29.

32. Bhargav S.S. and Prabha I., Removal of Arsenic and Copper Metals from Contaminated Water using Iron (III) Oxide Nanoparticle, International Journal of Chemistry and Chemical Engineering, 3, 2013, 107-112.

33. Acharylu N. P.S., Dubey R. S. and Swaminadham V., Green Synthesis of CuO Nanoparticles using Phyllanthus Amarus Leaf Extract and their Antibacterial Activity Against multidrug Resistance Bacteria, International Journal of Engineering Research and Technology, 3, 2014, 639-641.

34. Devi H. S. and Singh T. D., Synthesis of Copper oxide Nanoparticles by a Novel Method and its Application in the Degradation of Methyl Orange, Advance in Electronic and Electric Engineering,4, 2014, 83-88.

35. Kumar B., SMita K., Debut A. and Angulo Y. Biofabrication of Copper pxide nanoparticles using Andean blackberry (Rubus glaucusBenth.) fruit and leaf, Jurnal of Saudi Chemical Society, 21, 2017, S475- S480.

36. Ansilin S., Kavya Nair J., Aswathy C., Rama V., Peter J. and Jeyachynthaya Persis J, Journal of Nanoscience and Technology, 2, 2016, 221-223.

37. Mekala J., and Rajan M. R., Green Synthesis of Copper oxide nanoparticles using Aqueous WilayathThulsi (HyptisSuveolens) Extract- Characterisation and Study of Antibacterial Effects, International Journal of Current Research, 8, 2016, 39655- 39661.

38. Niraimathi K. I., Lavanya R., Sudha V., Narendran R., and Brindha P., Bio-Reductive Synthesis and Characterisation of Copper Oxide nanoparticles (CuONPs) Using Alternanthera sessilis Linn. Leaf Extract, Journal of Pharmacy Research , 10, 2016, 29-32.

39. Saif S., Tahir A., Asim T. and Chen Y., Plant Mediated Green Synthesis of CuO Nanoparticles: Comparison of Toxicity of Engineered and Plant Mediated CuO Nanoparticles towards Daphnia magna, Nanomaterials, 6, 2016, 1-15.

40. Vanathi P., Rajiv P. and Sivaraj R., Synthesis and characterization of Eichhornia-mediated copper oxide nanoparticles and assessing their antifungal activity against plant pathogens, Bull. Mater. Sci., 39, 2016, 1165–1170.

41. Aminuzzaman M., Kei L. M., and Liang W. H., Green Synthesis of Copper Oxide (CuO) nanoparticles using Banana Peel Extract and Their Photocatalytic Activities, Green and Susstainable Technology, AIP Conference proceedings, 1828, 2017, 020016-1-020016-5.

42. Prasad, K. S., Patra, A., Shruthi, G. & Chandan S., Aqueous Extract of Saraca indica Leaves in the Synthesis of Copper Oxide Nanoparticles : Finding a Way towards Going Green. J. Nanotechnol. 2017, (2017), 6pages.

43. Karthikarani S. and Suresh G., Green Synthesis, Characterization And Its Antibacterial Activity of Copper Oxide Nanoparticles Using Oscimum Sanctum Leaves And Piper Nigrum Extract, International Journal for Research in Applied Science & Engineering Technology, 5, 2017, 411-419.

44. Narasaiah P., Kunar B. and Sarada N. C., Biosunthesis of Copper Oxide nanoparticles from Drypetessepiaria Leaf extract and thir catalytic activity to dye degradation, IOP Conf. Series: Materials Science and Engineering, 263, 2017, 1-9.

45. Yugandhar, P., Vasavi, T., Maheswari, U. and Savithramma N., Bioinspired green synthesis of copper oxide nanoparticles from Syzygiumalternifolium (Wt.) Walp ., Characterization and Evaluation of its synergistic antimicrobial and anticancer activity, Appl. Nanosci., 7, 2017, 417-427.

46. Rajendran A., Dhanraj S. E. C. and Senthilkumar S., A Green and Facile Approach for the Synthesis Copper Oxide Nanoparticles Using Hibiscus rosa-sinensis Flower Extracts and It's Antibacterial Activities, J Bioprocess Biotech., 8, 2018, 1-4.

47. Batool M., Hashmi F., Mehboob N., Qureshi Z. and Daoush W. M., Studies on Adsorption of Congo red (Acid Red 28) by Nano Copperoxide, Adv. Nanoscie. Nanotec., 2, 2018, 1-7.

48. Meshram S. p., Mulik U. P., Adhyapak A and Amalnerkar D. P., Facile synthesis of CuOnanomorphs and their morphology dependent sunlight driven photocatalytic properties, Chemical Engineering Journal, 204, 2012, 158-168.

49. Alabi A. B., Coppede N., Vilani M., Calestani D., Zappetini A., Babalola O. A. and Salvatore I., Photocatalytic Activity of Nanostructured Copper (II) oxide particles, Journal of Science, 15, 2013, 409-414.

50. Farghali A. A., Bahgat M., Enaiet Allah A. and Khedr M. H., Adsorption of Pb(II) ions from aqueous solutions using copper oxide nanostructures, beni-suef university journal of basic and applied sciences, 2, 2013, 61-71.

51. Anandhavalli N., Bency Mol., Manikandan S., Anisha N., Ponnisami V. and Rajan K. S., Green Synthesis of Cupric Oxide Nanoparticles Using the Water Extract of Murryakoenigi and its photocatalytic Activity, Asian Journal of Chemistry, 26, 2014, 1-4.

52. Farrouji A E., Eddine A. C., Bouzit S. E., Boualy B., Mehdi A., Firdoussi L. E. and Ali M. A., Degradation of Methylene Blue using Synthesized Nanostructured CuO with High Specific Surface Area through Catalytic oxidation, International Research Journal of Pure & Applied Chemistry, 8, 2015,190-197.

53. Katwal R., Kaur H., Sharma G., NAushad M. and Pathina D., Electrochemical synthesized copper oxide nanoparticles for enhanced photocatalytic and antimicrobial activity, Journal of Industrial and Engineering Chemistry, 2566, 2015, 1-12.

54. Ijaz, F., Shahid, S., Khan, S. A., Ahmad, W. and Zaman S., Green synthesis of copper oxide nanoparticles using Abutilon indicum leaf extract : Antimicrobial , antioxidant and photocatalytic dye degradation activities. Trop. J. Pharm. Res. April 16, 2017, 743–753.

55. Radhakrishnan A., Padmavathi R., Beena B., CuO nano structures as an ecofriendly nano photo catalyst and antimicrobial agent for environmental remediation. Int. J. Nano Dimens. 9, 2018, 145-157.

56. Elumalaia K and Velmurugan S, Green synthesis, characterization and antimicrobial activities of zinc oxide nanoparticles from the leaf extract of Azadirachta indica (L.), Applied Surface Science, 345, 2015, 329–336.

57. Mansoore H.K., Behzad S., Ali Akbar Saboury., Fateme D., Aboulfazl S and Mina E ,Green synthesis of zinc oxide nanoparticles and their effect on the stability and activity of proteinase K,RSC Adv,6, 2016, 42313-42323.

58. Sheela T., Arthoba Nayaka Y., Viswanatha R., Basavanna S and Venkatesha T.G, Kinetics and thermodynamics studies on the adsorption of Zn(II), Cd(II) and Hg(II) from aqueous solution using zinc oxide nanoparticles, Powder Technology, 217, 2012, 163–170.

59. Wang Y., Li X., Wang N., Quan X and Chen Y, Controllable synthesis of ZnO nanoflowers and their morphology-dependent photocatalytic activities, Sep. Purif. Technol, 62, 2008, 727–732.

60. Li X., Lv K., Deng K., Tang J., Su R., Sun J and Chen L, Synthesis and characterization of ZnO and TiO_2 hollow spheres with enhanced photoreactivity, Mater. Sci. Eng. B, 158, 2009, 40–47.

61. Mohajerani M.S., Lak A and Simchi A, Effect of morphology on the solar photocat-alytic behavior of ZnO nanostructures, J. Alloys Compd, 485, 2009, 616–620.

62. Li B and Wang Y, Facile synthesis and enhanced photocatalytic performance of flower-like ZnO hierarchical microstructures, J. Phys. Chem. C, 114 ,2010, 890–896.

63. Okorn M., Pongsapak P., Piyasan P and Joongjai P, Effects of synthesis conditions and annealing post-treatment on the photocatalytic activities of ZnO nanoparticles in the degradation of methylene blue dye, Chemical Engineering Journal, 164,2010, 77–84.

64. Nina K., Irina S., Vladimir B., Yanko D., Assya B and Ceco D, A comparative study on the photocatalytic efficiency of ZnO thin films prepared by spray pyrolysis and sol–gel method, Surface & Coatings Technology, 207, 2012, 5–10.

65. Subrata Kundu, A facile route for the formation of shape-selective ZnO nano architectures with superior photo-catalytic activity, Colloids and Surfaces A: Physicochem. Eng. Aspects, 446, 2014, 199–212.

66. Wen Z., Guoping T., HuajiZ.,Ying Z and LiLi Y, Synthesis and antibacterial activity of mesoporous zinc oxide particle with high specific surface area, Materials Letters,114,2014,119–121.

67. Li W. G. Amino-functionalization of Nanocrystalline Cellulose and Its Absorption Behavior. Jinan: Qilu University of Technology, 2015

68. Liu P., Borrell P. F., Bozic M., Kokol V., Okaman K., Mathew A. P. Nanocellulose and their phosphorylated derivatives for selective adsorption of Ag+, Cu2+ and Fe3+ from industrial effluents. Journal of Hazardous Materials, 2015, 294: 177-18.

69. Anirudhan T. S. and Shainy F. Adsorption behavior of 2-mercaptobenzamide modified itaconic acid-grafted-magnetite nanocellulose composite for cadmium (II) from aqueous solutions. Journal of Industrial and Engineering chemistry, 32, 2015, 157-166.

70. Zhao G, Zhang N and Sun K ,Porous MoO_3 films with ultra-short relaxation time used for supercapacitors Mater. Res. Bull. 48, 2013, 1328-1332.

71. Si-Wei Zhao, Chong-Rui Guo, Ying-Zhu Hu, Yuan-Ru Guo and Qing-Jiang Pan, The preparation and antibacterial activity of cellulose/ZnO composite: a review, Open Chem., 16, 2018, 9–20.

72. Zhang L., Ge H., Xu M., Cao J. and Dai y., Physicochemical properties, antioxidant and antibacterial activities of dialdehyde microcrystalline cellulose, Cellulose, 24, 2017, 1–12.

73. Zeng, J.; Liu, S.; Cai, J.; Zhang, L. TiO2 Immobilized in Cellulose Matrix for Photocatalytic Degradation of Phenol under Weak UV Light Irradiation , J. Phys. Chem. C, 114, 2010, 7806–7811.

74. Xu, X.,. Y. Q. Yang, Y. Y. Xing, J. F. Yang, and S. F. Wang. Properties of novel polyvinyl alcohol/cellulose nanocrystals/silver nanoparticles blend membranes. Carbohydrate Polymers, 98 , 2013, 1573–7.

75. Tu K., Wang, Q., Lu, A. and Zhang, L,Portable Visible-Light Photocatalysts Constructed from Cu2O Nanoparticles and Graphene Oxide in Cellulose Matrix, J. Phys. Chem. C, 118, 2014, 7202–7210.

76. Mohammed, N., Grishkewich, N., Waeijen, H. A., Berry, R. M., and Tam, K. C., Continuous flow adsorption of methylene blue by cellulose nanocrystal-alginate hydrogel beads in fixed bed columns, Carbohydr. Polym. , 136, 2016, 1194–1202.

77. Sharma, P. R.; Cattopadhyay, A.; Sharma, S. K.; Geng, L.; Amiralian, N.; Martin, D. and Hsiao,B. S., Nanocellulose from Spinifex as an Effective Adsorbent to Remove Cadmium(II) from Water, ACS Sustainable Chem. Eng., 6,2018, 279–290.

78. Liou, P., F. X. Nayigiziki, F. Kong, A. Mustapha, and M. Lin., Cellulose nanofibers coated with silver nanoparticles as a SERS platform for detection of pesticides in apples, Carbohydrate Polymers 157, 2017, 643–50.

79. Singla, R., S. Soni, P. M. Kulurkar, A. Kumari, M. S, V. Patial, Y. S. Padwad, and S. K. Yadav., In situ functionalized nanobiocomposites dressings of bamboo cellulose nanocrystals and silver nanoparticles for accelerated wound healing. Carbohydrate Polymers, 155, 2017, 152–62.

80. Ahmed, J., Y. A. Arfat, E. Castro-Aguirre, and R. Auras., Mechanical, structural and thermal properties of Ag-Cu and ZnO reinforced polylactide nanocomposite films, International Journal of Biological Macromolecules, 86, 2016, 885–892.

81. Arfat, Y. A., J. Ahmed, N. Hiremath, R. Auras, and A. Joseph., Thermo-mechanical, rheological, structural and antimicrobial properties of bionanocomposite films based on fish skin gelatin and silver-copper nanoparticles, Food Hydrocolloids, 62, 2017, 191–202.

82. Tani T., Madler L and Pratsinis S.E, Synthesis of Zinc Oxide /Silica Composite nanoparticles by Flame Spray Pyrolysis, Journal of Materials Science, 37, 2002, 4627-4632.

83. Brunauer S., Emmett P.H and Teller E, Adsorption of gases in multimolecular layers, Journal of the Am. Chem. Soc. 60, 1938, 309–319.

84. Kagan C.R., Murthy C.B and Bawendi M.G, Long range resonance transfer of electronic excitations in close packed CdSe quantum dot solids, Phys Rev B, 54, 1996, 8633-8643.

85. Timothy H Gfroerer, Photoluminescence in analysis of Surfaces and Interfaces, Encyclopedia of Analytical Chemistry ,John Wiley &Sons Ltd, Chichester, 2000,9209-9231.

86. Anirudhan T.S., Rejeena S.R and Binusree J., Adsorptive separation of myoglobin from aqueous solutions using iron oxide magnetic nanoparticles modified with functionalized nanocrystalline cellulose, J. Chem. Eng. Data, 58 ,2013, 1329–1339.

87. Ho Y.S., Wase D.A J and Forster C.F, Kinetic Studies of Competitive Heavy Metal Adsorption by Sphagnum Moss Peat, Environ. Technol., 17, 1996, 71–77.

88. Sips R, On the structure of a catalyst surface, J. Chem. Phys, 16, 1948, 490-495.

89. Yogesh K.K., Muralidhara H.B and Arthoba Y, Hiararchically assembled mesoporous ZnO nanorods for the removal of lead and cadmium by using differential pulse anodic stripping voltametric method, Powder Technology, 239, 2013, 208-216.

90. Li X., Wang D., Cheng G., Luo Q., An J., Wang Y.g, Preparation of polyaniline-modified TiO_2 nanoparticles and their photocatalytic activity under visible light illumination, Appl. Cat. B 81, 2008, 267-273.

91. Brayner R., Ferrari-Iliou R., Brivois N., Djediat S., Benedetti M.F and Fievet F, Toxicological impact studies based on Escherichia coli bacteria in ultrafine ZnO nanoparticles colloidal medium, Nano Lett., 6, 2006, 866–870

92. Aanchal J., Richa B., and Pankaj P, Probing interaction of Gram-positive and Gram-negative bacterial cells with ZnO nanorods, Mater Sci. and Eng C, 33, 2013, 1247–1253.

93. Anita S, Ramachandran T., Rajendran R., Koushik C. V. and Mahalakshmi M., A study of the antimicrobial property of encapsulated copper oxide nanoparticles on cotton fabric, Text. Res. Jl., 81, 2011, 1081–1088.

94. Manikandan A and Sathiyabama M, Greensynthesis of copper chitosan nanoparticles and study of its antibacterial activity, Nanomed. Nanotechnol. 6, 2015, 1–5.

95. Wang. P, Zhao. J, Xuan. R., Wang. Y, Zou. C, Zhang. Z, Wan. Y and Xu. Y, Flexible and monolithic zinc oxide bionanocomposite foams by a bacterial cellulose mediated approach for antibacterial applications, Dalton Transactions, 431, 2014, 6762-6768.

96. Zhao S.W, Zheng. M, Zou. X.H, Guo. Y and Pan. Q.J, Self- Assembly of Hierarchically Structured Cellulose @ ZnO Composite in Solid-Liquid Homogeneous Phase: Synthesis, DFT Calculations, and Enhanced Antibacterial Activities, Acs Sustainable Chemistry & Engineering, 51, 2017, 6585-6596.

97. Prasanna V.L and Vijayaraghavan R, Insight into the Mechanism of Antibacterial Activity of ZnO: Surface Defects Mediated Reactive Oxygen Species Even in the Dark, Langmuir, 311, 2015, 9155-9162.

98. Ba-Abbad M.M, Takriff M.S, Benamor A, Mahmoudi E and Mohammad A.W, Arabic gum as green agent for ZnO nanoparticles synthesis: properties, mechanism and antibacterial activity, Journal of Materials Science-Materials in Electronics, 281, 2017, 12100-12107.

99. AliS.S.,QuasiI.A., Muhammed Arshad, ZahiruddinKhan, Thomas C. Voice, Ch.Tahir Mehmood, Photocatalytic degradation of low density polyethylene (LDPE) films using titania nanotubes. Environmental Nano technology, Monitoring & Management, 5, 2016, 44-53.

100. Daneshvar.D, Ashassi Sorkhabi & Tizpar, Decolorization of orange II by electrocoagulation method, Separation and Purification Technology, vol 31(2)2003 153-162.

101. Tim Luttrell, Sandamali Haipegamage, Junguang Alan Kramer, Eli Sutter & Matthias Batzill, Why is anatase a better photocatalyst than rutile?- Model studies on epitaxial TiO_2 films,Sci.Rep,10; 2014,4:4043 .

102. Hosseini A.H, RaminSaeedi, Bulletin of Chemical Reaction Engineering & Catalysis 12(1)2017, 96-105.

103. Evaluation of Polyaniline Nanocomposites of TiO_2 and ZnO for Environmental Remediation: Shanavas Khan, Ph.D Thesis Submitted to Kerala University in 2018.

104. Nano Composites of Copper Oxide and Trimanganese Tetra Oxide for Environmental and bio medical Applications: Sreekala, Ph.D Thesis Submitted to Kerala University in 2020.

105. Synthesis and Evaluation of Nano Zinc Oxide and its Composites for Environmental Remediation: Rejani P, Ph.D Thesis Submitted to The Kerala University in 2016.

106. Evaluation of Size / Morphology Dependent Properties and Applications of Zinc oxide Copper Oxide and Their Nano composites: Asha Radhakrishnan, Ph.D Thesis Submitted to The Kerala University in 2016.

Annexure - I

LIST OF PUBLICATION

1. *Baiju V, Dedhila Devadathan, Sajeevkumar G and* ***Raveendran,*** *(2020), PANI based metaloxide nanocomposite-A novel material for water purification, Aadvances in Nanoscience and Nanotechnology, 4, 37-40.*
2. *Nahi Jamal, Asha Radhakrishnan,* ***Raveendran Raghavan*** *and Beena Bhaskaran,(2020)Efficient photocatalytic degradation of organic dye from aqueous solutions over zinc oxide incorporated nanocellulose under visible light irradiation,Main Group Met. Chem.,43,84-91.*
3. *Megha S, Dedhila Devadathan,V Baiju and* ***R Raveendran****, (2019), Structural, Optical and Photocatalytic Degradation Studies of Polymer Based* Fe_2O_3 *Nanocomposite, IOP Conf. Series: Journal of Physics: Conf. Series 1172, 012051*
4. *P K Anjali Nambiar, Dedhila Devadathan, V Baiju and* ***R Raveendran****, (2019), Structural and antibacterial studies of rice straw based ZnO nanocomposite, IOP Conf. Ser.: Mater. Sci. Eng. 577 012136*
5. *Deepika R, Dedhila Devadathan, Rejani P and* ***Raveendran R****, (2019), Structural and photocatalytic degradation studies of rice straw based MgO nanocomposite, IOP Conf. Ser.: Mater. Sci. Eng. 577 012137*
6. *Dedhila Devadathan, Baiju V,* ***Raveendran R****, (2018), Antibacterial studies of polyindole based metal oxide nanocomposites, Bulletin of Pure and Applied Sciences, Vol.37 C (Chemistry), No.1, 42-52.*
7. *Baiju V, Dedhila Devadathan,* ***Raveendran R****, (2018), Photocatalytic degradation of an acidic dye and a basic dye using heterostructured photocatalyst, Bulletin of Pure and Applied Sciences, Vol.37 C (Chemistry), No.1, 35-41.*
8. *Dedhila Devadathan, Baiju V, Biju R,* ***Raveendran R****, (2017), Synthesis, Characterization and Application ofNiO/ZnOHeterostructured Adsorbent for Heavy Metal Ions, International Journal of Advance Research in Science and Engineering, 6, Special Issue No. 03, 194 – 198.*

9. *Baiju V, Dedhila Devadathan, Biju R,* ***Raveendran R****, (2017), Photocatalytic Degradation Studies of Polyaniline Based ZnO-Al_2O_3 Nanocomposite, International Journal of Advance Research in Science and Engineering, 6, Special Issue No. 03, 120 – 124.*

10. *Bhagya J, Dedhila Devadathan, Baiju V, Biju R,* ***Raveendran R****, (2017), Synthesis, Characterization and Photocatalytic Activity of MgO Nanoparticles, International Journal of Advance Research in Science and Engineering, 6, Special Issue No. 03,142 – 150.*

11. *Dhanuja B. S, Dedhila Devadathan, Baiju V, Biju R,* ***Raveendran R,*** *(2017), Synthesis, Characterization and Antibacterial Activity ofNiO Nanoparticles, International Journal of Advance Research in Science and Engineering, 6, Special Issue No. 03, 162 – 167.*

12. *mJoyal Mary, Dedhila Devadathan, Baiju V, Biju R,* ***Raveendran R****, (2017), Photocatalytic Degradation Of Azo Dye Congo Red Using Copper Oxide/Nickel Oxide Nanocomposite, International Journal of Advance Research in Science and Engineering, 6, Special Issue No. 03, 284 – 287.*

13. *C R Indulal , R Biju, Deepak Nand,* ***R Raveendran*** *(2017) Structural, optical studies of zinc magnesium oxide and zinc copper oxide nanocomposites* **,** *International Journal of Advance Research in Science and Engineering, 6, Special Issue No. 03, 316 – 318.*

14. *C R Indulal , R Biju, Deepak Nand,* ***R Raveendran*** *(2017)Optical and Anti Bacterial Studies of Zinc Magnesium Oxide Nano Composite, Oriental Journal of Chemistry, Vol.33.No(3).1545-1549.*

15. *C R Indulal , R Biju, Deepak Nand,* ***R Raveendran*** *(2017) Dielectric and Optical Band Gap Studies of Nano Structured Manganese Nickel Oxide and Cobalt Nickel Oxide, Oriental Journal of Chemistry, Vol.33.No(3).1581-1588.*

PAST

ISSN: 2640-557

Research Article

Advances in Nanoscience and Nanotechnology

PANI Based Metal Oxide Nanocomposite – A Novel Material for Water Purificatio

Baiju V[1,2]*, Dedhila Devadathan[1,2], Sajeevkumar G[1,2] and Raveendran R[1,2]

[1]Nanoscience Research Laboratory, Department of Physics, Sree Narayana College, Kollam, India

[2]Research Centre , University of Kerala, India

*Corresponding author

Baiju V, Nanoscience Research Laboratory, Department of Physics, Sree Narayana College, Kollam, India

Submitted: 20 Apr 2020; Accepted: 05 May 2020; Published: 30 May 2020

Abstract

In the present work NiO/ZnO was synthesized from combustion method, polyaniline and the polyaniline based NiO/ ZnO using chemical oxidation method. The synthesized materials were characterized using XRD and UV/Vis absorbance spectroscopy. From XRD, the formation of NiO/ZnO was confirmed. The study investigates the applicability of NiO/ ZnO Nanocomposite as photo catalyst for the degradation of organic dyes. Results suggested an increase in degradation efficiency in the case of polymer nanocomposite when compared to counter parts.

Keywords: Nanocomposite, Chemical oxidation, Combustion, Photocatalysis

Introduction

Water contamination becomes a serious issue due to the facts that 2% of dyes produced in the industries are discharged directly in aqueous effluent [1]. So it was necessary to find a new way to remove coloured dyes before discharging them into the environment [2, 3]. The various conventional technologies currently employed in the removal of effluents in industrial water are classical and do not lead to complete destruction of pollutants. In the case of industrial dyes, these methods do not work efficiently due to high solubility of dyes as well as their resistance to chemical and biological degradation; also they just transfer the contaminants from one phase to another [4]. Therefore, there is a need to develop a novel treatment method that is more effective. Photo catalysis is a promising technology in the field of green technology for the removal of dyes. Presently nanotechnology is widely applied for purification and treatment of waste water. The novel properties of nano materials such as large surface area, potential for self-assembly, high specificity, high reactivity and catalytic potential make them an excellent candidate for this application [5]. An expanding trend for the nanomaterials is the fabrication of composite structures and devices with materials capable of enhancing the properties of the composite material. This can be achieved either by utilizing the size advantage through templating on the nanomaterials and enhancing the properties to drive new synergetic properties of two combined materials [6]. In the present study Polyaniline based NiO/ZnO nanocomposite was prepared, analysed and used as photo catalyst for the degradation of Congo red and Malachite green.

Materials and Methods

AR grade chemicals obtained from Merck were used for the preparation of NiO/ZnO, Polyaniline and the Polyaniline based Nanocomposite. NiO/ZnO (NZF) was prepared by the combustion method. Polyaniline (PANI) and the polyaniline based NiO/ZnO Nanocomposite (PANINZ) was prepared using chemical oxidation method. NiO/ZnO annealed at 5000c for three hours, Polyaniline and Polyaniline based nanocomposite are as prepared form were used for analysis. For the preparation of the Polyaniline nanocomposite NZF was used. XRD study was carried out using XPERT-PRO model powder diffractometer (PAN analytical, Netherlands) employing Cu-Kα radiation (λ = 1.54060A°) operating at 40kV, 30mA. The absorbance spectra of these samples were studied using JASCO V 650, UV/V is spectrophotomer. Photo catalytic studies in the present work were carried out using JASCO V 650, UV/V is spectrophotomer.

Results and Discussion

XRD Analysis

NZF showed well defined X-ray diffraction peaks which indicated that NZF had crystalline nature. Again, the broader diffraction peaks indicated the smaller crystallite size. The inter planar spacing (d_{hkl} values), 2θ values and relative intensity values of NZF corresponding to the observed diffraction peaks were compared with the standard values of NiO and ZnO as reported by JCPDS-International Centre for Diffraction Data. The data obtained for NZF matched with JCPDS-ICDD pattern number #78-0423 of NiO and JCPDS-ICDD pattern number #79-0205 of ZnO separately. From JCPDS, NiO shows cubic system with FCC lattice and ZnO shows hexagonal system with primitive lattice. The variation observed in the d values of the crystal planes in case of NZF when compared to NiO and ZnO from JCPDS, confirms the formation of composites. The average crystallite size of NZF calculated from the line broadening of the XRD pattern, using FWHM values of seven major peaks in the XRD spectrum making use of Scherer formula,

$$D = \frac{K\lambda}{\beta \cos\theta} \quad (1)$$

Here, D is the average crystallite size normal to the reflecting planes, k – is the shape factor which lies between 0.95 and 1.15 depending on the shape of the grains (k =1 for spherical crystallites), λ-is the

wavelength of x-ray used and ($_{hkl}$) measured is the FWHM of the diffraction line in radians and θ_{hkl} is the Bragg angle corresponding to the diffraction line arising from the planes designated by Miller indices (hkl). The crystallite size for the sample is 18.73 ± 3 nm.

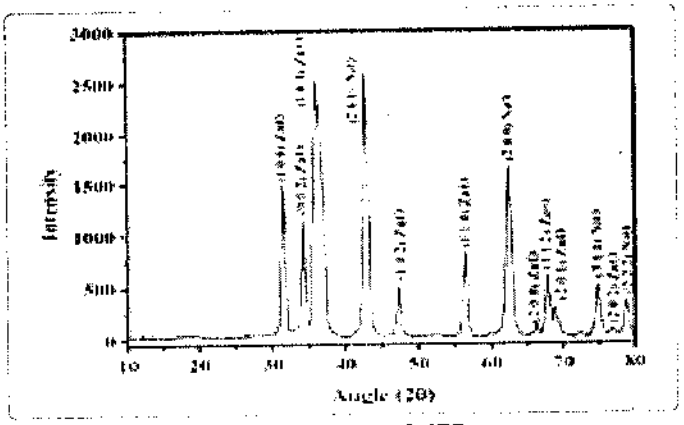

Figure 1: XRD of NZF

XRD of PANI shows an amorphous nature of the polymer. XRD of PANINZ confirms the formation of Nanocomposite. The well-defined peaks of planes of ZnO and NiO were found to be incorporated into the XRD spectrum of Polyaniline (Figure 2a). It is clear that the metal oxide particles are well distributed in the polymer matrix. Here also the crystalline peaks in the region between 150 and 300 observed in PANINZ showed variations when compared to the XRD of polyaniline which also supports the formation of Nanocomposite (Figure 2b).

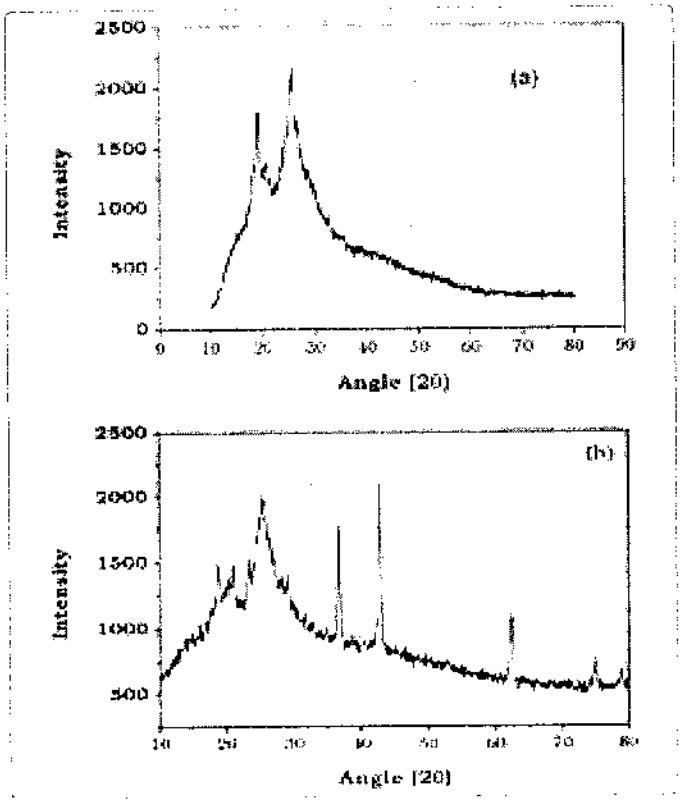

Figure 2: XRD of (a) PANI and (b) PANINZ

UV Analysis

The UV/Vis absorption and reflectance spectra of NZF taken in the wavelength range 210 to 870 nm with 1 nm resolution are shown in the Figure 3(a). Presence of a weak absorption band was observed in the range 225 nm – 270 nm with λ_{max} situated at 256nm and also another strong absorption band in the range 260 nm – 400 nm with λ_{max} situated at 360 nm was also obtained. The second band can be attributed to the presence of ZnO which could be assigned to the intrinsic band-gap absorption of ZnO due to the electron transitions from the valence band to the conduction band (O2p → Zn3d). The absorption edge (AE) is calculated from the equation, $E = hc/\lambda_{max}$ where h is Plank's constant and c is the velocity of light. The absorption edge was found to be 3.44 eV for NZF.

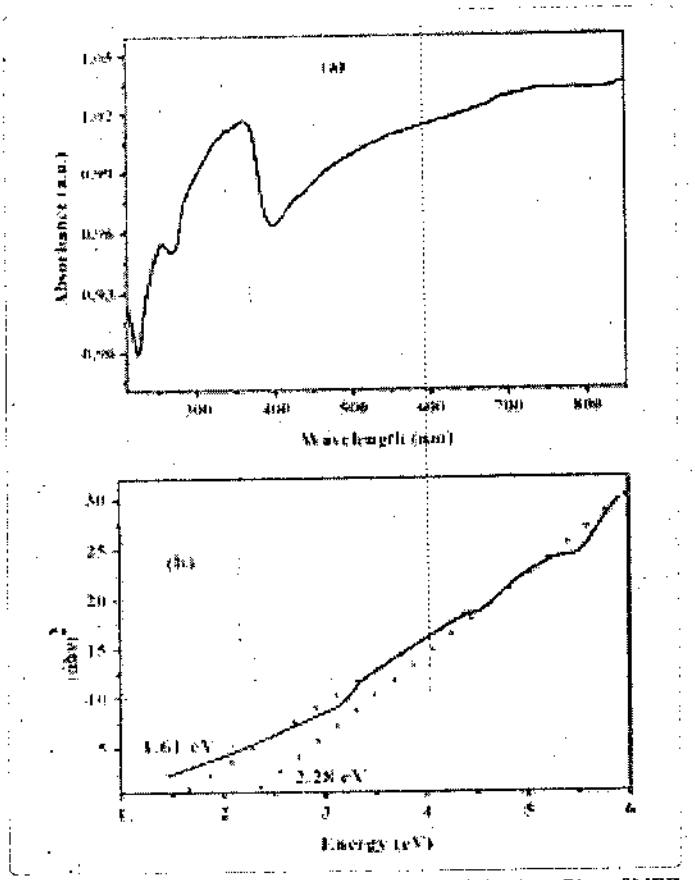

Figure 3: (a) UV/Vis Absorbance spectrum and (b) Tauc Plot of NZF

The optical band gap determined from the absorption spectra using Tauc's relation for NZF is shown in Figure 3 (b). The material showed multiple band gaps. Polyaniline showed sharp absorption in the range 225-325 nm with λ_{max} situated at 292 nm, attributed to the conjugation of benzene ring. [7, 8]. Presence of small absorption band is observed in the range 435 – 543 nm with λ_{max} situated at 478 nm due to the π - π^* transitions of the benzene ring in the polyaniline molecular chains [7]. The results indicate presence of enhanced conjugated segments and easy flow of charge in polyaniline molecular matrix. This band also relates to the extent of conjugation between adjacent rings in the polymer chain. The absorption edge is found to be 4.19 eV and 2.6 eV for the peaks corresponding to 292 nm and 478 nm respectively.

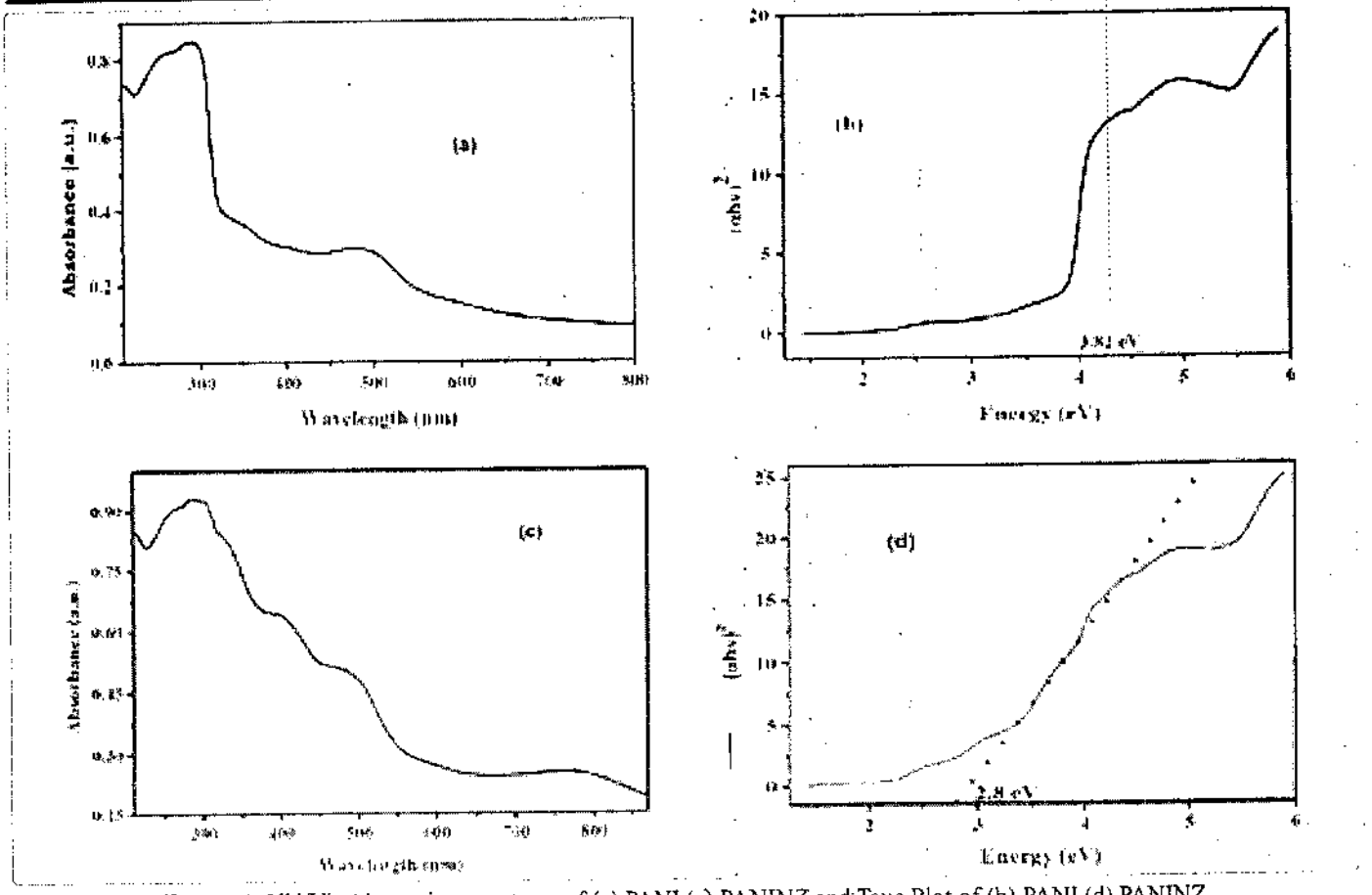

Figure 4: UV/Vis Absorption spectrum of (a) PANI (c) PANINZ and Tauc Plot of (b) PANI (d) PANINZ

The optical band gap of the material determined from the absorption spectrum using Tauc's relation was 3.82 eV. Tauc's plot drawn for polyaniline is shown in Figure 4. Due to large value of the optical band gap, the material is most suited in many applications in modern electronic industries.

The UV/Vis absorbance spectrum of PANINZ showed multiple absorption peaks in addition to the main peak observed in polyaniline due to π - π^* transitions The peak of polyaniline around 292 nm became a broad absorption band with peak value at 288 nm. This could be attributed to the interactions between polyaniline chains and nickel oxide – zinc oxide nano particles. The shift in λ_{max} of polyaniline indicates the incorporation of nickel oxide – zinc oxide nano particles into the polymer matrix. The multiple peaks observed might be due to the n- π^* and n-π transitions as a result of the interactions between polyaniline chains and nickel oxide – zinc oxide nano particles. This causes easy charge transfer from polyaniline to nickel oxide – zinc oxide. The absorption edge corresponding to 288 nm was found to be 4.3 eV.

Photo catalytic Studies

The organic dyes used for the present study are Congo Red (CR) and Malachite Green (MG). Pure CR absorbs at λ_{max} values of 344 nm and 498 nm whereas pure MG absorbs at λ_{max} 369 nm and 616 nm respectively. In the case of photo degradation studies the λ_{max} value 498 nm was taken as reference for CR and in case of MG both λ_{max} values at 369 nm and 616 nm were considered.

The photo catalytic activity of samples for the degradation of the dyes; Congo red (CR) and Malachite green (MG) were studied using the respective photo catalyst in the presence of UV illumination in a photo reactor. The experiments were performed by suspending the desired amount of photo catalyst into 300 ml of dye solution of desired concentration of 50 ppm. The experiment was carried out isothermally at 300 K. The concentration of residual dye in the solution after irradiation for two and a half hours was determined by monitoring the absorbance intensity of solution samples at their maximum absorbance wavelength by using UV-Vis spectrophotometer (JASCO V 650 UV/Vis spectrophotometer). To study the effect of contact time on the photo degradation of organic dyes, the respective dye solution of concentration, 50 ppm in 300 ml solution kept at 300 K, 0.1 g of the photo catalyst was added and was kept under UV light. After desired time intervals [30, 60, 90, etc.], 10 mL of the solution was taken out, centrifuged and UV/Vis absorption spectra was recorded. The photo catalytic degradation efficiency was calculated as follows:

$$\text{Photocalytic Degradation Efficiency (\%)} = \frac{(C_0 - C_t)}{C_0} \times 100$$

C0: initial concentration of dye solution [mgL-1],
Ct: final concentration of dye solution [mgL-1],

The photo degradation of Congo red using the Nanocomposite PANINZ as well as its counterparts were studied in detail. From the Figure 5 it is evident that the absorption peak at 498 nm showed a

decrease in peak intensity with increase in time. The results show high rate of photo degradation of the dye with increase in contact time. With further increase in contact time the rate of degradation can be further increased. When compared to Nanocomposite the rate of degradation of counterparts were low.

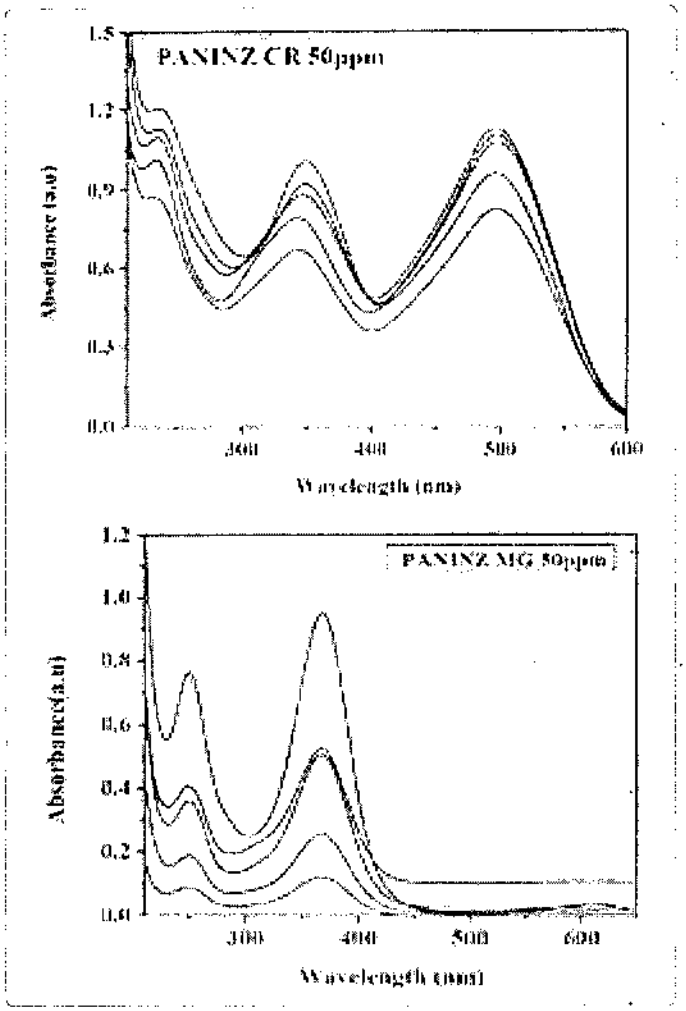

Figure 5: Photo catalytic degradation of CR and MG using PANINZ

The photo degradation efficiency of PANINZ for degradation of Malachite green after 120 minute was found to be 95%. The percentage of photo degradation increased with increase in contact time of the dye and the catalyst. Here also, the rate of degradation of counterparts was low when compared to Nanocomposite. Comparatively the Nanocomposite was found to be a fast acting photo catalyst for the degradation of Malachite green.

It was also found to be effective in case of Congo red also, but for complete degradation it may take longer time in comparison with malachite green. PANINZ reported in the present study showed very good photo catalytic activity. It was observed from the UV/Vis spectral analysis that the Nanocomposite showed absorption in visible range in addition to UV light. Hence these materials could be used as photo catalyst in the degradation of organic dyes under solar ray irradiation. Results suggested an increase in degradation efficiency in the case of polymer Nanocomposite when compared to metal oxides. It is suggested that these materials could be efficiently used as anti-bacterial, deodorizing, air purifying, anti-fogging and as other surface purification agents.

Conclusion

PANINZ reported in the present study showed very good photo catalytic activity. It was observed from the UV/Vis spectral analysis that the nanocomposite showed absorption in visible range in addition to UV light. Hence these materials could be used as photo catalyst in the degradation of organic dyes under solar ray irradiation. Results suggested an increase in degradation efficiency in the case of polymer nanocomposite when compared to metal oxides. It is suggested that these materials could be efficiently used as anti-bacterial, deodorizing, air purifying, anti-fogging and as other surface purification agents.

References

1. MA. Rauf, I. Shehadeh, A. Ahmed, A. Al-Zamly (2009) Removal of Methylene Blue from Aqueous Solution by Using Gypsum as a Low Cost Adsorbent, *World Academy of Science: Engineering and Technology* 55.
2. CI. Pearce, JR. Lloyd, JT. Guthrie (2003) The removal of colour from textile wastewater using whole bacterial cells: a review, *Dyes and Pigments* **58:** 179–196.
3. T. Robinson, G. McMullan, R. Marchant, P. Nigam (2001) Remediation of Dyes in Textile Effluent! A Critical Review on Current Treatment Technologies With a Proposed Alternative, *Bioresource Technology* 77: 247–255.
4. L. Mun (2008) Degradation of dyes using zinc oxide as the photocatalyst, *M.S. thesis*, Putra University, Serdang, Malaysia.
5. Shuna Zhang, Fangyi Cheng, Zhanliang Tao, Feng Gao, Jun Chen (2006) Removal of nickel ions from wastewater by Mg(OH)2/MgO nanostructures embedded in Al2O3 membranes, *Journal of Alloys and Compounds* **426:** 281-285.
6. Neamtu J and Verga N (2011) Magnetic Nanoparticles for Magneto-Resonance Imaging and Targeted Drug Delivery, *J.of Nanomat. and Biostru* 6: 969-978.
7. Eraldemir O, Sari B, Gok A, Unal HB (2008) Synthesis and Characterization of Polyindole/Poly(vinyl acetate) Conducting Composites, J. Macromol Sci.Part A Pure Appl. Chem. 45: 205-211.
8. Xu J, Hou J, Zhou W, Nie G, Pu S et al. (2006) 1H NMR spectral studies on the polymerization mechanism of indole and its derivatives, Spectrochim.Acta, Part A, 63: 723-728.

Copyright: ©2020 Baiju V, et al. This is an open-access article distributed under the terms of the Creative Commons Attribution License, which permits unrestricted use, distribution, and reproduction in any medium, provided the original author and source are credited.

Research Article

Open Access

Nahi Jamal, Asha Radhakrishnan, Raveendran Raghavan and Beena Bhaskaran*

Efficient photocatalytic degradation of organic dye from aqueous solutions over zinc oxide incorporated nanocellulose under visible light irradiation

https://doi.org/10.1515/mgmc-2020-0009
Received September 15, 2018; accepted April 29, 2020.

Abstract: Increased growth of textile industries leads to the tremendous accumulation of dyes on water and surrounding environments. This terrific increase of dyes is the major cause of water pollution which in turn adversely affects the aquatic lives and the balance of our ecosystem. Purpose of the present study is to report the synthesis and characterization of a composite namely zinc oxide incorporated nanocellulose (ZnO/NC) for effective degradation of an anionic dye, Congo red. Fourier transform infrared spectroscopy (FTIR), X-ray diffraction (XRD), Brunaeur, Emmett and Teller (BET) surface area analysis and scanning electron microscopy (SEM) studies have helped to characterize the composite. The optical properties of the samples were studied by UV-Visible spectroscopy. Feasibility of the photocatalyst in the degradation of Congo red was tested. Experimental conditions such as time of contact, concentration of the dye solution, catalyst dosage, pH were altered to find out the optimum conditions of degradation. The optimum pH was found to be 5.5 and dosage of ZnO/NC was optimized as 0.075 g for a dye concentration of 20 ppm. Equilibrium was attained at 120 min. The studies reveal that the photocatalyst ZnO/NC is efficient for the photodegradation of Congo red. Photodegradation was due to electron hole interaction between metal oxides and nanocellulose.

Keywords: zinc oxide; sugar cane bagasse; photodegradation; photocatalyst

1 Introduction

In recent decades, due to rapid industrialization, huge amount of toxic effluents are being discharged to water bodies (Ansari et al., 2015). A large number of industries such as leather, paper, plastic, textile, food processing, printing, cosmetics and pharmaceuticals, etc., deal with dyes. The dye containing waste water can adversely affect the aquatic environment due to decreased sunlight penetration. In addition to these, some of the dyes can cause serious health problems such as mutation and cancer (Kumar et al., 2013). Serious issues of this water pollution are the shortage of safe water for drinking, household uses, agriculture, farming, etc., (Radhakrishnan et al., 2015). Therefore it is necessary to eliminate water pollution (Pourmortazavi et al., 2017). Physical methods such as adsorption and chemical methods such as chlorination and ozonation are some of the most frequently used methods for the removal of textile dyes (Chennakesavulu et al., 2015). Floculation and reverse osmosis are also some other methods commonly used, but these methods are not destructive. They just transfer the contaminants from one phase to another for which further treatments are required (Guillard et al., 2003). But Advanced oxidation process (AOP) like heterogeneous photocatalysis is a promising technology for water purification going on the surface of photocatalyst under the irradiation of photons, leading to total mineralization of dyes (Nagaveni et al., 2004), pesticides, organic-inorganic pollutants and other deleterious pollutants. In

* **Corresponding author: Beena Bhaskaran,** Department of Chemistry, Kumbalath Sankupilla Memorial Devaswom Board College, Sasthamcotta, Kollam, Kerala, India
Nahi Jamal, Department of Chemistry, Kumbalath Sankupilla Memorial Devaswom Board College, Sasthamcotta, Kollam, Kerala, India
Asha Radhakrishnan, Department of Chemistry, Devaswom Board Pampa College, Parumala, Kerala, India
Raveendran Raghavan, Department of Physics, Sree Narayana College, Kollam, Kerala, India

Open Access. © 2020 Jamal et al., published by De Gruyter. This work is licensed under the Creative Commons Attribution alone 4.0 License.

photocatalysis, organic pollutants are degraded by using reusable photocatalysts, energetic light source such as sunlight or an artificial light and an oxidizing agent such as oxygen or air (Hachem et al., 2001). For a photocatalyst, as the particle size decreases, surface area increases and the number of active sites increases which leads to high reactivity (Alaton et al., 2002). As the number of active sites increases, the absorbance of pollutants on the surface of the catalyst increases (Augugliaro et al., 2002). The promoting of photoreaction in presence of a catalyst is termed as heterogeneous photocatalysis, a low cost and sustainable technology for the treatment of organic and inorganic pollutants present in water. In photocatalysis degradation takes place when the photocatalyst adsorbs photons of energy greater than its band gap energy (Anirudhan et al., 2015). A hole-electron generation occurs when the electron excites from the valence band to conduction band of the semiconductor. These electrons react with O_2 to form $O_2^{\cdot-}$ and holes react with OH^- or H_2O to form $OH^{\cdot}$ which are the active species to react with organic dyes.

Photocatalysis by semiconductors has gained much more attention due to its applications in hydrogen production, refractory pollutants elimination and self-cleaning surface. Wide band gap of metal oxides limit their ability to absorb visible light. Therefore many efforts such as metal or non-metal doping (Wang et al., 2014), composite synthesis (Mukherjee et al., 2014), etc., have been made to lower their band gap. Among these processes fabrication of composites with polymers has been shown to effectively lower the band gap and allows greater absorption in the visible region (Ansari et al., 2015). Such composites are expected to achieve synergetic and complementary behavior between the components.

In the present work we report the synthesis of a composite assembled from nano zincoxide (ZnO) and nanocellulose (NC). Nano ZnO is a photocatalyst with excellent properties and has many applications. Semiconducting metal oxides have photocatalytic activities for the degradation of pollutants. Metal oxide nanoparticles like ZnO and TiO_2 have been used to degrade non-biodegradable pollutants such as dyes via photocatalytic routes. In the present work, nanocellulose prepared from sugarcane bagasse was selected for the synthesis of composites with ZnO. Sugarcane bagasse is a waste product produced by the sugar and alcohol industries (Simkovic et al., 1990). It is used as a raw material for industrial applications like electricity generation, pulp and paper production and products based on fermentation (Pandey et al., 2000). Nanocellulose has been obtained from the inexpensive and readily available lignocellulosic material namely sugarcane bagasse by acid hydrolysis (Bondeson et al., 2006). For the preparation of NC, we hereby suggest a modified acid hydrolysis approach by an ecofriendly method. On the conversion of cellulose to nanocellulose, efficiency is enhanced due to the increase in the number of available functional groups, increase in surface area and crystalline nature. The NC prepared is made into a composite with nano ZnO and it is well characterized by different experimental techniques like XRD, FTIR, UV-Visible spectroscopy, SEM and BET surface area measurements. The photocatalytic activity of the materials was studied through the degradation of Congo red (CR). CR is an anionic dye frequently used in textile industry. Experiments were carried out to optimize the conditions like pH, time, initial concentration and adsorbent dosage.

2 Results and discussion

2.1 XRD analysis

The XRD of the synthesized ZnO samples (Figure 1) show broad peaks at 2θ values of 31.9, 34.6, 36.4, 47.7, 56.7, and 63.1 which are typical for the hexagonal ZnO wurtzite structure with lattice parameters a and c of 3.249 and 5.205 A°, respectively. The observed peaks of the nano crystallites match well with standard JCPDS files (36-1451), and no other crystalline phases were detected. The XRD of NC gives a broad hump between 16.1° and 23.2° indicating its amorphous nature. The XRD of ZnO/NC confirms the formation of nanocomposites. The well-defined peaks

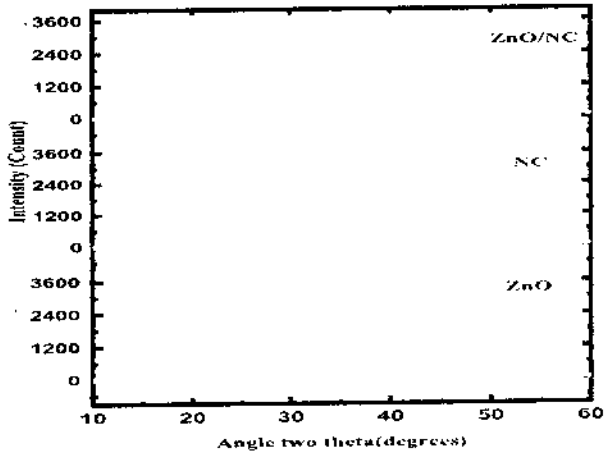

Figure 1: XRD of ZnO, NC, and ZnO/NC.

corresponding to the crystal planes (1 0 0), (0 0 2) and (1 0 1) of nano ZnO were found to be incorporated into the XRD of NC. It is thus clear that the metal oxide particles are well distributed in the nanocellulose matrix. Further, a change in intensity is observed in the characteristic peak of NC ($2\theta = 23.2°$) which again confirms the formation of nanocomposite. The average size of the particles was determined from full width at half maximum (FWHM) of the diffraction peaks using Scherrer's equation (Ahmmad et al., 2010):

$$D = \frac{k\lambda}{\beta\cos\theta} \quad (1)$$

where K is the shape factor ($K = 0.9$), β represents the full width at half maximum (FWHM), θ is the Bragg angle and λ is the wavelength of X-rays used. The particle size calculated for ZnO was found to be 26 nm.

2.2 FTIR analysis

The FTIR spectrum of ZnO (Figure 2) shows bands at around 566 cm^{-1}, which can be assigned to the vibrations of Zn (II)–O bonds. The absorption peaks observed at ~2500 cm^{-1} and ~1400 cm^{-1} may be due to the the adsorbed water and CO_2 molecules. The characteristic peaks of cellulose (Li et al., 2012) at 3400 cm^{-1}, 2800 cm^{-1} (due to O–H stretching and C–H stretching vibrations), 1371 cm^{-1}, and 897 cm^{-1} (due to O–H bending and C–H deformation vibration) are observed in the FTIR of NC prepared in the present study. In the FTIR spectrum of the composites, the main characteristic bands of NC and ZnO are retained. However, the incorporation of metal oxides leads to the shift of some bands of NC.

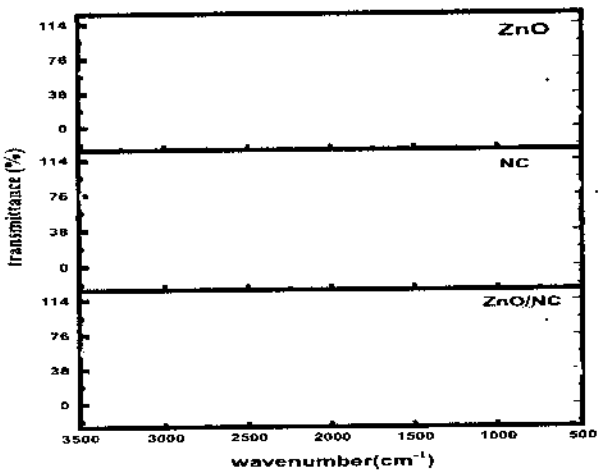

Figure 2: FTIR spectra of ZnO, NC, and ZnO/NC.

2.3 SEM analysis

The SEM results of the prepared samples are shown in Figure 3. SEM of ZnO consists of homogeneous; almost flower shaped nanostructures with less agglomeration. The SEM of NC reveals its sheet like morphology. ZnO/NC shows morphology entirely different from the flower like and sheet like morphologies of its components via ZnO and NC.

2.4 UV analysis

The room temperature UV-Visible spectra of the prepared samples were taken in the range of 250 to 600 nm are shown Figure 4. The spectrum of ZnO shows absorption peak at 380 nm which can be consigned to the intrinsic

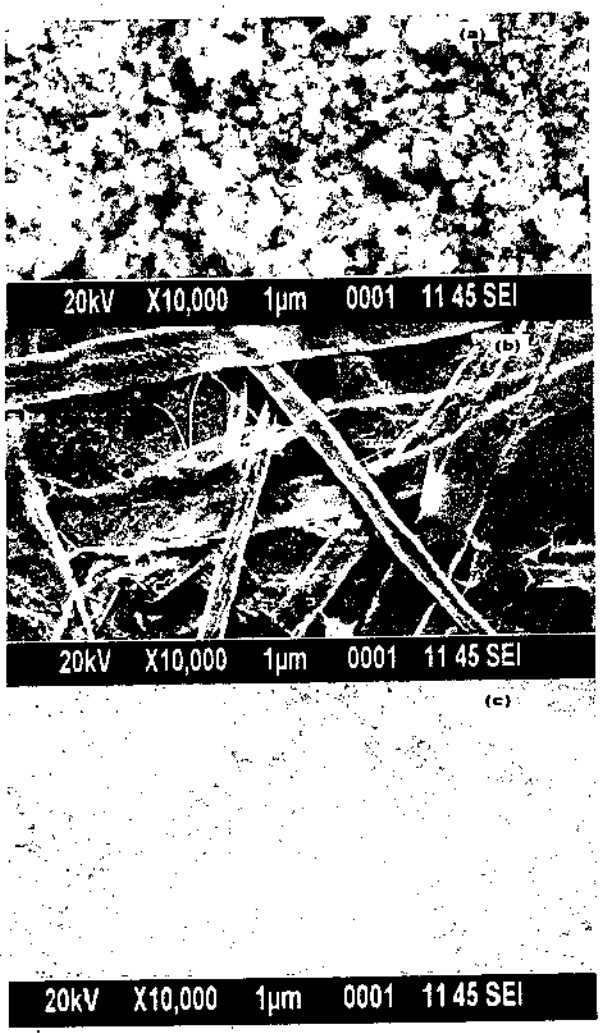

Figure 3: SEM images of (a) ZnO, (b) NC, and (c) ZnO/NC.

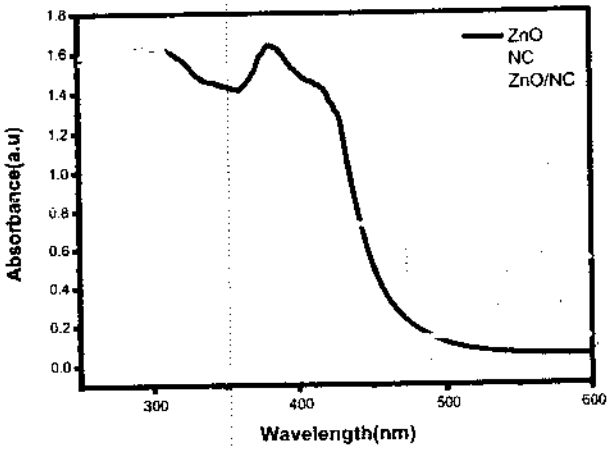

Figure 4: UV-Visible spectra of ZnO, NC, and ZnO/NC.

band gap absorption of ZnO due to the transition of electrons from valence band to conduction band (O2p–Zn3d) (Khorsand Zak et al., 2011). The spectrum of NC shows absorption band with λ_{max} value of 300 nm. When ZnO nanoparticles are doped into NC, broad and strong absorption with a maximum at 360 nm was perceived, which was blue shifted relative to the ZnO (380 nm) due to the quantum confinement (Prasad et al., 2006). The band gap of the samples was determined from the absorption spectra using Wood-Tauc's relation (Khorsand Zak et al., 2011).

$$\alpha h\vartheta = D\,(h\vartheta - Eg)^n \quad (2)$$

where $h\vartheta$ is the energy of the photon, Eg is the band gap of the material and D is a constant. The band gap values obtained for ZnO, NC, and ZnO/NC are 3.33, 3.8, and 2.75 eV, respectively. Thus the absorption of the composite is in the visible region due to its low band gap energy compared to that of ZnO and NC.

2.5 BET surface area measurement

The Brunauer-Emmett-Teller (BET) surface area measured for ZnO, NC, and ZnO/NC were found to be 82.3, 75.9, and 184.5 m^2/g, respectively. Surface area of the composite ZnO/NC is highest which also accounts for its good photo catalytic activity.

2.6 Evaluation of photocatalytic activity

To study the efficiency of the composite for the degradation of dyes, a synthetic anionic dye namely Congo red was selected, the structures of which is shown in Scheme 1.

2.6.1 Effect of time

The changes in optical absorption spectra of Congo red using 0.1 g of photocatalyst for 25 ppm of dye solution of pH 7.5 irradiated under visible light irradiation for different time intervals are shown in Figure 5. From the plots it is evident that there is a decrease in intensity with increase in time for all the samples. High rate of photodegradation of the dye was observed with increase in time for all the samples. The photodegradation efficiency of NC for degradation of CR after a time interval of 120 min was found to be 52% whereas for ZnO it was 72% and for ZnO-NC 98%.

2.6.2 Effect of catalyst dosage

As the catalyst dosage was increased from 0.025 to 0.25 g for 25 ppm dye solution of pH 7.5 and irradiated for 120 min, the percentage degradation of the Congo red dye was found to increase for all the catalysts as shown in Figure 6. The increase in amount of catalyst load increased the number of active sites on the photocatalytic surface, which in turn, increased the number of hydroxyl radicals (Wang et al., 2007). It is also observed that further increase in the load of photocatalyst dosage decreased the degradation efficiency in all the samples. This is because, with increasing catalyst loading, though the number of active sites increases the penetration of light decreases due to shielding effect (Jang et al., 2006). In comparison with ZnO and NC, very small amount of ZnO/NC was required for maximum degradation of Congo red.

2.6.3 Effect of concentration

The effect of concentration of the dyes (Figure 7) on the degradation was observed by varying the initial concentration of dyes from 10 to 50 ppm using 0.1 g of catalyst for 120 min of pH 7.5 under visible light irradiation. At low concentrations, the rate of degradation and substrate concentrations are directly

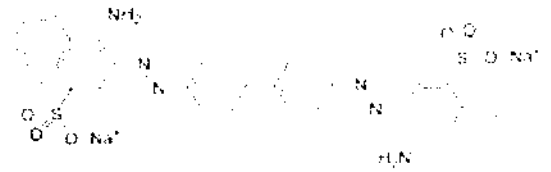

Scheme 1: Structure of Congo red.

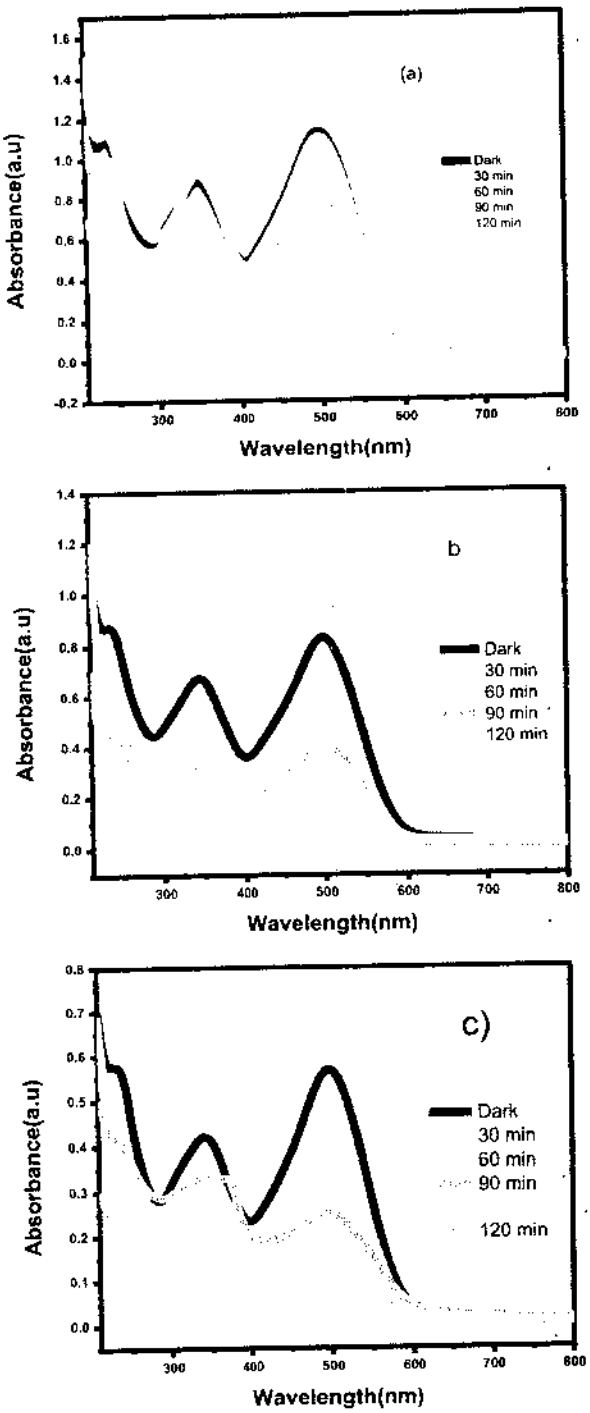

Figure 5: Time dependant absorption spectra of Congo red dye under visible light irradiation with (a) ZnO, (b) NC, and (c) ZnO/NC.

related. As the concentration increased, the degradation efficiency decreased for all the catalysts. The reduced rate of degradation at higher concentrations are due to unavailability of photoactive sites by increased adsorption of dye molecules, decreased rate of light penetration due

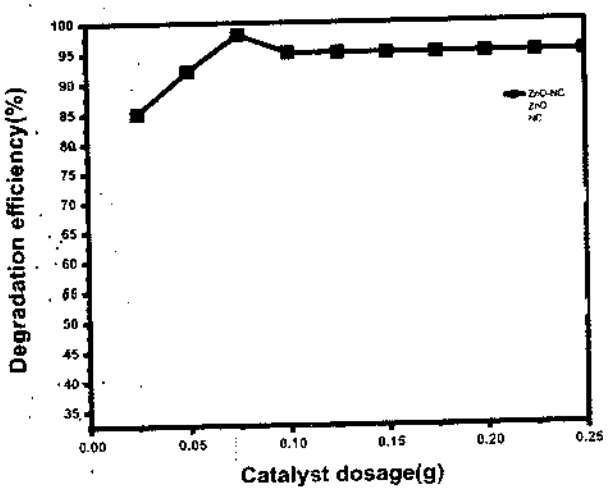

Figure 6: Degradation efficiency vs catalyst dosage for CR.

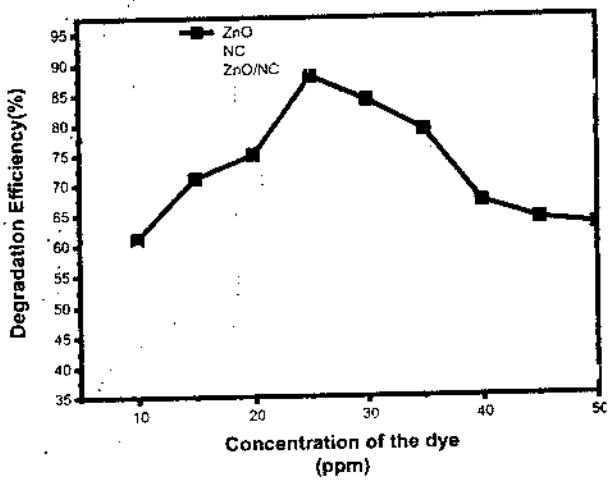

Figure 7: Degradation efficiency vs concentration for CR.

to screening effect and high rate of aggregation of dye molecules (Gopal et al., 2015). The highest degradation was obtained at concentrations 20, 25, and 30 ppm respectively for NC, ZnO, and ZnO/NC.

2.6.4 Effect of pH

Photodegradation capability of the photocatalyst depends on solution pH. Studies were conducted to evaluate the effect of pH on the CR degradation using 25 ppm dye solution and 0.1 g of photocatalyst for 120 min under visible light irradiation. For the degradation process, the effect of pH was studied over the pH range of 2.0-9.0 (Figure 8). The pH of the CR solution was altered by using diluted HCl or NaOH. The results obtained are shown in Figure 9, which show a maximum degradation

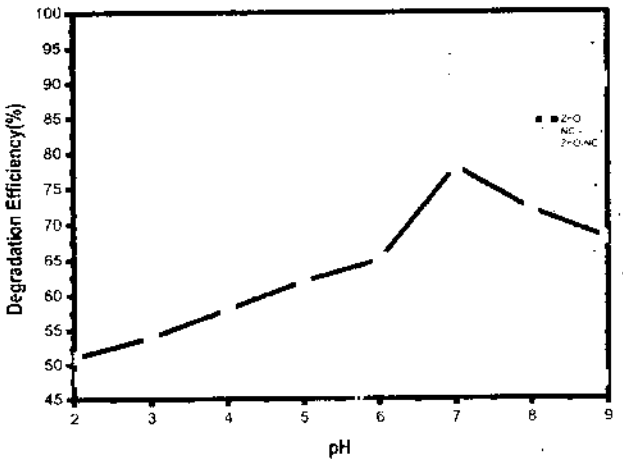

Figure 8: Degradation efficiency vs pH for CR.

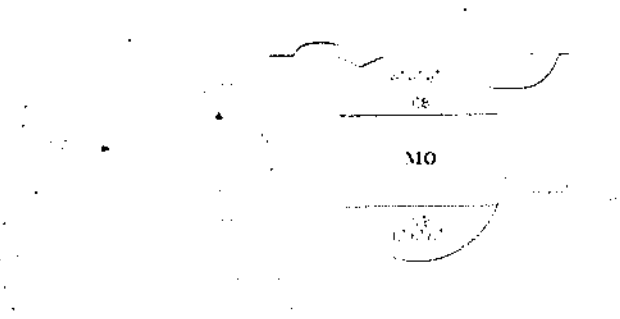

Figure 9: Mechanism of photodegradation by metal oxide nanocellulose composites.

of CR at pH 7.5, 4, and 5.5 for ZnO, NC, and ZnO/NC respectively. From literature it was found that the point of zero charge (pH_{pzc}) for ZnO is 8 (Benhebal et al., 2013). So its surface charge is zero at this pH. When the pH values are lower than pH_{pzc}, surface charge is positive and it is neutral at pH_{pzc} and negative at higher pH. As CR is an anionic dye, lower pH values show higher degradation efficiency.

Photodegradation of the dyes on the composites can be explained by the mechanism given in Figure 9. When metal oxide-nanocellulose composites are illuminated under visible light, the electrons are excited from the highest occupied molecular orbital (HOMO) to lowest unoccupied molecular orbital of (LUMO) NC and subsequently into the CB of metal oxide, holes will be left in the HOMO of NC. The electrons in the VB of metal oxide can migrate to the HOMO of NC and recombine with holes creating holes in the VB of metal oxide. As a result of this large number of electrons and holes are formed. These electrons react with O_2 to form O_2^- and holes react with OH^- or H_2O to form OH^- which are the active species to react with organic dyes. The dyes undergo degradation through intermediates which are oxidized finally to CO_2 and H_2O.

The mechanism of the degradation process can be expressed as

$$MO - NC \rightarrow MO - NC^* + e^- \quad (3)$$

$$e^- + O_2 \rightarrow O_2^- \quad (4)$$

$$MO - NC^* \rightarrow MO - NC + h^- \quad (5)$$

$$OH^- + h^- \rightarrow OH^- \quad (6)$$

$$H_2O + h^+ \rightarrow OH^- + H^+ \quad (7)$$

$$Dye + O_2^- \text{ or } OH^- \rightarrow intermediates \rightarrow CO_2 + H_2O \quad (8)$$

where e^- and h^+ are the electrons and holes respectively.

Mostly semiconducting metal oxides are used as catalyst in the UV region. Here in the present study by the incorporation of ZnO into NC the resulting composite could be used as an effective photocatalyst in the visible region. Overall the process of photodegradation was found to be simple and complete. Almost complete (98%) degradation was obtained using the nanocomposite. No significant degradation of the dye was observed when experiments were conducted without photocatalyst and without light. The composite prepared was from cellulose which is bio compactable, readily available and thus cost effective. The above study also points towards the utilization of such composites for the removal of pollutants from waterbodies.

3 Conclusion

The present work mainly covers the synthesis, characterization and photocatalytic degradation efficiency of ZnO, NC, and ZnO incorporated NC. Pure hexagonal phase ZnO with flower like morphology was synthesized using zinc acetate and HMT. Nanocellulose was prepared by a novel biogenic method using sugarcane bagasse. The composite of NC with ZnO was synthesized and well characterized. Photocatalytic degradation of the Congo red using the above materials was well studied. The study reveals that the catalytic activity of the composite is higher when compared to its counterparts. The variation in different experimental conditions such as time, concentration of the dye, catalyst dosage and pH that affects the photocatalytic degradation was also studied.

The composite ZnO/NC was found to be a promising catalyst for environmental applications.

Experimental

Materials and methods

All chemicals: zinc acetate dehydrate ($Zn(CH_3COOH)_2 H_2O$), hexa methylene tetraammine {$(CH_2)_6N_4$} (HMT), and Congo red (CR) were purchased from Merck Company as analytical grade and were used as received. Sugarcane bagasse was collected locally, cut into small pieces, washed and dried in sunlight. The dried bagasse was grained and the obtained powder was used for further studies.

Preparation of ZnO

To an aqueous solution of 0.02M zinc acetate dihydrate (50 mL), a 0.25 M hexa methylene tetraammine solution in water was added dropwise under constant stirring. The prepared solution was then stirred well for 120 min to obtain a homogeneously turbid liquid. This liquid was sonicated in an ultra-sonication bath for 30 min. The curdy white precipitate obtained was cooled at room temperature, filtered, and washed with water followed by drying in hot air oven at 100°C for 2 h. The main steps involved in the formation of ZnO are as follows (Rejani et al., 2014):

$$CH_2N_4 + 6H_2O \rightarrow 4NH_3 + 6HCHO \quad (9)$$

$$NH_3 + H_2O \rightarrow NH_4^+ + OH- \quad (10)$$

$$Zn^{2+} + 2OH- \rightarrow ZnO + H_2O \quad (11)$$

HMT a moderate alkali was used to generate hydroxide anion.

Preparation of nanocellulose (NC) from sugar cane bagasse (SCB)

The dried SCB was boiled with 25% (w/v) NaOH (fiber to liquid ratio 1:20) for 6 h and allowed to cool at room temperature. The obtained product was acid hydrolyzed with 50% (w/v) sulfuric acid under stirring for another 6 h. About 500 mL of distilled water was added to the above solution, cooled and centrifuged. This washing and centrifugation was continued for 24 h. The obtained colloidal solution was then sonicated for 2 h in ice bath in order to avoid overheating (Dong et al., 1998). The suspension obtained was collected, dried, and stored for further studies.

Preparation of ZnO/NC

About 4 g NC was dispersed in 50 mL water and stirred well for 1 h. Simultaneously 2 g ZnO was dispersed in 50 mL water and was stirred for 1 h. The above solutions were mixed under constant stirring and sonicated for 3 h using ultra sonication bath. The obtained composite was washed and dried.

Characterization

X-ray diffractogram (2Θ = 10–90°) was obtained on XPERT-PRO powder diffractometer with Cu-Kα radiation. The FTIR spectrum was recorded using KBr wafer on the Thermo Nicolet FTIR model AVATAR 370 DTGS. In the present study, SEM of the sample was recorded using a JED-2300 system. The UV-Visible spectra were recorded at room temperature using JASCOV 650 UV-2550 UV Visible spectrophotometer. BET surface area of the samples was measured using SMART SORB 93 Surface area analyzer.

Photocatalytic degradation of CR

In a typical experiment, 0.1g of the prepared catalyst was added to aqueous solution of CR (25 ppm, 300 mL, pH 7.5) taken in a cylindrical photoreactor of capacity 500 mL. The mixture was kept in the dark for 90 min to obtain equilibrium adsorption of CR onto the photo catalyst. The photoreactor was then illuminated with visible light (160 W, Hg vapour lamp) for 120 min. Aliquant were withdrawn from the reaction mixture at regular time intervals and centrifuged immediately to remove the catalyst before absorbance was recorded using a JASCOV 650, UV-Visible spectrophotometer.

To study the effect of pH, experiments were conducted in the pH range 2.0 to 9.0 using 0.1 g of photocatalyst with 25 ppm of dye solution and 120 min of irradiation. To optimize the amount of photocatalyst, a series of experiments were carried out by varying the catalyst amount from 0.025 to 0.25 g for 25 ppm dye solution of pH 7.5 irradiated for 120 min. The effect of initial dye concentration was investigated by varying the initial concentration from 10 to 50 ppm using 0.1 g of catalyst for 120 min of irradiation. Here also the pH of the solution was maintained at 7.5. Blank experiments were also performed in the absence of catalyst and absence of light.

The photocatalytic degradation efficiency was calculated as follows (Radhakrishnan et al., 2016):

$$Removal\ (R\%) = \frac{C_o - C_e}{C_o} \times 100 \quad (12)$$

where $R\%$ is the degradation efficiency of CR, C_o – initial concentration of dye solution (mg/L), Ce equilibrium concentration of dye solution (mg/L).

Acknowledgements: The authors are thankful to the Management and the Principal of Kumbalath Sankupilla Memorial Devaswom Board College (K.S.M.D.B. College) for providing necessary laboratory facilities, STIC Cochin for instrumental analysis. One of the authors (N.J.) is thankful to the University of Kerala for financial assistance.

References

Ahmmad B., Kusumoto Y., Islam M.S., One-step and large scale synthesis of non-metal doped TiO_2 submicrospheres and their photocatalytic activity. Adv. Powder Technol., 2010, 21, 292-297.

Alaton I.A., Balcioglu I.A., Bahnemann D.W., Advanced oxidation of a reactive dyebath effluent: comparison of O_3, H_2O_2/UV-C and TiO_2/UV-A processes. Water Res., 2002, 36, 1143-1154.

Anirudhan T.S., Deepa J.R., Binusreejayan, Synthesis and characterization of multi carboxyl-functionalized nanocellulose/nanobentonite composite for the adsorption of uranium (VI) from aqueous solutions: Kinetic and equilibrium profiles. Chem. Eng. J., 2015, 273, 390-400.

Ansari M.O., Khan M.M., Ansari S.A., Cho M.H., Polythiophene nanocomposites for photodegradation applications: Past, present and future. J. Saudi Chem. Soc., 2015, 19, 494-504.

Augugliaro V. Baiocchi C., Bianco Prevot A., García-López E., Loddo V., Malato S., et al., Azo-dyes photocatalytic degradation in aqueous suspension of TiO_2 under solar irradiation. Chemosphere, 2002, 49, 1223-1230.

Benhebal H., Chaib M., Salmon T., Geens J., Leonard A., Lambert S.D., Photocatalytic degradation of phenol and benzoic acid using zinc oxide powders prepared by the sol–gel process. Alexandria Eng. J., 2013, 52, 517-523.

Bondeson D., Mathew A., Oksman K., Optimization of the isolation of nanocrystals from microcrystalline cellulose by acid hydrolysis. Cellulose, 2006, 13, 171-180.

Chennakesavulu K., Madhusudhana Reddy M., Ramanjaneya Reddy G., Rabel A.M., Brijitta J., Vinita V., et al., Synthesis, Characterization and Photo catalytic studies of the composites by Tantalum oxide and Zinc oxide Nanorods. J. Mol. Struct., 2015, 1091, 49-56.

Dong X.M., Revol J.F., Gray D.G., Effect of Microcrystallite Preparation Conditions on the Formation of Colloid Crystals of Cellulose. Cellulose, 1998, 5, 19-32.

Gopal P., Mira P., Kim H.-Y., Lee S.-Y., Park S.-J., Electrospun ZnO hybrid nanofibers for photodegradation of wastewater containing organic dyes. A review. J. Ind. Eng. Chem., 2015, 21, 26-35.

Guillard C., Lachheb H., Houas A., Ksibi M., Elaloui E., Herrmann J.M., Influence of chemical structure of dyes of pH and of inorganic salts on their photocatalytic degradation b TiO_2 comparison of the efficiency of powder and supported TiO_2. J. Photochem. Photobiol. A-Chem., 2003, 158, 27-36.

Hachem C., Bocquillon F., Zahraa O., Bouchy M., Decolourization of textile industry wastewater by the photocatalytic degradation process. Dyes Pigments, 2001, 49, 117-125.

Jang Y.J., Simer C., Ohm T., Comparison of zinc oxide nanoparticles and its nano-crystalline particles on the photocatalytic degradation of methylene blue. Mater. Res. Bull., 2006, 41, 67-77.

Khorsand Zak R., Razali R., Majid W.H.A., Darroudi M., Green synthesis and evolution of metabolic activity of starchmediated nanoceria. Int. J. Nanomed., 2011, 6, 1399-1403.

Kumar M., Sivakumar V., Tamilarasan R., Adsorption of Victoria blue by carbon/Ba/Alignate beads: Kinetics, Thermodynamics and Isotherm studies. Carbohydr. Polym., 2013, 98, 505-513.

Li J., Wei X., Wang Q., Chen J., Chang G., Kong L., et al., Homogeneous Isolation of Nanocellulose from Sugarcane Bagasse by High Pressure Homogenization. Carbohydr. Polym., 2012, 90, 1609-1613.

Mukherjee D., Barghi S., Ray A.K., Preparation and characterization of the TiO_2 immobilized polymeric photocatalyst for degradation of aspirin under UV and solar light. Processes, 2014, 2, 12-23.

Nagaveni K., Sivalingam G., Hegde M.S., Madras G., Solar photocatalytic degradation of dyes high activity of combustion synthesized Nano-TiO_2. Appl. Catal. B-Env., 2004, 48, 83-93.

Pandey A., Soccol C.R., Nigam P., Soccol V.T., Biotechnological potential of agro-industrial residues I: Sugarcane bagasse. Bioresour. Technol., 2000, 74, 69-80.

Pourmortazavi S.M., Rahimi-Nasrabadi M., Aghazadeh M., Ganjali M.R., Karimi M.S., Norouzi P., Synthesis, characterization and photocatalytic activity of neodymium carbonate and neodymium oxide nanoparticles. J. Mol. Struct., 2017, 1150, 411-418.

Prasad V., Souza C.D., Yadav D., Shaikh A.J., Vigneshwaran N., Spectroscopic characterization of zinc oxide nanorods synthesized by solid-state reaction. Spectrochim. Acta A, 2006, 65, 173-178.

Radhakrishnan A., Rejani P., Bhaskaran B., CuO/polypyrrole nanocomposites as a marker of toxic lead ions for ecological remediation in contrast with CuO and polypyrrole. Main Group Met. Chem., 2015, 38, 133-143.

Radhakrishnan A., Rejani P., Shanavas Khan J., Bhaskaran B., Effect of annealing on the spectral and optical characteristics of nano ZnO: Evaluation of adsorption of toxic metal ions from industrial waste water. Ecotoxicol. Environ. Saf., 2016, 133, 457-465.

Rejani P., Radhakrishnan A., Bhaskaran B., Photo Catalytic Decomposition of Malachite Green in Aqueous Solutions under UV Irradition Using Nano ZnO Rod. Iranica J. Energy Environ., 2014, 5, 233-239.

Simkovic I., Mlynar J., Alfoldi J., Micko M.M., New aspects in cationization of lignocellulose materials. XI. Modification of bagasse with quaternary ammonium groups. Holzforschung, 1990, 44, 113-116.

Wang H., Xie C., Zhang W., Cai S., Yang Z., Gui Y, Comparison of dye degradation efficiency using ZnO powders with various size scales. J. Hazard. Mater., 2007, 141, 645-652.

Wang Y., Zhang R., Li J., Li L., Lin S., First-principles study on transition metaldoped anatase TiO_2. Nanoscale Res. Lett., 2014, 9, 46-53.

Structural, Optical and Photocatalytic Degradation Studies of Polymer Based Fe2o3 Nanocomposite

Megha.S[1,2] , DedhilaDevadathan[1], Baiju V[1], Raveendran R[1]

[1] Nanoscience Research Laboratory, Department of Physics, Sree Narayana College, Kollam 691001, Kerala, India
[2] Department of Physics, Amrita Vishwa Vidyapeetham, Amritapuri, Kollam 690525, Kerala, India

E-mail: Phone Number: 9746377111

Abstract: The present study is focused on the comparison of structural and optical properties of nanocomposite of Fe2O3 formed with both rice straw, a biopolymer and polyindole, a conducting polymer. For comparison, counter parts were also synthesized. Nanoparticles of iron oxide were synthesized through controlled co-precipitation method in presence of citric acid. Structural characterizations of all the synthesized samples were carried out using XRD. Comparison of XRD of metal oxide with JCPDS confirmed that the formed metal oxide was Fe2O3. Optical studies of all the samples were carried out using UV/Vis spectroscopy. From band gap calculation it was seen that all of them except polyindole showed subgaps. Also these samples were employed as photocatalyst in the photocatalytic degration study of organic acidic dye Congo Red. Results suggested that the nanocomposites prepared in the present study are promising photocatalysts. Also an increase in degradation efficiency was observed in the case of nanocomposites when compared to their counterparts.
Keywords: Nanocomposite, Co- Precipitation, Conducting Polymer, Biopolymer, Photocatalyst

1. Introduction

Synthesis of nanocomposites is an expanding trend of nanoscience. Currently, the applications of natural products as eco-friendly materials, in waste disposal have gained a great deal of attention from researchers, particularly, for the synthesis of composites [1]. The utilization of inexpensive, renewable, accessible, and biodegradable farming residues such as rice straw, rice husks and corn stover can rationalize the cost effect. Because of the availability of natural/bio-fibers from renewable resources, the use of bio-composites is expanding in recent years. In order to exploit the full potential of the technological applications of the nanomaterials, the scientists were guided towards the conventional polymers as one component of the nanocomposite. First major discovery in the field of electrically conducting polymers took place around 1978 when Shirakawa and co-workers reported the synthesis of doped polyacetylene which was formed accidentally [2]. The instability of polyacetylene in air further intensified this research which resulted in many novel conducting polymers and their derivatives [3]. Nanocomposite materials formed by metal nanoparticles that appropriately incorporated into the polymer matrix were found to be very significant due to their diversity in electrical, catalytic and optical properties. These diversities have potential applications in the fields of electronic, photonic, catalysis and bioengineering.

Content from this work may be used under the terms of the . Any further distribution of this work must maintain attribution to the author(s) and the title of the work, journal citation and DOI.
Published under licence by IOP Publishing Ltd

In the present work we are focussed on the comparison of structural, optical properties and photocatalytic degradation studies of the nanocomposite of Fe_2O_3 formed with both rice straw, a biopolymer and polyindole, a conducting polymer.

2 Experimental

AR grade chemicals obtained from Merck were used for the preparation of polyindole based Fe_2O_3 nanocomposite and rice straw based nanocomposite. Nanoparticles of Fe_2O_3 were prepared by the co-precipitation method in presence of capping agent.

Metal oxide Fe_2O_3 were prepared as follows. Ferric nitrate nonahydrate, and sodium hydroxide were used as starting materials. Citric acid was used as stabilizer. Aqueous solutions of 25ml 0.1 M ferric nitrate, and 50ml 1 M of sodium hydroxide were slowly mixed drop wise into a beaker containing aqueous solution of 25 ml 0.02 M citric acid and stirred well using a magnetic stirrer for two hours. The stabilizer was used to prevent growth and agglomeration of the particles. The particle size was governed by the experimental parameters like concentration of the reactants, rate of mixing, pH, viscosity of the solutions etc. The stabilizers used for controlling the precipitation reaction should be easily and completely removable from the sample so as to avoid any possible contamination of the samples. After two hours of continuous stirring, the precipitate formed was in hydroxide form. The hydroxide precipitate formed was washed several times in distilled water to free it from ions and other impurities. The wet precipitate obtained was dried at room temperature and thoroughly grounded using an agate motor to obtain the hydroxide precursor in the form of fine powder. The powder so obtained was annealed at 600^0C for 3 hours in a muffle furnace to obtain the respective metal oxide nanoparticles.

Nanostructures of polyindole were synthesized using a simple and direct chemical oxidative polymerization method conducted at room temperature as follows. About 3.5 g of indole was dissolved in a solution of 10 ml methanol with 15 ml distilled water. For the oxidation and doping purpose, 12 ml of freshly prepared 2 M HCl solution was added to the monomer solution. The reaction mixture was gradually and constantly stirred. After the reaction duration of 1 hour, the polymerized product formed was collected by centrifugation, and thoroughly washed with deionized water, dried at room temperature and collected [4,5]. Polyindole based Fe_2O_3 nanocomposite were also prepared using the same procedure with some modifications. After adding 12 ml of freshly prepared 2 M HCl solution to the monomer solution, the reaction mixture was gradually and constantly stirred for 10 minutes and then the already annealed sample of Fe_2O_3 was added by 5% of weight. After 1 hour the product formed was collected by centrifugation, thoroughly washed with de-ionized water, dried at room temperature and collected.

After proper cleaning and drying process rice straw waste was used. For the treatment of rice straw waste, basic NaOH solution and methanol were used. Small pieces of 5g rice straw washed using distilled water. NaOH solution was prepared by measuring NaOH equal to the weight of 10% of rice straw (.5g) and making it upto 50ml by dissolving NaOH in distilled water. Liquor to fiber ratio was taken as 10:1, ie, 50g of methanol for 5g of rice straw. Liquor and NaOH solution were added to the rice straw and were cooked on a heater for 20 minutes until the solution reduced to some amount on open air. It cool for some time and the pulps were further applied for acid pulping, where nitric acid (69% concentration) diluted (2.5 ml of acid and making it upto 25 ml using distilled water) was used in the pulp for heating until it reduces. It was cooled for some time. Again 25 ml of concentrated acid was added. After reduction and cooling process another 25 ml of acid was added and heated. The pulp turned to particles. After cooling distilled water was added to it and stirred for 15 minutes on a magnetic stirrer. After some time the powder settled. Water was decanted. The process was repeated thrice and finally washing was done using 50 ml of methanol. The solution was filtered using filter paper and dried at room temperature. Dried rice straw powder was collected and used for analysis. In case of nanocomposite based on rice straw annealed Fe_2O_3 was added at the time of pulp formation.

XRD studies were carried out using XPERT-PRO model powder diffractometer (PAN analytical, Netherlands) employing Cu- Kα radiation (λ = 1.54060A°) operating at 40kV, 30mA.The UV/Vis

spectrum was obtained using JASCO V-650 UV visible spectrophotometer. Adsorption studies were carried out using GBC-AAS spectrometer having lamb current 5milli ampere and wavelength 270nm.

Table 1 Sample notations used in the present work

Sample	Notations
Iron oxide nanoparticles annealed at 600^{0}C	FS
Polyindole	PI
Polyindole based Iron oxide nanocomposite	PIFS
Rice Straw	RS
Rice Straw based Iron oxide nanocomposite	RSFS

3 Results and Discussions

Metal oxide prepared in the present study was obtained in the form of hydroxide. The iron hydroxide was obtained as light brown powders. But the annealed iron oxide as dark brown in colour. Rice straw was obtained as pale yellow and where as rice straw based nanocomposite was observed as brown powders. Polyindole was obtained as pale white powder where as polyindole based nanocomposites was observed as light brown powders.

3.1 XRD Analysis

1. XRD analysis of PI

The XRD pattern of PI was found to match well with the XRD patterns in literature [5]. The XRD of polyindole shows the presence of numerous sharp crystalline peaks in the diffraction pattern having 2θ values between 15^0 and 30^0. This can be related to the scattering from bare polymeric chains at the inter-planar spacing. Figure 1 shows the XRD diffraction pattern of PI.

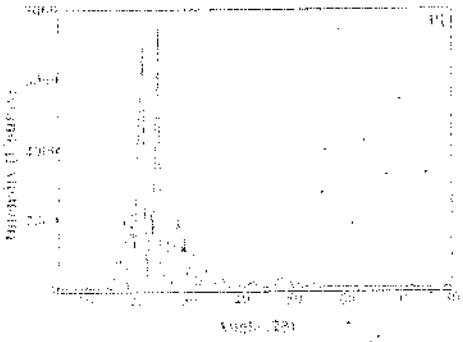

Figure 1 XRD Spectrum of PI

An XRD peak is known to be the measure of crystallinity and the appearance of peaks in the XRD of the polymer confirms the crystalline nature rather than amorphous nature. Higher the degree of regularity in arrangement or ordering of the polymer chain, higher is the crystallinity [6]. The presence of sharp crystalline peaks in the XRD graph indicates good electrostatic (dipole–dipole) interactions among the adjoining molecular chains in the PI matrix and also their highly ordered state [7]. The XRD results justify the PI nanostructures as crystalline in nature.

2 XRD analysis of FS and PIFS

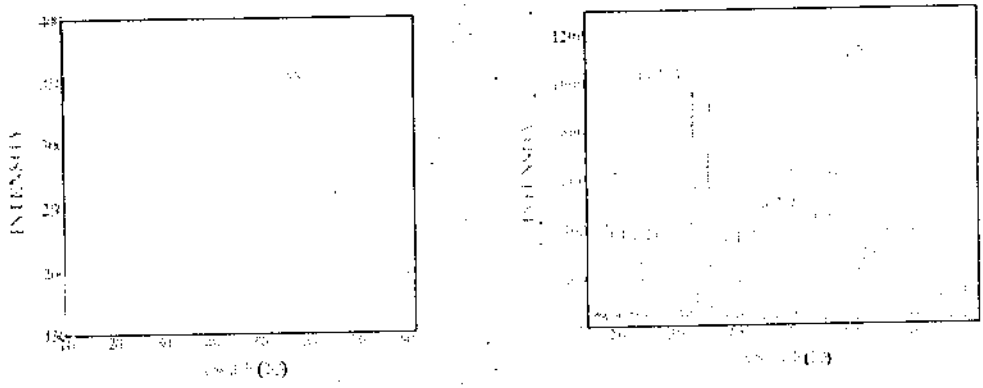

Figure 2 XRD of FS and FN

Figure 2 shows XRD of FS. Though the peaks were not sharp diffraction peaks at 2 the values 24.33°, 33.06°, 35.76°, 49.46° and 54.15° corresponding to the crystal planes of (102), (104), (110), (024), (116) and (018) was observed. The sample was again annealed at 900°c for six hours inorder to study the structure of the formed sample and the sample was named FN. Figure 2 shows XRD of FN. The interplanar spacing (d_{hkl} values), 2θ values and relative intensity values of iron oxide corresponding to the observed diffraction peaks were compared with the standard values of iron oxide as reported by JCPDS-International Centre for Diffraction Data. The data obtained for Fe_2O_3 in case of FN was matched with JCPDS-ICDD pattern number #84-0311. For FN diffraction peaks at 2θ the values 24.06°, 33.20°, 35.61°, 40.84°, 49.60°, 54.26°, 57.43°, 62.64°, 63.95° 71.95° and 75.49° corresponds to the crystal planes of (012), (104), (110), (113), (024), (116), (122), (214), (300) (1010) and (220) respectively with no characteristic peaks corresponding to the impurities were detected, which further confirms the formation of pure stable Fe_2O_3 phase. JCPS matching confirmed the rhombohedral structure for Fe_2O_3. The average crystallite size of FN calculated from the line broadening of the XRD pattern, using FWHM values of four major peaks in the XRD spectrum making use of Scherrer formula are shown in Tables 2. The Scherrer equation is

$$t = K\lambda / \beta_{hkl} \cos \theta_{hkl} \qquad (1)$$

Here t is the average crystallite size normal to the reflecting planes, K is the shape factor which lies between 0.95 and 1.15 depending on the shape of the grains (K= 1 for spherical crystallites), λ is the wavelength of X-rays used, β_{hkl} is the full width at half maximum of the diffraction line in radians and β_{hkl} is the Bragg angle corresponding to the diffraction line arising from reflections from the planes designated by Miller indices (h k l).

Table 2 Crystallite size calculation of FN using Scherrer equation

2θ	θ	Cosθ	FWHM	D (nm)
33.2	16.60	0.9584	0.443	18.72
35.61	17.81	0.9522	0.465	17.95
49.6	24.80	0.9079	0.346	25.30
54.26	27.13	0.8901	0.564	15.83

Average Crystallite size = 10.28 nm

XRD of PIFS confirms the formation of nanocomposite. The well defined peaks corresponding to the planes (1 0 4), (1 1 0) and (1 1 6) of iron oxide were found to be incorporated into the XRD spectrum of polyindole. The variations in the peaks observed in PIFS and PI in the region between 15^0 and 30^0 supports the formation of nanocomposites. It is clear that the metal oxide particles are well distributed in the polymer matrix. Since FS is doped in the polymer matrix sharp peaks of metal oxide are not observed.

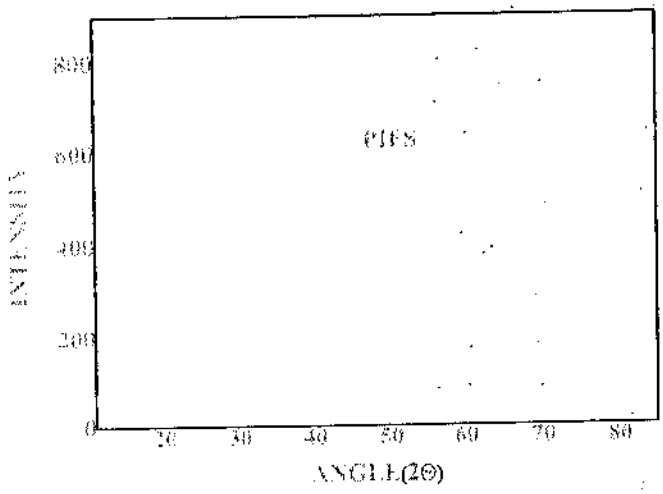

Figure 3 XRD Spectrum of PIFS

3. XRD analysis of RS and RSFS

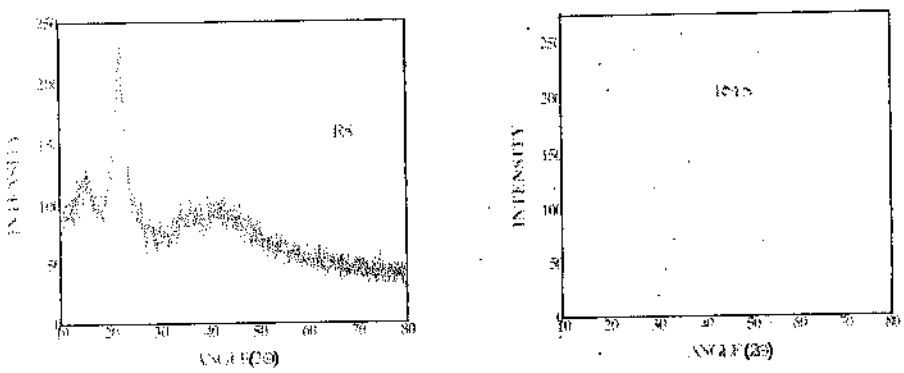

Figure 4 XRD Spectrum of RS and RSFS

The XRD of rice straw showed the presence of a sharp crystalline peak in the diffraction pattern having 2 value at 22.03^0. Figure 4 shows the XRD diffraction pattern of RS and RSFS. The variation of XRD of RSFS between 30^0 and 50^0 when compared to RS confirms the formation of nanocomposite.

3.2. UV/Vis Analysis

1 UV/Vis spectrum analysis of PI

The UV/Vis absorption spectrum of the Polyindole taken in the wavelength range 210 to 800 nm with 1 nm resolution is shown in Figure 5 (a). Polyindole nanobelts depict a sharp absorption in the range 225-325 nm with λ_{max} situated at 292 nm, attributed to the conjugation of benzene ring in the indole unit [8,9]. The Presence of small absorption band is observed in the range 435 – 543 nm with λ_{max} situated at 478 nm due to the π - π^* transitions of the benzene ring in the PI molecular chains [8]. The results indicate presence of enhanced conjugated segments and easy flow of charge in PI molecular matrix. This band also relates to the extent of conjugation between adjacent rings in the polymer chain. The absorption edge (AE) is calculated from the equation, $E = hc/\lambda_{max}$ where h is Plank's constant and c is the velocity of light. The absorption edge is found to be 4.19 eV and 2.6 eV for the peaks corresponding to 292 nm and 478 nm respectively. The optical band gap of the material determined from the absorption spectrum using Tauc's relation was 3.82 eV. Tauc's plot drawn for PI is shown in Figure 5(b). Due to large value of the optical band gap, the material is most suited in many applications in modern electronic industries.

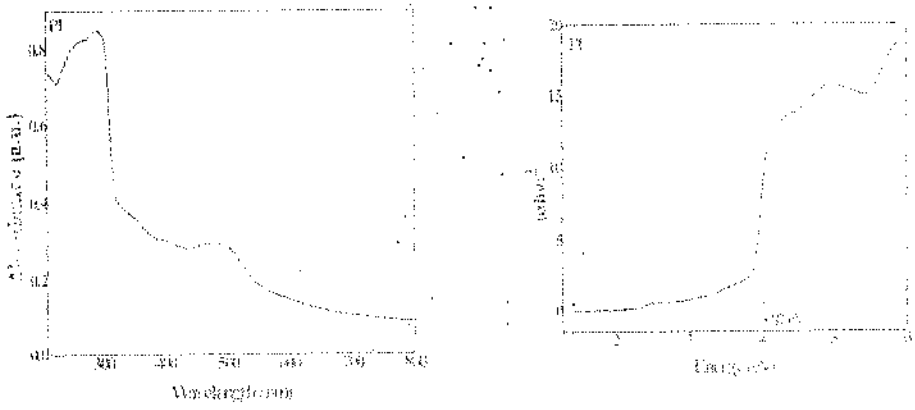

Figure 5 (a) UV/Vis Absorbance spectrum of PI (b) Tauc's Plot for PI

1 UV/Vis spectrum analysis of FS and PIFS

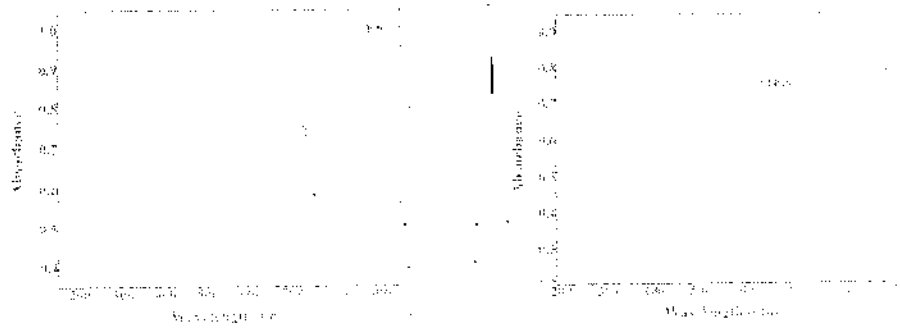

Figure 6 (a) UV/Vis Absorbance spectrum of FS (b) UV/Vis Absorbance spectrum of FS

The UV/Vis absorption spectrum of the FS and PIFS taken in the wavelength range 210 to 870 nm with 1 nm resolution is shown in Figure 6. In case of FS a broad absorption peak was observed in UV and visible region. No sharp peak was observed. But PIFS depict a sharp absorption in the range 225-325 nm with λ_{max} situated at 297 nm, attributed to the conjugation of benzene ring in the indole unit. The shift when compared to PI can be due to the presence of metal oxide nanoparticles in the polymer structure.

The absorption edge (AE) is calculated from the equation, $E = hc/\lambda_{max}$ where h is Plank's constant and c is the velocity of light. The absorption edge is found to be 4.18 eV for the peak corresponding to 297 nm. The optical band gap of the material determined from the absorption spectrum using Tauc's relation was found and Tauc's plot drawn for FS and PIFS is shown in Figure 7. Due to large value of the optical band gap, the material is most suited in many applications in modern electronic industries.

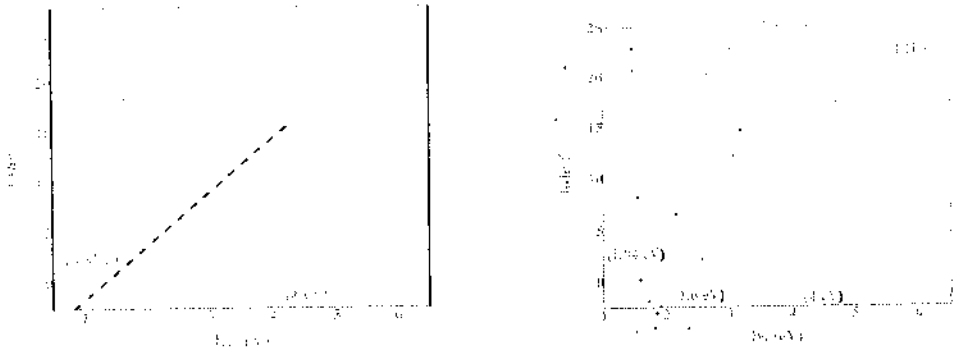

Figure 7(a) UV/Vis Absorbance spectrum of PI (b) Tauc's Plot for PI

1 UV/Vis spectrum analysis of RS and RSFS

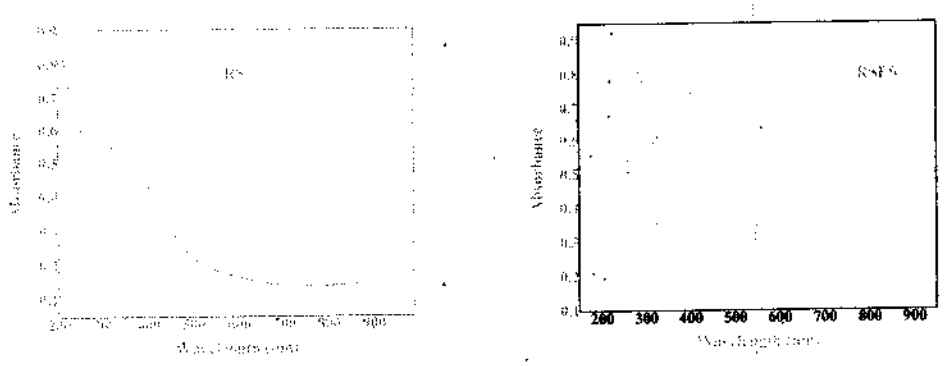

Figure 8 (a) UV/Vis Absorbance spectrum of RS (b) UV/Vis Absorbance spectrum of RSFS

The UV/Vis absorption spectrum of the RS and RSFS taken in the wavelength range 210 to 870 nm with 1 nm resolution is shown in Figure 8. In case of RS a small absorption peak was observed in UV region. No sharp peak was observed. A variation in absorption was obtained in case of RSFS. The presence of additional small absorption peak in RSFS can be attributed to the presence of metal ions. The optical band gap of the material determined from the absorption spectrum using Tauc's relation drawn for RS and RSFS is shown in Figure 9.

International Conference on Applied Physics, Power and Material Science IOP Publishing
IOP Conf. Series: Journal of Physics: Conf. Series **1172** (2019) 012051 doi:10.1088/1742-6596/1172/1/012051

Figure 9 (a) Tauc's Plot for FS (b) Tauc's Plot for RSFS

From band gap calculation it was seen that all of the samples except PI showed subgaps. Multiple band gaps were obtained in case of both nanocomposite.

1 Photocatalytic Degradation Studies

Acidic dye Congo Red (CR), and basic dye of 1000 ppm concentration were prepared and the desired concentrations were taken and used as dye samples.

The photocatalytic activity of samples for the degradation of the dyes; Congo red (CR) was studied using the respective photocatalyst in the presence of visible light illumination in a photoreactor. The experiments were performed by suspending the desired amount of photocatalyst into 300 ml of dye solution of desired concentration which was varied and done at two different concentrations, 50 ppm to 75 ppm. The experiment was carried out isothermally at 300 K. The concentration of residual dye in the solution after irradiation for 24 hrs was determined by monitoring the absorbance intensity of solution samples at their maximum absorbance wavelength by using UV-Vis spectrophotometer (JASCO V 650 UV/Vis spectrophotometer).

In the present work the factors affecting photocatalytic degradation like effect of contact time, amount of photocatalyst and dye concentration were also investigated.

To study the effect of contact time on the photodegradation of organic dyes, the following procedure was adopted. To the respective dye solution of concentration, 50 ppm in 300 ml solution kept at 300 K, 0.1 g of the photocatalyst was added and was kept under UV light. After desired time intervals [1, 2, 3 and 24 hrs], 10 mL of the solution was taken out, centrifuged and UV/Vis absorption spectra was recorded.

In the above experiment, the amount of photocatalyst was varied. 0.1 g and 0.15 g was used to study its effect on photodegradation.

Dye solutions of two different concentrations were selected (50 ppm and 75 ppm) to study the effect of initial dye concentration on photodegradation efficiency.

The photocatalytic degradation efficiency was calculated as follows:

$$\textbf{Photocatalytic Degradation Efficiency}(\%) = \frac{(C_0 - C_t)}{C_0} \times 100 \qquad 1$$

C_0: initial concentration of dye solution [mgL^{-1}],

C_t final concentration of dye solution [mgL^{-1}]

The photodegradation of Congo Red (CR) using the nanocomposite RSFS as well as PIFS and their counterparts FS, PI and RS were studied in detail. The results show high rate of photodegradation of the dye with increase in contact time. The photodegradation rate after 24 hrs for all the samples for Congo Red (CR) are given in Table 1.

The amount of catalyst loading is one of the main parameters for the degradation efficiency. In order to avoid the use of excess catalyst it is necessary to find out the ...m loading for efficient removal of dye. The results showed that when catalyst dosage was in... ...e was a slight decrease in the degradation percentage. The percentage degradation sign... ...tly ... ...reased due to decrease of formation of hydroxyl radicals. It should be pointed out that, the cata... ...t loa... ...affects both the number of active sites on photocatalysts and the penetration of UV light throu... ...h the ... ...nsion [10]. With increasing catalyst loading the number of active sites increases, but the penetrat... ...f UV light decreases due to shielding effect [11]. It should also be noted that the optimum value o... ...catalyst loading is strongly dependent on the type and initial concentration of the dye and the operating conditions of the photoreactor [12].

The results indicate that the rate of photocatalytic degradation decreased with the increasing initial dye concentration. As the initial concentration of a dye increases, the colour of dye solution becomes deeper which results in less penetration of light to the surface of the catalyst, decreasing the number of excited dye molecules. With increase in initial concentration of dye more and more organic substances are adsorbed on the surface of the photocatalyst. Therefore, the generation of hydroxyl radicals is reduced, since there are only fewer active sites in the system [13]. The activity of the nanocomposite was also compared with the counter parts. All nanocomposites showed higher activity when compared to their counter parts.

Table 1 Photodegradation % of Congo Red using Synthesized samples

Sample	Weight (g)	Concentration (ppm)	% Photodegradation
RS, CR	0.1	50 ppm	59.54
	0.15	50 ppm	54.23
	0.1	75 ppm	53.24
	0.15	75 ppm	46.36
FS, CR	0.1	50 ppm	70.75
	0.15	50 ppm	69.33
	0.1	75 ppm	65.45
	0.15	75 ppm	60.25
RSFS, CR	0.1	50 ppm	96.89
	0.15	50 ppm	91.39
	0.1	75 ppm	89.48
	0.15	75 ppm	86.53
PI, CR	0.1	50 ppm	60.55
	0.15	50 ppm	53.35

PIFS, CR	0.1	75 ppm	54.05
	0.15	75 ppm	47.25
	0.1	50 ppm	94.89
	0.15	50 ppm	89.08
	0.1	75 ppm	88.99
	0.15	75 ppm	85.44

4. Conclusions

Structural characterizations of all the five synthesized samples were carried out using XRD. Comparison of XRD of metal oxide with JCPDS confirmed that the formed metal oxide was Fe_2O_3. Phase purity and crystallinity of the sample was confirmed from XRD. Crystallite size was calculated using Scherrer equation. FS, PI and PIFS prepared in this work showed strong UV as well as visible absorption, but RS and RSFS showed more absorption in UV region. Hence all these materials could be suitable for anti UV applications such as anti UV glass, anti UV sunscreen, etc. Also these materials could be a good candidate as photocatalyst for photocatalysis in presence of UV, as antibacterial agents, etc. From band gap calculation it was seen that all of them showed subgaps. This property is found to increase the photocatalytic activity of the photocatalyst. FS, PI and PIFS showed visible range absorption in addition to UV range. So these materials can be used as photocatalyst in presence of solar light. The metal oxides and their nanocomposites in the present study showed very good photocatalytic activity. The variations in different experimental conditions affecting photocatalytic oxidation were also studied. Results suggested an increase in degradation efficiency in the case of polymer nanocomposites when compared to their counter parts. It is suggested that these materials could be efficiently used as anti-bacterial, deodorizing, air purifying, anti fogging and as other surface purification agents.

References

[1] Roshanak Khandanlou, Mansor B. Ahmad, Kamyar Shameli, Elnaz Saki and Katayoon Kalantari, Studies on Properties of Rice Straw/Polymer Nanocomposites Based on Polycaprolactone and Fe_3O_4 Nanoparticles and Evaluation of Antibacterial Activity, International journal of molecular sciences, 2014, *15*(10), 18466-18483.

[2] Shirakawa H, Louis E J, MacDiarmid A G, Chiang C K and Heeger A J, Synthesis of electrically conducting organic polymers: Halogen derivatives of polyacetylene, (CH)x" J. Chem.Soc. Chem. Commun.,16, 1977, 578-580.

[3] Bakhshi A K and Bhalla G, Electrically conducting polymers: Materials of the twenty first century, Journal of Scientific & Industrial Research, 63, 2004, 715 – 728.

[4] Goel S, Mazumdar N A and Gupta A, Growth of one-dimensional polyindole nanostructures, J. Nanosci. Nanotechnol. 11, 2011, 10164-10172.

[5] Goel S, Synthesis of polyindole nanoflakes through direct chemical oxidative route Advanced Science, Engineering and Medicine, 4, 2012 438–441.

[6] Hutten P F V and Hadziioannou G, Handbook of Organic Conductive Molecules and Polymers, edited by H. S. Nalwa, John Wiley, New York, 3, 1997, 1–85.

[7] Taylan N B, Sari B and Unal H I, Preparation of conducting poly(vinyl chloride)/polyindole composites and freestanding films via chemical polymerization,J. Polym. Sci.: Part B: Polym.Phys.,48, 2010, 1290-1298.

[8] Eraldemir O, Sari B, Gok A, and Unal H B, Synthesis and characterization of polyindole/poly(vinylacetate) conducting composites, J. Macromol. Sci.Part A Pure Appl. Chem. 45,

2008, 205-211.

[9] Xu Z, Liu W and Li H, Titanium dioxide doped polyaniline, *Mater. Sci. Eng. C*, 25, 2005, 444-447.

[10] Daneshvar N, Salari D and Khataee A R, Photocatalytic degradation of azo dye acid red in water: investigation of the effect of operational parameters, J. Photochem, Photobiol. A. Chem., 157, 2003, 111-116.

[11] Gouvea CAK, Wypych F, Moraes SG, Durán N and Peralta- Zamora P, Semiconductor-assisted photocatalytic degradation of reactive dyes in aqueous solution, Chemosphere, 40, 2000, 433–440.

[12] Gogate P R and Pandit A B, A review of imperative technologies for wastewater treatment II: hybrid methods, Adv. Environ. Res., 8, 2004, 553–597.

[13] Daneshvar N, Salari D and Khataee A R, Photocatalytic Degradation of Azo Dye Acid Red 14 in Water on ZnO as an Alternative Catalyst to TiO_2, J. Photochem. Photobiol., A: Chem., 162, 2004, 317-322.

IOP Publishing

Structural and antibacterial studies straw based zno nanocomposite

P K Anjali Nambiar[1,2], Dedhila Dev[illegible]atha[illegible][1],V Baiju[1] and R Raveendran[1]

[1] Nanoscience Research Laboratory, Department of Physics, Sree Narayana College, Kollam 691001, Kerala, India
[2] Department of Physics, Amrita Vishwa Vidyapeetham, Amritapuri, Kollam 690525, Kerala, India

E-mail:anjalipknambiar@gmail.com

Abstract. The present study is focused on the structural and antibacterial studies of rice straw based ZnO nanocomposite. For comparison, counterparts were also synthesized. Nanoparticles of ZnO were synthesized through combustion method and co-precipitation method. Structural characterizations of all the synthesized samples were carried out using XRD. Antibacterial studies of the synthesized samples were carried out. The present study investigates the antimicrobial activity of the synthesized samples as antibacterial agents. The selected microbes for the present study are gram-positive bacteria: Bacillus cereus (B. cereus), the gram-negative bacteria: Escherichia coli (E. coli)..

1. Introduction

Natural fiber has many advantages like biodegradability, flammability, and non-toxicity [1, 2]. The source of natural fiber are stalks, leaves, and seeds, for instance, kenaf, sisal, flax, wheat straw and rice straw [3, 4]. In most countries, straw is an abundant cellulosic by-product from the production of crops such as wheat, corn, soybean, and rice. The utilization of easily available biodegradable farming residues like rice straw, rice husks and corn Stover can be used to rationalize the cost effect. Rice straw is best known to be a potential source of energy and also a value-added by-product [5]. Due to the availability of natural/bio-fibers from the renewable resources, the use of bio-composites has been found to be expanding in the recent years. Nanocomposite materials formed by metal nanoparticles that have been appropriately incorporated into the polymer matrix were experimentally found to be very significant due to their diversity in electrical, catalytic and optical properties. These diversities have potential applications in the fields of electronic, photonic, catalysis and bioengineering [6]. Synthesis of nanocomposites is an expanding trend of nanoscience. In order to exploit the full potential of the technological applications of the nanomaterials, the scientists were guided towards the conventional polymers as one component of the nanocomposite. The control of the proliferation of microbes in nature is one of the most important concepts for the survival of human beings, animals and plants. Antimicrobial operators are of incredible significance in businesses, for example, water cleansing, materials, bundling, development, medication and sustenance bundling [7,8]. As of late, nonstop endeavors have been made to create polymer-based nanocomposites with antimicrobial capacity. The polymeric frameworks are considered as great host materials for metal and metal oxide nanoparticles. They give extra characteristics, for example, processability, solvency and warm

Content from this work may be used under the terms of the Creative Commons Attribution 3.0 licence. Any further distribution of this work must maintain attribution to the author(s) and the title of the work, journal citation and DOI.
Published under licence by IOP Publishing Ltd

solidness to the frameworks shaped[9]. Several efforts have been made for the fabrication of polymeric material with potential antimicrobial activity [10]. Moreover, the nanocomposites prepared using inorganic metal oxide nanoparticles and organic polymers can find better utilization due to the enhanced antimicrobial activity. All these open the possibility of the formulation of a new generation of bactericidal materials. In the present work, we are focussed on the comparison of structural and antibacterial properties of the nanocomposite of ZnO formed with rice straw.

2. Experimental

AR review synthetics got from Merck were utilized for the arrangement of rice straw based ZnO nanocomposite. ZnO nanoparticles were set up by the co-precipitation method in presence of capping agent and also by combustion method.

Metal oxide ZnO was prepared as follows. Zinc nitrate dihydrate and sodium hydroxide were used as beginning materials. The citrus extract was utilized as the stabilizer. Aqueous solutions of 25ml 0.1 M zinc nitrate, and 50ml 1 M of sodium hydroxide were slowly mixed drop wise into a beaker containing aqueous solution of 25 ml 0.02 M citric acid and stirred well using a magnetic stirrer for two hours. The stabilizer was used to prevent growth and agglomeration of the particles. The molecule measure was driven by the test parameters, for example, the convergence of the reactants, rate of blending, pH, thickness of the arrangements and so forth. The stabilizers used for controlling the precipitation reaction should be easily and completely removable from the sample so as to avoid any possible contamination of the samples. After two hours of continuous stirring, the precipitate formed was in hydroxide form. The hydroxide precipitate formed was washed several times in distilled water to free it from ions and other impurities The wet accelerate got was dried at room temperature and completely grounded utilizing an agate engine to get the hydroxide antecedent as fine powder. The powder so obtained was annealed at 600^0C for 3 hours in a muffle furnace to to acquire the particular metal oxide nanoparticles.

Nanoparticles of zinc oxide were prepared by combustion method using analytical grade chemicals. Zinc nitrate dehydrates and urea was used as starting materials. Urea was used as fuel. 5 g zinc nitrate was taken to which urea and glycol were added mixed to get a clear solution. pH of the solution was made neutral by controlling the amount of urea and glycol. The solution was then heated. The chemical reactions between the reactants produce exothermic energy and as a resulting flame is produced and fine powders of the nanoparticles were formed.

The powder so obtained was annealed at 600^0c for 3 hours in a muffle furnace to obtain nanoparticles of zinc oxide.

After legitimate cleaning and drying process rice straw waste was utilized. For the treatment of rice straw waste, basic NaOH solution and methanol were used. Small pieces of 5g rice straw washed using distilled water. NaOH solution was prepared by measuring NaOH equal to the weight of 10% of rice straw (.5g) and making it up to 50ml by dissolving NaOH in distilled water. Liquor to fiber ratio was taken as 10:1, ie, 50g of methanol for 5g of rice straw. Liquor and NaOH solution were added to the rice straw and were cooked on a heater for 20 minutes until the solution reduced to some amount on open air. It cool for some time and the pulps was further applied for acid pulping, where nitric acid (69% concentration) diluted (2.5 ml of acid and making it up to 25 ml using distilled water) was used in the pulp for heating until it reduces. It was cooled for some time. Again 25 ml of concentrated acid was added. After reduction and cooling process, another 25 ml of acid was added and heated. The pulp turned to particles. After cooling distilled water was added to it and stirred for 15 minutes on a magnetic stirrer. After some time the powder settled. Water was decanted. The process was repeated thrice and finally, washing was done using 50 ml of methanol. The solution was filtered using filter paper and dried at room temperature. Dried rice straw powder was collected and used for analysis. In case of nanocomposite based on rice straw annealed ZnO prepared from combustion and co-precipitation methods added at the time of pulp formation, separately.

Table 1. Sample notations used in the present work.

Sample	Notations
ZnO nanoparticles prepared from co-precipitation annealed at 600^{0}C	ZS
ZnO nanoparticles prepared from combustion method annealed at 600^{0}C	ZCS
Rice straw	RS
Rice straw based zinc oxide nanocomposites	RSZS

3. Results and discussions

Metal oxide prepared using co-precipitation method in the present study was obtained in the form of hydroxide. In the case of combustion method, black powder was obtained. Both annealed samples of zinc oxide are obtained as white powders. Rice straw and rice straw based nanocomposites were obtained as pale yellow.

3.1. XRD Analysis

3.1.1. XRD analysis of ZS and ZCS

XRD studies were done by XPERT-PRO model powder diffractometer (PAN analytical, Netherlands) employing Cu- Kα radiation (λ = 1.54060A°) operating at 40kV, 30mA. Figure 1 shows XRD of ZS and ZCS. The interplanar spacing (d_{hkl} values), 2 values and relative intensity values of zinc oxide (ZS and ZCS prepared in the present work) corresponding to the observed diffraction peaks were compared with the standard values of zinc oxide as reported by JCPDS-International Centre for Diffraction Data which also matched with JCPDS-ICDD pattern number pattern number #79-0205 of zinc oxide. Both ZS and ZCS matched with the standard ZnO hexagonal system with a primitive lattice of ZnO (JCPDS: #79-0205). For ZS the diffraction peaks at 2 values 31.71°, 34.39°, 36.27°, 47.49°, 56.61°, 62.68°, 66.29°, 67.99°, 69.1°, 72.75° and 77.12° corresponds to the crystal planes of (100), (002), (101), (102), (110), (103), (200), (112), (201), (004) and (202) respectively with no characteristic peaks corresponding to the impurities, which further confirms the formation of pure stable ZnO phase. In case of ZCS, the diffraction peaks at 2 . values 31.73°, 34.40°, 36.28°, 47.50°, 56.61°, 62.88°, 66.29°, 67.82°, 69.15°, 72.58° and 76.99° corresponds to the crystal planes of (100), (002), (101), (102), (110), (103), (200), (112), (201), (004) and (202) respectively with no characteristic peaks corresponding to the impurities, which further confirms the formation of pure stable ZnO phase.

The average crystallite size of ZS and ZCS calculated from the line broadening of the XRD pattern, utilizing FWHM values of three noteworthy tops in the XRD spectrum making use of Scherrer equation are shown in Tables 2 and Table 3. The Scherrer equation is

$$t = K\lambda/\beta cos\theta_{hkl}$$

Here t is the average crystallite size normal to the reflecting planes, K is the shape factor which lies between 0.95 and 1.15 depending on the shape of the grains (K= 1 for spherical crystallites), l is the wavelength of X-rays used, β_{hkl} is the full width at half maximum of the diffraction line in radians and β_{hkl} is the Bragg angle corresponding to the diffraction line arising from reflections from the planes designated by Miller indices (h k l).

Table 2. Crystallite size calculation of ZCS using Scherrer equation.

2θ	θ	Cosθ	FWIIM	D (nm)
31.73	15.87	0.9619	0.3814	21.65
34.40	17.20	0.9553	0.3919	21.22
36.28	18.14	0.9503	0.4661	17.94

Average Crystallite size = 20.27 nm

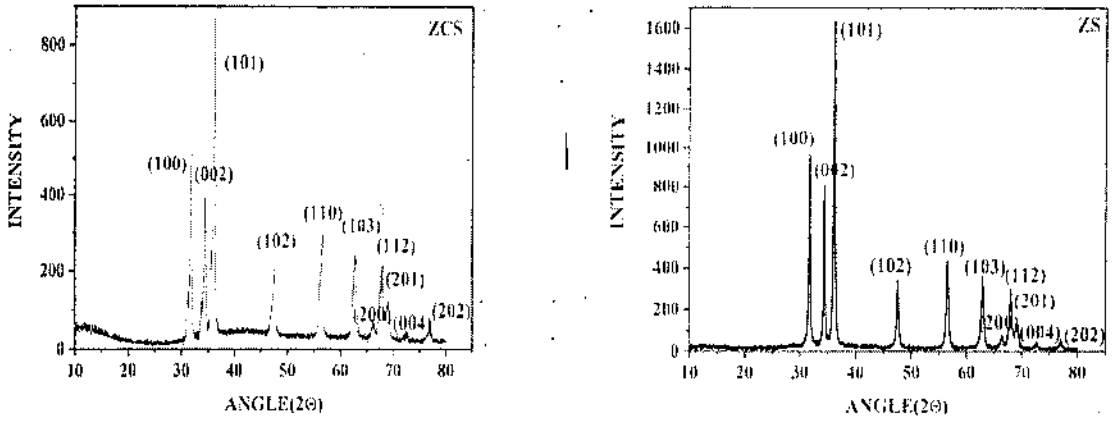

Figure 1 XRD Spectrum of ZCS and ZS

Table 3. Crystallite size calculation of ZS using Scherrer equation.

2θ	θ	Cosθ	FWHM	D (nm)
31.71	15.86	0.9619	0.3945	20.94
34.39	17.19	0.9553	0.3603	23.08
36.27	18.14	0.9504	0.4308	19.40

Average Crystallite size = 21.14 nm

3.1.2. XRD analysis of RS

The XRD pattern of RS was found to match well with the XRD patterns in literature [7]. The XRD of RS showed the presence of a few crystalline peaks in the diffraction pattern having 2θ values

between 15^0 and 30^0 and broad peaks between 30^0 and 50^0. Figure 2 shows the XRD diffraction pattern of RS.

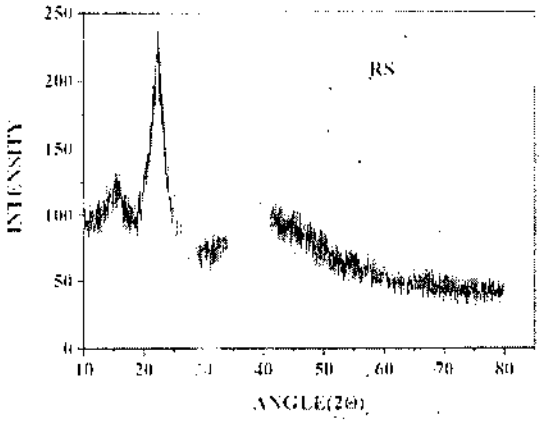

Figure 2 XRD Spectrum of RS

3.XRD analysis of RSZS and RSZCS

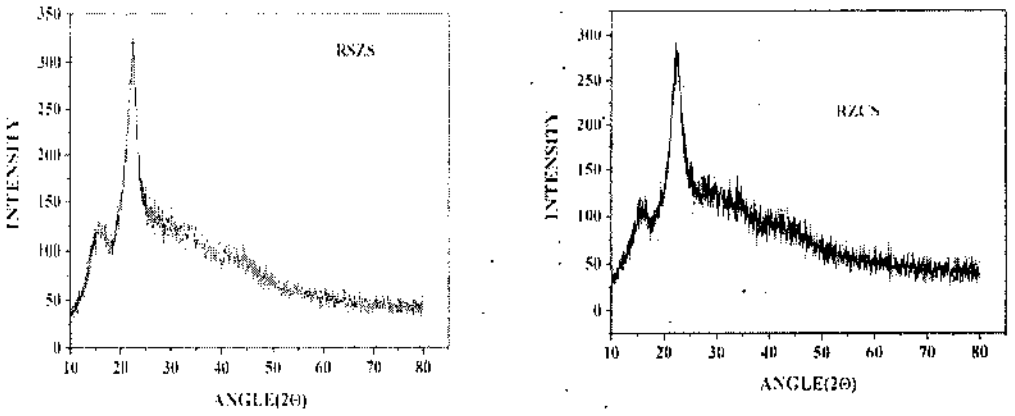

Figure 3 XRD Spectrum of RSZS and RSZCS

Figure 3 shows the XRD diffraction pattern of RSZS and RSZCS respectively. The variation of XRD of RSZS and RSZCS when compared with RS confirms the formation of nanocomposites. Since doping level of metal oxide was low no sharp peaks of metal oxide was obtained in case of nanocomposites.

3.2. Antibacterial Studies

There is a pressing demand in the present world to develop new antimicrobial agents and to find out novel strategies due to the emerging infectious diseases and the development of drug resistance in the pathogenic bacteria and fungi. The present study investigates the antimicrobial activity of the synthesized samples as antibacterial agents. The selected microbes for the present study are the gram positive bacteria: Bacilus cereus (B. cereus), the gram negative bacteria: Escherichia coli (E. coli). These test organisms were collected from Institute of Microbial Technology, Microbial Type Culture Collection Centre (IMTECH), Chandigarh. The strains were maintained on their respective medium in slants at 2-8^{0}C.

The antibacterial activities of the prepared samples in the laboratory had been calculated using the modified Kirby-Bauer disc diffusion method. The pure cultures of the given organisms were subcultured in the Müller-Hinton broth at a temperature range of 35°C ± 2°C on an orbital shaking incubator at 160 rpm. For the microbial growth, a large lawn of culture was prepared by spreading the 100 µL freshly prepared culture having 106 colony-forming units (CFU)/mL of each testing organism on nutrient agar plates by the assistance of a sterile glass-rod spreader. Plates were left standing for 10 minutes to allow the culture to get absorbed into the plates. Thereafter, 8 mm wells were punched into the nutrient agar plates to test the nanomaterial antimicrobial activity. Wells had been sealed with one drop of molten agar (0.8% agar) to avoid leakage of nanomaterials from the bottom of the wells. Using a micropipette, 100 µL (50 µg) of the prepared sample of nanoparticle suspension was poured onto each of the wells on all plates. After an overnight incubation at a temperature range of 35°C±2°C, the various levels of the zone of inhibition were measured around the disc in units of millimeter. The Solvent blank was used as negative control and Antibiotic tetracycline was used as a positive control.

The antibacterial activities of all the five samples were studied in detail. The antimicrobial activity of the nanoparticles with which is in contact with the microorganisms is generally known to be a function of the surface area. Since, the reactions take place at the surface of a chemical or material, smaller the size, higher is the surface to volume ratio i.e., in case of larger surface area, better interaction with the microbes is seen. Figure 4 shows the comparison of antibacterial activity of ZS, ZCS, RS, RSZS and RSZCS. Table 4 shows this comparison. Antimicrobial effects of ZnO nanoparticles can be attributed to several mechanisms: ROS (reactive oxygen species) generation results in induction of oxidative stress, due to accumulation of nanoparticles in the bacterial membrane, membrane disorganization occurs and also their cellular internalization, antimicrobial activity may also be due to the release of metal ions and their binding to the membrane of microorganisms.

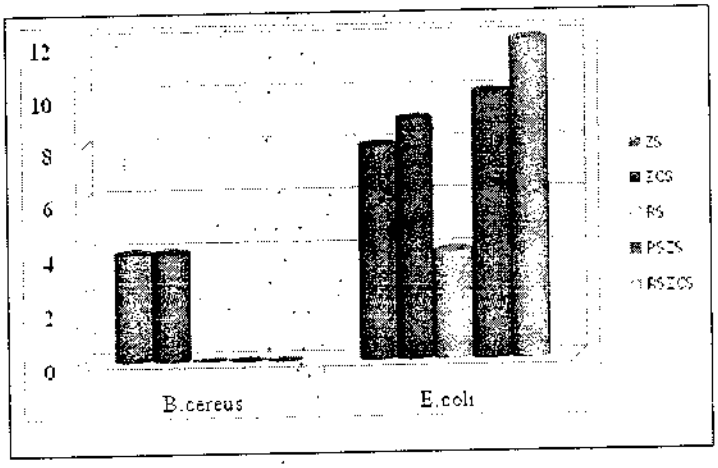

Figure 4 Comparison of Antibacterial activity of ZCS, ZS, RS, RSZS and RSZCS

The destruction of the outer membrane of bacteria by the generated superoxide anion radicals ($\cdot O^{2-}$), which acts as the reactive species, results in antibacterial activity. At the catalyst's surface, the reactive species such as $\cdot OH$ and $\cdot O^{2-}$ are generated. Hence the high surface area is very beneficial for degradation of bacteria. The activity was found to be highest in case of gram negative bacteria. All the five samples showed very low activity for B.cereus. The variation in the sensitivity or resistance to both gram positive and gram negative bacteria populati[illegible]e to the differences in the cell structure, physiology, metabolism or degree of contact o[illegible]gani[illegible]with nanoparticles.

Table 4 Zone of inhibition of ZS, [illegible] RS, RSZS and RSZS

Samples	B.cereus	E. coli
ZS	4 mm	8 mm
ZCS	4 mm	9 mm
RS	No zone	4 mm
RSZS	No zone	10 mm
RSZCS	No zone	12 mm

4. Conclusions

In the present work we are focussed on the comparison of structural and antibacterial properties of nanocomposite of ZnO formed with rice straw. ZnO nanoparticles were prepared using co-precipitation and combustion methods. Structural characterizations of all the five synthesized samples were carried out using XRD. Comparison of XRD's of metal oxide with JCPDS confirmed that the formed metal oxide was ZnO. Crystallite sizes were calculated using Scherrer equation. Crystallite sizes calculated for ZCS was 18.54 nm and that of ZS 19.33 nm. The variation of XRD of RSZS and RSZCS when compared with XRD of RS confirms the formation of nanocomposites. Since doping level of metal oxide was low no sharp peaks of metal oxide was obtained in case of nanocomposites. The present study investigates the antimicrobial activity of the synthesized samples as antibacterial agents. The selected microbes for the present study are the gram positive bacteria: Bacilus cereus (B. cereus), the gram negative bacteria: Escherichia coli (E. coli). The activity was found to be highest in case of gram negative bacteria. Antibacterial activity of RS can be attributed to the activity of organic groups which are present in the biopolymer chain. The presence of polyfunctional groups is supposed to be a perfect recipe for making an antibacterial agent. In addition to this, the presence of metal oxide in the biopolymer chain might have enhanced the antibacterial activity of the nanocomposite. All the five samples showed very low activity for B.cereus. The variation in the sensitivity or resistance to both gram positive and gram negative bacteria populations may be due to the differences in the cell structure, physiology, metabolism or degree of contact of organisms with nanoparticles.

References

[1] Wang S.S, Shanks R.A and Hodzic A, Poly(L-lactic acid) composites with flax fibers modified by plasticizer adsorption. Polym. Eng. Sci. 2003, 43, 1566–75.Mohammad M. K, Debabrata Pradhan and Youngku Sohn2017*Springer* 19-40.

[2] Satyanarayana K.G, Arizaga G.G.C and Wypych F, Biodegradable composites based on

lignocellulosic fibers—An overview, Prog. Polym. Sci. 2009, 34, 982–1021.

[3] Garsia, M.; Garmendia, I.; Garsia, J. Influence of natural fiber type in eco-composites. J. Appl. Polym. Sci. 2008, 107, 2994–3004.

[4] Shanks, R.A.; Hodzic, A.; Ridderhof, D. Composites of poly(lactic acid) with flax fibers modified by interstitial polymerization. J. Appl. Polym. Sci. 2006, 99, 2305–13.

[5] Fu P, Hu S, Xiang J, Sun L.S, Yang, T, Zhang A.C and Zhang J.Y, Mechanism study of rice straw pyrolysis by fourier transform infrared technique, Chin. J. Chem. Eng. 2009, 17, 522–29..

[6] Roshanak Khandanlou, Mansor B. Ahmad, Kamyar Shameli, Elnaz Saki and Katayoon Kalantari, Studies on Properties of Rice Straw/Polymer Nanocomposites Based on Polycaprolactone and Fe_3O_4 Nanoparticles and Evaluation of Antibacterial Activity, International journal of molecular sciences, 2014, 15(10), 18466-483.

[7] Li Q L, Mahendra S, Lyon D Y, Brunet L, Liga M V, Li D and Alvarez P J J, Antimicrobial nanomaterials for water disinfection and microbial control: potential applications and implications, Water Res., 42, 2008a, 4591–602.

[8] Yamamoto O, Influence of particle size on the antibacterial activity of zinc oxide, Int. J. Inorganic Materials, 3, 2001, 643–646.

[9] Naka K, Itoh H, Park S and Chujo Y, Synthesis of nanocomposites of metal nanoparticles utilizing miscible polymers, Poly. Bull., 52, 2004, 171-176.

[10] Siedenbiedel F and Tiller J C, Antimicrobial polymers in solution and on surfaces: overview and functional principles, Polymers, 4, 2012, 46-71.

[11] Roshanak Khandanlou, Mansor Bin Ahmad, Kamyar Shameli and Katayoon Kalantari, Synthesis and Characterization of Rice Straw/Fe_3O_4 Nanocomposites by a Quick Precipitation Method, Molecules 2013, 18, 6597-607.

[12] Li Q L, Mahendra S, Lyon D Y, Brunet L, Liga M V, Li D and Alvarez P J J, Antimicrobial nanomaterials for water disinfection and microbial control potential applications and implications, Water Res., 42, 2008a, 4591–602..

Structural and photocatalytic degradation studies of rice straw based MgO nanocomposite

Deepika R[1,2], Dedhila Devadathan[1], Rejani P[1,3] and Raveendran R[1]

[1] Nanoscience Research Laboratory, Department of Physics, Sree Narayana College, Kollam 691001, Kerala, India
[2] Department of Physics, Amrita Vishwa Vidyapeetham, Amritapuri, India
[3] Department of Chemistry, MMNSS College, Kottiyam, Kollam 691571, India

E-mail: 956deepika@gmail.com

Abstract. The present study is focused on the comparison of structural and photocatalytic degradation activities of nanocomposite of MgO formed with rice straw, a biopolymer. For comparison, counter parts were also synthesized. Nanoparticles of magnesium oxide were synthesized through controlled co-precipitation method in presence of citric acid. Structural characterizations of all the synthesized samples were carried out using XRD. Comparison of XRD of metal oxide with JCPDS confirmed that the formed metal oxide was MgO. Photocatalytic degradation of organic dyes Congo Red, an acidic dye and Methylene Blue, a basic dye was done.

1. Introduction

Photocatalysis is a special method that can be used for a variety of purposes such as degradation of different types of organic pollutants in wastewater, hydrogen production, air purification and antibacterial activity [1]. Photocatalysis based research is growing rapidly and gaining researchers more attention due to its advantages like low cost and high quality efficiency when compared to other methods. It is a unique method for rectifying issues related to energy and environment. With the various efficient methods that have come up in the technologies for the treatment of wastewater, low cost and less time consuming methods is the need to access pure water [2]. Natural materials applications as eco-friendly products, for disposing waste is the field gained great attention of the researchers, especially, in the synthesis of composites [3]. The use of farm residues like rice straw, rice husks and corn stover that are cheaper, available, renewable and biodegradable, can make profitable results. Since nature is the huge source of natural/bio-fibers, the utilization of bio-composites is expanding at a brisk pace. Because of the diversity in the optical, electrical and catalytic properties of nanocomposites prepared by incorporating metal nanoparticles into polymer matrix were found very significant applications. These have huge applications in the field of bioengineering, electronics, catalysis, and photonics [3]. Synthesis of nanocomposites is an expanding trend of nanoscience. In order to exploit the full potential of the technological applications of the nanomaterials, the scientists were guided towards the conventional polymers as one component of the nanocomposite. In the present work, we are focussed on the comparison of structural and photocatalytic degradation activity of nanocomposite of MgO formed with rice straw, a biopolymer.

Content from this work may be used under the terms of the . Any further distribution of this work must maintain attribution to the author(s) and the title of the work, journal citation and DOI.
Published under licence by IOP Publishing Ltd

2. Experimental

Merck's AR grade chemicals were used in the precipitation of rice straw based MgO nanocomposite. Co-precipitation method was applied in order to prepare MgO nanoparticles in presence of capping agent.

Metal oxide of MgO nanoparticles was prepared as follows. Starting materials used were Magnesium nitrate dihydrate and sodium hydroxide with Citric acid as a stabilizer. Aqueous solutions of 25 ml, 0.1 M magnesium nitrate and 50 ml, 0.5 M sodium hydroxide were added drop wise into a beaker containing 25 ml, 0.01 M aqueous solution of citric acid while stirring using a magnetic stirrer. The stabilizer was used to prevent growth and agglomeration of the particles. The particle size was governed by the experimental parameters like concentration of the reactants, rate of mixing, pH, viscosity of the solutions etc. The stabilizers used for controlling the precipitation reaction should be easily and completely removable from the sample so as to avoid any possible contamination of the samples. After two hours of continuous stirring, the precipitate formed was in hydroxide form. The precipitated hydroxide that contains ions and other impurities was washed several times using distilled water to free from it. The wet precipitate was filtered and dried at room temperature and used an agate motor to obtain the hydroxide precursor in the form of fine powder. The powder so obtained was annealed at 600^0C for 4 hours in a muffle furnace to obtain the respective metal oxide nanoparticles.

After proper cleaning and drying process rice straw waste was used. For the treatment of rice straw waste, basic NaOH solution and methanol were used. Small pieces of 5g rice straw washed using distilled water. NaOH solution was prepared by measuring NaOH equal to the weight of 10% of rice straw (0.5g) and making it upto 50 ml by dissolving NaOH in distilled water. Liquor to fiber ratio was taken as 10:1, ie, 50g of methanol for 5g of rice straw. Liquor and NaOH solution were added to the rice straw and were cooked on a heater for 20 minutes until the solution reduced to some amount on open air. It cool for some time and the pulps were further applied for acid pulping, where nitric acid (69% concentration) diluted (2.5 ml of acid and making it upto 25 ml using distilled water) was used in the pulp for heating until it reduces. It was cooled for some time. Again 25 ml of concentrated acid was added. After reduction and cooling process another 25 ml of acid was added and heated. The pulp turned to particles. After cooling distilled water was added to it and stirred for 15 minutes on a magnetic stirrer. After some time the powder settled. Water was decanted. The process was repeated thrice and finally washing was done using 50 ml of methanol. The solution was filtered using filter paper and dried at room temperature. Dried rice straw powder was collected and used for analysis. In case of nanocomposite based on rice straw annealed MgO was added at the time of pulp formation.

Table 1. Sample notations used in the present work.

Sample	Notations
Magnesium oxide nanoparticles annealed at 600^0C	MS
Rice Straw	RS
Rice Straw based Magnesium oxide nanocomposite	RSMS

3. Results and discussions

Metal oxide prepared using co-precipitation method in present study was obtained in the form of hydroxide. Magnesium hydroxide and after annealing Magnesium oxide both were obtained as white powders. Rice straw and rice straw based nanocomposite was obtained as pale yellow.

3.1. XRD Analysis

XRD studies were done with XPERT-PRO model powder diffractometer (PAN analytical, Netherlands) that employing Cu- Kα radiation (λ = 1.54060A°) operating at 40kV, 30mA.

3.1.1. XRD analysis of MS

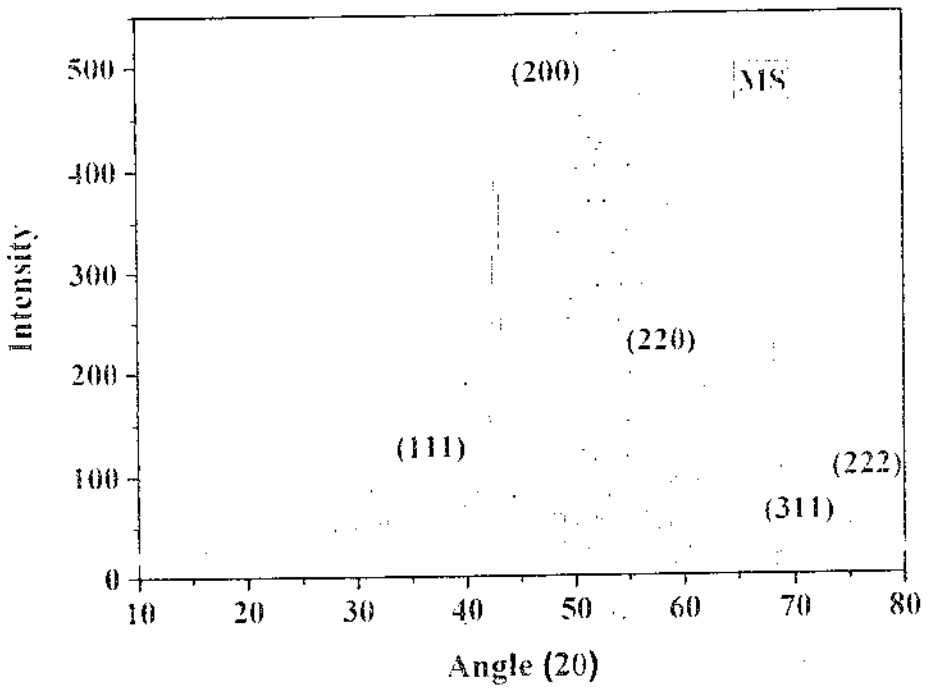

Figure 1. XRD of MS.

Figure 1 shows XRD of MS. The interplanar spacing (d_{hkl} values), 2θ values and relative intensity values of magnesium oxide corresponding to the observed diffraction peaks were compared with the standard values of magnesium oxide as reported by JCPDS-International Centre for Diffraction Data. The data obtained for MgO in case of MS was matched with JCPDS-ICDD pattern number #89-7746. For MS diffraction peaks at 2θ the values 36.67°, 42.88°, 62.19°, 74.6° and 78.51° corresponding to the crystal planes of (111), (200), (220), (311) and (222) respectively with no characteristic peaks corresponding to the impurities were detected, which further confirms the formation of pure stable MgO phase. JCPDS matching confirmed the cubic structure for MgO with FCC lattice. The average crystallite size of MS calculated from the line broadening of the XRD pattern, using FWHM values of three major peaks in the XRD spectrum making use of Scherrer formula are shown in Tables 2.

Table 2. Crystallite size calculation of MS using Scherrer equation.

2θ	θ	Cosθ	FWHM	D (nm)
42.88	21.44	0.9309	0.745	11.45
62.19	31.09	0.8565	0.779	11.90
78.51	39.26	0.7746	0.789	12.99

Average Crystallite size = 12.11 nm

3.1.2. XRD analysis of RS and RSMS

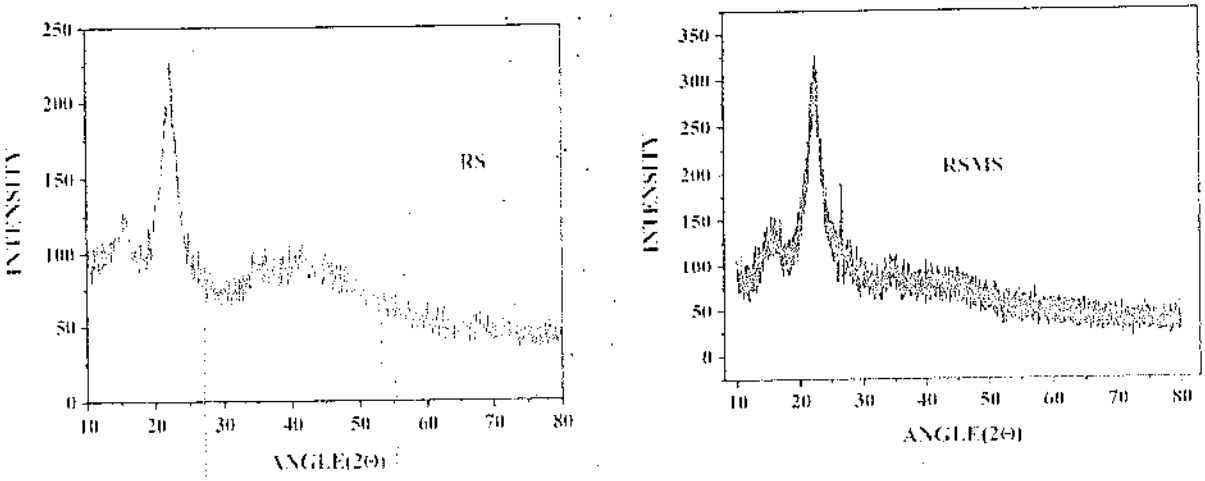

Figure 2. XRD Spectrum of RS and RSMS.

The XRD pattern of RS was found to match well with the XRD patterns in literature [4]. The XRD of rice straw showed the presence of a sharp crystalline peak in the diffraction pattern having 2θ value at 22.03^0. The XRD of RS showed a few peaks having 2θ values between 15^0 and 30^0 and broad peaks between 30^0 and 50^0. Figure 2 shows the XRD diffraction pattern of RS. The variation of XRD of RSMS when compared with RS confirms the formation of nanocomposite. Since doping level of metal oxide was low no sharp peaks of metal oxide was obtained in case of nanocomposite.

3.2. Photocatalytic Studies

Acidic dye Congo red and basic dye Methylene Blue of 1000 ppm concentration were prepared and the desired concentrations were taken and used as dye samples.

The photocatalytic activity of samples for the degradation of the dyes; Congo red (CR) and Methylene Blue (MB) were studied using the respective photocatalyst under the visible light illumination in a photoreactor. The experiments were performed by suspending the required quantity of photocatalyst into 300 ml of dye solution of needed concentration which was varied from 50 ppm to 75 ppm. The experiment was done isothermally at 300 K. The concentration of remaining dye in the solution after irradiation for 24 hrs was determined by monitoring the absorbance intensity of solution samples at their maximum absorbance wavelength by using UV-Vis spectrophotometer (JASCO V 650 UV/Vis spectrophotometer).

In the present work the factors affecting photocatalytic degradation like effect of contact time, amount of photocatalyst and dye concentration were also investigated.

To study the effect of contact time on the photodegradation of organic dyes, to the respective dye solution of concentration, 50 ppm in 300 ml solution kept at 300 K, 0.1 g of the photocatalyst was added and was kept under visible light. After desired time intervals [1, 2, 3 and 24 hrs], 10 mL of the solution was taken out, centrifuged and UV/Vis absorption spectra was recorded.

In the above experiment, the amount of photocatalyst was varied. 0.1 g and 0.15 g was used to study its effect on photodegradation.

Dye solutions of two different concentrations were selected (50 ppm and 75 ppm) to study the effect of initial dye concentration on photodegradation efficiency.

The photocatalytic degradation efficiency was calculated as follows:

$$\text{Photocatalytic Degradation Efficiency}(\%) = \frac{(C_0 - C_t)}{C_0} \times 100 \quad (1)$$

C_0: initial concentration of dye solution [mgL^{-1}],

C_t: final concentration of dye solution [mgL^{-1}]

The photodegradation of Congo red and Methylene Blue using the nanocomposite RSMS as well as its counterparts RS and MS were studied in detail. The results show high rate of photodegradation of the dye with increase in contact time. The photodegradation rate after 24 hrs for all the samples for both Congo Red and Methylene Blue are given in Table 3 and Table 4 respectively. Figure 3 shows the absorbance spectrum obtained for a few samples at various contact time.

In the calculation of degradation efficiency, the amount of loading catalyst is one of the chief parameters. For the efficient dye removal, it is required to find optimal loading in order to avoid the excessive use of the catalyst. The results showed that there was a slight decrease in the degradation percentage when catalyst dosage was increased. The significant decrease was due to the decrease in the formation of hydroxyl radicals. It should mention here that, the number of active sites on photocatalysts and the visible light penetration through the suspension, both affect the catalyst loading [5]. The number of active sites increases with the increase catalyst loading, but the visible light penetration decreases because of the shielding effect [6]. It should also be noted that the optimum value of catalyst loading is strongly dependent on the type and initial concentration of the dye and the operating conditions of the photoreactor [7].

The results imply that the photocatalytic degradation rate decreased according to the increasing of initial dye concentration. The colour of dye solution becomes deeper as the initial dye concentration increase, which reduces the light penetration into the catalyst's surface and thereby decreasing the excited dye molecule. With the increase of initial dye concentration more and more organic substances get adsorbed on the surface of the photocatalyst. Therefore, the hydroxyl radicals generation is reduced, since there are only fewer active sites in the system [8]. The activity of the nanocomposite was also compared with the counter parts.

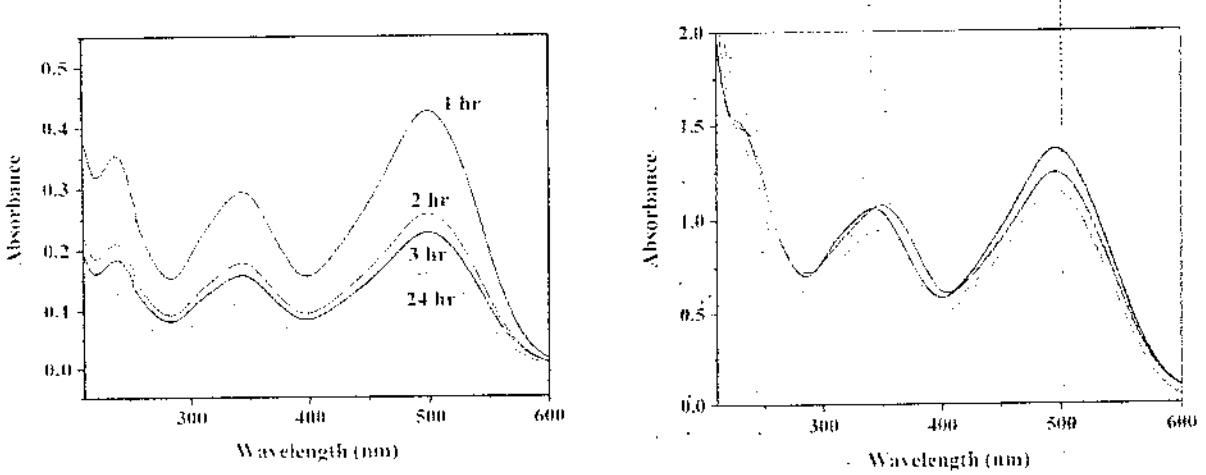

Figure 3. Absorbance spectrum showing photodegradation of CR using MS, 50 ppm and RS, 75 ppm.

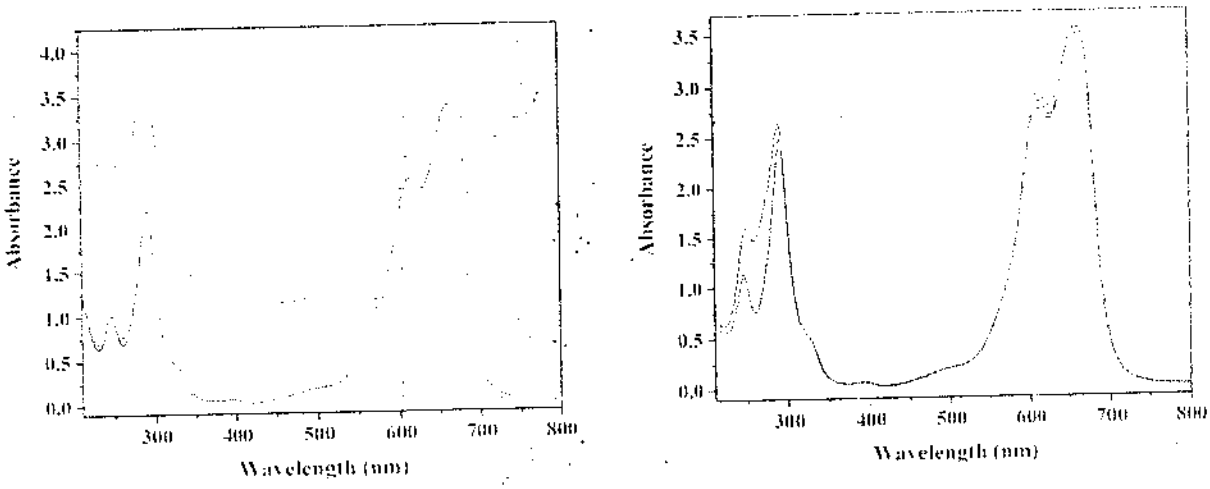

Figure 4. Absorbance spectrum showing photodegradation of MB using RS, 50 ppm and RS, 75 ppm.

Table 3. % Photodegradation of Congo Red using Synthesized samples.

Sample	Weight (g)	Concentration (ppm)	% Photodegradation
MS, CR	0.1	50 ppm	85.23
	0.15	50 ppm	80.15
	0.1	75 ppm	82.05
	0.15	75 ppm	78.43
RS, CR	0.1	50 ppm	59.54
	0.15	50 ppm	54.23
	0.1	75 ppm	53.24
	0.15	75 ppm	46.36
RSMS, CR	0.1	50 ppm	96.46
	0.15	50 ppm	90.54
	0.1	75 ppm	91.45
	0.15	75 ppm	87.23

Table 4. % Photodegradation of Methylene Blue using Synthesized samples.

Sample	Weight (g)	Concentration (ppm)	% Photodegradation
MS, MB	0.1	50 ppm	73.56
	0.15	50 ppm	68.12
	0.1	75 ppm	70.24
	0.15	75 ppm	64.81
RS, MB	0.1	50 ppm	43.12
	0.15	50 ppm	35.84
	0.1	75 ppm	34.29
	0.15	75 ppm	29.15
RSMS, MB	0.1	50 ppm	82.15
	0.15	50 ppm	75.19
	0.1	75 ppm	76.20
	0.15	75 ppm	68.15

4. Conclusions

Structural characterizations of all the three synthesized samples were carried out using XRD. Comparison of XRD of metal oxide with JCPDS confirmed that the formed metal oxide was MgO. Phase purity and crystallinity of the sample was confirmed from XRD. Crystallite size was calculated using Scherrer equation. Photocatalytic degradation of organic dyes Congo Red, an acidic dye and Methylene Blue, a basic dye was done. In the present work the factors affecting photocatalytic degradation like effect of contact time, amount of photocatalyst and dye concentration were also investigated. The results show high rate of photodegradation of the dye with increase in contact time. Also, when catalyst dosage was increased, there was a slight decrease in the degradation percentage. The results also, indicate that the photocatalytic degradation rate decreased with the increasing initial dye concentration. The synthesized nanocomposite is a good photocatalyst for the photodegradation of organic dyes.

References

[1] Gupta V K, Ali I, Saleh T A, Nayak A and Agarwal S 2012 *RSC Adv.* **2**(16) 6380-6388.
[2] Mohammad M K, Debabrata Pradhan and Youngku Sohn 2017 *Nanocomposites for visible light-induced photocatalysis* Springer 19-40.

[3] Roshanak Khandanlou, Mahsor B Ahmad, Kamyar Shameli, Elnaz Saki and Katayoon Kalantari 2014 *Int. J. of Mol. Sci.* **15** 18466-83.
[4] Roshanak Khandanlou, Mansor Bin Ahmad, Kamyar Shameli and Katayoon Kalantari 2013 *Molecules* **18**, 6597-607.
[5] Daneshvar N, Salari D and Khataee A R 2003 *J. Photochem. Photobiol. A: Chem.* **157** 111-6.
[6] Gouvea CAK, Wypych F, Moraes SG, Durán N and Peralta- Zamora P 2000 *Chemosphere* **40** 433–40.
[7] Gogate P R and Pandit A B 2004 *Adv. Environ. Res.* **8** 553–97.
[8] Daneshvar N, Salari D and Khataee A R 2004 *J. Photochem. Photobiol. A: Chem.* **162** 317-22.

Original Article

Bulletin of Pure and Applied Sciences.
Vol.37 C (Chemistry), No.1, 2018: P.42-52
Print version ISSN 0970 4620
Online version ISSN 2320 320X
DOI 10.5958/2320-320X.2018.00007.9

Antibacterial studies of polyindole based metal oxide nanocomposites

Dedhila Devadathan[1]*, Baiju V[1], Raveendran R[1]

Author Affiliations
[1]Nanoscience Research Laboratory, Department of Physics, Sree Narayana College, Kollam 691001

Corresponding Author
***Dedhila Devadathan,** Nanoscience Research Laboratory, Department of Physics, Sree Narayana College, Kollam 691001

E-mail: dedhila@yahoo.com

Received on 16th January 2018
Accepted on 28th January 2018

Abstract

In the present work, polyindole based metal oxide nanocomposites were synthesised through chemical oxidation method. For comparative study, the counterparts, polyindole was synthesised through chemical oxidation method and the metal oxides were synthesised through chemical co-precipitation method. Structural studies were done using XRD. Phase purity and crystallinity of these samples were confirmed from XRD. XRD confirmed the formation of nanocomposites. Crystallite sizes were calculated using Scherrer equations for metal oxides. The present study investigates the antimicrobial activity of the synthesized samples as antibacterial agent. The gram [illegible] oxide nanocomposites. Samples prepared by the co-precipitation method [illegible] the antibacterial properties of metal oxide nanoparticles.

1. INTRODUCTION

The advances in the field of nanosciences and nanotechnology led to the development of inorganic and organic nanocomposites that are nowadays widely used as antimicrobials. It is a matter of fact that the binding of the particles to the bacteria depends on the surface area available for interaction. Since the reactions takes place at the surface of a chemical or material; the greater the surface for the same volume, the greater will be the reactivity. The smaller size of nanoparticles helps them to easily reach the nuclear content of bacteria which will give more bactericidal effect than the larger particles.

Conducting polymers because of its ability to be doped in reduced or oxidized form (redox properties) has facilitated its usefulness in certain biological applications [1]. Also they can be used in the form of powders, aqueous dispersions and as coatings on variety of substrates. In addition to

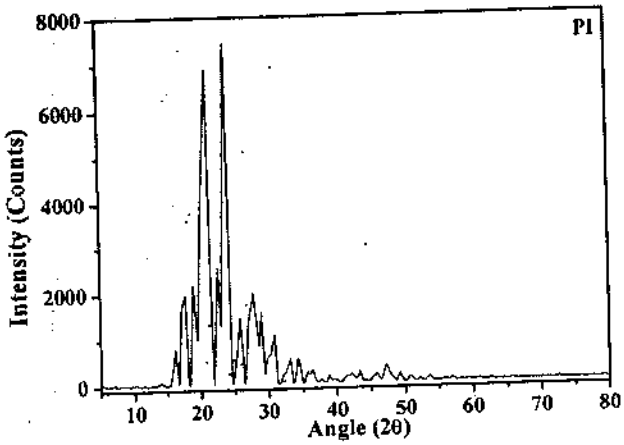

Fig. 1: XRD Spectrum of PI

X-ray diffractograms of NF and NS are shown in Figures 2 and 3 respectively. The well defined X-ray diffraction peaks in the case of NF and NS indicate that NiO formed are crystalline in nature. Also, the diffraction peaks are notably broadened indicating the smaller crystallite size.

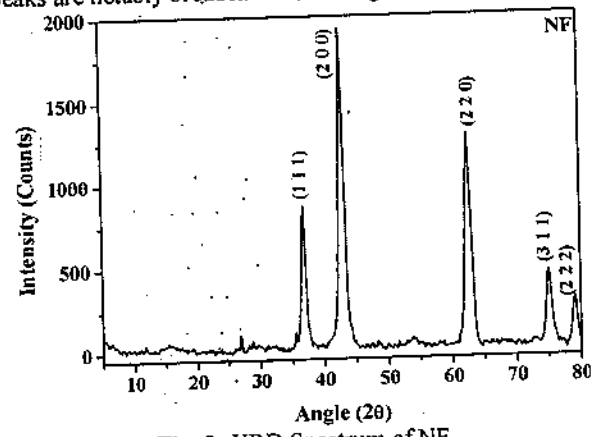

Fig. 2: XRD Spectrum of NF

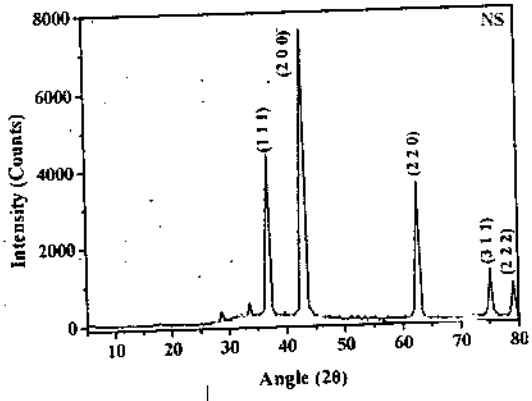

Fig. 3: XRD Spectrum of NS

Similar to NF and NS, NZF and NZS also showed well defined X-ray diffraction peaks which indicated that NZF and NZS too had crystalline nature. Again, the broader diffraction peaks indicated the smaller crystallite size. The interplanar spacing (d_{hkl} values), 2θ values and relative intensity values of NZF and NZS corresponding to the observed diffraction peaks were compared with the standard values of NiO and ZnO as reported by JCPDS-International Centre for Diffraction Data. The obtained pattern for ZnO (ZF) was found to match well with JCPDS-ICDD pattern number #79-0205. The data obtained for NiO/ZnO matched with JCPDS-ICDD pattern number #78-0423 of NiO and JCPDS-ICDD pattern number #79-0205 of ZnO separately. From JCPDS, NiO shows cubic system with FCC lattice and ZnO shows hexagonal system with primitive lattice. Figures 6 and 7 show XRD patterns obtained for NZF and NZS respectively.

The variation observed in the d values of the crystal planes in case of NZF and NZS when compared to NiO and ZnO, confirmes the formation of composites. This is also supported by the disappearance of the peak corresponding to (1 0 3) of ZnO in the XRD of the nanocomposite.

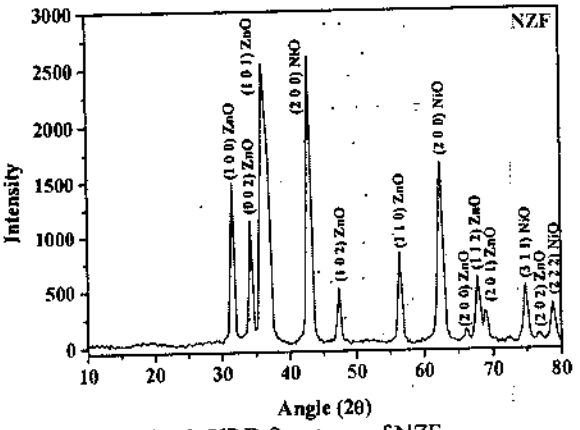

Fig. 6: XRD Spectrum of NZF

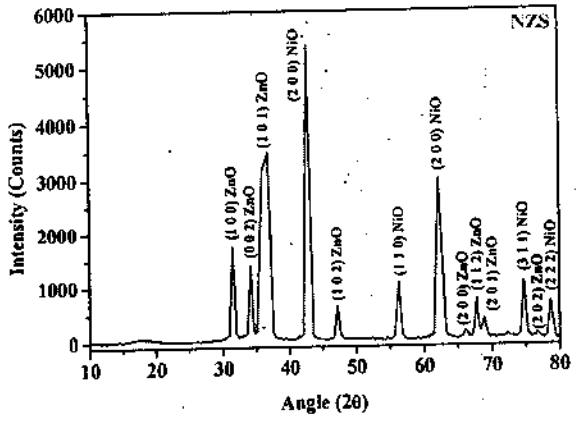

Fig. 7: XRD Spectrum of NZS

NMF and NMS also showed well defined X-ray diffraction peaks which indicated the crystalline nature of NMF and NMS. Here also the broader diffraction peaks obtained indicated the smaller crystallite size. The interplanar spacing (d_{hkl} values), 2θ values and relative intensity values of NMF and NMS corresponding to the observed diffraction peaks were compared with the standard values of NiO and MgO separately. Figure 9 shows XRD diffraction pattern obtained for MgO. The obtained pattern for MgO was found to match well with JCPDS-ICDD pattern number #89-7746. The obtained data for NMF and NMS were matched with JCPDS-ICDD pattern number #78-0423 of NiO and JCPDS-ICDD pattern number #89-7746 of MgO separately. From JCPDS comparison it is clear that MgO like NiO has a cubic system with FCC lattice. Hence it could be concluded that NMF and NMS also formed a cubic system with FCC lattice. Figures 10 and 11 show XRD pattern obtained for NMF and NMS respectively.

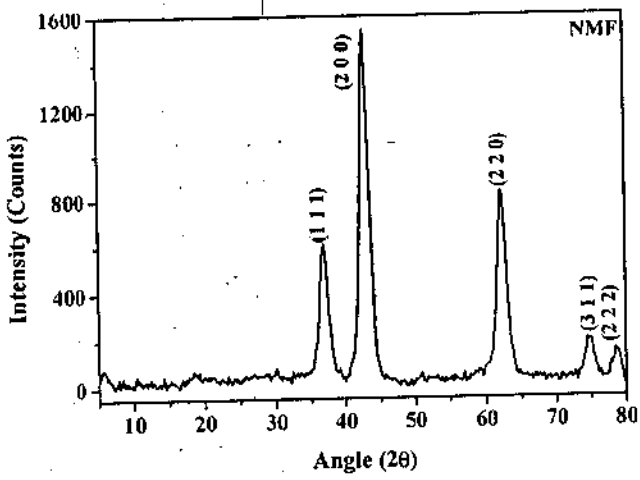

Fig. 10: XRD Spectrum of NMF

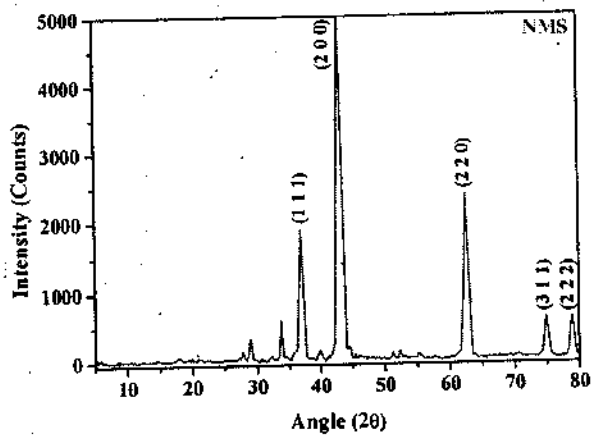

Fig. 11: XRD spectrum of NMS

Among NF, NZF and NMF the activity was found to be highest for the metal oxide composite, NZF. Here the activity can be attributed to the combined activities of NiO and ZnO. Antimicrobial effects of ZnO nanoparticles can be attributed to several mechanisms:

1. Induction of oxidative stress due to ROS (reactive oxygen species) generation,
2. Membrane disorganization due to accumulation of ZnO nanoparticles in the bacterial membrane and also their cellular internalization,
3. Release of Zn ions that may be responsible for antimicrobial activity by binding to the membrane of microorganisms.

These factors when combined with the activity of Ni^{2+}could have resulted in its higher antimicrobial activity when compared to NF. The zone of inhibition area of NZF is shown in Table 2.

In the case of NMF also the activity was found to be higher than NF. Here the inhibition of microbial growth can be attributed to the combined effect of NiO and MgO. The mechanism of the antibacterial activity of the MgO nanoparticles are mainly attributed to the presence of defects or oxygen vacancies at the surface of the nanoparticles which lead to the lipid peroxidation and reactive oxygen species generation. The activity was higher for NZF. This might be due to the specific activity of NZF to the selected microbes when compared to NMF. Furthermore, other factors such as nanoparticle diffusion rates may also affect bacterial strain differently. The zone of inhibition area of NMF and NMS are given in Table 3.

These materials also being good photocatalysts, their antibacterial mechanism can also be attributed to the destruction of the outer membrane of bacteria by the generated superoxide anion radicals ($\cdot O^{2-}$) as the reactive species. The reactive species such as $\cdot OH$ and $\cdot O^{2-}$ are generated at the catalyst's surface, hence the high surface area is very beneficial for degradation of bacteria.

Polyindole prepared in the present study, was found to have significant antimicrobial activity. Like polyailine, polyindole also contains quarternary ammonium salts (QAS) and halamines. Hence the antibacterial activity of PI can be attributed to the activity of QAS and halamines which are present in the polymer chain due to the presence of charged nitrogen as well as due to chloride ions. Nitrogen is present in the PI structure itself and the presence of chloride ions in the polymer chain as dopant. The presence of these two combined with the polycationic nature of polymer and the presence of polyfunctional groups is supposed to be a perfect recipe for making an antibacterial agent.

Table 1: Comparison of Antibacterial and Antifungal activity of NF, NS, PI and PIN

Samples	E. coli ZOI (mm)	C. perfringens ZOI (mm)	V. cholerae ZOI (mm)	S. epidermidis ZOI (mm)
NF	10	12	9	13
NS	9	10	7	11
PI	8	9	7	10
PIN	15	18	14	19

Composite of PI with metal oxides; PIN, PINZ and PINM have higher activities when compared to their counter parts. All the factors of PI combined with the activity of metal oxides was found to enhance the activity of the respective nanocomposite. The activity was found to be highest for PINZ than for PINM. Among the polyindole nanocomposites, PIN had lowest activity. The value of zone of inhibition area (ZOI) for PIN is given in Table 1. The corresponding values for PINZ and PINM are given in Table 2 and 3 respectively.

[10] Chen J, Schmidt, Chen J, Wang L, Weidner D J, Zhang J and Wang Y, Journal of Materials Science, 40, 2005, 5763–5766.
[11] Mattei G, Mazzoldi P, Post M L, Buso D, Guglielmi M and Martucci A, Advanced Materials 19, 2007, 561–564.

Original Article

Bulletin of Pure and Applied Sciences.
Vol.37 C (Chemistry), No.1, 2018: P.35-41
Print version ISSN 0970 4620
Online version ISSN 2320 320X
DOI 10.5958/2320-320X.2018.00006.7

Photocatalytic degradation of an acidic dye and a basic dye using heterostructured photocatalyst

Baiju V[1,*], Dedhila Devadathan[1], Raveendran R[1]

Author Affiliations
[1]Nanoscience Research Laboratory, Department of Physics, Sree Narayana College, Kollam, 691001, Kerala.

Corresponding Author
***Baiju V,** Nanoscience Research Laboratory, Department of Physics, Sree Narayana College, Kollam, 691001, Kerala.

E-mail: baijuvkollam@gmail.com

Received on 15th January 2018
Accepted on 30th January 2018

Abstract

Most of the natural resources of drinking water are found to be contaminated with various toxic materials. One of the most relevant pollutants is organic dyes. Photocatalysis is a promising green technology for the removal of dyes. In the present work heterostructured NiO/ZnO nanocomposite was prepared using co-precipitation method, analyzed using XRD, SEM and UV/Vis spectroscopy. For comparison purpose NiO was also prepared. Comparison of XRD's of metal oxides with JCPDS confirmed the formation of heterojunctions. UV/Vis absorption studies confirmed the shift of the optical absorption towards the visible region. The photocatalytic degradations of dyes namely Malachite Green, a basic and Congo Red, an acidic dye were carried out using the prepared composites. Factors affecting photocatalytic degradation like effect of contact time, amount of photocatalyst, dye concentration were also investigated. Results suggested an increase in degradation efficiency by the use of the heterojunction nanocomposites as compared to individual metal oxides.

Keywords: Photocatalysis, Heterojunction, Nanocomposite, Photocatalytic degradation

1. INTRODUCTION

Nature has its own mechanism for water recycling to provide us with sufficient quantity of fresh water with consumable purity level. Modern human activities have however disrupted the balance between the usage and natural purification process, leading to a shortage of potable water. Most of the natural resources of drinking water are found to be contaminated with various toxic materials and pathogenic microorganisms. One of the most relevant pollutants is organic dyes. The dyes have diverse applications in various industries of paper, leather, cosmetics, drugs, electronics, plastics and printing and approximately 80% of the synthetic dyes are consumed by the textile industry. Dyes are non biodegradable compounds and human exposure to wastewater which contains dyes is highly dangerous and these carcinogenic compounds show high resistance against biological, physical and

chemical reactions. Many researchers consider advanced oxidation process as the most effective, economically feasible and applicable technology for the removal of organic dye pollutants. Nanotechnology is widely applied for purification and treatment of waste water. The novel properties of nanomaterials such as large surface area, potential for self assembly, high specificity, high reactivity and catalytic potential make them excellent candidates for this application. An expanding trend for the nanomaterials is the fabrication of composite structures with materials capable of enhancing the properties. Many efforts have been made for the synthesis of different coupled semiconductors [1–4]. The synthesized coupled semiconductors significantly improve the photocatalytic efficiency by decreasing the recombination rate of the photogenerated electron–hole pairs and present potential application in water splitting, organic decomposition and photovoltaic device [5]. In the present study heterojuction NiO/ZnO nanocomposite is prepared and applied as photocatalyst.

2. MATERIALS AND METHODS

AR grade chemicals obtained from Merck were used for the preparation of NiO/ZnO heterojunction. NiO (NF) and NiO/ZnO (NZF) were prepared by the co–precipitation method in presence of capping agent. NF and NZF annealed at 5000c for three hours, was used for analysis. XRD studies were carried out using XPERT–PRO model powder diffractometer (PAN analytical, Netherlands) employing Cu–Kα radiation (λ = 1.54060Ao) operating at 40kV, 30mA. SEM of the samples was obtained using JEOL/EO Model JSM–6390LV scanning electron microscope. The absorbance spectra, reflectance spectra and photocatalysis studies of the sample was studied using JASCO V 650, UV/Vis spectrophotomer.

Metal oxides prepared in the present study were obtained in the form of hydroxides. The nickel hydroxide was obtained as dark green powder where as in the case of NiO/ZnO was obtained as light pista green powders. But both the annealed samples were black in colour.

3. RESULTS AND DISCUSSION

X–ray diffractograms of NF and NZF is shown in Figure 1. The well defined X–ray diffraction peaks in the case of NF and NZF indicate that NiO and NiO/ZnO formed are crystalline in nature. Also, the diffraction peaks are notably broadened indicating the smaller crystallite size. In order to confirm the phase purity of the samples prepared, the interplanar spacing (dhkl values), 2θ values and relative intensity values corresponding to the observed diffraction peaks were compared with the standard values of NiO in case of NF and in case of NZF the observed diffraction peaks were compared with the standard values of NiO and ZnO as reported by JCPDS–International Centre for Diffraction Data.

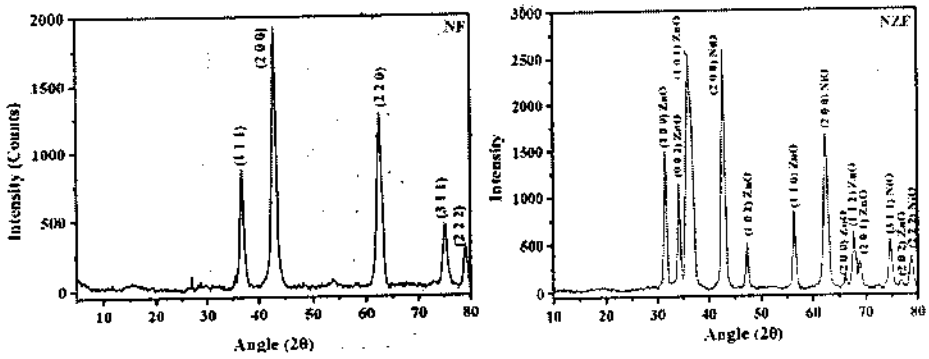

Fig. 2: XRD Spectrum of NF and NZF

Fig. 2: SEM images of (a) NF and (b) NZF

The UV–Vis absorption spectrum of the NF taken in the wavelength range 210 to 850 nm with 1 nm resolution is shown in the Figure 3. Presence of an absorption band is observed in the range 225 nm – 270 nm with λ_{max} situated at 249nm in case of NF.

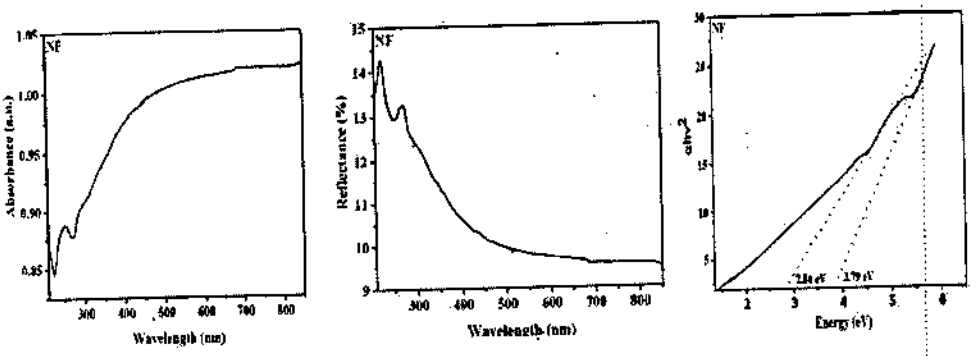

Fig. 3: UV/VisAbsorbance, Reflectance spectra and Tauc Plot of NF

An additional absorption band is observed in the wavelength range 270 nm – 305 nm. It is reported in literature that optical energy band gap of NiO lies in the range (3.6–4.0 eV) [Adler and Feinleib, 1970] and is attributed to charge–transfer transition between the valence bands of O (p) states to conduction bands of Ni d (e_{2g}) states [7]. The absorption edge is found to be 4.98 eV for NF. Figure 3 also shows the reflectance spectrum obtained for NF. The percentage reflectance corresponding to λ_{max} situated at 249 nm was found to be 12.94 %.

The materials also showed sub band gaps. This might be due to d–d transitions. The optical band gap of NF determined from the absorption spectra using Tauc's relation were 2.84 eV and 3.79 eV. Tauc's plot drawn for NF is also shown in Figure 3.

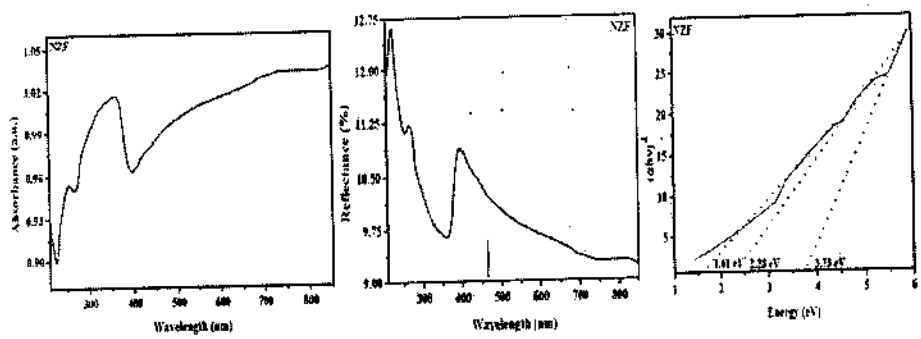

Fig. 4: UV/Vis Absorbance, Reflectance spectra and Tauc Plot of NZF

The UV–Vis absorption and reflectance spectra of NZF taken in the wavelength range 210 to 870 nm with 1 nm resolution is shown in the Figure 4. Presence of a weak absorption band was observed in the range 225 nm – 270 nm with λ_{max} situated at 256nm and also another strong absorption band in the range 260 nm – 400 nm with λ_{max} situated at 360 nm was also obtained. The shift of peak from 252 nm of NF to 256 nm in NZF can be attributed to the interaction between NiO and ZnO. The second band can be attributed to the presence of ZnO which could be assigned to the intrinsic band–gap absorption of ZnO due to the electron transitions from the valence band to the conduction band ($O_{2p} \rightarrow Zn_{3d}$) [8]. The absorption edge was found to be 3.44 eV for NZF. Figure 4 also shows the

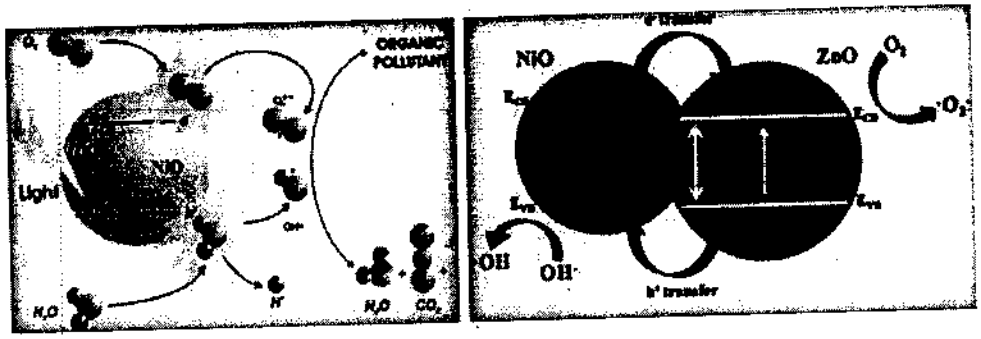

Fig. 5: Mechanism of Photocatalytic degradation process using NiO and NiO/ZnO hetrojunction nanocomposite

The percentage of photodegradation increased with increase in contact time of the dye and the catalyst. The amount of catalyst loading is one of the main parameters for the degradation efficiency. In order to avoid the use of excess catalyst it is necessary to find out the optimum loading for efficient removal of dye. The results showed that when catalyst dosage was increased from 0.025 to 0.075 g, the percentage de-colorization increased. However, on further increase in dosage of the catalyst beyond 0.1 g, there was a slight decrease in the degradation percentage. In the absence of photocatalyst it was found that CR dye is difficult to be oxidized by only UV light. The increase in degradation rate with increase in the catalyst loading is due to increase in total active surface area i.e. availability of more active sites on catalyst surface [9]. However, it increases significantly upon addition of photocatalyst due to the generation of higher amount of hydroxyl radical through the interaction of UV light with photocatalyst. But above 0.1 g, the percentage degradation significantly decreased due to decrease of formation of hydroxyl radicals. It should be pointed out that, the catalyst loading affects both the number of active sites on photocatalysts and the penetration of UV light through the suspension [10]. With increasing catalyst loading the number of active sites increases, but the penetration of UV light decreases due to shielding effect [11]. It should also be noted that the optimum value of catalyst loading is strongly dependent on the type and initial concentration of the dye and the operating conditions of the photoreactor [12]. The optimum concentration of the catalyst for efficient UV photodecolorization and degradation was found to be 0.1 g/300ml.

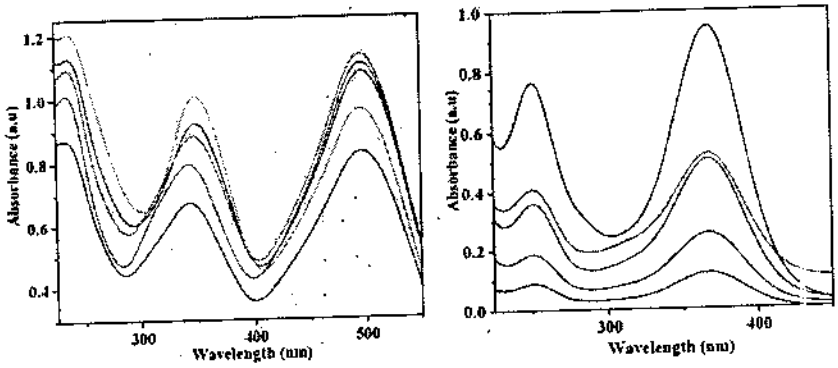

Fig. 6: Photocatalytic degradation of CR and MG

The rate of photocatalytic degradation decreased with the increasing initial dye concentration. As the initial concentration of a dye increases, the colour of dye solution becomes deeper which results in less penetration of light to the surface of the catalyst, decreasing the number of excited dye molecules. With increase in initial concentration of dye more and more organic substances are adsorbed on the surface of the photocatalyst. Therefore, the generation of hydroxyl radicals is reduced, since there are only fewer active sites in the system [13]. Similar results have been reported by other researchers for

International Journal of Advance Research in Science and Engineering
Volume No 06, Special Issue No. 03, September 2017, AFM-2017
www.ijarse.com
IJARSE
ISSN: 2319-8354

SYNTHESIS, CHARACTERIZATION AND APPLICATION OF NiO/ZnO HETEROSTRUCTURED ADSORBENT FOR HEAVY METAL IONS

Dedhila Devadathan[1], Baiju V[2], Biju R[3], Raveendran R[4]

Nanoscience Research Laboratory, Department of Physics, Sree Narayana College, Kollam 691001, Kerala, India

Abstract

In the present work heterostructured NiO/ZnO nanocomposite was prepared using co-precipitation method, analyzed using XRD and UV/Vis spectroscopy. For comparison purpose NiO and ZnO was also prepared. Comparison of XRD's of metal oxides with JCPDS confirmed the formation of heterojunctions. UV/Vis absorption studies confirmed the shift of the optical absorption towards the visible region. The batch type adsorption mechanism is utilized to study adsorption of heavy metal ions using synthesised samples as adsorbent in the present work. The factors affecting adsorption process such as contact time, pH, concentration of adsorbates, adsorbent dose, agitation speed and temperature were investigated and compared for the synthesized materials. Adsorption was found to be high in the case of nanocomposites than counterparts.

Keywords: Nanocomposite, Adsorbent

1. INTRODUCTION

Environmental pollution and its harmful effect on ecosystem have been studied intensively during the last decade. Heavy metals are very harmful for human beings, animals and plants. Industrial discharge of waste water containing elevated levels of heavy metals is a major environmental concern. Global and local agencies have established certain limits on the quantities of heavy metals being discharged into the environment. Adsorption is one of the conventional but efficient techniques used to remove heavy metals and organics from aqueous solutions. Presently nanotechnology is widely applied for purification and treatment of waste water. The novel properties of nanoparticles such as large surface area, potential for self assembly, high specificity, high reactivity and catalytic potential make them an excellent candidate for this application [1]. An expanding trend for nanomaterials is the fabrication of composite structures and devices with materials capable of enhancing the properties of the material [2]. In the present investigation, we report synthesis of NiO/ZnO heterostructured nanocomposite using the well known co-precipitation method. The nanocomposite has

International Journal of Advance Research in Science and Engineering
Volume No 06, Special Issue No. 03, September 2017, AFM-2017
www.ijarse.com
IJARSE
ISSN: 2319-8354

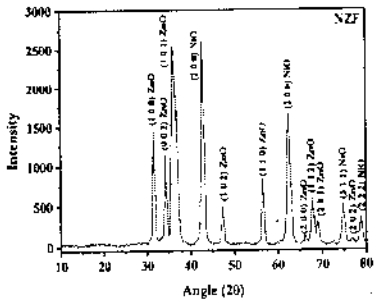

Fig.1 XRD of NZF

3.2 UV/Vis Spectrum Analysis

The UV/Vis absorption of NZF taken in the wavelength range 210 to 870 nm with 1 nm resolution is shown in the Figure 2. Presence of a weak absorption band was observed in the range 225 nm – 270 nm with λ_{max} situated at 256nm and also another strong absorption band in the range 260 nm – 400 nm with λ_{max} situated at 360 nm was also obtained. The second band can be attributed to the presence of ZnO which could be assigned to the intrinsic band-gap absorption of ZnO due to the electron transitions from the valence band to the conduction band ($O_{2p} \rightarrow Zn_{3d}$) [4]. The absorption edge was found to be 3.44 eV for NZF.

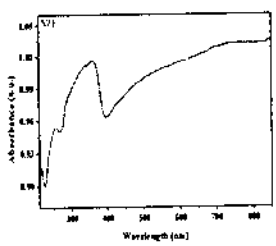

Fig.2 UV Absorbance spectrum of NZF

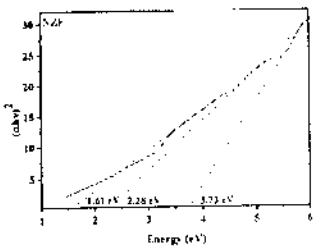

Fig.3 Tauc plot for NZF

From absorbance spectrum, Tauc plot was drawn and the corresponding energy gap was found. $(\alpha h\nu)^2$ vs hv was also plotted. The optical band gap determined from the absorption spectra using Tauc's relation for NZF is shown in Figure 3.

3.3 Adsorption Studies

Adsorption studies were performed by batch process by taking 0.1 gm of synthesized NZF in a 100 ml clean and dried stoppered bottle. Known concentration of 50 ml Cd^{2+} solution was added in the same stoppered flask. This flask was placed on a mechanical shaker at 160 rpm and the rate of adsorption of cadmium on NZF nanocomposite was studied. After desired time intervals [20, 40, 60, 80, 100 min etc], the solution was filtered using Whatman filter paper no. 41 and reserved for atomic absorption spectroscopy study. The factors affecting adsorption process such as contact time, pH, concentration of adsorbates, adsorbent dose, agitation speed and temperature were

higher mobility of ions. Results suggest that these adsorbents show endothermic nature of adsorption. The effect of agitation speed on the adsorption amount and percentage removal has been investigated. To study this parameter, the agitation speed (rpm) was varied from 50 to 200 rpm. There is increase in adsorption with respect to agitation speed with a maximum at 150 rpm. At 200 rpm the adsorption amount decreased. Hence the agitation speed was fixed at 150 rpm for studying the effect of all other factors on the adsorption process. The increase in agitation rate improves the diffusion of metal ions towards the adsorbent surface [6]. The diffusion rate of adsorbate ions (Pb^{2+}/Cd^{2+}) from the bulk liquid to the liquid boundary layer surrounding the particles becomes higher when the agitation rate is increased due to enhancement of turbulence and a decrease in the thickness of the liquid boundary layer. Thus, the external diffusion resistance can be neglected. A too vigorous agitation rate would result in more desorption of adsorbate from adsorbed sites.

4 CONCLUSIONS

Proper tuning can make NiO/ZnO heterostructured nanocomposite a good adsorbent for the removal of heavy metal ions.

5. REFERENCES

[1]. S. Zhang et.al., Journal of Alloys and Compounds, 426, 281 (2006).

[2]. J. Neamtu and N. Verga, J.of Nanomat. and Biostru. 6,969 (2011) .

[3]. S.H. Abdel-Halim et.al., Water research, 37, 1678 (2003).

[4]. Y. Haldorai, S. Chitra and J. J. Shim, Advanced Science, Engineering and Medicine 5, 2013, 1–7.

[5]. A. Ozar and H. B. Pirincci, J. Hazard. Mater., 2006, B137, 849.-855.

[6]. S. M. Nomanbhay and K. Palanisamy, Electronic J. Biotechnol. 8, 2005, 43 – 53.

International Journal of Advance Research in Science and Engineering
Volume No 06, Special Issue No. 03, September 2017, AFM-2017
www.ijarse.com
IJARSE
ISSN: 2319-8354

PHOTOCATALYTIC DEGRADATION STUDIES OF POLYANILINE BASED ZnO-Al_2O_3 NANOCOMPOSITE

Baiju V[1], Dedhila Devadathan[2], Biju R[3], Raveendran R[4]

Nanoscience Research Laboratory, Department of Physics, Sree Narayana College, Kollam 691001, Kerala,(India)

Abstract

In the present work polyaniline based ZnO-Al_2O_3 nanocomposite and its counterparts were synthesized. The synthesized materials were characterized using XRD. UV/Vis absorption spectroscopy of the synthesized samples was studied. From band gap calculation it was seen that all of them showed subgaps. The photocatalytic activities of the synthesized samples for the degradation of organic dye Congo Red were studied. The study also investigates the factors affecting photocatalytic processes of the nanocomposite such as dye concentration, illumination time and amount of catalyst loading.

Keywords: Nanocomposite, Conducting Polymer, Photocatalysis

I. INTRODUCTION

Water contamination has become a serious issue due to the fact that 2% of dyes produced in the industries are discharged directly in aqueous effluent [1]. So it was necessary to find a new way to remove coloured dyes [2, 3] before discharging them into the environment. Due to the economic constraints, development of a cost effective and clean process is essential. The various conventional technologies currently employed in the removal of effluents in industrial water are classical and do not lead to complete destruction of pollutants. In the case of industrial dyes, these methods do not work efficiently due to high solubility of dyes as well as their resistance to chemical and biological degradation; also they just transfer the contaminants from one phase to another [4]. Therefore, there is a need to develop a novel treatment method that is more effective. Photocatalysis is a promising technology in the field of green technology for the removal of dyes. Presently nanotechnology is widely applied for purification and treatment of waste water. The novel properties of nanomaterials such as large surface area, potential for self assembly, high specificity, high reactivity and catalytic potential make them an excellent candidate for both applications [5]. An expanding trend for the nanomaterials is the fabrication of composite structures and devices with materials capable of enhancing the properties of the composite material. This can be achieved either by utilizing the size advantage through templating on the nanomaterials and enhancing the properties to drive new synergetic properties of two combined materials [6]. In the present study polyaniline based ZnO-Al_2O_3 nanocomposite was prepared, analyzed and used as photocatalyst for the

diffraction line arising from the planes designated by Miller indices (hkl). The particle size for the sample is 15.32 ± 3 nm. From the XRD's of the polyaniline based nanocomposite it is clear that the metal oxide particles are well distributed in the polymer matrix. The well defined peaks of the metal oxides were found to be incorporated into the XRD peaks of polyaniline.

3.2 UV/Vis Spectrum Analysis

The UV/Vis absorption spectra of all the samples were taken in the wavelength range 210 to 870 nm with 1 nm resolution. In case of ZAT one weak band with λ_{max} situated at 257 nm between 223nm and 265 nm and another peak with λ_{max} situated at 323 nm between 270 nm and 420 nm were observed. The absorption edge is found to be 4.85 eV and 3.84 eV for the peaks corresponding to 256 nm and 323 nm respectively. The optical band gap of the material determined from the absorption spectrum using Tauc's relation.

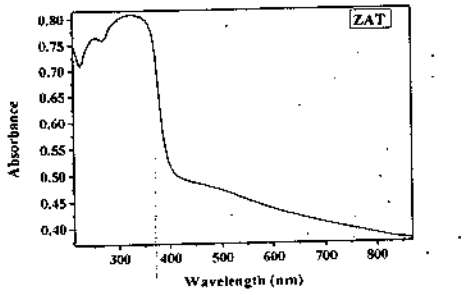

Fig.2 UV/Vis Absorbance spectra of ZAT

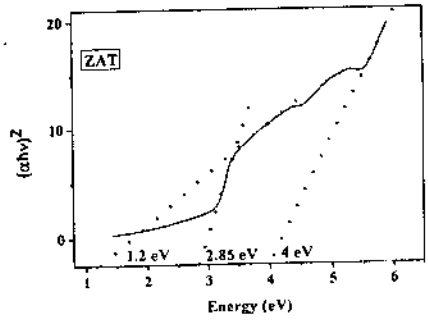

Fig.3 UV/Vis Absorbance spectra of ZAT

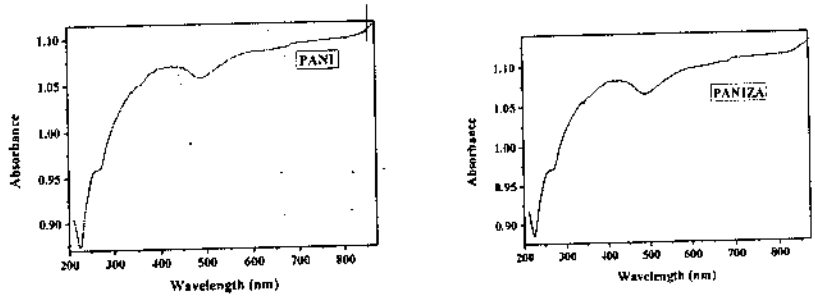

Fig. 4 UV/Vis Absorbance of PA and PANIZA

The absorption spectra of PANI and PANIZA are shown in the Figure 4. In case of PANI presence of a weak absorption band was observed in the range 220 nm – 265 nm with λ_{max} situated at 258 nm, which can be attributed to the conjugation of benzene ring in the indole unit and also another strong absorption band in the range 270 nm – 490 nm with λ_{max} situated at 426 nm was also obtained, which could be due to the π - π^* transitions of the benzene ring in the PI molecular chains [7]. The results indicate presence of enhanced conjugated segments and easy flow of charge in PANI molecular matrix. This band also relates to the extent of conjugation between adjacent rings in the polymer chain.. The absorption edge is found to be 4.81 eV and 2.91 eV for the peaks corresponding to 258 nm and 426 nm respectively. In case of PANIZA, the peak values were observed at 260 nm between 223 nm and 265 nm. The second peak was observed at 428 nm between 265 nm and 490 nm. The absorption edge is found to be 4.77 eV

reach to integrated model for the photocatalytic degradation of Congo red. The effect of illumination time on photodegradation efficiency of Congo Red was carried out by measuring the photodegradation efficiency at different periods of time using 0.1 gm of catalyst and 300mL of 50 ppm dye solution under UV light at 30°C. The results revealed that the photocatalytic activity increases with increase of the illumination time and reaches to 100% after 150 minutes illumination time. Such data reveals the relative high activity of the prepared catalysts which enables the complete degradation of the Congo red in such short illumination time and the catalyst has active sites for carrying out the reaction. The effect of catalyst loading dose on the photodegradation efficiency of Congo red was observed by taking different amounts of catalyst ranging from 0.05 to 0.15 gm into 300mL of 50 ppm dye solution under UV light at 30°C for two hours. The results showed that increment of catalyst loading from 0.05 to 0.1 gm increased the photodegradation efficiency of Congo red from 95 to 100% and after that the further increase in catalyst loading dose above 0.125 gm does not affect on the photodegradation efficiency. This is attributed to the increase in the catalyst loading dose which increased the number of active sites available on the catalyst surface for the reaction, which in turn increased the number of holes and hydroxyl radicals. The increase in initial dye concentration showed decreased photodegradation efficiency.

VI. CONCLUSIONS

XRD analysis confirmed the formation of nanocomposite. From the present work it is concluded that proper tuning of the formation of PANIZA nanocomposite can make it a good photocatalyst.

REFERENCES

[1]. M. A. Rauf, I. Shehadeh, A. Ahmed, and A. Al-Zamly, *World Academy of Science: Engineering and Technology*, 55, 2009.

[2]. C. I. Pearce, J. R. Lloyd, and J. T. Guthrie, *Dyes and Pigments*, 58, 2003, 179–196.

[3]. T. Robinson, G. McMullan, R. Marchant, and P. Nigam, *Bioresource Technology*, 77, 2001, 247–255.

[4]. L. Mun, Degradation of dyes using zinc oxide as the photocatalyst, *M.S. thesis*, Putra University, Serdang, Malaysia, 2008.

[5]. S. Zhang et.al., *Journal of Alloys and Compounds*, 426, 2006, 281-285.

[6]. Neamtu J and Verga N, *J.of Nanomat. and Biostru.* 6, 2011, 969-978.

[7]. Eraldemir O, Sari B, Gok A, and Unal H B, *J. Macromol. Sci.Part A Pure Appl. Chem.* 45, 2008, 205-211.

International Journal of Advance Research in Science and Engineering
Volume No 06, Special Issue No. 03, September 2017, AFM-2017
www.ijarse.com
IJARSE
ISSN: 2319-8354

SYNTHESIS, CHARACTERIZATION AND PHOTOCATALYTIC ACTIVITY OF MgO NANOPARTICLES

Bhagya J[1,2], Dedhila Devadathan[1], Baiju V[1], Biju R[1], Raveendran R[1]

1 Nanoscience Research Laboratory, Department of Physics, Sree Narayana College, Kollam 691001, Kerala, India

2 Department of Physics, Sree Narayana College, Sivagiri, Sreenivasapuram P.O, Varkala Thiruvananthapuram 695145, Kerala, India

Abstract

In the present study, nanoparticles of MgO were synthesised through controlled co-precipitation method and microwave assisted fast synthesis method. In both methods MgO was synthesised in presence of citric acid and also in presence of polyvinyl alcohol (PVA). Structural characterizations of all the four synthesized samples were carried out using XRD. Comparison of XRD's of metal oxides with JCPDS confirmed that the formed metal oxide was MgO. Phase purity and crystallinity of these samples were confirmed from XRD. Crystallite sizes were calculated using Scherrer equation. Magnesium oxide nanoparticles showed visible range absorption in addition to UV range. From band gap calculation it was seen that all of them showed subgaps. The metal oxide reported in the present study showed very good photocatalytic activity. It was observed from the UV/Vis spectral analysis that the nanomaterial showed absorption in visible range in addition to UV light. Hence these materials could be used as photocatalyst in the degradation of organic dyes under solar ray irradiation.

Keywords: Nanoparticles, Photocatalysis, Photocatalyst

1. INTRODUCTION

Industrial waste water tainted with dyes is often discharged into natural water ways. Most of these dyes represent severe harms to the ecological system and the ejection of these colored wastes into natural water bodies may increase the toxicity and the chemical oxygen demand (COD). So it was necessary to find a new way to remove coloured dyes [1, 2] before discharging them into the environment. In the case of industrial dyes, the various conventional technologies do not work efficiently due to high solubility of dyes as well as their resistance to chemical and biological degradation; also they just transfer the contaminants from one phase to another [3]. Photocatalysis is a promising technology in the field of green technology for the removal of dyes. Presently nanotechnology is widely applied for purification and treatment of waste water. The novel properties of nanomaterials such as large surface area, potential for self assembly, high specificity, high reactivity and catalytic potential make them an excellent candidate for both applications [5]. In the present work magnesium oxide (MgO) nanoparticles is prepared in presence of capping agent, citric acid using co-precipitation method. The aim of the work is to study the variations in the properties

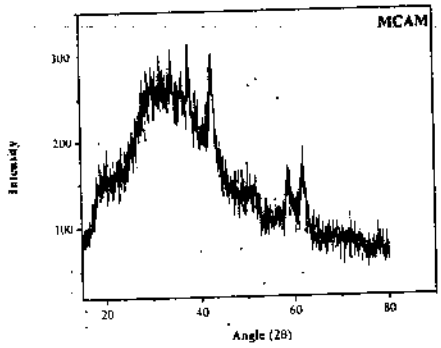

Fig.2 XRD of MCAM

Figure 1 shows the XRD of MCA. From the XRD itself it is clear that all the samples formed shows crystalline nature with sharp crystalline peaks. The broader diffraction peaks obtained indicated the smaller crystallite size. The interplanar spacing (d_{hkl} values), 2θ values and relative intensity values of magnesium oxide corresponding to the observed diffraction peaks were compared with the standard values of magnesium oxide as reported by JCPDS-International Centre for Diffraction Data.

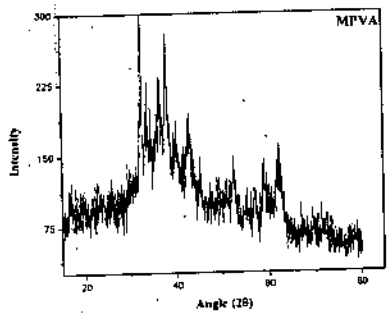

Fig. 3 XRD of MPVA

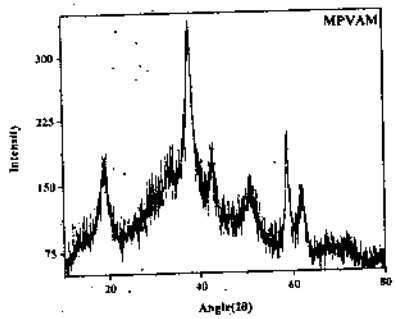

Fig.4 XRD of MPVAM

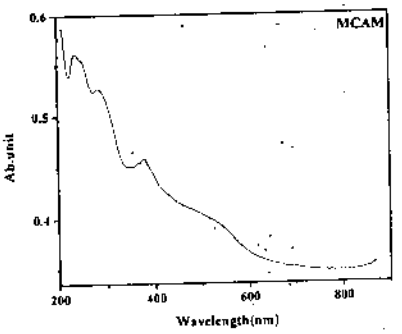

Fig.6 UV/Vis Absorbance spectrum of MCAM

The absorbance spectrum of all the four samples were studied and compared. In case of all the four samples of magnesium oxide, MCA, MCAM, MPVA and MPVAM showed a wide band of absorption in both UV and Visible range. In addition to the main peak a weak absorption peak was observed in UV region in case of all the four samples. Figure 5 shows the absorption spectrum of MCA. All the samples showed absorbance in both UV and visible region and also multiple peaks were obtained which shows the presence of subgaps.

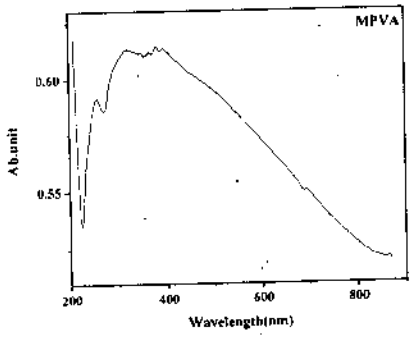

Fig.7 UV/Vis Absorbance spectrum of MPVA

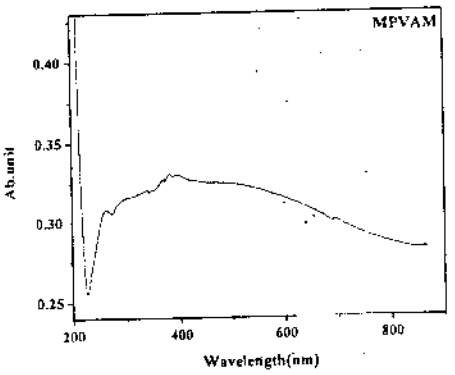

Fig.8 UV/Vis Absorbance spectrum of MPVAM

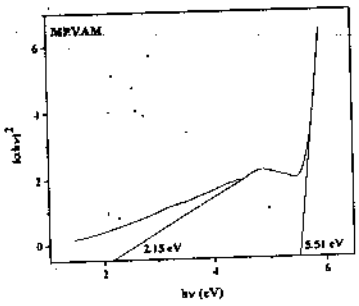

Fig.12 Tauc plot for MPVAM

3.3 Photocatalytic Studies

The photocatalytic activity of samples for the degradation of the dye; Congo red (CR) were studied using the respective photocatalyst (MCA, MCAM, MPVA, MPVAM) in the presence of UV illumination in a photoreactor. The experiments were performed by suspending the desired amount of photocatalyst into 300 ml of dye solution of desired concentration which was 75 ppm. The experiment was carried out isothermally at 300 K. The concentration of residual dye in the solution after irradiation for 4 hrs was determined by monitoring the absorbance intensity of solution samples at their maximum absorbance wavelength by using UV-Vis spectrophotometer (JASCO V 650 UV/Vis spectrophotometer). To study the effect of contact time on the photodegradation of organic dyes, the following procedure was adopted. To the respective dye solution of concentration, 75 ppm in 300 ml solution kept at 300 K, 0.1 g of the photocatalyst was added and was kept under UV light. After desired time intervals [60, 90, 120, etc], 10 mL of the solution was taken out, centrifuged and UV/Vis absorption spectra was recorded. Figure 13 shows the results obtained for the photodegradation studies of Congo Red done for seven different time intervals, using MCA as photocatalyst. Comparatively MCAM showed enhanced activity. MCA and MPVA showed similar photodegradation activity. Among the four samples MPVAM showed lower level of activity. The activity for four hours was studied. Further increase in time can completely degrade Congo Red completely.

them showed subgaps. The metal oxide reported in the present study showed very good photocatalytic activity. It was observed from the UV/Vis spectral analysis that the nanomaterial showed absorption in visible range in addition to UV light. Hence these materials could be used as photocatalyst in the degradation of organic dyes under solar ray irradiation.

5. REFERENCES

[1]. C. I. Pearce, J. R. Lloyd, and J. T. Guthrie, *Dyes and Pigments*, 58, 2003, 179–196.

[2]. T. Robinson, G. McMullan, R. Marchant, and P. Nigam, *Bioresource Technology*, 77, 2001, 247–255.

[3]. L. Mun, Degradation of dyes using zinc oxide as the photocatalyst, *M.S. thesis*, Putra University, Serdang, Malaysia, 2008.

[4]. S. Zhang et.al., *Journal of Alloys and Compounds*, 426, 2006, 281-285.

[5]. Neamtu J and Verga N, *J.of Nanomat. and Biostru.* 6, 2011, 969-978.

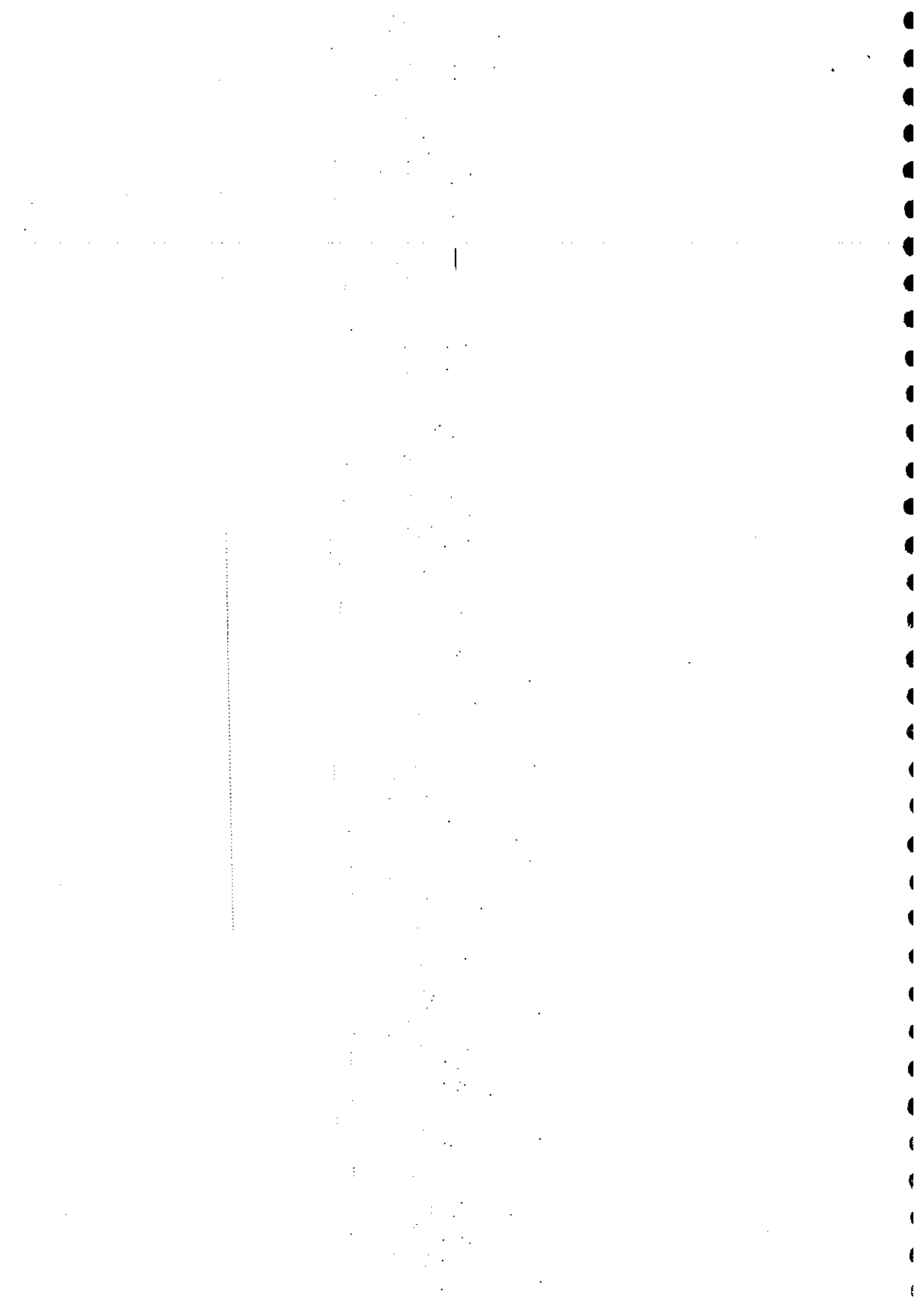

International Journal of Advance Research in Science and Engineering
Volume No 06, Special Issue No. 03, September 2017, AFM-2017
www.ijarse.com
IJARSE
ISSN: 2319-8354

SYNTHESIS, CHARACTERIZATION AND ANTIBACTERIAL ACTIVITY OF NiO NANOPARTICLES

Dhanuja B. S[1,2], Dedhila Devadathan[1], Baiju V[1], Biju R[1], Raveendran R[1]

[1]*Nanoscience Research Laboratory, Department of Physics, Sree Narayana College, Kollam, Kerala, (India)*

[2]*Department of Physics, Sree Narayana College, Sivagiri, Sreenivasapuram P.O, Varkala Thiruvananthapuram , Kerala, (India)*

Abstract

In the present study, nanoparticles of NiO were synthesised through controlled co-precipitation method and microwave assisted fast synthesis method. In both methods NiO was synthesised in presence of citric acid and also in presence of polyvinyl alcohol (PVA). Structural characterizations of all the four synthesized samples were carried out using XRD. Comparison of XRD's of metal oxides with JCPDS confirmed that the formed metal oxide was NiO. Phase purity and crystallinity of these samples were confirmed from XRD. Crystallite sizes were calculated using Scherrer equation. Nickel oxide nanoparticles showed visible range absorption in addition to UV range. From band gap calculation it was seen that all of them showed subgaps. The present study investigates the antimicrobial activity of the synthesized samples as antibacterial agents. The gram positive bacteria: Staphylococcus aureus and the gram negative bacteria: Escherichia coli are the microbes used in the present study. The study confirms that the nickel oxide samples prepared in the present study can be used as antibacterial agent against Escherichia coli. The results suggest that proper tuning can make them good antimicrobial agent.

Keywords: Nanoparticles, Antibacterial Agents

i.INTRODUCTION

Among transition metal oxides, nickel oxide (NiO) bulk and nano size have received considerable attention due to their wide range of applications in different fields [1-3]. Because of the quantum size and surface effects, NiO nanoparticles exhibit catalytic, optical, electronic, and magnetic properties that are significantly different than those of bulk-sized NiO particles [4, 5]. The novel properties of nanomaterials such as large surface area, potential for self assembly, high specificity, high reactivity and catalytic potential make them an excellent candidate for various applications [6]. In the present work nickel oxide (NiO) nanoparticles is prepared in presence of capping

agent, citric acid using co-precipitation method. The aim of the work is to study the variations in the properties obtained when NiO is prepared using microwave assisted fast synthesis method. Also when NiO was prepared in presence of polyvinyl alcohol instead of citric acid using co-precipitation method and microwave assisted fast synthesis method. The NiO nanoparticles synthesized is characterized using X-ray Diffraction Spectroscopy (XRD). The optical studies of the prepared samples are done using UV/Vis spectroscopy. In the present work there is a pressing demand to develop new antimicrobial agents and discover novel strategies due to the emerging infectious diseases and the development of drug resistance in the pathogenic bacteria and fungi. The present study investigates the antimicrobial activity of the synthesized samples as antibacterial agents. The results of all the four samples are compared.

2 EXPERIMENTAL

AR grade chemicals obtained from Merck were used for the preparation of NiO nanoparticles. NiO was prepared in presence of citric acid by the co-precipitation (NCA) and microwave method (NCAM) and in presence of polyvinyl alcohol (PVA) NPVA and NPVAM. The samples annealed at 500^0c were used for analysis. XRD study was carried out using XPERT-PRO model powder diffractometer (PAN analytical, Netherlands) employing Cu-K_α radiation (λ = 1.54060A°) operating at 40kV, 30mA. The UV/Vis spectrum was obtained using JASCO V-650 UV visible spectrophotometer.

3 RESULTS AND DISCUSSIONS

3.1 XRD Analysis

Figure 1 shows the XRD of NCA. From the XRD itself it is clear that all the samples formed shows crystalline nature with sharp crystalline peaks. The broader diffraction peaks obtained indicated the smaller crystallite size. In order to confirm the phase purity of the samples prepared, the interplanar spacing ($d_{h,l}$ values), 2θ values and relative intensity values of nickel oxide corresponding to the observed diffraction peaks were compared with the standard values of nickel oxide as reported by JCPDS-International Centre for Diffraction Data. From the comparison of diffraction peaks NF and NS with JCPDS-ICDD pattern number #78-0423 it is clear that NiO formed was a cubic system with FCC lattice. The well defined X-ray diffraction peaks in the case of all samples indicate that NiO formed are crystalline in nature. Also, the diffraction peaks are notably broadened indicating the smaller crystallite size.

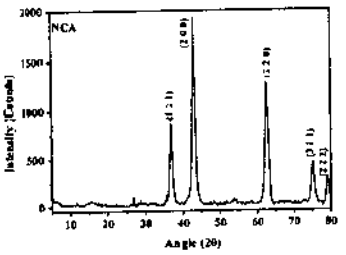

Fig.1 XRD of NCA

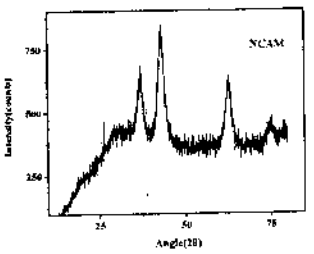

Fig.2 XRD of NCAM

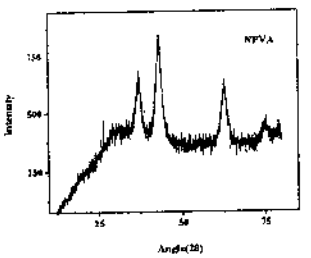

Fig.3 XRD of NPVA

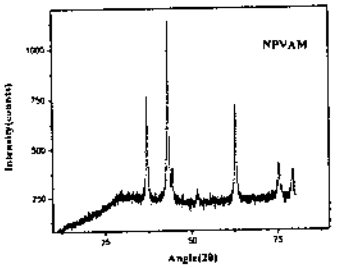

Fig.4 XRD of NPVAM

For NPVA, NCAM and NPVAM the diffraction peaks in addition to the 2θ values seen in NCA additional peaks were found. The presence of unremoved PVA might have created these impurity peaks. Annealing the samples at higher degrees can remove PVA completely and can give pure crystalline peaks. Using curve fitting the full width at half maximum of the major peaks was found and from this the crystallite size of all the samples were found. The result obtained NCA was 10.84 nm For NCAM 18.49 nm, NPVA 30.86 nm and NPVAM 17.81 nm respectively.

3.2 UV/Vis Spectrum Analysis

The absorbance spectrum of all the four samples were studied and compared. It is reported in literature that optical energy band gap of NiO lies in the range (3.6–4.0 eV) and is attributed to charge-transfer transition between the valence bands of O (p) states to conduction bands of Ni d (e_{2g}) states. Figure 5 shows the absorption spectrum of NCA. All the samples showed absorbance in both UV and visible region. The multiple peaks obtained which shows the presence of subgaps.

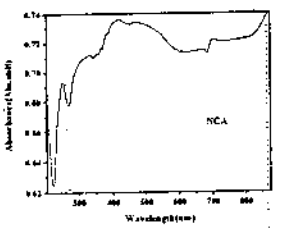

Fig.5 UV Absorbance spectrum of NCA

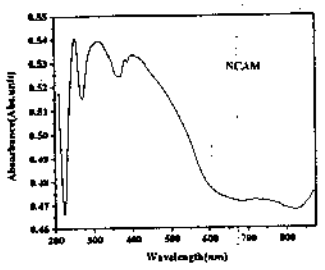

Fig.6 UV Absorbance of spectrum NCAM

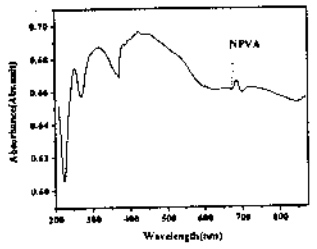

Fig. 7 UV Absorbance of spectrum NPVA

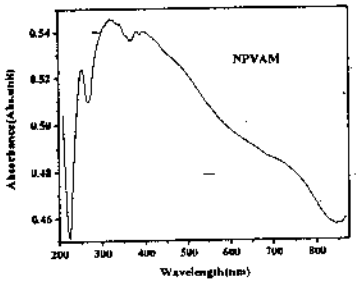

Fig. 8 UV Absorbance spectrum of NPVAM

From absorbance spectrum, Tauc plot was drawn and the corresponding energy gap was found. The energy band gap of the material is related to the absorption coefficient α by the Tauc relation, $\alpha = A (h\nu - E_g)^n$, where A is a constant, hν is the photon energy ($\nu = c/\lambda$), E_g is the band gap and n is either 2 for an indirect transition or ½ for a direct transition. The $(\alpha h\nu)^2$ vs hν for all the samples were also plotted. Figure 9 shows Tauc plots drawn for NCA. Similar results were obtained for other three samples.

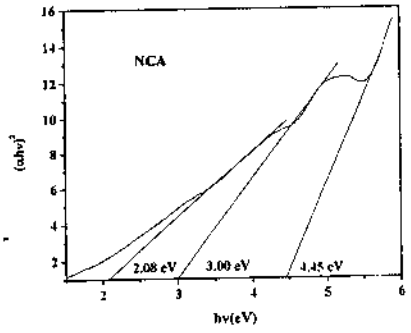

Fig.9 Tauc plot for NCA

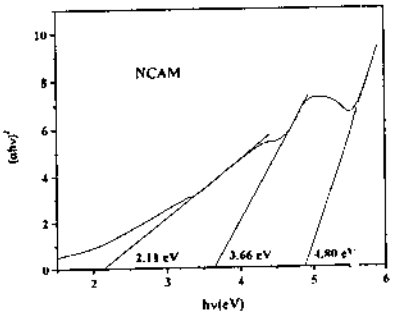

Fig.10 Tauc plot for NCAM

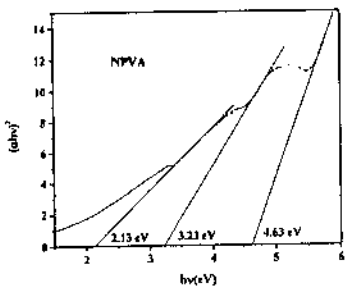

Fig.11 Tauc plot for NPVA

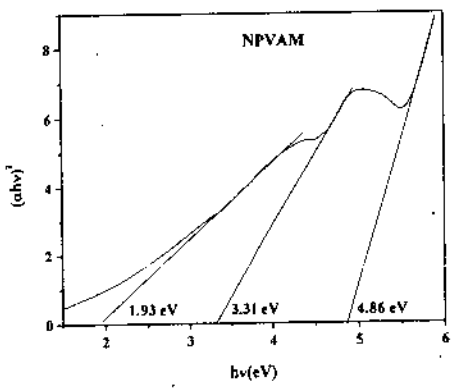

Fig.12 Tauc plot for NPVAM

3.3 Antibacterial Studies

The antibacterial activities of all the four samples were studied in detail. The antimicrobial activity of the nanoparticles is generally known to be a function of the surface area which is in contact with the microorganisms. Reactions take place at the surface of a chemical or material. Hence, the smaller size and the higher surface to volume ratio i.e., larger surface area, enhanced interaction with the microbes is seen. Figure 13 shows the comparison of antibacterial activity of NCA, NCAM, NPVA and NPVAM. Antimicrobial effects of NiO nanoparticles can be attributed to several mechanisms:

1. Induction of oxidative stress due to ROS (reactive oxygen species) generation,
2. Membrane disorganization due to accumulation of nanoparticles in the bacterial membrane and also their cellular internalization,
3. Release of metal ions that may be responsible for antimicrobial activity by binding to the membrane of microorganisms.

The antibacterial mechanism can also be attributed to the destruction of the outer membrane of bacteria by the generated superoxide anion radicals ($\bullet O^{2-}$) as the reactive species. The reactive species such as •OH and $\bullet O^{2-}$ are generated at the catalyst's surface, hence the high surface area is very beneficial for degradation of bacteria. The activity was found to be highest in case of gram negative bacteria. All the four samples showed no activity for S.aureus. The variation in the sensitivity or resistance to both gram positive and gram

negative bacteria populations could be due to the differences in the cell structure, physiology, metabolism or degree of contact of organisms with nanoparticles.

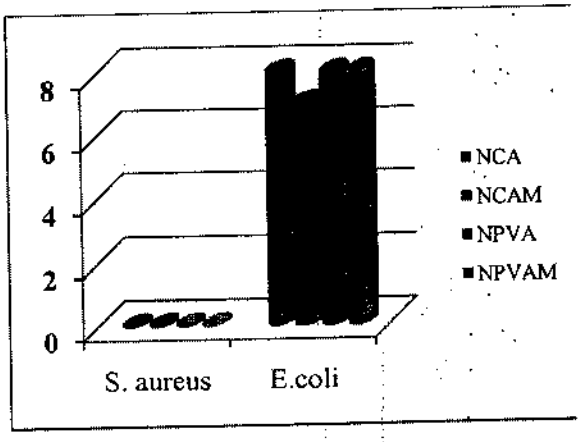

Fig.13 Comparison of Antibacterial activity of NCA, NCAM, NPVA and NPVAM

4 CONCLUSIONS

Comparison of XRD's of metal oxides with JCPDS confirmed that the formed metal oxide was NiO. Crystallite sizes were calculated using Scherrer equation. All the four samples prepared in this work showed strong UV as well as visible absorption. Hence all these materials could be suitable for anti UV applications. Also these materials could be a good candidate as photocatalyst for photocatalysis in presence of UV, as antibacterial agents, etc. From band gap calculation it was seen that all of them showed subgaps. The antibacterial activity was found to be highest in case of gram negative bacteria. All the four samples showed no activity for S.aureus. Nickel oxide samples prepared in present study showed comparable activity towards E.coli. The results suggest that proper tuning can make them good antimicrobial agent.

5. REFERENCES

[1]. N. M. Deraz, M. M. Selim, M. Ramadan, Mater. Chem. Phys. 2009, 113, 269–275.

[2]. I. Hotovy, J. Huran, L. Spiess, S. Hascik, V. Rehacek,Sens. Actuators B Chem. 1999, 57, 147–152.

[3]. W. Y. Li, L. N. Xu, J. Chen, Adv. Funct. Mater. 2005, 15, 851–857.

[4]. M. Meyer, A. M. Albrecht-Gary, C. O. Dietrich-Buchecker, J. P. Sauvage, J. Am. Chem. Soc. 1997, 119, 4599–4607.

[5]. G. Li, D. H. Shi, H. L. Zhu, H. Yan, S. W. Ng, Inorg. Chim. Acta 2007, 360, 2881–2889.

[6]. S. Zhang et.al., *Journal of Alloys and Compounds*, 426, 2006, 281-285.

International Journal of Advance Research in Science and Engineering
Volume No 06, Special Issue No. 03, September 2017, AFM-2017
www.ijarse.com
IJARSE
ISSN: 2319-8354

PHOTOCATALYTIC DEGRADATION OF AZO DYE CONGO RED USING COPPER OXIDE/NICKEL OXIDE NANOCOMPOSITE

Joyal Mary[1,2], Dedhila Devadathan[1], Baiju V[1], Biju R[1], Raveendran R[1]

1 Nanoscience Research Laboratory, Department of Physics, Sree Narayana College, Kollam, Kerala, (India)

2 Department of Physics, Sacred Heart College, Thevara, Ernakulam, Kerala,(India)

Abstract

Nanocomposite of CuO/NiO was prepared using controlled co-precipitation method. The synthesized materials were characterized using XRD. UV/Vis absorption spectroscopy of the synthesized samples was studied. The Photocatalytic activity of the nanocomposite for the photodegradation of Congo red was studied at different pH values, different illumination time and at different amount of catalyst loading.

Keywords: Nanocomposite, Co-precipitation, Photocatalytic activity, Photocatalyst.

INTRODUCTION

Wastewater from textile industries poses a threat to the environment as large amount of chemically different dyes are used for various industrial applications. They also uses substantial amount of water in their processes to form highly colored effluent which generally has hazardous effect in our ecosystem due to the presence of organic chemicals. Water contamination becomes a serious issue due to the fact that 2% of dyes produced in these industries are discharged directly in aqueous effluent [1]. So it was necessary to find a new way to remove colored dyes before discharging them into the environment [2, 3]. The various conventional technologies currently employed in the removal of colored effluents in industrial water are classical and do not lead to complete destruction of the dyes. These methods do not work efficiently due to high solubility of dyes as well as their resistance to chemical and biological degradation; also they just transfer the contaminants from one phase to another [4]. Therefore, there is a need to develop a novel treatment method that is more effective. In recent years, photocatalytic reaction has attracted extensive interests as a potential way to treat wastewater. The aim of the present work is to study the factors effecting on photocatalytic oxidation process of Congo red using CuO/NiO nanocomposite and to find out the optimal conditions used in photocatalytic process.

II. EXPERIMENTAL

AR grade chemicals obtained from Merck were used for the preparation of CuO/NiO heterojunction. CuO/NiO (CNF) were prepared by the co-precipitation method in presence of capping agent. CNF annealed at 500^0c for three hours, was used for analysis.

XRD studies were carried out using XPERT-PRO model powder diffractometer (PAN analytical, Netherlands) employing Cu- K_α radiation (λ = 1.54060A°) operating at 40kV, 30mA.The UV/Vis spectrum was obtained using JASCO V-650 UV visible spectrophotometer.

III. RESULTS AND DISCUSSIONS

3.1 XRD Analysis

X-ray diffractograms of CNF is shown in Figure 1. In order to confirm the phase purity of the samples prepared, the interplanar spacing (d_{hkl} values), 2θ values and relative intensity values corresponding to the observed diffraction peaks were compared with the standard values of CNF the observed diffraction peaks were compared with the standard values of CuO and NiO as reported by JCPDS-International Centre for Diffraction Data. The data obtained for CuO/NiO matched with JCPDS-ICDD pattern number #78-0423 of NiO and JCPDS-ICDD pattern number #80-1917 of CuO separately. The variation observed in the d values of the crystal planes in case of CNF when compared to NiO and CuO, confirms the formation of composites. The average crystallite size was calculated from the line broadening of the XRD pattern, making use of Scherrer formula. Average Crystallite size of CNF is 16.29 nm.

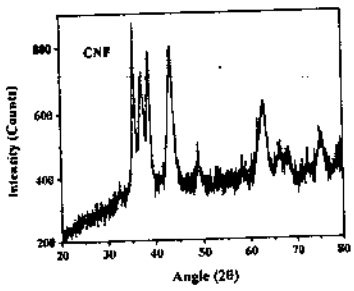

Fig.1 XRD of CNF

3.2 UV/Vis Spectrum Analysis

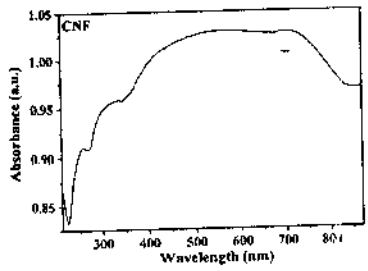

Fig.2 UV Absorbance spectrum of CNF

The UV/Vis absorption of CNF taken in the wavelength range 210 to 870 nm with 1 nm resolution is shown in the Figure 2. A wide range of absorption in UV and visible range was observed. Absorbance spectrum shows the presence of multiple peaks which confirms the presence of subgaps.

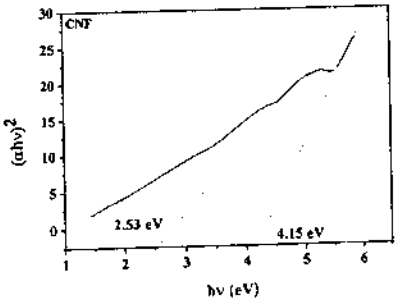

Fig.3 Tauc plot for CNF

From absorbance spectrum, Tauc plot was drawn and the corresponding energy gap was found. $(\alpha h\nu)^2$ vs hν was also plotted. The optical band gap determined from the absorption spectra using Tauc's relation for CNF is shown in Figure 3.

3.3 Photocatalytic Studies

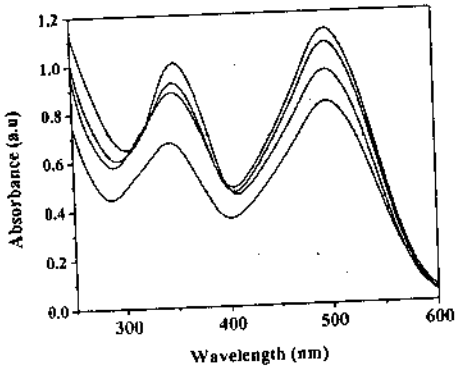

Fig.4 Absorbance spectrum showing photocatalytic degradation of Congo Red

A set of Photocatalytic degradation of Congo red was carried out to measure the photocatalytic activity of CuO/NiO Photocatalyst. A black light blue flourescent bulb was positioned at the axis to supply UV illumination. The experiments were performed by suspending photocatalyst into reactor with Congo red dye solution. The reaction was carried out isothermally at 30°C. The concentration of residual Congo red in the solution after irradiation was determined by monitoring the absorbance intensity of solution samples at their maximum absorbance wavelength by using UV-Vis spectrophotometer which was recorded on a JASCO V 650 with a spectrometric quartz cuvette at room temperature.

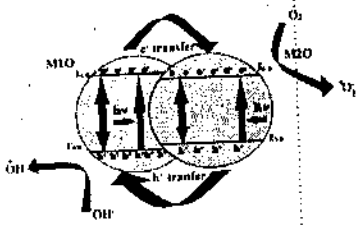

Fig.5 Mechanism suggested in the case of Photocatalytic degradation process using M1O/M2O (CuO/NiO)

The variations in different experimental conditions affecting on Photocatalytic oxidation of Congo red using catalyst CuO/NiO such as, pH value, illumination time and amount of catalyst loaded were taken into account to reach to integrated model for the photocatalytic degradation of Congo red. Generally, the effect of pH on organic degradation assisted by the semiconductor oxides has been related to the establishment of acid-base equilibrium governing the surface chemistry of metal oxides in water. The role of the effect of pH on the photodegradation of Condo red over CuO/NiO catalyst is reported in the pH range of 2–9 using 0.1 gm of catalyst and 300mL of 50 ppm dye solution under UV light at 30°C for two hours. Maximum efficiency was obtained for pH 6. The effect of illumination time on photodegradation efficiency of Congo red was carried out by measuring the photodegradation efficiency at different periods of time using 0.1 gm of catalyst and 300mL of 50 ppm dye solution under UV light at 30°C. The results revealed

that the photocatalytic activity increases with increase of the illumination time and reaches maximum after 120 min illumination time. Such data reveals the relative high activity of the prepared catalysts which enables the complete degradation of the Congo red in such short illumination time and the catalyst has active sites for carrying out the reaction. The effect of catalyst loading dose on the photodegradation efficiency of Congo red was observed by taking different amounts of catalyst ranging from 0.05 to 0.15 gm into 300mL of 50 ppm dye solution under UV light at 30^0C for two hours. These results showed that increment of catalyst loading from 0.05 to 0.1 gm increased the photodegradation efficiency of Congo red from 85 to 96% and after that the further increase in catalyst loading dose above 0.125 gm does not affect on the photodegradation efficiency. This is attributed to the increase in the catalyst loading dose which increased the number of active sites available on the catalyst surface for the reaction, which in turn increased the number of holes and hydroxyl radicals. Figure 3 shows the UV spectrum analysis for different time intervals done for the photodegradation of Congo red for time variation with 0.1 g 300mL of 50 ppm dye solution under UV light at 30^0C for two hours.

4 CONCLUSIONS

Nanocomposite of CuO/NiO was prepared through controlled co-precipitation method in presence of capping agent. Results show that CuO/NiO is a good Photocatalyst for degradation of Congo red.

5. REFERENCES

[1]. M. A. Rauf, I. Shehadeh, A. Ahmed, and A. Al-Zamly, World Academy of Science: Engineering and Technology, **55** (2009)..

[2]. C. I. Pearce, J. R. Lloyd, and J. T. Guthrie, Dyes and Pigments, **58**, 179–196 (2003).

[3]. T. Robinson, G. McMullan, R. Marchant, and P. Nigam, Bioresource Technology, 77, 247–255 (2001).

[4]. L. Mun, M.S. thesis, Degradation of dyes using zinc oxide as the photocatalyst, Putra University, Serdang, Malaysia, (2008).

International Journal of Advance Research in Science and Engineering
Volume No 06, Special Issue No. 03, September 2017, AFM-2017
www.ijarse.com
IJARSE
ISSN: 2319-8354

STRUCTURAL, OPTICAL STUDIES OF ZINC MAGNESIUM OXIDE AND ZINC COPPER OXIDE NANOCOMPOSITES

C R Indulal[1], R Biju[2], Deepak Nand[3],R Raveendran[4]

[1] *Department of Physics, S.G. College, Kottarakara, Kerala, India*

[2]*Nanoscience Research laboratory, S.N. College, Kollam, Kerala, India*

Abstract

Nanocomposites of Zinc Magnesium Oxide (ZnMgO) and Zinc Copper Oxide (ZnCuO) were synthesized by chemical co-precipitation method. The nanocomposites annealed at 500°C were used for further structural and optical studies. The Scherrer equation was used to calculate the average particle sizes of the prepared nanocomposites. The optical characterizations of the metal oxide nanocomposites were carried out by UV/Visible analysis. From the analysis of the absorption spectra, the optical bandgaps of the nanocomposites were calculated.

Keywords: Nanocomposite, XRD, Optical bandgap

1 INTRODUCTION

Metal oxide nano composites with large surface to volume ratio acquire unique magnetic, electronic, optical and chemical applications. Zinc oxide is a wide bandgap semiconducting material with a lot of applications including light emitting diodes, piezoelectric transducers, photocatalysts etc[1-3].

Nanomaterials exhibit large surface to volume ratio and thereby most of their properties are selectively controlled by engineering the size, morphology and composition. Such nano crystalline metal oxides exhibiting this large surface area can be applied to devices including sensors for which a betteAr surface effect is required. These new nanomaterials can have enhanced properties from their parent bulk materials[4]. The metal oxide nanocomposites exhibit exceptional UV absorbing ability, high stability at high temperatures and reactivity as catalyst[5-6].

2 EXPERIMENTAL

Nanocomposite of Zinc Magnesium Oxide (ZnMgO) was prepared by arrested precipitation using analytical grade 0.1M Zinc Nitrate, 0.1M Magnesium Nitrate, 0.02M citric acid and 0.5M sodium hydroxide as the reagents. However in the synthesis of Zinc Copper Oxide (ZnCuO), instead of Magnesium nitrate, 0.1 M copper nitrate was used. Among the reagents, citric acid was used as a stabilizer to prevent agglomeration. The precipitates so formed by stirring were separated from the reaction combination and washed with distilled water to remove all impurities. The dried precipitates at room temperature were thoroughly grounded using an agate mortar to obtain its fine powder. On heating to 500°C, their corresponding nanocomposites were formed.

2.1 CHARACTERIZATION

XRD analysis is a finger print tool for the structural analysis of nanocomposites. The XRD patterns of the powdered samples were recorded using XPERT-PRO powder diffractometer using Cu- K_α radiation in the 2θ range 10° to 80° at 30mA, 40kV. The UV spectra were recorded using Shimadzu UV-2550 UV visible spectrophoto meter.

3 RESULTS AND DISCUSSIONS

3.1 XRD STUDIES

The nano crystalline natures of ZnMgO and ZnCuO are verified using XRD analysis. There is a definite line broadening of the XRD peaks indicates the synthesized materials consist of particles in nanometer scale. The peak intensity, position and full width at half maximum data are obtained from the XRD pattern. The nanoparticle sizes are calculated using Debye-Scherrer equation, $t = k\lambda/(\beta\cos\theta)$; where k is the Scherrer constant and its value is taken as 0.9; β is the full width at half maximum of XRD peaks, θ is the Bragg diffraction angle and λ is wavelength of X-rays used in XRD analysis, λ = 1.54060 [Å]. The XRD patterns of ZnMgO and ZnCuO sintered at 500°C are shown in fig 1A and 1B respectively. The average particle sizes for ZnMgO and ZnCuO nanocomposites are found to be 32 and 23nms respectively. The XRD peaks of ZnMgO and ZnCuO confirms that they are almost free from impurities.

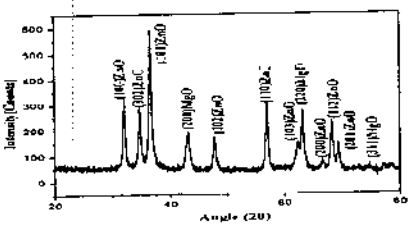

Fig. 1A XRD Patterns of ZnMgO

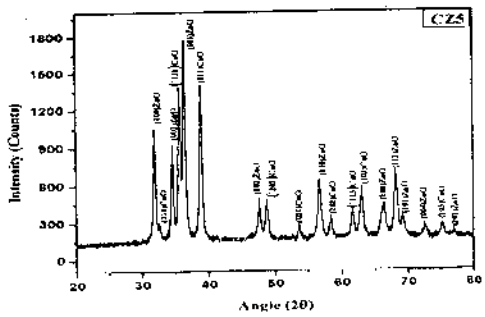

Fig. 1B *XRD Patterns of* ZnCuO

3.2 UV-SPECTRAL STUDIES

The UV spectra of ZnMgO and ZnCuO nanocomposites sintered at 500°C taken in the wavelength range of 210 to 870 nm are shown in fig 2A and 2B respectively. The optical bandgap details of the nanocomposites can be directly calculated using UV absorption spectra. The decrease in absorbance with increase in wavelength from the UV spectra is due to the presence of optical bandgap in the nanomaterials. Using Tauc's relation, the direct optical bandgaps of the nanomaterials are calculated[8]. The value of direct optical bandgaps of ZnMgO and ZnCuO nanocomposites are 3.29eV and 3.95eV respectively and are depicted in the figures 3A and 3B respectively.

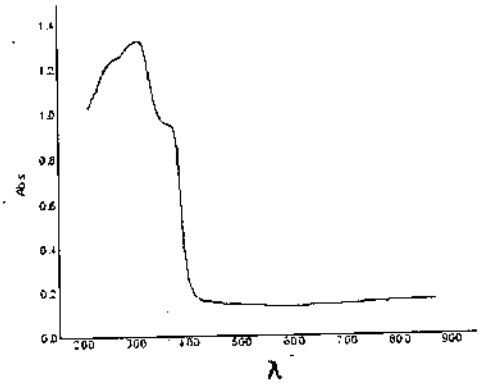

Fig. 2A UV spectrum of ZnMgO

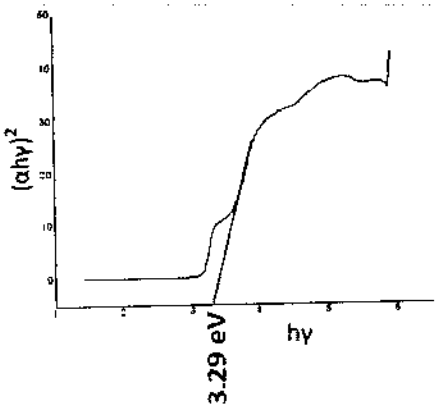

Figure 3A: Optical bandgap calculation of ZnMgO

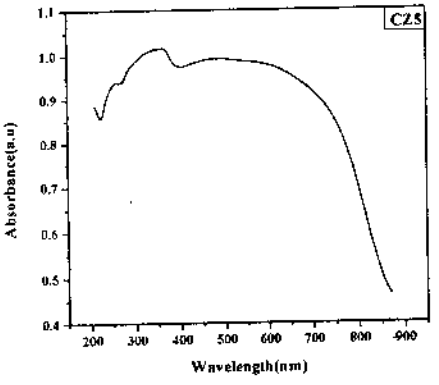

Fig. 2B UV spectrum of ZnCuO

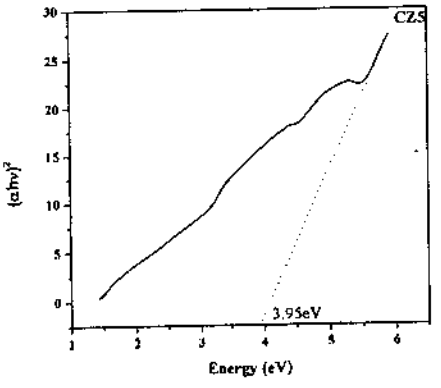

Fig. 3B Optical bandgap calculation of ZnCuO

4 CONCLUSIONS

Nanocomposites of Zinc Magnesium Oxide and Zinc Copper Oxide are prepared by chemical co-precipitation method. Average particle sizes obtained from XRD studies are 32nm for Zinc Magnesium Oxide nanocomposite and 23nm for Zinc Copper Oxide nanocomposite and are in the nano meter scale. Value of direct optical bandgaps of Zinc Magnesium Oxide and Zinc Copper Oxide nanocomposites are is 3.29eV and 3.95eV respectively.

5. REFERENCES

[1] J. Bao; M. A. Zimmler, F. Capasso, *Nano Letters*, 6, 1719-1722, 2006,.

[2] X. D. Bai, P. X. Gao, Z. L. Wang, E. G. Wang, *Applied Physics Letters*, 82, 4806-4808, 2003,.

[3] H. F. Lin, S. C. Liao, S. W. Hung, *Journal of Photochemistry and Photobiology A*, 174, 82-87, 2005.

[4] Kenneth J. Klabunde; Cathymohs, Manhanttan Kansas second Edition, 1998.

[5] M. S. Tsai, *Mater. Sci. Eng. B*, 110, 132-134, 2004

[6] Mori, Y. R. Wang, Drennan; *J Solid State Ionics*, 175, 641-649, 2004,.

[7] B. D. Cullity, Elements of X-ray diffraction, Addison-wesley publishing company Inc.California, 1970, 102.

[8] D. Mohanta, S S Nath, N C Mishra, A Choudhury, *Bull. Mater. Sci.*, 26, 289-294, 2003.

(19)

ORIENTAL JOURNAL OF CHEMISTRY
An International Open Free Access, Peer Reviewed Research Journal
www.orientjchem.org
Est. 1904
ISSN: 0970-020 X
CODEN: OJCHEG
2017, Vol. 33, No. (3):
Pg. 1545-1549

Optical and Antibacterial Studies of Zinc Magnesium Oxide Nanocomposite

C R INDULAL[1*], R BIJU[2], DEEPAK NAND[2] and R.RAVEENDRAN[2]

[1]Department of Physics, S.G. College, Kottarakara, Kerala, India.
[2]Nanoscience Research laboratory, S.N. College, Kollam, Kerala, India.
*Correspnding author E-mail: itdrindulal@gmail.com

http://dx.doi.org/10.13005/ojc/330359

(Received: April 08, 2017; Accepted: May 11, 2017)

ABSTRACT

Through the microwave assisted fast synthesis method, Zinc Magnesium Oxide nanocomposite was prepared. Zinc Magnesium Oxide nanocomposite heated at 500ºC was used for further structural, optical and antibacterial studies. The Debye Scherrer equation was used to calculate the average particle size of the nanocomposite. The optical characterization of the oxide nanocomposite was carried out by UV analysis. From the analysis of the absorption spectra, the optical direct band gap of the Zinc Magnesium Oxide nanocomposite was calculated and the result was compared with Zinc Oxide and Magnesium Oxide nanocomposites. Antibacterial studies were done in detail.

Keywords: Nanocomposites, XRD, Optical band gap, Antibacterial studies

INTRODUCTION

Nanooxide materials with large surface to volume ratio acquire unique magnetic, electronic, optical, antibacterial properties and potential applications. In the early 1950s, scientists had already started the research on Zinc related materials as antibacterial agents[1]. In the areas related with textile industries, water disinfection, medicine, food packaging etc. these antibacterial agents have a major role. Instead of organic compounds, inorganic disinfectants like metal oxide nanocomposites have several advantages, including their non toxicity to the human body. Zinc oxide is a wide band gap semiconducting material with a lot of applications including light emitting diodes, piezoelectric transducers, photocatalysts etc[2-4].

Nanomaterials exhibit large surface to volume ratio and most of their properties are selectively controlled by engineering the size, morphology and composition. Such nano crystalline metal oxides exhibiting this large surface area can be applied to devices including sensors for which a better surface effect is required. These new nanomaterials can have enhanced properties from their parent bulk

materials[5]. The metal oxide nanocomposites exhibit exceptional UV absorbing ability, high stability at high temperatures and reactivity as catalyst[6-7].

Experimental procedure

Zinc Magnesium Oxide nanocomposite was prepared by microwave assisted fast synthesis method using analytical grade Magnesium Nitrate and Zinc Nitrate as the reagents. When compared with other methods, this method has revealed several advantages. It was already reported that molecules undergo excitations due to electromagnetic radiations. By converting microwave radiation into heat energy with high efficiency, superheating becomes possible at ambient pressure. Zinc Nitrate, Magnesium Nitrate and Sodium hydroxide were used as starting materials. Citric acid was used as stabilizer. Aqueous solutions of 0.1M Zinc Nitrate, 0.1 M Magnesium Nitrate and 0.5 M Sodium hydroxide were mixed drop wise and stirred simultaneously into a beaker containing aqueous solution of 0.02 M Citric acid. The process was carried out in few minutes. Then the beaker was kept in a microwave oven. The stabilizer is used to prevent growth/agglomeration of the particles.

CHARACTERIZATION

XRD studies are ideal for the of nanocomposites size determination of powder samples. The XRD patterns of the powdered samples were recorded using XPERT-PRO powder diffractometer using Cu- K_{α} radiation in the 2θ range 10° to 80° at 30 mA, 40 kV. Based on the line broadening, few techniques involving Scherrer equation, integral breadth analysis or Hall-Williamson approach and Fourier method of Warren-Averbach have been developed[8-10]. The UV spectrum were recorded using Shimadzu UV-2550 UV visible spectrophotometer. Antibacterial activity of the sample was carried out using diffusion disk method.

RESULTS AND DISCUSSIONS

XRD Studies

The nano crystalline nature of Zinc Magnesium Oxide is verified using XRD analysis. There is a definite line broadening of the XRD peaks which indicates the synthesized materials consist of particles in nanometer scale. The peak intensity, position and full width at half maximum data are obtained from the XRD pattern. The nanoparticle sizes are calculated using Debye-Scherrer formula, $d = 0.9\lambda/\beta\cos\theta$[11], where 0.9 is the Scherrer constant,

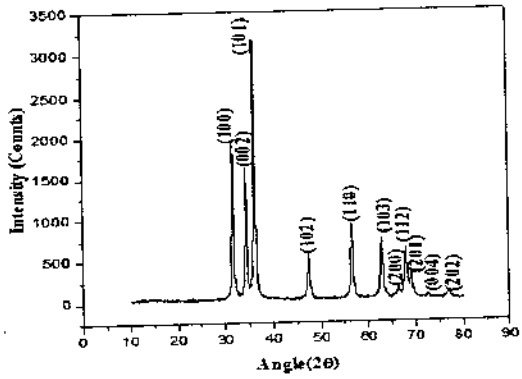

Fig. 1A: XRD Pattern of ZnO

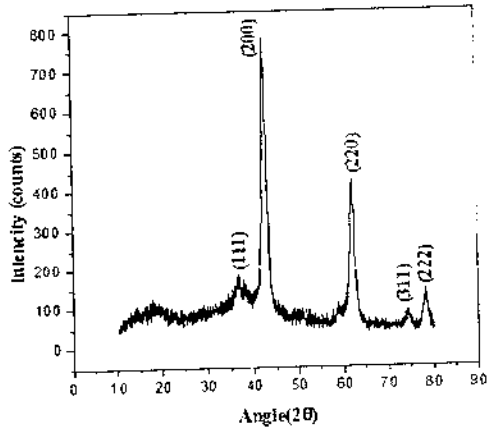

Fig. 1B: XRD Pattern of MgO

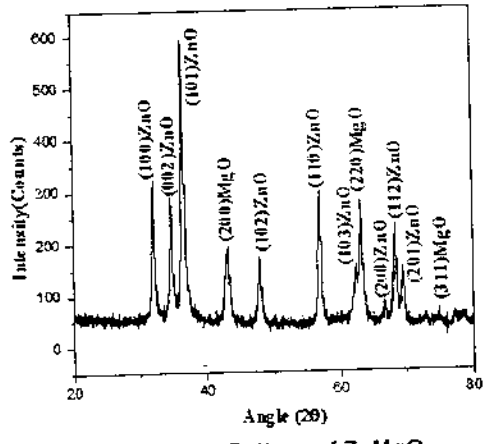

Fig. 1C: XRD Pattern of ZnMgO

β is the full width at half maximum of XRD lines, β is Bragg diffraction angle and wavelength of X-rays, λ= 1.54060 [Å]. The XRD pattern of Zinc Oxide (ZnO), Magnesium Oxide (MgO) and Zinc Magnesium Oxide (ZnMgO) heated at 500ºC are shown in fig 1A,

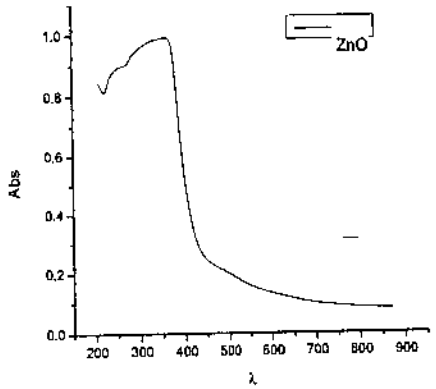

Fig. 2A: UV spectrum of ZnO

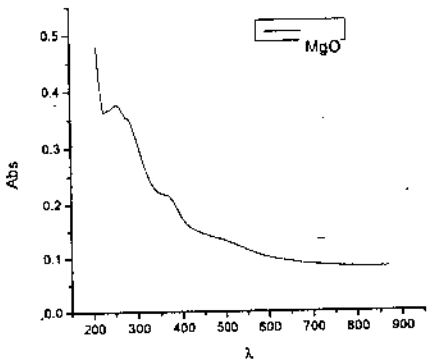

Fig. 2B: UV spectrum of MgO

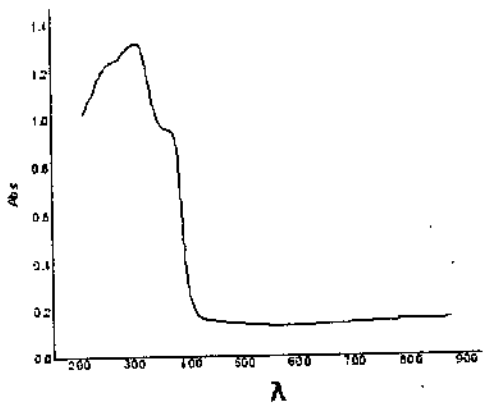

Fig. 2C: UV spectrum of ZnMgO

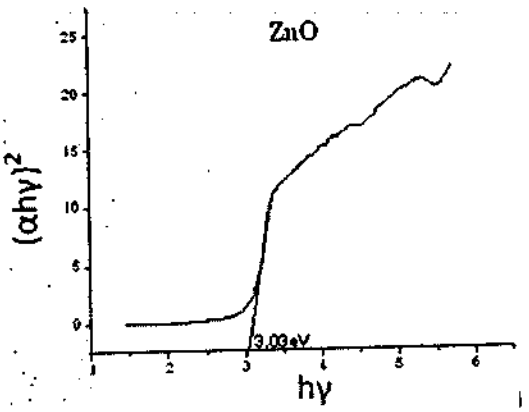

Fig. 3A: Optical bandgap calculation of ZnO

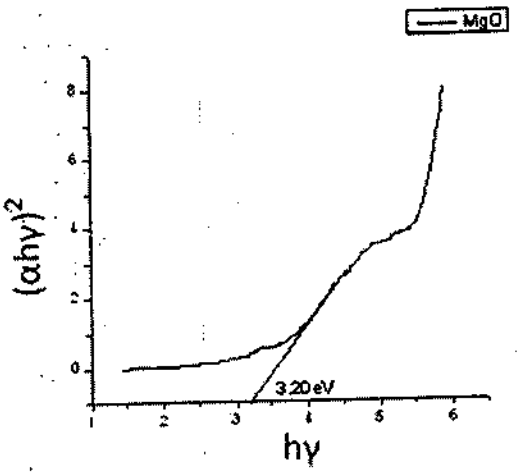

Fig. 3B: Optical bandgap calculation of MgO

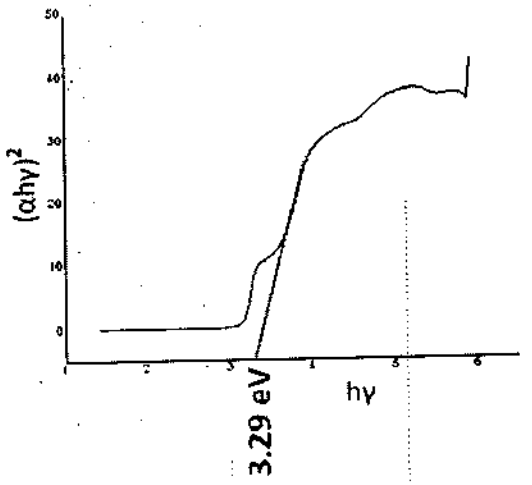

Fig. 3C: Optical bandgap calculation of ZnMgO

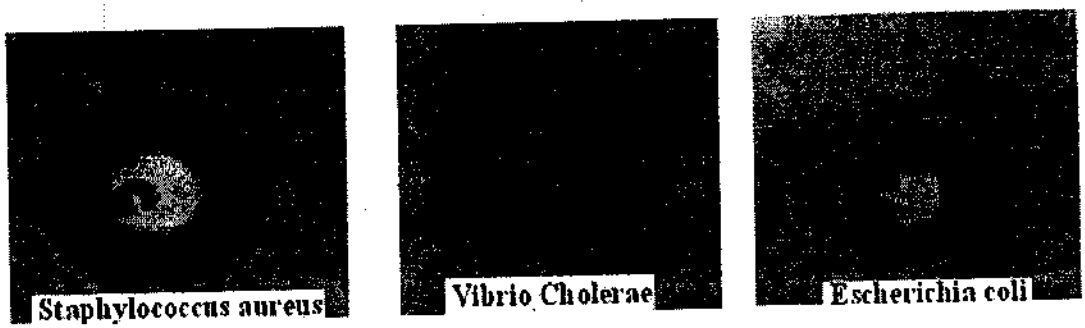

Fig. 4A: Antibacterial studies of ZnMgO

1B and 1C respectively. The average particle size for Zinc Oxide is 19nm, Magnesium Oxide is 7nm and Zinc Magnesium Oxide is 46nm. The micro straining of crystal structures due to various defects such as dislocations and twinning are the major reasons behind the broadening of the peaks in the XRD pattern. These defects are supposed to be linked with chemically synthesized nanocomposites. When the crystals suddenly grows during chemical reaction, the legands do not get enough time to diffuse to an energetically positive site resulting in crystal defects[12]. The XRD peaks of Zinc Oxide, Magnesium Oxide and Zinc Magnesium Oxide confirms that they are almost free from impurities.

UV spectral studies

The UV spectra of Zinc Oxide, Magnesium Oxide and Zinc Magnesium Oxide heated at 500ºC taken in the wavelength range of 210 to 870 nm are shown in fig 2A, 2B and 2C respectively. The optical band gap details of the nanocomposites can be directly calculated using UV absorption spectra. The decrease in absorbance with increase in wavelength from the UV spectra is due to the presence of optical band gap in the nanomaterials. Using Tauc's relation, the optical direct band gap of the nanomaterials can be calculated[13]. The value of optical direct band gap of Zinc Oxide is 3.03 eV, Magnesium Oxide is 3.2 eV and Zinc Magnesium Oxide nano composite is 3.29 eV and are depicted in the figures 3A, 3B and 3C respectively. So compared to their single counter parts, the nano composites have a considerably large band gap value.

Antibacterial studies

In order to investigate the antibacterial ability of Zinc Magnesium Oxide nanocomposite, the diffusion disk method was employed. *Staphylococcus aureus, Vibrio Cholerae, Escherichia coli and Bacillus cereus* were selected as test strains[14]. The inhibition zone diameters of *Staphylococcus aureus, Vibrio Cholerae, Escherichia coli and Bacillus cereus* found to be 14, 20, 15 and 0 mm respectively (Fig4A). Zinc Magnesium Oxide nanocomposite is found to be an efficient antibacterial agent towards Vibrio Cholerae. However it shows very poor activity towards Bacillus cereus.

CONCLUSIONS

Nanocomposite of Zinc Magnesium Oxide was prepared by microwave assisted fast synthesis method. Mean particle sizes obtained from XRD studies are 46 nm for Zinc Magnesium Oxide, 19 nm for Zinc Oxide and 7nm for magnesium oxide and are in the nano meter scale. Particle size of nanocomposite is greater than their single counter parts. The value of direct band gap of Zinc Magnesium Oxide nanocomposite is 3.29 eV which is greater than Zinc oxide or Magnesium oxide nanoparticles. It can be concluded that highly reactive metal oxide nanocomposites of Zinc Magnesium Oxide exhibit exceptional antibacterial activity against both gram-positive and gram-negative bacteria except Bacillus cereus.

REFERENCES

1. Bartels, H.A.; The effect of eugenol and oil of cloves on the growth of micro.overddot. organisms. *Am J Orthod Oral Surg.* 1947,*33*, 458-465.

2. Bao, J; Zimmler, M A; Capasso, F; Broadband ZnO single-nanowire light-emitting diode *Nano Letters.* **2006**, *6*, 1719-1722.
3. Bai, X. D.; Gao, P. X.; Wang, Z. L.; Wang, E. G.; Dual-mode mechanical resonance of individual ZnO nanobelts, *Applied Physics Letters.* **2003**, *82*, 4806-4808.
4. Lin, H. F.; Liao, S. C.; Hung, S. W.; The dc thermal plasma synthesis of ZnO nanocomposites for visible- light photocatalyst, *Journal of Photochemistry and Photobiology A.* **2005**, *174*, 82-87.
5. Kenneth J. Klabunde; Cathymohs, Department of Chemistry, Kansas state university, *Manhanttan Kansas second Edition*, **1998.**
6. Tsai, M. S.; *Mater. Sci. Eng. B* **2004**, *110*, 132-134.
7. Mori; Wang, Y. R.; Drennan; J *Solid State Ionics.* **2004**, *175*, 641-649.
8. Scherrer, P; *Math. Phys. K.* **1918**, 1, 187-188.
9. Williamson, G. K.; Hall, W. H.; Acta Metall. **1953**, *1*, 22-31.
10. Warren, B. E.; Averbach, B. L.; *J. Appl. Phys.* **1950**, *21*, 595-599.
11. Cullity, B. D.; *Elements of X-ray diffraction*, Addison - wesley publishing company Inc. California, **1970**, *102.*
12. Warad, H. C.; Ghosh, S C; Hemtanon; *Sci. Technol. Adv. Mater.* **2005**, *6*, 296-301.
13. Mohanta, D.; Nath, S. S.; Mishra, N. C.; Choudhury, A.; *Bull. Mater. Sci.* **2003**, *26*, 289- 294.
14. Shalumon, K. T.; *International Journal of Biological Macromolecules* **2011**, *49*, 247-254.

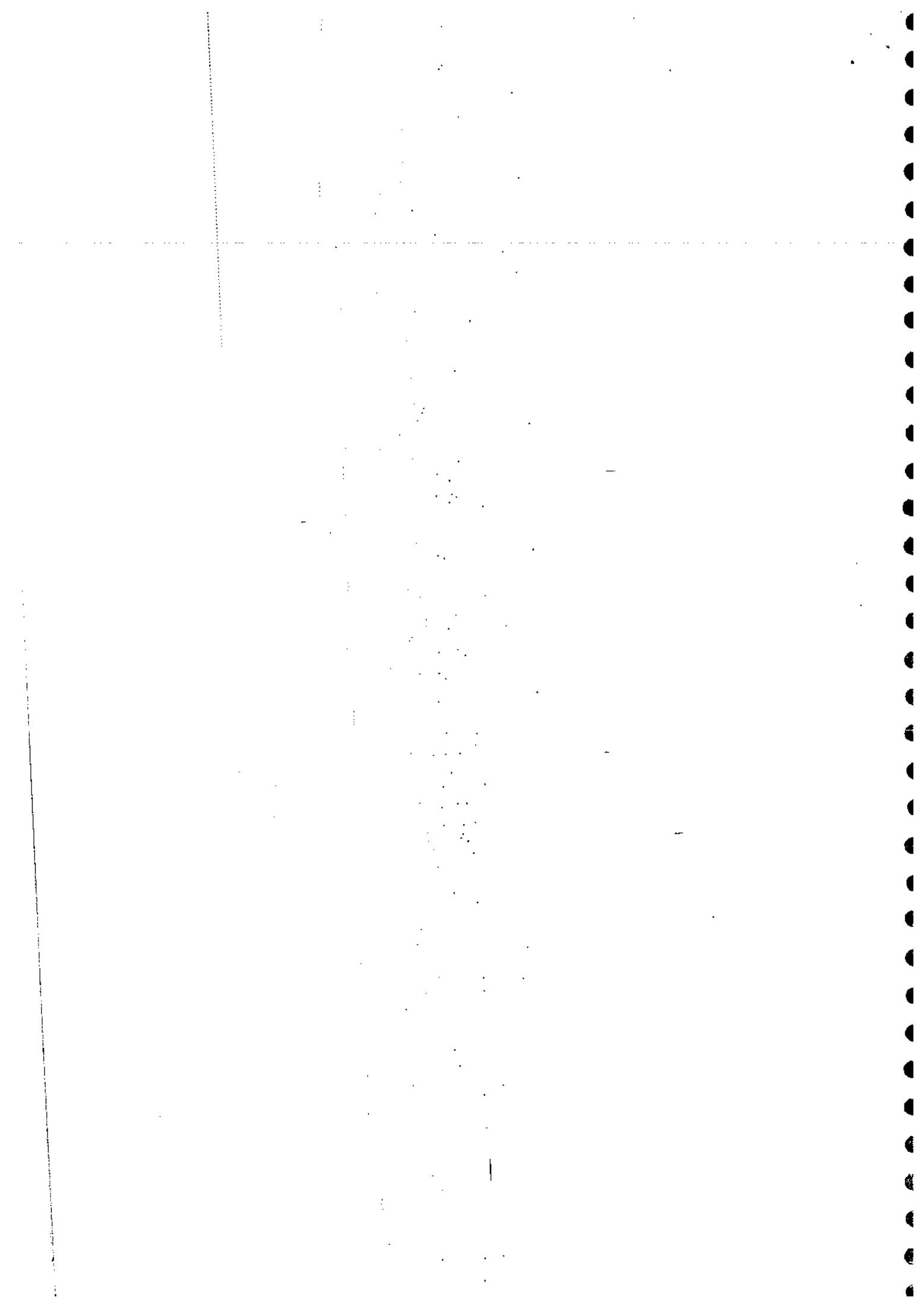

(15)

ORIENTAL JOURNAL OF CHEMISTRY
An International Open Free Access, Peer Reviewed Research Journal
www.orientjchem.org
Est. 1984
ISSN: 0970-020 X
CODEN: OJCHEG
2017, Vol. 33, No. (3):
Pg.1581-1588

Dielectric and Optical Band Gap Studies of Nanostructured Manganese Nickel Oxide and Cobalt Nickel Oxide

C R INDULAL[1*], R BIJU[2], DEEPAK NAND[2] and R RAVEENDRAN[2]

[1]Department of Physics, S.G. College, Kottarakara, Kerala, India.
[2]Nanoscience Research laboratory, S.N. College, Kollam, Kerala, India.
*Corresponding author E-mail: itdrindulal@gmail.com

http://dx.doi.org/10.13005/ojc/330365

(Received: April 08, 2017; Accepted: May 06, 2017)

ABSTRACT

Nano oxides of Manganese Nickel and Cobalt Nickel were synthesized by chemical co-precipitation method from the reaction of respective metal sulfides of manganese, nickel, cobalt and sodium carbonate using ethylene diamene tetra acetic acid as an effective capping agent. The carbonate precursors were heated at different temperatures so as to form their oxides. Through the X-ray line broadening technique, the mean particle sizes were calculated at different temperatures. The elastic micro strains versus particle size variations were thoroughly studied. The metal oxide formations of Manganese Nickel and Cobalt Nickel were confirmed with the help of FTIR spectra. EDX spectra of Manganese Nickel oxide and Cobalt Nickel oxide provide chemical composition of the samples. The crystallite shapes were studied using the scanning electron microscopy images. The optical direct band gap values of both Manganese Nickel and Cobalt Nickel oxides were calculated using Tauc's relation.

Keywords: Nanoparticles, SEM, EDX, Optical band gap, Dielectric properties

INTRODUCTION

Oxides of cobalt are stable and are available in abundance which are cheaper than other noble metals. In the recent past, oxide nanomaterials have been drawing wide attention due to their comparatively excellent electrical, optical[1-2] or magnetic[3] properties. Generally nanoparticles have large surface to volume ratio. So their properties such as electrical, optical, etc. can be tuned by engineering size, morphology or composition. Nano oxides of Manganese Nickel and Cobalt Nickel with large surface area can be used in gas sensors. These nano oxide systems may have entirely different properties compared to their parent bulk materials[4]. The ultra fine oxide nanoparticles exhibit unique UV absorbing ability, excellent stability at elevated temperatures, very high hardness and reactivity as catalyst[5-6]. Manganese-Nickel oxide and Cobalt-Nickel oxide systems can be considered as potential candidates for electrodes in batteries, in super capacitor, in sensors, switches etc.

MATERIALS AND METHODS

The nano particles of both Manganese-Nickel oxide (MnNiO) and Cobalt-Nickel oxide (CoNiO) were synthesized by arrested precipitation from AR grade 0.4 M cobalt sulphate, 0.4 M nickel sulphate, 0.4 M manganese sulphate and 0.6 M sodium carbonate using ethylene diamene tetra acetic acid as an effective capping agent. The carbonate precipitates so formed were separated from the reaction combination and were washed with distilled water and ethanol to remove all impurities. The dried precipitates at room temperature were thoroughly grounded using an agate mortar to obtain their metal carbonate precursor in the form of fine powder. On heating to sufficient temperatures (400, 600 and 800 ºC), these carbonate precursor decomposes to their corresponding metal oxides.

Characterization

XRD is one of the ideal techniques used for the determination of crystallite size of the nano powders. Based on the broadening of diffraction peaks, a few techniques involving Scherrer equation, Integral breadth analysis or Hall-Williamson approach and Fourier method of Warren-Averbach etc. were developed[7-9]. Warren and Averbach proposed the first theory related with the broadening of diffraction peaks. XRD studies were done on XPERT-PRO powder diffractometer with Cu- K_α radiation in the 2θ range 10° to 70° at 30mA, 40 kV. The surface morphological studies of the powder samples were evaluated by a scanning electron microscope. The energy dispersive analyses of X- rays were carried out on the nano samples to ascertain its precise composition. The ultra violet spectroscopic studies were carried out using Shimadzu UV-2550 UV visible spectrophotometer.

RESULTS AND DISCUSSION

XRD Studies

The nano crystallanity of the powder samples are verified using XRD analysis. The nano particle sizes are calculated using Debye-Scherrer equation, $d = 0.9\lambda/\beta\cos\theta$[10], where β represents the full width at half maximum of XRD lines, λ = 1.54060 [Å]. Figure 1A and 1B represents the XRD patterns of MnNiO and CoNiO sintered at 600 ºC. The most intense peaks are obtained from the (311) planes. The crystallite sizes of MnNiO and CoNiO at 400, 600 and 800 ºC using Debye-Scherrer equation are as recorded in Table 1A and 1B respectively. On analyzing the table, it is confirmed that when the temperature increases, the particle size also increases. So temperature of the reaction can be considered as one of the prime parameters on the crystallites size[11]. The reason for increasing

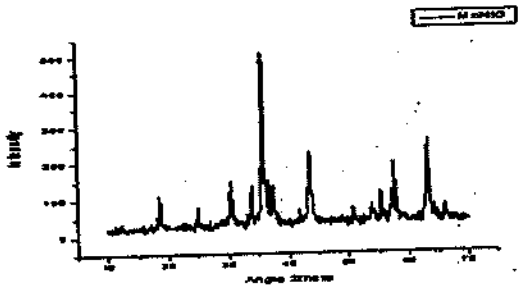

Fig. 1A: XRD pattern of MnNiO sintered at 600ºC

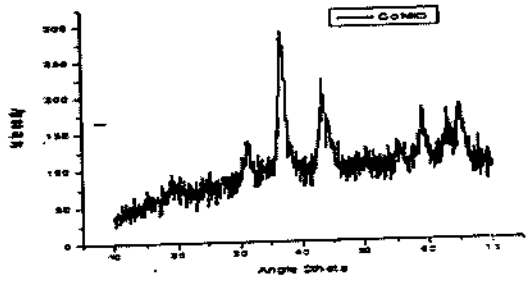

Fig. 1B: XRD pattern of CoNiO sintered at 600ºC

Table 1A

Sintering temp ºC	Particle size (nm)	Elastic strains	Band gap (eV)
400	8	0.002620	1.44
600	17	0.001313	1.41
800	41	0.000562	1.37

Table 1B

Sintering temp ºC	Grain size (nm)	Elastic strains	Band gap (eV)
400	6	0.003820	1.43
600	20	0.001159	1.39
800	42	0.000689	1.33

particle size with increase in sintering temperature is either due to the Ostwald ripening or oriented attachment. Ostwald ripening happens mainly because, larger particles are energetically more stable than smaller ones and it is also due to the effect of potential energy difference between larger and smaller particles which may happens through solid state diffusion. The crystallographic phases

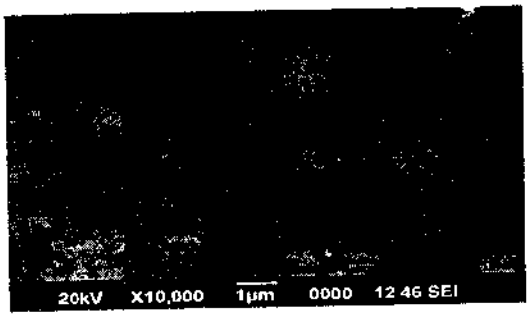

Fig. 2A: SEM image of MnNiO

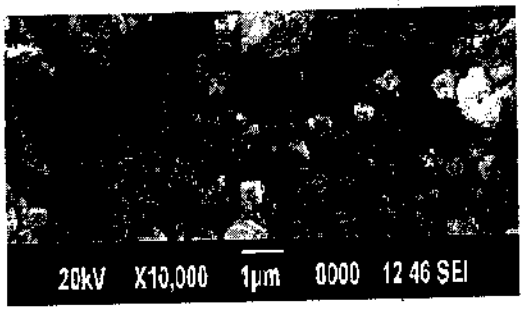

Fig. 2B: SEM image of CoNiO

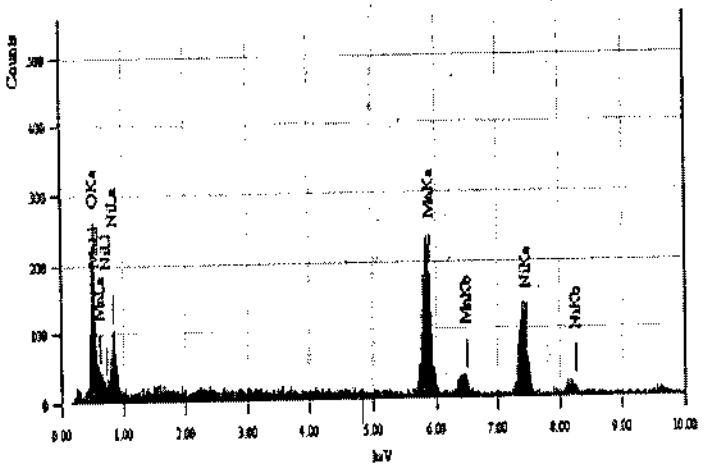

Fig. 3A: EDX spectrum of MnNiO

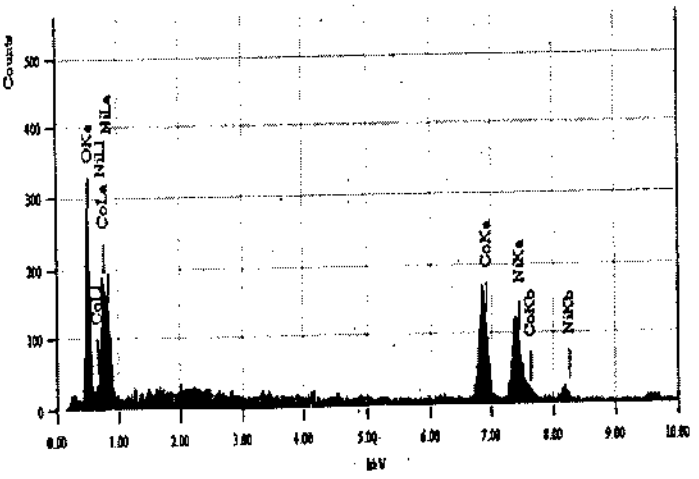

Fig. 3B: EDX spectrum of CoNiO

and cubic structure of the synthesized nano particles are confirmed by comparing it with JCPDS files (File No 01-1110 and 20-0781). The basic reason for the broadening of the peaks in the XRD pattern is micro straining of the crystal structures which are arising from the various defects like dislocations/ twinning. They are supposed to be connected with chemically synthesized nanoparticles. At the time of crystals growth, the ligand may get only negligible time to diffuse to an energetically positive site which results in crystal defects[12].

The elastic strain of MnNiO and CoNiO are found out using the values of full width at half maximum of XRD lines[13]. From the table 1A and 1B, it is confirmed that, as the nano particle size increases elastic strain decreases. This strain is one of the major reasons behind the broadening of the XRD peak of the nanomaterials.

Microstructural studies

For the surface morphological studies, the nano powders heated at 600 °C were transferred in to the SEM chamber. SEM images along with EDX of both MnNiO and CoNiO nanoparticles are shown in the Fig. 2A, 2B, 3A and 3B respectively. The nanoparticles are found to be almost spherica with some agglomerations.

FTIR Studies

The FTIR spectra of both MnNiO and CoNiO are shown in Fig. 4A and 4B respectively. The absorption bands found in the regions 3420 cm^{-1} for MnNiO and 3430 cm^{-1} for CoNiO are

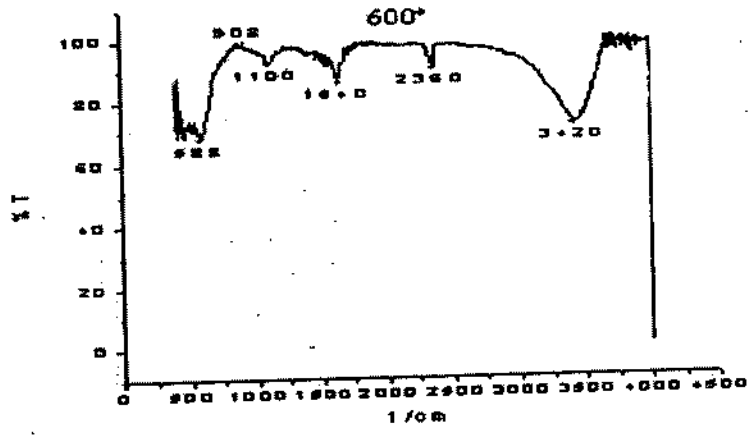

Fig. 4A: FTIR spectrum of MnNiO

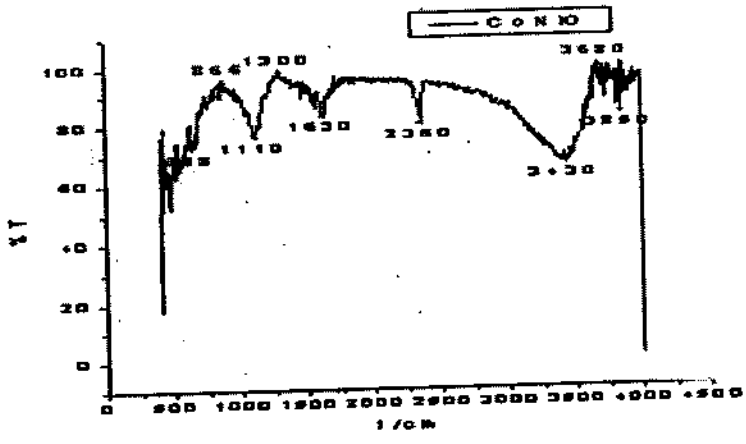

Fig. 4B: FTIR spectrum of CoNiO

broad and are due to the presence of co-ordinated or entrapped water in the samples. The bands in the regions 1640 and 1630 cm^{-1} for both MnNiO and CoNiO correspond to carboxylate ions[14,15]. There are some bands around 600cm^{-1} which might be due to the bending modes of the metal oxides in the nanoparticles.

UV spectral studies

The ultra violet spectra of both MnNiO and CoNiO sintered at 400, 600 and 800 ºC are taken in the wavelength range 200 to 800 nm are shown in fig 5A and 5B respectively. The optical band gaps of the nanoparticles are found out using the UV spectra.

On analyzing the UV spectra, there is a decrease in absorbance with increase in wavelength which can be considered as an indication of the presence of optical band gaps in the materials. This decrease corresponds to excitation of surface plasmons in the nano composite. The Tauc's relation connects energy band of the material and the absorption coefficient by the formula $\alpha h\upsilon = A(h\upsilon - Eg)^n$, where A is a constant, $h\upsilon$ is the photon energy, Eg is the band gap energy; for an allowed direct transition the value of n is 1/2. $(\alpha h\upsilon)^2$ versus $h\upsilon$ graphs in Fig 6A and 6B gives the of direct band gap values[16] of MnNiO and CoNiO sintered at 600 ºC.

When the sintering temperature increases, the nano particle size increases. However the band gap decreases. The reason for decreasing band gap with increase in sintering temperature may be due to the surface defects on the nanocomposite. So it is concluded that the band gap has an

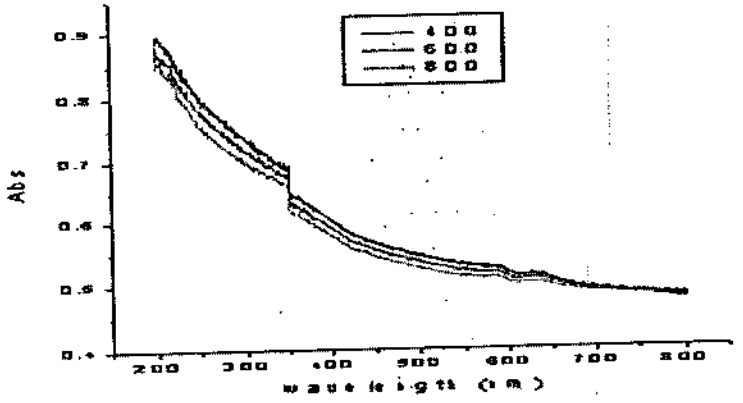

Fig. 5A: Absorbance versus wavelength graph for MnNiO sintered at different temperatures

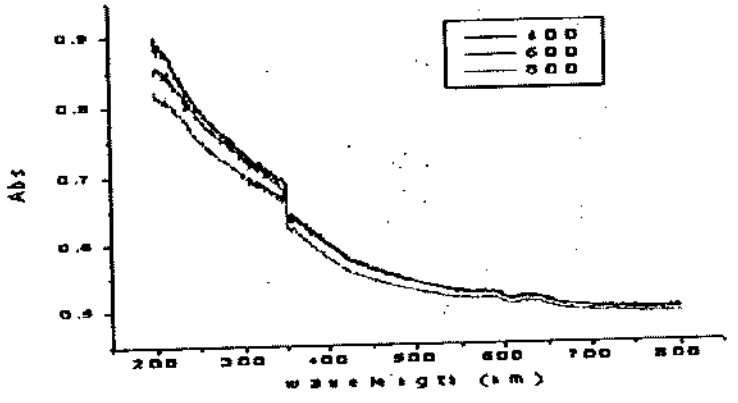

Fig. 5B: Absorbance versus wavelength graph for CoNiO sintered at different temperatures

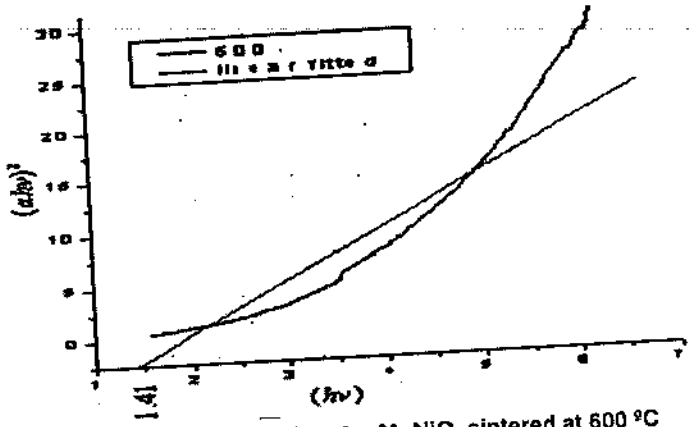

Fig. 6A: $(\alpha h\upsilon)^2$ vs $h\upsilon$ graph for MnNiO sintered at 600 °C

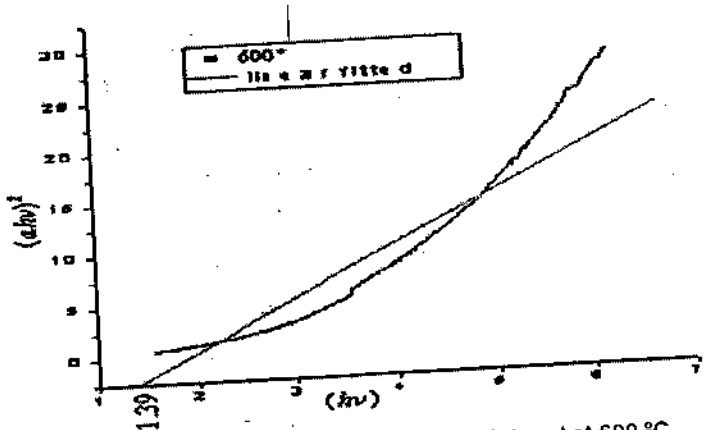

Fig. 6B: $(\alpha h\upsilon)^2$ vs $h\upsilon$ graph for CoNiO sintered at 600 °C

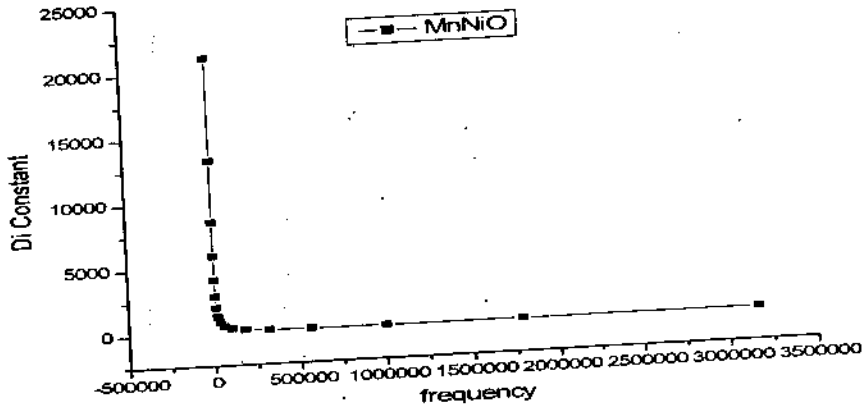

Fig. 7A: Dielectric constant-frequency graph of MnNiO at 600 °C

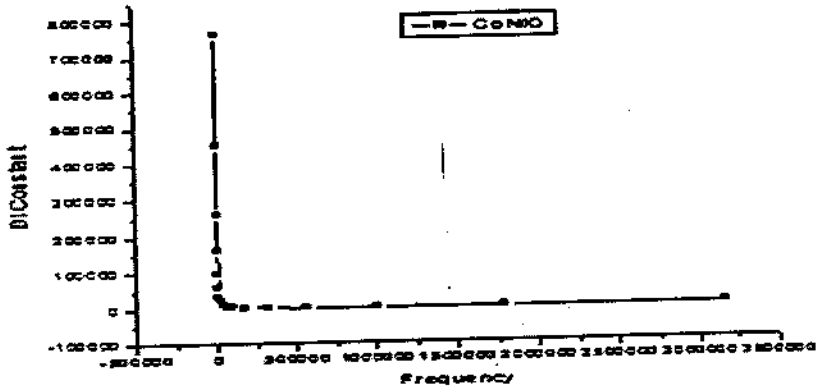

Fig. 7B: Dielectric constant-frequency graph of CoNiO at 600 ºC

inverses dependence on the particle size of these nanocomposite.

Dielectric studies

To study the dielectric constant values of both MnNiO and CoNiO, the nanopowders were first pelletized and then studied about the variations of dielectric constant with frequency of the applied field. Fig 7A and 7B represents the dielectric constant versus frequency graphs of both MnNiO and CoNiO at 600 ºC. The dielectric constant decreases very fast in the low frequency region but after that it reaches a constant value which shows that it is independent of frequency at high frequency region. The dielectric nature of the nanoparticles is mainly due to space charge and rotational polarizations[17]. Nanoparticles possess a large number of interfaces and the defects in these interfaces can cause a change of positive as well as negative space charge distribution. In the presence of an electric field these space charges can move and may be trapped by the defects which results in the formation of dipole moments. Interfaces found in nanoparticles contain several oxygen ion vacancies, and are equivalent to positive charges giving dipole moments. When exposed to an electric field, these dipoles can rotate, giving a resultant dipole moment in the direction of the field. These are the reasons for the high value of dielectric constant at low frequencies[18].

CoNiO nanoparticles are found to be better dielectric material than MnNiO nanoparticles at all frequencies especially in the lower regime.

CONCLUSIONS

Nanoparticles of Manganese-Nickel Oxide and Cobalt-Nickel oxide were prepared by arrested precipitation. The X-ray diffractograms compared with JCPDS data confirms the presence of the cubic phases with prominent peaks at (311). From the XRD analysis, there is a direct dependence of sintering temperature and particle size. The nanoparticles are found to be almost spherical in shape with agglomerations to a certain extend. Optical absorption studies indicate that Manganese-Nickel Oxide and Cobalt-Nickel oxides have the direct band gaps which decrease with increase in temperatures. Variations in the dielectric constant with frequency of the applied field are thoroughly studied for both the samples so as to recommend CoNiO as a better dielectric material compared to MnNiO nanoparticles.

REFERENCES

1. Lopez, R.; Haynes, T .E.; Boatner, L. A.; Haglund, R. F.; *Opt. Lett.* **2002**, *27*, 1327-1329.
2. Ikeyama, M.; Nakao, S.; Tazawa, M.; Kamada, K.; *Nucl Instrum Methods Phys. Res. B* **2001**, *652*, 175-177.
3. Muroi, M.; Street, R.; McCormick, P. G.; *J. Appl. Phys.* **2000**, *87*, 3242-3244.

4. Kenneth J. Klabunde; Cathymohs, Department of Chemistry, Kansas state university, *Manhanttan Kansas second Edition*, **1998**.
5. Tsai, M. S.; *Mater. Sci. Eng. B.* **2004**, *110*, 132-134.
6. Mori, Wang, Y. R.; Drennan, *Solid State Ionics*, **2004**, *175*, 641-649.
7. Scherrer, P.;, *Math. Phys. K.* **1918**, *1*, 187.
8. Williamson, G. K.; Hall, W. H.; Acta Metall. **1953**, *1*, 22-31.
9. Warren, B. E.; Averbach, B. L.; *J. Appl. Phys.* **1950**, *21*, 595-599.
10. Cullity, B. D.; *Elements of X-ray diffraction*, Addison - wesley publishing company Inc California, **1970** . 102.
11. Wang, L. P.; Hong, G. Y.; Qu, S. C.; Wang, Z. G.; *Nanotechnology*. **2005**, *16*, 1469-1473.
12. Warad, H. C.; Ghosh, S. C.; Hemtanon; *Sci. Technol. Adv. Mater.* **2005**, *6*, 296-301.
13. Robert Kelsall; Ian Hamley; Mark Geoghegan; *Nano Scale Science & technology*, (John Wiley, Chichester), **2005**.
14. Ehrlich, G.; J Am Chem Soc. **1954**, *76*, 5263-5268.
15. Douville, F.; Duval, G.; Lecomte, J.; Compt Rend Acad Sci. **1941**,*963*, 212.
16. Mohanta, D.; Nath, S. S.; Mishra, N. C.; Choudhury, A.; *Bull. Mater. Sci.* **2003**, *26*, 289-294.
17. Mo Chi-Mei; Zhang Lide; Wang Guozhong, *Nanostuctr Mater.* **1995**,*6*, 823-826.
18. *Tareev, B.; Physics of dielectric materials (Mir Publishers, Moscow), 1979.*

Research Article

Open Access

Nahi Jamal, Asha Radhakrishnan, Raveendran Raghavan and Beena Bhaskaran*

Efficient photocatalytic degradation of organic dye from aqueous solutions over zinc oxide incorporated nanocellulose under visible light irradiation

https://doi.org/10.1515/mgmc-2020-0009
Received September 15, 2018; accepted April 29, 2020.

Abstract: Increased growth of textile industries leads to the tremendous accumulation of dyes on water and surrounding environments. This terrific increase of dyes is the major cause of water pollution which in turn adversely affects the aquatic lives and the balance of our ecosystem. Purpose of the present study is to report the synthesis and characterization of a composite namely zinc oxide incorporated nanocellulose (ZnO/NC) for effective degradation of an anionic dye, Congo red. Fourier transform infrared spectroscopy (FTIR), X-ray diffraction (XRD), Brunaeur, Emmett and Teller (BET) surface area analysis and scanning electron microscopy (SEM) studies have helped to characterize the composite. The optical properties of the samples were studied by UV-Visible spectroscopy. Feasibility of the photocatalyst in the degradation of Congo red was tested. Experimental conditions such as time of contact, concentration of the dye solution, catalyst dosage, pH were altered to find out the optimum conditions of degradation. The optimum pH was found to be 5.5 and dosage of ZnO/NC was optimized as 0.075 g for a dye concentration of 20 ppm. Equilibrium was attained at 120 min. The studies reveal that the photocatalyst ZnO/NC is efficient for the photodegradation of Congo red. Photodegradation was due to electron hole interaction between metal oxides and nanocellulose.

Keywords: zinc oxide; sugar cane bagasse; photodegradation; photocatalyst

1 Introduction

In recent decades, due to rapid industrialization, huge amount of toxic effluents are being discharged to water bodies (Ansari et al., 2015). A large number of industries such as leather, paper, plastic, textile, food processing, printing, cosmetics and pharmaceuticals, etc., deal with dyes. The dye containing waste water can adversely affect the aquatic environment due to decreased sunlight penetration. In addition to these, some of the dyes can cause serious health problems such as mutation and cancer (Kumar et al., 2013). Serious issues of this water pollution are the shortage of safe water for drinking, household uses, agriculture, farming, etc., (Radhakrishnan et al., 2015). Therefore it is necessary to eliminate water pollution (Pourmortazavi et al., 2017). Physical methods such as adsorption and chemical methods such as chlorination and ozonation are some of the most frequently used methods for the removal of textile dyes (Chennakesavulu et al., 2015). Floculation and reverse osmosis are also some other methods commonly used, but these methods are not destructive. They just transfer the contaminants from one phase to another for which further treatments are required (Guillard et al., 2003). But Advanced oxidation process (AOP) like heterogeneous photocatalysis is a promising technology for water purification going on the surface of photocatalyst under the irradiation of photons, leading to total mineralization of dyes (Nagaveni et al., 2004), pesticides, organic-inorganic pollutants and other deleterious pollutants. In

* **Corresponding author: Beena Bhaskaran,** Department of Chemistry, Kumbalath Sankupilla Memorial Devaswom Board College, Sasthamcotta, Kollam, Kerala, India
Nahi Jamal, Department of Chemistry, Kumbalath Sankupilla Memorial Devaswom Board College, Sasthamcotta, Kollam, Kerala, India
Asha Radhakrishnan, Department of Chemistry, Devaswom Board Pampa College, Parumala, Kerala, India
Raveendran Raghavan, Department of Physics, Sree Narayana College, Kollam, Kerala, India

Open Access. © 2020 Jamal et al., published by De Gruyter. This work is licensed under the Creative Commons Attribution alone 4.0 License.

photocatalysis, organic pollutants are degraded by using reusable photocatalysts, energetic light source such as sunlight or an artificial light and an oxidizing agent such as oxygen or air (Hachem et al., 2001). For a photocatalyst, as the particle size decreases, surface area increases and the number of active sites increases which leads to high reactivity (Alaton et al., 2002). As the number of active sites increases, the absorbance of pollutants on the surface of the catalyst increases (Augugliaro et al., 2002). The promoting of photoreaction in presence of a catalyst is termed as heterogeneous photocatalysis, a low cost and sustainable technology for the treatment of organic and inorganic pollutants present in water. In photocatalysis degradation takes place when the photocatalyst adsorbs photons of energy greater than its band gap energy (Anirudhan et al., 2015). A hole-electron generation occurs when the electron excites from the valence band to conduction band of the semiconductor. These electrons react with O_2 to form $O_2^{\cdot -}$ and holes react with OH^- or H_2O to form $OH^{\cdot}$ which are the active species to react with organic dyes.

Photocatalysis by semiconductors has gained much more attention due to its applications in hydrogen production, refractory pollutants elimination and self-cleaning surface. Wide band gap of metal oxides limit their ability to absorb visible light. Therefore many efforts such as metal or non-metal doping (Wang et al., 2014), composite synthesis (Mukherjee et al., 2014), etc., have been made to lower their band gap. Among these processes fabrication of composites with polymers has been shown to effectively lower the band gap and allows greater absorption in the visible region (Ansari et al., 2015). Such composites are expected to achieve synergetic and complementary behavior between the components.

In the present work we report the synthesis of a composite assembled from nano zincoxide (ZnO) and nanocellulose (NC). Nano ZnO is a photocatalyst with excellent properties and has many applications. Semiconducting metal oxides have photocatalytic activities for the degradation of pollutants. Metal oxide nanoparticles like ZnO and TiO_2 have been used to degrade non-biodegradable pollutants such as dyes via photocatalytic routes. In the present work, nanocellulose prepared from sugarcane bagasse was selected for the synthesis of composites with ZnO. Sugarcane bagasse is a waste product produced by the sugar and alcohol industries (Simkovic et al., 1990). It is used as a raw material for industrial applications like electricity generation, pulp and paper production and products based on fermentation (Pandey et al., 2000). Nanocellulose has been obtained from the inexpensive and readily available lignocellulosic material namely sugarcane bagasse by acid hydrolysis (Bondeson et al., 2006). For the preparation of NC, we hereby suggest a modified acid hydrolysis approach by an ecofriendly method. On the conversion of cellulose to nanocellulose, efficiency is enhanced due to the increase in the number of available functional groups, increase in surface area and crystalline nature. The NC prepared is made into a composite with nano ZnO and it is well characterized by different experimental techniques like XRD, FTIR, UV-Visible spectroscopy, SEM and BET surface area measurements. The photocatalytic activity of the materials was studied through the degradation of Congo red (CR). CR is an anionic dye frequently used in textile industry. Experiments were carried out to optimize the conditions like pH, time, initial concentration and adsorbent dosage.

2 Results and discussion

2.1 XRD analysis

The XRD of the synthesized ZnO samples (Figure 1) show broad peaks at 2θ values of 31.9, 34.6, 36.4, 47.7, 56.7, and 63.1 which are typical for the hexagonal ZnO wurtzite structure with lattice parameters a and c of 3.249 and 5.205 A°, respectively. The observed peaks of the nano crystallites match well with standard JCPDS files (36-1451), and no other crystalline phases were detected. The XRD of NC gives a broad hump between 16.1° and 23.2° indicating its amorphous nature. The XRD of ZnO/NC confirms the formation of nanocomposites. The well-defined peaks

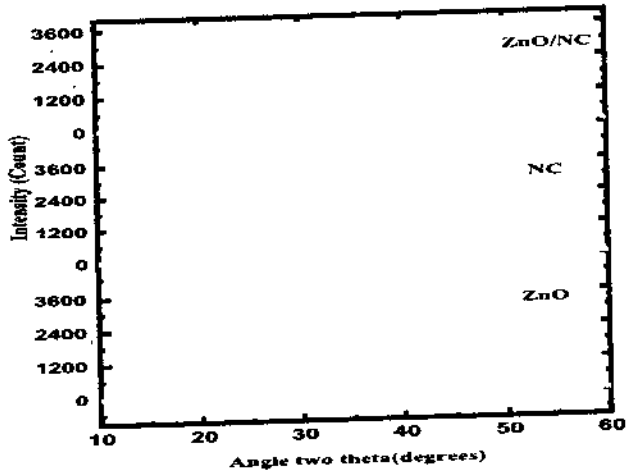

Figure 1: XRD of ZnO, NC, and ZnO/NC.

corresponding to the crystal planes (1 0 0), (0 0 2) and (1 0 1) of nano ZnO were found to be incorporated into the XRD of NC. It is thus clear that the metal oxide particles are well distributed in the nanocellulose matrix. Further, a change in intensity is observed in the characteristic peak of NC ($2\theta = 23.2°$) which again confirms the formation of nanocomposite. The average size of the particles was determined from full width at half maximum (FWHM) of the diffraction peaks using Scherrer's equation (Ahmmad et al., 2010):

$$D = \frac{k\lambda}{\beta\cos\theta} \quad (1)$$

where K the shape factor ($K = 0.9$), β represents the full width at half maximum (FWHM), Θ is the Bragg angle and λ is the wavelength of X-rays used. The particle size calculated for ZnO was found to be 26 nm.

2.2 FTIR analysis

The FTIR spectrum of ZnO (Figure 2) shows bands at around 566 cm^{-1}, which can be assigned to the vibrations of Zn (II)–O bonds. The absorption peaks observed at ~2500 cm^{-1} and ~1400 cm^{-1} may be due to the the adsorbed water and CO_2 molecules. The characteristic peaks of cellulose (Li et al., 2012) at 3400 cm^{-1}, 2800 cm^{-1} (due to O–H stretching and C–H stretching vibrations), 1371 cm^{-1}, and 897 cm^{-1} (due to O–H bending and C–H deformation vibration) are observed in the FTIR of NC prepared in the present study. In the FTIR spectrum of the composites, the main characteristic bands of NC and ZnO are retained. However, the incorporation of metal oxides leads to the shift of some bands of NC.

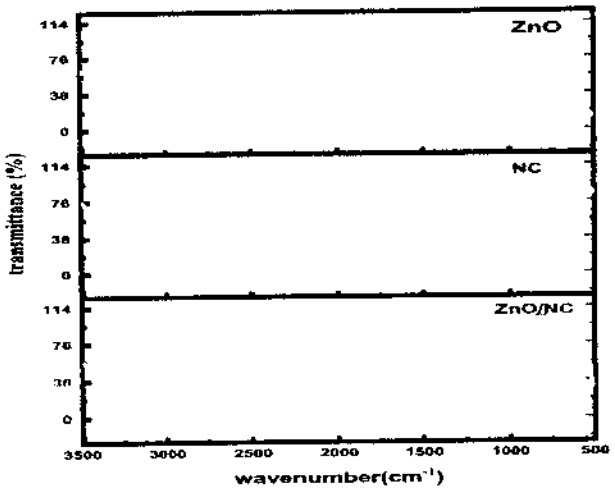

Figure 2: FTIR spectra of ZnO, NC, and ZnO/NC.

2.3 SEM analysis

The SEM results of the prepared samples are shown in Figure 3. SEM of ZnO consists of homogeneous; almost flower shaped nanostructures with less agglomeration. The SEM of NC reveals its sheet like morphology. ZnO/NC shows morphology entirely different from the flower like and sheet like morphologies of its components via ZnO and NC.

2.4 UV analysis

The room temperature UV-Visible spectra of the prepared samples were taken in the range of 250 to 600 nm are shown Figure 4. The spectrum of ZnO shows absorption peak at 380 nm which can be consigned to the intrinsic

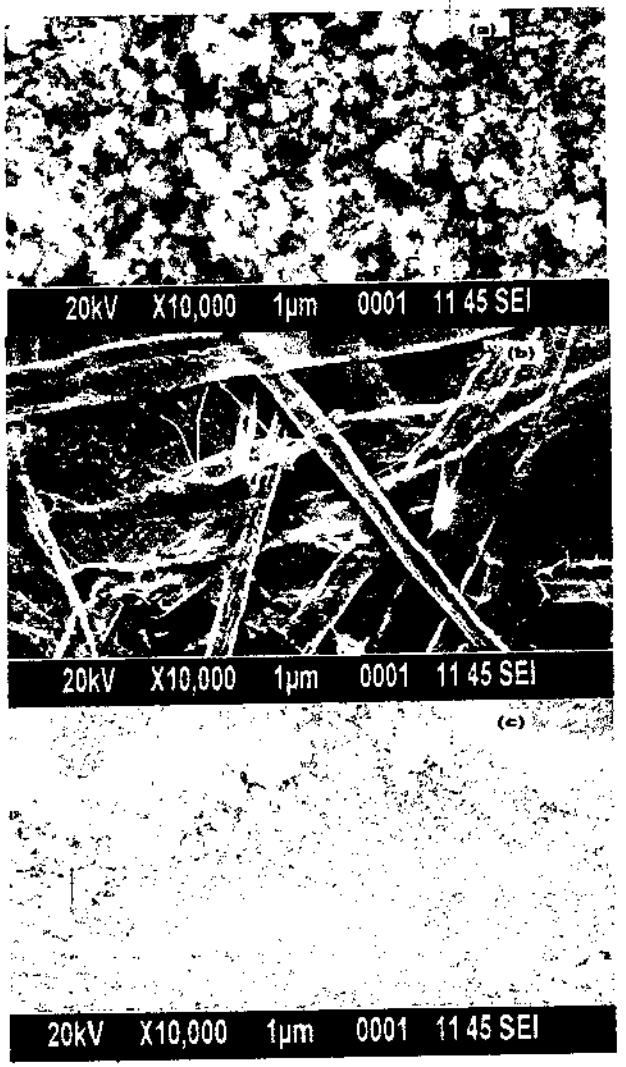

Figure 3: SEM images of (a) ZnO, (b) NC, and (c) ZnO/NC.

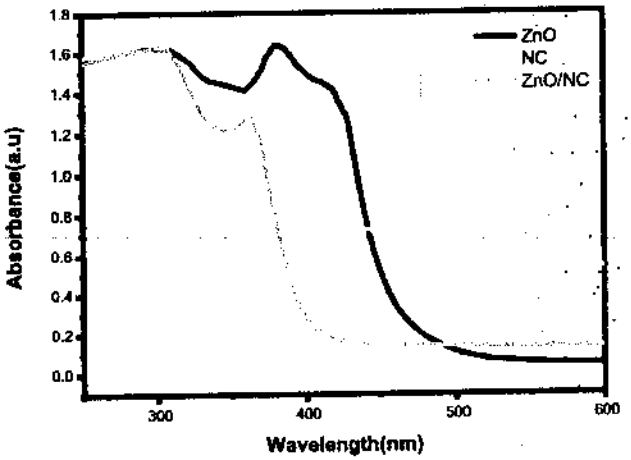

Figure 4: UV-Visible spectra of ZnO, NC, and ZnO/NC.

band gap absorption of ZnO due to the transition of electrons from valence band to conduction band (O2p–Zn3d) (Khorsand Zak et al., 2011). The spectrum of NC shows absorption band with λ_{max} value of 300 nm. When ZnO nanoparticles are doped into NC, broad and strong absorption with a maximum at 360 nm was perceived, which was blue shifted relative to the ZnO (380 nm) due to the quantum confinement (Prasad et al., 2006). The band gap of the samples was determined from the absorption spectra using Wood-Tauc's relation (Khorsand Zak et al., 2011).

$$\alpha h\vartheta = D\,(h\vartheta - Eg)^n \quad (2)$$

where $h\vartheta$ is the energy of the photon, Eg is the band gap of the material and D is a constant. The band gap values obtained for ZnO, NC, and ZnO/NC are 3.33, 3.8, and 2.75 eV, respectively. Thus the absorption of the composite is in the visible region due to its low band gap energy compared to that of ZnO and NC.

2.5 BET surface area measurement

The Brunauer-Emmett-Teller (BET) surface area measured for ZnO, NC, and ZnO/NC were found to be 82.3, 75.9, and 184.5 m^2/g, respectively. Surface area of the composite ZnO/NC is highest which also accounts for its good photo catalytic activity.

2.6 Evaluation of photocatalytic activity

To study the efficiency of the composite for the degradation of dyes, a synthetic anionic dye namely Congo red was selected, the structures of which is shown in Scheme 1.

2.6.1 Effect of time

The changes in optical absorption spectra of Congo red using 0.1 g of photocatalyst for 25 ppm of dye solution of pH 7.5 irradiated under visible light irradiation for different time intervals are shown in Figure 5. From the plots it is evident that there is a decrease in intensity with increase in time for all the samples. High rate of photodegradation of the dye was observed with increase in time for all the samples. The photodegradation efficiency of NC for degradation of CR after a time interval of 120 min was found to be 52% whereas for ZnO it was 72% and for ZnO-NC 98%.

2.6.2 Effect of catalyst dosage

As the catalyst dosage was increased from 0.025 to 0.25 g for 25 ppm dye solution of pH 7.5 and irradiated for 120 min, the percentage degradation of the Congo red dye was found to increase for all the catalysts as shown in Figure 6. The increase in amount of catalyst load increased the number of active sites on the photocatalytic surface, which in turn, increased the number of hydroxyl radicals (Wang et al., 2007). It is also observed that further increase in the load of photocatalyst dosage decreased the degradation efficiency in all the samples. This is because, with increasing catalyst loading, though the number of active sites increases the penetration of light decreases due to shielding effect (Jang et al., 2006). In comparison with ZnO and NC, very small amount of ZnO/NC was required for maximum degradation of Congo red.

2.6.3 Effect of concentration

The effect of concentration of the dyes (Figure 7) on the degradation was observed by varying the initial concentration of dyes from 10 to 50 ppm using 0.1 g of catalyst for 120 min of pH 7.5 under visible light irradiation. At low concentrations, the rate of degradation and substrate concentrations are directly

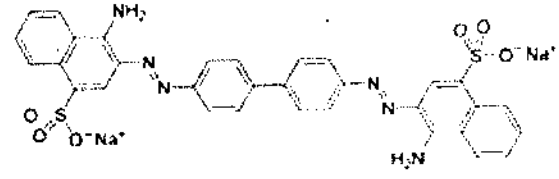

Scheme 1: Structure of Congo red.

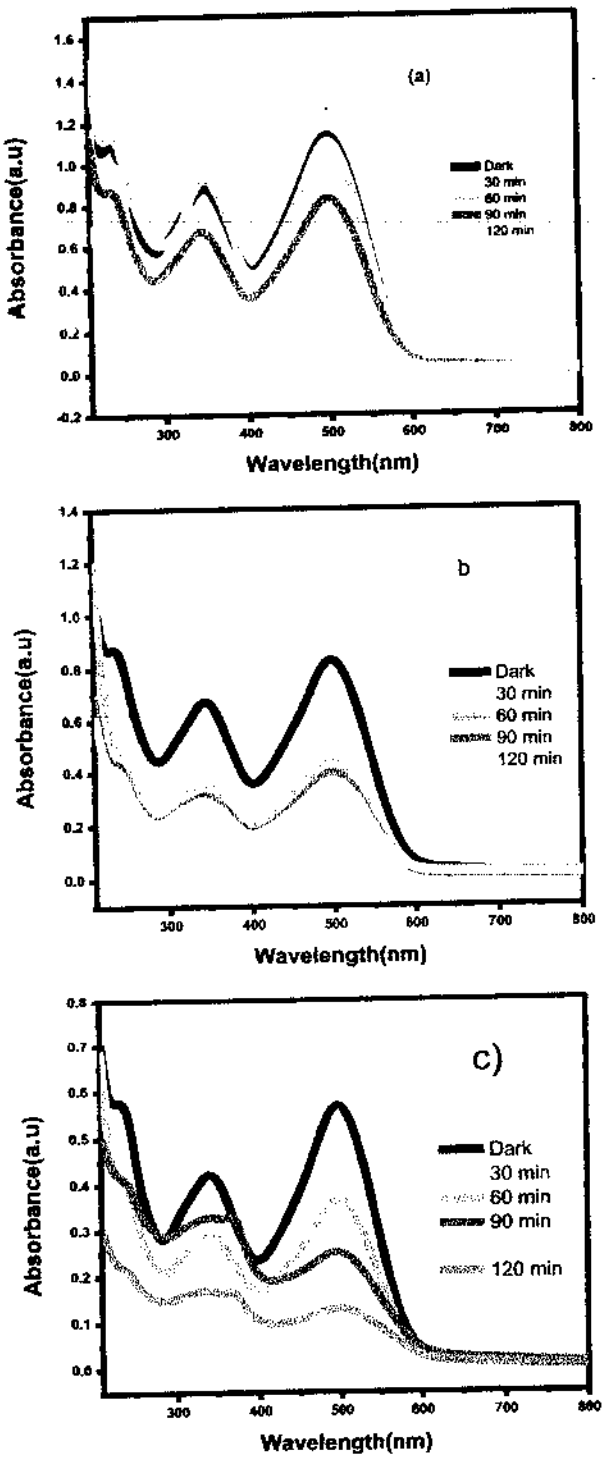

Figure 5: Time dependant absorption spectra of Congo red dye under visible light irradiation with (a) ZnO, (b) NC, and (c) ZnO/NC.

related. As the concentration increased, the degradation efficiency decreased for all the catalysts. The reduced rate of degradation at higher concentrations are due to unavailability of photoactive sites by increased adsorption of dye molecules, decreased rate of light penetration due

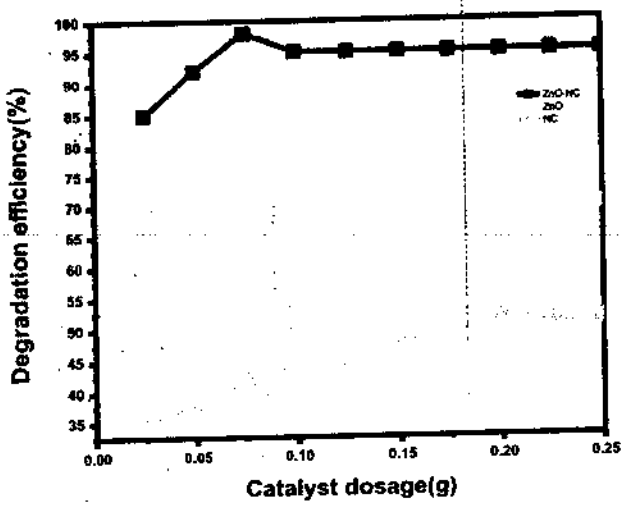

Figure 6: Degradation efficiency vs catalyst dosage for CR.

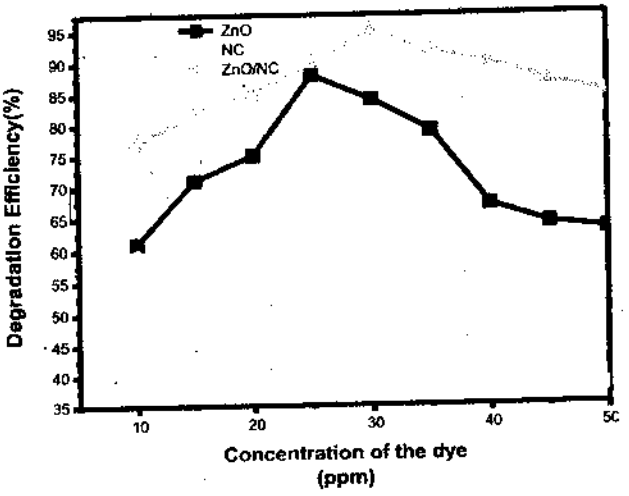

Figure 7: Degradation efficiency vs concentration for CR.

to screening effect and high rate of aggregation of dye molecules (Gopal et al., 2015). The highest degradation was obtained at concentrations 20, 25, and 30 ppm respectively for NC, ZnO, and ZnO/NC.

2.6.4 Effect of pH

Photodegradation capability of the photocatalyst depends on solution pH. Studies were conducted to evaluate the effect of pH on the CR degradation using 25 ppm dye solution and 0.1 g of photocatalyst for 120 min under visible light irradiation. For the degradation process, the effect of pH was studied over the pH range of 2.0-9.0 (Figure 8). The pH of the CR solution was altered by using diluted HCl or NaOH. The results obtained are shown in Figure 9, which show a maximum degradation

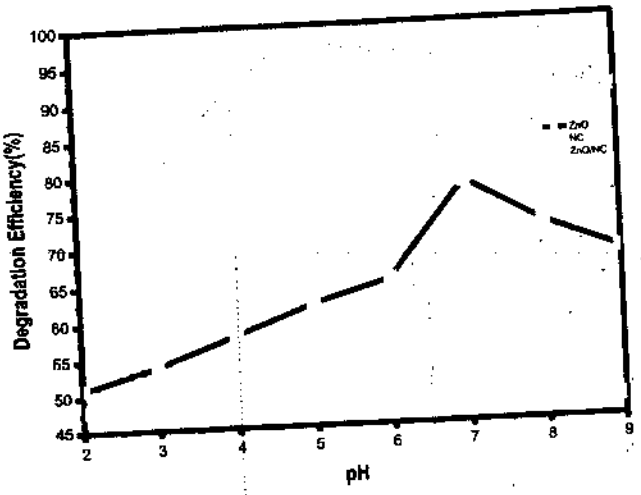

Figure 8: Degradation efficiency vs pH for CR.

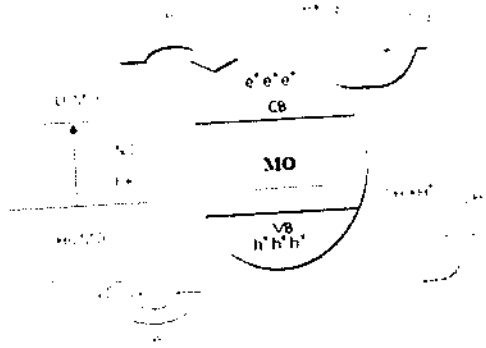

Figure 9: Mechanism of photodegradation by metal oxide nanocellulose composites.

of CR at pH 7.5, 4, and 5.5 for ZnO, NC, and ZnO/NC respectively. From literature it was found that the point of zero charge (pH_{pzc}) for ZnO is 8 (Benhebal et al., 2013). So its surface charge is zero at this pH. When the pH values are lower than pH_{pzc}, surface charge is positive and it is neutral at pH_{pzc} and negative at higher pH. As CR is an anionic dye, lower pH values show higher degradation efficiency.

Photodegradation of the dyes on the composites can be explained by the mechanism given in Figure 9. When metal oxide-nanocellulose composites are illuminated under visible light, the electrons are excited from the highest occupied molecular orbital (HOMO) to lowest unoccupied molecular orbital of (LUMO) NC and subsequently into the CB of metal oxide, holes will be left in the HOMO of NC. The electrons in the VB of metal oxide can migrate to the HOMO of NC and recombine with holes creating holes in the VB of metal oxide. As a result of this large number of electrons and holes are formed. These electrons react with O_2 to form $O_2^{\cdot-}$ and holes react with OH^- or H_2O to form $OH^{\cdot}$ which are the active species to react with organic dyes. The dyes undergo degradation through intermediates which are oxidized finally to CO_2 and H_2O.

The mechanism of the degradation process can be expressed as

$$MO - NC \rightarrow MO - NC^* + e^- \quad (3)$$

$$e^- + O_2 \rightarrow O_2^- \quad (4)$$

$$MO - NC^* \rightarrow MO - NC + h^+ \quad (5)$$

$$OH^- + h^+ \rightarrow OH^{\cdot} \quad (6)$$

$$H_2O + h^+ \rightarrow OH^{\cdot} + H^+ \quad (7)$$

$$Dye + O_2^{\cdot-} \text{ or } OH^{\cdot} \rightarrow intermediates \rightarrow CO_2 + H_2O \quad (8)$$

where e^- and h^+ are the electrons and holes respectively.

Mostly semiconducting metal oxides are used as catalyst in the UV region. Here in the present study by the incorporation of ZnO into NC the resulting composite could be used as an effective photocatalyst in the visible region. Overall the process of photodegradation was found to be simple and complete. Almost complete (98%) degradation was obtained using the nanocomposite. No significant degradation of the dye was observed when experiments were conducted without photocatalyst and without light. The composite prepared was from cellulose which is bio compactable, readily available and thus cost effective. The above study also points towards the utilization of such composites for the removal of pollutants from waterbodies.

3 Conclusion

The present work mainly covers the synthesis, characterization and photocatalytic degradation efficiency of ZnO, NC, and ZnO incorporated NC. Pure hexagonal phase ZnO with flower like morphology was synthesized using zinc acetate and HMT. Nanocellulose was prepared by a novel biogenic method using sugarcane bagasse. The composite of NC with ZnO was synthesized and well characterized. Photocatalytic degradation of the Congo red using the above materials was well studied. The study reveals that the catalytic activity of the composite is higher when compared to its counterparts. The variation in different experimental conditions such as time, concentration of the dye, catalyst dosage and pH that affects the photocatalytic degradation was also studied.

The composite ZnO/NC was found to be a promising catalyst for environmental applications.

Experimental

Materials and methods

All chemicals: zinc acetate dehydrate ($Zn(CH_3COOH)_2 H_2O$), hexa methylene tetraammine ($(CH_2)_6N_4$) (HMT), and Congo red (CR) were purchased from Merck Company as analytical grade and were used as received. Sugarcane bagasse was collected locally, cut into small pieces, washed and dried in sunlight. The dried bagasse was grained and the obtained powder was used for further studies.

Preparation of ZnO

To an aqueous solution of 0.02M zinc acetate dihydrate (50 mL), a 0.25 M hexa methylene tetraammine solution in water was added dropwise under constant stirring. The prepared solution was then stirred well for 120 min to obtain a homogeneously turbid liquid. This liquid was sonicated in an ultra-sonication bath for 30 min. The curdy white precipitate obtained was cooled at room temperature, filtered, and washed with water followed by drying in hot air oven at 100°C for 2 h. The main steps involved in the formation of ZnO are as follows (Rejani et al., 2014):

$$CH_2N_4 + 6H_2O \rightarrow 4NH_3 + 6HCHO \quad (9)$$

$$NH_3 + H_2O \rightarrow NH_4^+ + OH- \quad (10)$$

$$Zn^{2+} + 2OH- \rightarrow ZnO + H_2O \quad (11)$$

HMT a moderate alkali was used to generate hydroxide anion.

Preparation of nanocellulose (NC) from sugar cane bagasse (SCB)

The dried SCB was boiled with 25% (w/v) NaOH (fiber to liquid ratio 1:20) for 6 h and allowed to cool at room temperature. The obtained product was acid hydrolyzed with 50% (w/v) sulfuric acid under stirring for another 6 h. About 500 mL of distilled water was added to the above solution, cooled and centrifuged. This washing and centrifugation was continued for 24 h. The obtained colloidal solution was then sonicated for 2 h in ice bath in order to avoid overheating (Dong et al., 1998). The suspension obtained was collected, dried, and stored for further studies.

Preparation of ZnO/NC

About 4 g NC was dispersed in 50 mL water and stirred well for 1 h. Simultaneously 2 g ZnO was dispersed in 50 mL water and was stirred for 1 h. The above solutions were mixed under constant stirring and sonicated for 3 h using ultra sonication bath. The obtained composite was washed and dried.

Characterization

X-ray diffractogram ($2\Theta = 10–90°$) was obtained on XPERT-PRO powder diffractometer with Cu-Kα radiation. The FTIR spectrum was recorded using KBr wafer on the Thermo Nicolet FTIR model AVATAR 370 DTGS. In the present study, SEM of the sample was recorded using a JED-2300 system. The UV-Visible spectra were recorded at room temperature using JASCOV 650 UV-2550 UV Visible spectrophotometer. BET surface area of the samples was measured using SMART SORB 93 Surface area analyzer.

Photocatalytic degradation of CR

In a typical experiment, 0.1g of the prepared catalyst was added to aqueous solution of CR (25 ppm, 300 mL, pH 7.5) taken in a cylindrical photoreactor of capacity 500 mL. The mixture was kept in the dark for 90 min to obtain equilibrium adsorption of CR onto the photo catalyst. The photoreactor was then illuminated with visible light (160 W, Hg vapour lamp) for 120 min. Aliquant were withdrawn from the reaction mixture at regular time intervals and centrifuged immediately to remove the catalyst before absorbance was recorded using a JASCOV 650, UV-Visible spectrophotometer.

To study the effect of pH, experiments were conducted in the pH range 2.0 to 9.0 using 0.1 g of photocatalyst with 25 ppm of dye solution and 120 min of irradiation. To optimize the amount of photocatalyst, a series of experiments were carried out by varying the catalyst amount from 0.025 to 0.25 g for 25 ppm dye solution of pH 7.5 irradiated for 120 min. The effect of initial dye concentration was investigated by varying the initial concentration from 10 to 50 ppm using 0.1 g of catalyst for 120 min of irradiation. Here also the pH of the solution was maintained at 7.5. Blank experiments were also performed in the absence of catalyst and absence of light.

The photocatalytic degradation efficiency was calculated as follows (Radhakrishnan et al., 2016):

$$Removal\ (R\%) = \frac{C_o - C_e}{C_o} X100 \quad (12)$$

where $R\%$ is the degradation efficiency of CR, C_o – initial concentration of dye solution (mg/L), Ce – equilibrium concentration of dye solution (mg/L).

Acknowledgements: The authors are thankful to the Management and the Principal of Kumbalath Sankupilla Memorial Devaswom Board College (K.S.M.D.B. College) for providing necessary laboratory facilities, STIC Cochin for instrumental analysis. One of the authors (N.J.) is thankful to the University of Kerala for financial assistance.

References

Ahmmad B., Kusumoto Y., Islam M.S., One-step and large scale synthesis of non-metal doped TiO_2 submicrospheres and their photocatalytic activity. Adv. Powder Technol., 2010, 21, 292-297.

Alaton I.A., Balcioglu I.A., Bahnemann D.W., Advanced oxidation of a reactive dyebath effluent: comparison of O_3, H_2O_2/UV-C and TiO_2/UV-A processes. Water Res., 2002, 36, 1143-1154.

Anirudhan T.S., Deepa J.R., Binusreejayan, Synthesis and characterization of multi carboxyl-functionalized nanocellulose/nanobentonite composite for the adsorption of uranium (VI) from aqueous solutions: Kinetic and equilibrium profiles. Chem. Eng. J., 2015, 273, 390-400.

Ansari M.O., Khan M.M., Ansari S.A., Cho M.H., Polythiophene nanocomposites for photodegradation applications: Past, present and future. J. Saudi Chem. Soc., 2015, 19, 494-504.

Augugliaro V. Baiocchi C., Bianco Prevot A., García-López E., Loddo V., Malato S., et al., Azo-dyes photocatalytic degradation in aqueous suspension of TiO_2 under solar irradiation. Chemosphere, 2002, 49, 1223-1230.

Benhebal H., Chaib M., Salmon T., Geens J., Leonard A., Lambert S.D., Photocatalytic degradation of phenol and benzoic acid using zinc oxide powders prepared by the sol–gel process. Alexandria Eng. J., 2013, 52, 517-523.

Bondeson D., Mathew A., Oksman K., Optimization of the isolation of nanocrystals from microcrystalline cellulose by acid hydrolysis. Cellulose, 2006, 13, 171-180.

Chennakesavulu K., Madhusudhana Reddy M., Ramanjaneya Reddy G., Rabel A.M., Brijitta J., Vinita V., et al., Synthesis, Characterization and Photo catalytic studies of the composites by Tantalum oxide and Zinc oxide Nanorods. J. Mol. Struct., 2015, 1091, 49-56.

Dong X.M., Revol J.F., Gray D.G., Effect of Microcrystallite Preparation Conditions on the Formation of Colloid Crystals of Cellulose. Cellulose, 1998, 5, 19-32.

Gopal P., Mira P., Kim H.-Y., Lee S.-Y., Park S.-J., Electrospun ZnO hybrid nanofibers for photodegradation of wastewater containing organic dyes. A review. J. Ind. Eng. Chem., 2015, 21, 26-35.

Guillard C., Lachheb H., Houas A., Ksibi M., Elaloui E., Herrmann J.M., Influence of chemical structure of dyes of pH and of inorganic salts on their photocatalytic degradation b TiO_2 comparison of the efficiency of powder and supported TiO_2. J. Photochem. Photobiol. A-Chem., 2003, 158, 27-36.

Hachem C., Bocquillon F., Zahraa O., Bouchy M., Decolourization of textile industry wastewater by the photocatalytic degradation process. Dyes Pigments, 2001, 49, 117-125.

Jang Y.J., Simer C., Ohm T., Comparison of zinc oxide nanoparticles and its nano-crystalline particles on the photocatalytic degradation of methylene blue. Mater. Res. Bull., 2006, 41, 67-77.

Khorsand Zak R., Razali R., Majid W.H.A., Darroudi M., Green synthesis and evolution of metabolic activity of starchmediated nanoceria. Int. J. Nanomed., 2011, 6, 1399-1403.

Kumar M., Sivakumar V., Tamilarasan R., Adsorption of Victoria blue by carbon/Ba/Alignate beads: Kinetics, Thermodynamics and Isotherm studies. Carbohydr. Polyn., 2013, 98, 505-513.

Li J., Wei X., Wang Q., Chen J., Chang G., Kong L., et al., Homogeneous Isolation of Nanocellulose from Sugarcane Bagasse by High Pressure Homogenization. Carbohydr. Polym., 2012, 90, 1609-1613.

Mukherjee D., Barghi S., Ray A.K., Preparation and characterization of the TiO_2 immobilized polymeric photocatalyst for degradation of aspirin under UV and solar light. Processes, 2014, 2, 12-23.

Nagaveni K., Sivalingam G., Hegde M.S., Madras G., Solar photocatalytic degradation of dyes high activity of combustion synthesized Nano TiO_2. Appl. Catal. B-Env., 2004, 48, 83-93.

Pandey A., Soccol C.R., Nigam P., Soccol V.T., Biotechnological potential of agro-industrial residues I: Sugarcane bagasse. Bioresour. Technol., 2000, 74, 69-80.

Pourmortazavi S.M., Rahimi-Nasrabadi M., Aghazadeh M., Ganjali M.R., Karimi M.S., Norouzi P., Synthesis, characterization and photocatalytic activity of neodymium carbonate and neodymium oxide nanoparticles. J. Mol. Struct., 2017, 1150, 411-418.

Prasad V., Souza C.D., Yadav D., Shaikh A.J., Vigneshwaran N., Spectroscopic characterization of zinc oxide nanorods synthesized by solid-state reaction. Spectrochim. Acta A, 2006, 65, 173-178.

Radhakrishnan A., Rejani P., Bhaskaran B., CuO/polypyrrole nanocomposites as a marker of toxic lead ions for ecological remediation in contrast with CuO and polypyrrole. Main Group Met. Chem., 2015, 38, 133-143.

Radhakrishnan A., Rejani P., Shanavas Khan I., Bhaskaran B., Effect of annealing on the spectral and optical characteristics of nano ZnO: Evaluation of adsorption of toxic metal ions from industrial waste water. Ecotoxicol. Environ. Saf., 2016, 133, 457-465.

Rejani P., Radhakrishnan A., Bhaskaran B., Photo Catalytic Decomposition of Malachite Green in Aqueous Solutions under UV Irradition Using Nano ZnO Rod. Iranica J. Energy Environ., 2014, 5, 233-239.

Simkovic I., Mlynar J., Alfoldi J., Micko M.M., New aspects in cationization of lignocellulose materials. XI. Modification of bagasse with quaternary ammonium groups. Holzforschung, 1990, 44, 113-116.

Wang H., Xie C., Zhang W., Cai S., Yang Z., Gui Y, Comparison of dye degradation efficiency using ZnO powders with various size scales. J. Hazard. Mater., 2007, 141, 645-652.

Wang Y., Zhang R., Li J., Li L., Lin S., First-principles study on transition metaldoped anatase TiO_2. Nanoscale Res. Lett., 2014, 9, 46-53.

Annexure-II

AS RESOURCE PERSON IN SEMINARS

1. Invited Talk on the topic: "ENVIRONMENT" in the Awareness Seminar organized by the National Service Scheme of S.N. College, Sivagiri , Varkala, Thiruvanthapuram on 05-06-2016.
2. Invited Talk in the National Seminar "Join The Race to Make The World a Better Place" on World Environmental Day celebrations--2016 sponsored by KSCSTE, Govt. of Kerala and organized by the Department of Physics, St. Gregorios College, Kottarakara, Kollam, Kerala on 15-06-2016.
3. Invited Talk on the topic: "NUCLEAR WARS" in the Awareness Seminar organized by the National Service Scheme of S.N. College, Sivagiri , Varkala, Thiruvanthapuram on 08-08-2016.
4. Invited Talk in the auspicious of Ozone Day Celebrations -2016" organized by the Department of Physics, S.N. College, Kollam , Kerala on 27-09-2016.
5. Invited Talk organized by the IQAC for an orientation programme on Internal Quality Assurances in Colleges at M.P.M.M S.N.Trusts College, Shoranur, Palakkad , Kerala on 04-11-2016.
6. Key Note Address and Invited Talk on the topic: "Recent trends in Science" in the one Day Seminar sponsored by KSCSTE, Govt. of Kerala and organized by the Science Club of S.N. College, Sivagiri, Varkala, Thiruvanthapuram on 10th February 2017.
7. Inauguration and Inaugural Address of ASPIRE-2017 : Multi Disciplinary Seminar Series ,15-17, February 2017 organized by the IQAC and PTA at Sree Narayana College, Chathannur.
8. Invited talk on the subject :"Future Scope of Nano Medical Research" in the National Seminar on "NANO MEDICINE – CURRENT SCENARIO AND FUTURE OPPORTUNITIES organized by the Post Graduate Department of Chemistry, Sree Narayana College, Chengannur, Alleppey Dist , Kerala during17th &18th of February 2017.
9. Key Note Address on the Topic : "Science and Technology for Specially abled Persons" in the National Science Day Celebrations -2017 organized by The

Department of Chemistry and Science Club of SREE NARAYANA COLLEGE, CHENGANNUR Sponsored by KSCSTE, Govt. of Kerala on 22nd February,2017.

10. Invited Talk on the topic: "Career Guidance for Science Students " organized by the Department of Physics, S.N. College, Kollam , Kerala on 23-02-2017.

11. Delivered an Invited Talk on National Science Day Celebrations -2017 organized by The Applied Science Department of Vidya Academy of Science and Technology Campus- Kilimanoor, Thiruvananthapuram, kerala Sponsored by KSCSTE, Govt. of Kerala on 28th February,2017.

12. Invited Speech on the Topic: "Science Enrichment Programme" organized on the Opening day of XIIth standard students of Sree Narayana Central School, Cherukunnam, Mavelikkara on 16th May -2017 .

13. Key Note Address and Invited Talk in the National Seminar "Connecting People to Nature" on World Environmental Day celebrations--2017 sponsored by KSCSTE, Govt. of Kerala and organized by the Department of Chemistry, D.B. Pamba College, Parumala, Pathanamthitta on 05-06- 2017.

14. Invited Talk on the topic: "NUCLEAR DISASTERS" in the Awareness Seminar organized by the National Service Scheme of S.N. College, Sivagiri , Varkala, Thiruvanthapuram on 09-08-2017.

15. Invited Talk on the topic: "Atomic Bomb Blast @ Hiroshima and Nagasaki " in the Awareness Seminar organized by the Department of Physics, S.N. College, Kollam, Kerala on 10-08-2017.

16. Inaugural talk for the inauguration of P.G. Courses of M.A English and M.Com at Sree Narayana Guru College of Advanced Studies, Nattika ,Trichur ,Kerala on 23-08-2017.

17. Key Note Address and Invited Talk on the topic: "CARING FOR ALL LIFE UNDER THE SUN" in the auspicious of Ozone Day Celebrations -2017" sponsored by KSCSTE, Govt. of Kerala and organized by the Department of Geology, S.N. College, Sivagiri, Varkala, Thiruvanthapuram on 15th September 2017.

18. Key Note Address and Invited Talk on the topic: "CARING FOR ALL LIFE UNDER THE SUN" in the auspicious of Ozone Day Celebrations -2017" sponsored by KSCSTE, Govt. of Kerala and organized by GHSS Thodiyoor, Thodiyoor North, Karunagappally, Kollam Kerala on 18th, 19th & 20th September 2017.

19. Key Note Address and Invited Talk on the topic: "CARING FOR ALL LIFE UNDER THE SUN" in the auspicious of Ozone Day Celebrations -2017" sponsored by KSCSTE, Govt. of Kerala and organized by the P.G. and Research Department of Chemistry, K.S.M.D.B. College, Sasthamcotta , Kollam, Kerala on 26-27 September 2017.

20. Orientation Class for Teachers, Topic: Psychological and Scientific Tenets of Teaching" at Sree Narayana Guru College of Advanced Studies, Pambanar, Idukki, Kerala on 04-10-2017.

21. One day Seminar on "Personality and Career Guidance "for B.Sc, B.A and B.Com students at Sree Narayana College of Arts & Science, Pambanar, Idukki, Kerala on 04-10-2017.

22. Invited Talk on the topic: "HOW TO JOIN INDIAN ARMY" in the Awareness Seminar sponsored organized by the National Cadets Corps (NCC) of S.N. College, Sivagiri, Varkala, Thiruvanthapuram on 03-11-2017.

23. One day Seminar on "Personality and Career Guidance "for B.Sc, B.A and B.Com students at Sree Narayana Guru College of Advanced Studies, Kannur on 21-11-2017.

24. Orientation Class for Teachers, Topic: NAAC Accreditation in New Format" dated 21-11-2017 at Sree Narayana College, Kannur.

25. Invited Talk in the One day Seminar "CHALLENGES OF NAAC ACCREDITATION IN HIGHER EDUCATION (NEW FORMAT)" organized by the IQAC, D.B. Pamba College, Parumala, Pathanamthitta on 28-11- 2017.

26. One Day Workshop on "New Guidelines on NAAC Accreditation "Dated 07-12-2017, T.K.M.M.College, Nangiarkulangara, Alleppey, Kerala.

27. Orientation Class for Teachers ,Topic: : NAAC Accreditation in New Format" dated 11-12-2017 at Sree Narayana College ,Chelannur, Kozhikkodu.

28. One day Seminar on "Career Development "2nd &3rd B.Com students at Sree Narayana Guru College of Advanced Studies, Chelannur on 11-12-2017.

29. Orientation Class for Teachers, Topic: :Challenges of NAAC Accreditation in Higher Education (New Format)" dated 12-12-2017 at Sree Narayana College, Chempazhanthy, Thiruvananthapuram, Kerala.

30. Orientation Class for Teachers , Topic: Changing Parameters of Quality Assessment" dated 13-12-2017 at Sree Narayana College ,Nattika, Trichur, Kerala.

31. Resource Person in an One Day Seminar organized by the Department of Physics , Sree Narayana College for Women, Kollam on "Funding Agencies in India & Abroad" Dated 14th December 2017.

32. Orientation Class for Teachers, Topic: UGC- NAAC ACCREDITATION" dated 22-12-2017 at Sree Narayana Arts & Science College, Kumarakom, Kottayam, Kerala.

33. Invited Talk in an One day Seminar "Institutional Information For Quality Assessment (IIQA) organized by the IQAC, S.N. College, Sivagiri, Varkala, Thiruvananthapuram (Dist),KERALA on 28th November 2017.

34. One day College Level Seminar on "Motivational Class for Science Students" dated 11-01-2018, S.N. College, Punalur.

35. Orientation Class for Teachers, Topic: NAAC Accreditation in New Format" dated 11-01-2018 at Sree Narayana College, Punalur.

36. Orientation Class for Teachers, Topic: NAAC Accreditation in New Format" dated 12-01-2018 at Sree Narayana College, Chathannur, Kollam, Kerala.

37. One day Seminar on "Personality Development "for Degree students at Sree Narayana Guru College of Advanced Studies, Mezhuveli, Pathanamthitta, on 16-01-2018.

38. Worked as a Member of TALENT SEARCH EXAMINATION-APT-TSE 2017 -2018 organized on 20th January 2018 at S.N. College, Kollam.

39. Invited Talk on the topic: "Personality Development for Science Students " organized by the Department of Physics, S.N. College, Kollam, Kerala on 01-02-2018.

40. Invited Talk organized by the IQAC for an orientation programme on New Trends in NAAC Accreditation at M.P.M.M S.N.Trusts College, Shoranur, Palakkad , Kerala on 02-02-2018.

41. Invited Talk on the topic: "No Wetland No Life" in the auspicious of World Wetland Day Celebrations -2018" sponsored by KSCSTE, Govt. of Kerala and organized by the P.G. and Research Department of Chemistry, K.S.M.D.B. College, Sasthamcotta , Kollam, Kerala on 08-02- 2018.

42. Inauguration and Inaugural Address on "National Science Day Celebrations -2018 on 19-02-2018 sponsored by KSCSTE, Govt. of Kerala and organized by the Department of Physics & Science Forum, S.N. College, Chengannur, Alleppey Dist, Kerala.

43. Inauguration and Inaugural Speech in the National Science Day Celebrations -2018 entitled "Technology Transfer from Lab to Land for Sustainable Development" organized by Sree Narayana College For Women, Kollam on 26th February 2018.

44. Invited Speech in the National Science Day Celebrations -2018 entitled "Technology Transfer from Lab to Land for Sustainable Development" organized by Sree Narayana College For Women, Kollam on 27 th February 2018.

45. Invited Speech on the Topic: "Science & Technology for Green Future" in the National Science Day Celebrations-2018 on 28-02-2018 sponsored by KSCSTE, Govt. of Kerala and organized by, Sree Narayana Training College, Nedunganda,Varkala, Thiruvananthapuram Dist, Kerala.

46. Key Note Address and Invited Talk in the Seminar on "Science & Technology for Sustainable Development" organized by the P.G. Department of Physics and IQAC of SAHODARAN AYYAPPAN SMARAKA SNDP YOGAM COLEGE, KONNI, PATHANAMTHITTA (Dist) on 8th March 2018.

47. "Science Enrichment Programme for the Students" at Sree Narayana Guru College of Advanced Studies, Chempazhanthy , Thiruvananthapuram ,Kerala on 28th March-2018.

48. Invited Speech on the Topic : "Nano Technology for Green and Sustainable Development" in the National Science Day Celebrations -2018 organized by CIPET-INSTITUTE OF PLASTIC TECHNOLOGY(IPT),Department of Chemicals and Petro Chemicals , CUSAT , Kochi , Kerala. Sponsored by KSCSTE, Govt. of Kerala on 11th May -2018.

49. Orientation Class for Teachers, Topic: Psychological and Scientific Tenets of Teaching" at Sree Narayana Guru College of Advanced Studies, Nattika,Trichur, Kerala on 27-06-2018.

50. Inaugural talk for the inauguration of Library Complex at Sree Narayana Guru College of Advanced Studies, Nattika, Trichur, Kerala on 27-06-2018.

51. Invited talk in a One Day Seminar for College Teachers on "Funding Agencies in India & Abroad" Dated 17th July 2018, Sree Narayana College Sivagiri, Varkala, Thiruvananthapuram.

52. One Day Seminar on “Quality Enhancement and Preparation for NAAC Accreditation “Dated 09-08-2108, at R. SANKAR MEMORIAL SNDP YOGAM ARTS & SCIENCE COLLEGE, KOYILANDY, CALICUT,KERALA.

53. Key Note Address and participation in an one day Seminar organized by The Department of Mathematics, S.N. College, Sivagiri, Varkala, Thiruvananthapuram Dist, Kerala Sponsored by KSCSTE, Govt. of Kerala on 10th August -2018.

54. Invited Talk organized by the IQAC for an orientation programme for the First Year Degree Students at S.N. College, Chengannur, Allepey , Kerala on 06-09-2018.

55. Inauguration and Inaugural Speech in the “*Two Day Zonal Workshop on Nano Materials and Nano Composites”* held on 12th & 13 th of September 2018 at S.N. College, Kollam in association with BEC on 2k18-19 & IIT Delhi.

56. Invited Talk on the topic: “CAREER IN DEFENCE” in the Awareness Seminar sponsored & organized by the National Cadets Corps (NCC) of S.N. College, Sivagiri, Varkala, Thiruvanthapuram on 03-11-2017.

57. Invited Talk in an One Day Seminar organized by the IQAC of ST. GEORGE’S COLLEGE ARUVITHURA ,KOTTAYAM on” NAAC ACCREDITATION IN NEW FORMAT” for the entire Teachers of the college on 27-10-2018.

58. Invited Talk in an One Day Seminar organized by the IQAC of SREE NARAYANA GURU COLLEGE, Chelannur, Kozhikkodu on” ASSESSMENT & ACCREDITATION IN THE NEW SCENARIO” for the entire Teachers of the college on 07-11-2018.